

Aminoglycoside resistance mechanisms and strategies to overcome them

Nicola Pontillo

Propositions

accompanying the dissertation

AMINGLYCOSIDE RESISTANCE MECHANISMS AND STRATEGIES TO OVERCOME THEM

by

Nicola PONTILLO

1. Aminoglycoside sensitivity is an energetic phenomenon: uptake is governed by respiratory driven PMF, and membrane hyperpolarization rather than mistranslation or ROS, is the key determinant of bactericidal action.
2. After four years of optimizing aminoglycosides, I'm convinced that adding a methyl group may not solve all problems in life, but it solves more than expected.
3. The structural plasticity of AAC(3)-IIIa is a primary driver of its broad substrate promiscuity, and targeting this adaptability (rather than the active site itself) could represent a more effective strategy for designing next generation aminoglycosides.
4. Reversible optical control of antibiotic activity challenges traditional chemical modifications strategies, decoupling drug potency from constant selective pressure.
5. Aminoglycoside optimization should prioritize structural features governing ribosomal engagement rather than tailoring drug design exclusively to evade resistance enzymes, whose recognition patterns are inherently heterogeneous.
6. Docking, and AI have each inspired their own hype cycles, sometimes with promises exceeding reality. Considering them together underscores their strengths, limits, and the need for scientific sobriety.
7. Resistance enzymes evolve faster through horizontal gene transfer than through point mutation and inhibitors targeting these enzymes could remain effective longer than next generation antibiotics designed to evade modification.
8. The Crystallization Oracle states: big, colorful crystals promise publications and academic careers; tiny, troublesome crystals lead to biotech, and cracked crystals send you to character development.

These propositions are regarded as opposable and defendable, and have been approved as such by the promotor prof. dr. A. Guskov.

Aminoglycoside resistance mechanisms and strategies to overcome them

Nicola Pontillo



university of groningen / faculty of mathematics and natural sciences / zernike institute for advanced materials





The work described in this thesis was performed in the research groups of Polymer Chemistry and Bioengeneering of the Zernike Institute for Advanced Materials, and Biomolecular X-ray Crystallography Group. Groningen Biomolecular Sciences and Biotechnology Institute, Faculty of Science and Engineering. The Netherlands.

This project received funding from the European Union's Horizon 2020 research and innovation programme under the Marie Skłodowska–Curie grant agreement No. 713482, and from the European Research Council Advanced Grant *Suprabiotics* (No. 694610).

Cover design: Nicola Pontillo

Cover image: A landscape defined by what is missing.

university of groningen

Aminoglycoside resistance mechanisms and strategies to overcome them

PhD thesis

to obtain the degree of PhD at the
University of Groningen
on the authority of the
Rector Magnificus Prof. J.M.A. Scherpen
and in accordance with
the decision by the College of Deans.

This thesis will be defended in public on

Tuesday 30 June 2026 at 12.45 hours

by

Nicola Pontillo

born on 14 February 1988

Supervisors
Prof. A. Guskov
Prof. D.J. Slotboom

Assessment Committee
Prof. B. Poolman
Prof. M.R. Groves
Prof. S.T. Arold

Even Odysseus needed three winds to return home.

Amicus exercitus; in spe certa
Dionysus inventus; cor apertum
Custos fortunae; tacita dilectio

Si intellegis, iam scis.

CONTENTS

Samenvatting **xiii**

Summary **xv**

1 General Introduction **1**
1.1 Aminoglycoside antibiotics . . . 2
New perspectives for an old class . . . 2
Aminoglicosides: structure and classes . . . 3
1.2 Aminoglycosides mechanism of action . . . 5
Aminoglycoside activity . . . 5
Antibiotic uptake . . . 6
Structural basis of antibiotic activity . . . 8
Adverse effects . . . 10
1.3 Mechanisms of resistance to aminoglycoside antibiotics . . . 11
General overview . . . 11
Aminoglycoside modifying enzymes . . . 12
Ribosomal alteration . . . 20
1.4 Common strategies adopted to counteract the resistance . . . 23
Semi-synthetic aminoglycoside derivatives . . . 23
1.5 Scope of this thesis . . . 26
References . . . 28

2 3-N-alkylation of Neomycin B **45**
2.1 Introduction . . . 47
2.2 Results and Discussion . . . 49
The Crystal Structure of AAC(3)-IIIa Reveals a Unique Fold Among Acetyltransferases . . . 49
The Catalytic Mechanism Features a Non-Canonical Catalytic Triad . . . 49
Kinetic Characterization and Substrate Promiscuity of AAC(3)-IIIa . . . 50
Synthesis of 3-C Modified NEO B Derivatives . . . 51
Evaluation of the Antibacterial Activity of NEO B Derivatives . . . 53
3-N-Methylation of NEO B Dramatically Reduces AAC(3)-IIIa Catalysis While Retaining Ribosomal Binding . . . 54
2.3 Conclusion . . . 56
2.4 Methods . . . 58
Protein Expression and Purification . . . 58
Further Purification by Size-Exclusion Chromatography . . . 59

2.5 AAC(3)-IIIa Structural Characterization . . . 61
Crystallization . . . 61
Data Collection, Model Building and Refinement . . . 61
2.6 Enzymatic Assay . . . 64
Protein Purification . . . 64
Enzymatic Assays of AAC(3)-IIIa . . . 64
Determination of Kinetic Parameters . . . 64
Cloning of *pBluescript-aacC3* . . . 65
MIC Determination . . . 65
2.7 Cryo-EM Structure of the 70S *E. coli* Ribosome . . . 66
Sample Preparation and Data Collection . . . 66
Data Processing and Reconstruction . . . 66
2.8 Synthesis of 3-*N*-Alkylated Neomycin B Derivatives. . . . 69
General Methods . . . 69
NMR Spectroscopy . . . 69
High-Resolution Mass Spectrometry (HRMS) . . . 69
Liquid Chromatography–Mass Spectrometry (LC–MS) . . . 70
High-Resolution Chromatographic Separations. . . . 70
HPLC Purification. . . . 70
2.9 Supporting Information. . . . 72
Synthesis of Imidazole-1-sulfonyl Azide. . . . 72
Characterization . . . 72
2.10 Synthesis of 3-C-Azido Neomycin B (Compound 1) . . . 72
Procedure. . . . 72
Characterization . . . 73
2.11 Synthesis of 1,2',2",6',6"-*N*-Penta-Cbz-3-C-Azido-Neomycin B (Compound 2) . . . 73
Procedure. . . . 73
Characterization . . . 74
2.12 Synthesis of 1,2',2",6',6"-*N*-Penta-Cbz-Neomycin B (Compound 3) . . . 74
Procedure. . . . 74
Characterization . . . 75
2.13 Synthesis of 1,2',2",6',6"-*N*-Penta-Cbz-3-*N*-Methyl-Neomycin B (Compound 4) as 5×TFA Salt . . . 75
Procedure. . . . 75
Characterization . . . 75
2.14 Synthesis of 1,2',2",6',6"-*N*-Penta-Cbz-3-*N*,*N*-Dimethyl-Neomycin B (Compound 5) as 5×TFA Salt . . . 76
Procedure. . . . 76
Characterization . . . 76
2.15 Synthesis of 1,2',2",6',6"-*N*-Penta-Cbz-3-*N*-Propyl-Neomycin B (Compound 6) . . . 77
Procedure. . . . 77
Characterization . . . 77

2.16 Synthesis of 1,2',2",6',6"-*N*-Penta-Cbz-3-*N*-Hexyl-Neomycin B (Compound 7) as 5×TFA Salt . . . 77
Procedure . . . 77
Characterization . . . 78
2.17 General Procedure for Amine Deprotection . . . 78
2.18 Synthesis of 3-*N*-Methyl-Neomycin B (Compound 8) as 5×HFBA Salt . . . 78
Procedure . . . 78
NMR Analysis . . . 79
2.19 Synthesis of 3-*N,N*-Dimethyl-Neomycin B (Compound 9) as 5×HFBA Salt . . . 79
Procedure . . . 79
NMR Analysis . . . 79
2.20 Synthesis of 3-*N*-Propyl-Neomycin B (Compound 10) as 5×HFBA Salt . . . 81
Procedure . . . 81
NMR Analysis . . . 82
2.21 Synthesis of 3-*N*-Hexyl-Neomycin B (Compound 11) . . . 83
Procedure . . . 83
NMR Analysis . . . 84
References . . . 86

3 Photo-Switchable Aminoglycosides 93
3.1 Introduction . . . 95
Background on Antibiotic Resistance . . . 95
Targeting the Ribosome: Mechanism of Action . . . 95
Novel strategies to overcome resistance . . . 95
Amminoglyside hybrid antibiotics . . . 98
Optical control of Antibiotic Activity . . . 99
Chemical modifications of azobenzenes . . . 100
3.2 Results and Discussion . . . 101
Design and Development of Photo-Switchable Paromomycin Dimers . . . 101
Synthesis and characterization of photo-switchable par dimers . . . 103
3.3 Photoisomerization studies . . . 105
Antibacterial Activity of Photo-Switchable Paromomycin Dimers . . . 108
Structural Insights into the Binding of Photo-Switchable Paromomycin Dimers to APH(3')-Ia . . . 110
3.4 Conclusions . . . 113
3.5 Materials and Methods . . . 115
General Procedures . . . 116
Materials . . . 116
Protein preparation . . . 116
Crystallization . . . 117
Data Collection, Processing, and Structure Determination . . . 118

3.6 Supporting Information . . . 119
Synthesis of Azobenzene-4,4'-dicarboxylic acid (5) . . . 120
Synthesis of 4,4'-Bis(2,5-dioxopyrrolidin-1-yl ester) azobenzene (6) . . . 120
Synthesis of Paromomycin–Azobenzene Conjugates . . . 120
Synthesis of H-dimer (compound 2) . . . 121
Synthesis of 2,6-difluoro-4-bromoaniline (compound 9) . . . 122
Synthesis of 4-amino-3,5-difluorobenzonitrile (**10**) . . . 122
Synthesis of 4-amino-3,5-difluorobenzoic acid (**11**) . . . 123
Synthesis of ethyl 4-amino-3,5-difluorobenzoate (12) . . . 123
Synthesis of diethyl 4,4'-(2,2',6,6'-tetrafluoro)azobenzene-4,4'-dicarboxylate (13) . . . 123
Synthesis of 4,4'-(2,2',6,6'-tetrafluoro)azobenzene-4,4'-dicarboxylic acid (14, F_4-diacid) . . . 124
Synthesis of F-dimer (compound 3) . . . 124
Synthesis of p-(phenylazo)benzoic acid (16) . . . 126
Synthesis of p-(phenylazo)benzoic acid-PAR conjugate (17) . . . 126
Synthesis of azobenzene-4,4'-dicarboxylic acid-mono-NHS-PAR conjugate (18) 127
References . . . 128

4 Site-Selective Modifications of Aminoglycosides 133
4.1 Introduction . . . 135
Aminoglycosides antibiotics . . . 135
Mechanism of Action and Bactericidal Effects. . . . 136
Gram-Negative Resistance and the Need for New Antimicrobial Strategies . . . 136
4.2 The Growing Challenge of Aminoglycoside Resistance . . . 137
4.3 Chemical Modifications to Overcome Aminoglycoside Resistance . . . 139
4.4 Results and Discussion . . . 141
Synthesis and Chemical Modifications of Aminoglycosides . . . 141
Microbiological Activity and Mechanism of Action . . . 141
Effect of 3'-OH Modifications on AG Activity . . . 142
Impact of 3'-OH Modifications on Protein Synthesis Inhibition . . . 144
Effect of 3'-OH Modifications on Phosphorylation by APH(3') . . . 144
Basal ATPase Activity of APH(3')-Ia: Case Study with SBI214 . . . 146
Assay Validation and Potential Overestimation of IC_{50} Values . . . 146
Structural Insights into APH(3')-Ia Recognition of Modified Aminoglycosides . 149
4.5 Conclusions. . . . 151
4.6 Materials and Methods . . . 153
Synthesis of Modified Aminoglycosides . . . 153
Microbiology . . . 153
Biochemical Assays . . . 154
APH(3')-Ia Inhibition Assays . . . 155
Structural determination of APH(3')-Ia . . . 155

4.7 Supporting Information . . . 159
General Methods . . . 159
UPLC-MS Analysis and qNMR-Based Purity Determination . . . 159
4.8 synthesis . . . 160
Synthesis of N-$(Cbz)_5$-Paromomycin (1) . . . 160
Synthesis of N-$(Cbz)_5$-3'-Keto-Paromomycin (3) . . . 161
Synthesis of N-$(Boc)_4$-Kanamycin (2) . . . 162
Synthesis of N-$(Boc)_4$-3'-Keto-Kanamycin (4) . . . 162
Synthesis of N-$(Cbz)_5$-3'-Allyl-Paromomycin (5) . . . 163
Synthesis of N-$(Cbz)_5$-3'-epi-Paromomycin (6) . . . 163
Synthesis of 3'-epi-Paromomycin × 5 AcOH (SBI237) . . . 164
Synthesis of 3'-Propyl-Paromomycin × 5 AcOH (SBI236) . . . 164
Synthesis of N-$(Boc)_4$-3'-Allyl-Kanamycin (7) and N-$(Boc)_4$-3',4"-Diallyl-Kanamycin (8) . . . 165
Synthesis of N-$(Boc)_4$-3'-Propargyl-Kanamycin (9) . . . 167
Synthesis of N-$(Boc)_4$-3'-Propyl-Kanamycin (10) . . . 168
4.9 Deprotection to Give SBI209, SBI214, SBI233, SBI238 . . . 168
Synthesis of 3'-Allyl-Kanamycin × 4 TFA (SBI209) . . . 168
Synthesis of 3',4"-Diallyl-Kanamycin × 4 TFA (SBI214) . . . 169
Synthesis of 3'-Propargyl-Kanamycin × 4 TFA (SBI233) . . . 169
Synthesis of 3'-Propyl-Kanamycin × 4 TFA (SBI238) . . . 170
References . . . 170

5 Design of methyltransferase inhibitors 175
5.1 Introduction . . . 177
rRNA methyl-transferases . . . 177
5.2 Computer-based methods in Drug Discovery . . . 179
Fragment-based drug design . . . 180
Fragment profiling . . . 182
5.3 Results and Discussion . . . 183
ArmA Pocket Analysis . . . 183
Building of the Fragment Library . . . 184
Docking results and Growing Strategy . . . 185
Lead selection and linker-angle hypothesis . . . 186
Synthetic feasibility and academic accessibility . . . 187
Commercial building blocks and in-silico combinatorial expansion . . . 187
5.4 Conclusions . . . 189
Summary of Findings . . . 191
Implications for Academic Research . . . 191
Addendum and Future Directions . . . 191

5.5 Methods . . . 194
Formulation of the initial compound library . . . 194
Fragment Evolution and Docking . . . 194
In-silico synthesis of analogs of compounds **3** and **4** . . . 194
Deep Docking Workflow . . . 195
Synthetic feasibility analysis . . . 196
High-Performance Computing Environment . . . 196
Experimental Characterization . . . 196
References . . . 196

6 General Discussion and Conclusions **203**
6.1 Overview . . . 204
Mechanistic Leverage Over AME Specificity . . . 206
Activity Modulation and Evolutionary Dynamics . . . 207
Targeting RMTs as Class-Wide Leverage . . . 207
6.2 Limitations . . . 208
Preclinical Priorities . . . 209
6.3 Concluding Remarks . . . 209
References . . . 210

Acknowledgements **211**

SAMENVATTING

Dit proefschrift onderzoekt strategieën om aminoglycoside-antibiotica (AG) nieuw leven in te blazen in het licht van de toenemende antimicrobiële resistentie (AMR). AG's zijn krachtige bacteriedodende middelen, maar hun klinisch gebruik wordt beperkt door toxiciteit en resistentiemechanismen zoals enzymatische modificatie en ribosomale methylatie. Het werk is verdeeld over zes hoofdstukken:

Hoofdstuk 1 – Achtergrond en Doelstelling Geeft een overzicht van AG-antibiotica, hun werkingsmechanisme en de belangrijkste resistentieroutes, waaronder aminoglycoside modificerende enzymen (AME's) en 16S rRNA-methyltransferasen. Het benadrukt de noodzaak van innovatieve benaderingen om AG's effectief te houden.

Hoofdstuk 2 – Overwinning van AAC(3)-Gemedieerde Resistentie Richt zich op N-acetyl transferase AAC(3)-IIIa. Structurele en kinetische studies tonen aan dat minimale chemische modificaties zoals 3-N-alkylering van neomycine, acetylatie kunnen voorkomen dit erwijl ribosomale binding behouden blijft. Dit is bevestigd door cryo-EM-analyse.

Hoofdstuk 3 – Fotofarmacologie en Dynamische Controle Introduceert foto-switchbare aminoglycoside-dimeren met azo-benzeenlinkers. Deze verbindingen maken een omkeerbare modulatie van antibiotische activiteit door middel van licht mogelijk, wat ruimtelijke en temporele controle biedt en selectiedruk voor resistentie vermindert.

Hoofdstuk 4 – Plaats-Specifieke Modificaties tegen APH-enzymen Onderzoekt structurele modificaties op de 3'-OH-positie van kanamycine en paromomycine om fosforylatie door APH(3')-Ia te vermijden. Verschillende derivaten behielden antibacteriële activiteit en werkten als competitieve remmers. Röntgenkristallografie onthulde sterische hinderingen bij de ATP-bindingsplaats, wat resistentie-ontwijking verklaart.

Hoofdstuk 5 – In-Silico Ontwerp van ArmA-Remmers Beschrijft fragment-gebaseerde en AI-ondersteunde computationele methoden om remmers te identificeren van ArmA-methyltransferase, een enzym dat pan-aminoglycoside-resistentie veroorzaakt. Twee leidende structuren werden ontworpen voor synthetische toegankelijkheid; voorlopige synthese bevestigde de haalbaarheid ondanks oplosbaarheidsproblemen.

Hoofdstuk 6 – Algemene Discussie en Conclusies Vat de bevindingen samen, bespreekt hun wetenschappelijke en technische implicaties en plaatst het onderzoek in een bredere maatschappelijke en translationele context. Het behandelt beperkingen, toekomstige richtingen en culturele aspecten van antibiotica innovatie.

Over het geheel genomen toont dit proefschrift een multidisciplinaire aanpak, door een combinatie van synthetische chemie, structurele biologie en computationeel ontwerp, om

zo AMR aan te pakken. Hoewel verdere validatie en optimalisatie nodig zijn, vormen deze resultaten een solide basis voor aminoglycosiden van de volgende generatie en resistentie remmers.

SUMMARY

This thesis explores strategies to revive aminoglycoside (AG) antibiotics in the face of growing antimicrobial resistance (AMR). AGs are potent bactericidal drugs, but their clinical use is compromised by toxicity and resistance mechanisms such as enzymatic modification and ribosomal methylation. The work is organized into six chapters:

Chapter 1 – Background and Rationale Provides an overview of AG antibiotics, their mechanism of action, and the major resistance pathways, including aminoglycoside-modifying enzymes (AMEs) and 16S rRNA methyltransferases. It establishes the urgent need for innovative approaches to restore AG efficacy.

Chapter 2 – Overcoming AAC(3)-Mediated Resistance Focuses on N-acetyltransferase AAC(3)-IIIa, a key AME. Through structural and kinetic studies, the chapter demonstrates that minimal chemical modifications such as 3-N-alkylation of neomycin can prevent acetylation while preserving ribosomal binding, validated by cryo-EM analysis.

Chapter 3 – Photopharmacology and Dynamic Control Introduces photo-switchable aminoglycoside dimers incorporating azobenzene linkers. These compounds enable reversible modulation of antibiotic activity using light, offering spatiotemporal control and reducing selective pressure for resistance.

Chapter 4 – Site-Selective Modifications Against APH Enzymes Investigates structural modifications at the 3'-OH position of kanamycin and paromomycin to evade phosphorylation by APH(3')-Ia. Several derivatives retained antibacterial activity and acted as competitive inhibitors. X-ray crystallography revealed steric hindrance at the ATP-binding site, explaining resistance evasion.

Chapter 5 – In-Silico Design of ArmA Inhibitors Explores fragment-based and AI-assisted computational approaches to identify inhibitors of ArmA methyltransferase, which confers pan-aminoglycoside resistance. Two lead scaffolds were designed for synthetic accessibility, and preliminary synthesis confirmed feasibility despite solubility challenges.

Chapter 6 – General Discussion and Conclusions Summarizes the findings, discusses their scientific and technical implications, and places the research in a broader societal and translational context. It addresses limitations, future directions, and the cultural aspects of antibiotic innovation.

Overall thi thesis demonstrates a multidisciplinary approach, combining synthetic chemistry, structural biology, and computational design, to address AMR. While experimental validation and optimization remain ongoing, these findings provide a foundation for next-generation aminoglycosides and resistance inhibitors.

1

General Introduction

Nicola Pontillo and Albert Guskov

"In the beginning, there was penicillin. Then came resistance.
Then we dug in the dirt and found hope again."

— Anonymous microbiologist, circa 1944, holding a very confused chicken

1

1.1. AMINOGLYCOSIDE ANTIBIOTICS

NEW PERSPECTIVES FOR AN OLD CLASS

Aminoglycosides (AG) constitute a well-known class of clinically relevant antibiotics employed in the management of bacterial infections both in humans and animals. The first member of this class of antibiotics which was identified is streptomycin (STR), which was isolated from the soil-dwelling *Streptomyces griseus* in 1944, and provided for the first effective treatment for tuberculosis (TB). [1, 2] STR remained the recommended component in TB treatments for the next forty years until the World Health Organization (WHO) changed the treatment guidelines after the insurgence of Multi-Drug Resistant (MDR) *Mycobacterium tuberculosis*, in favor for the more recent AG amikacin (AMK). [3–5]

During the two decades following the first report of STR, many other AGs were isolated from *Streptomyces, Micromonospora* and *Actinomycetes* species, notably neomycin (NEO)in 1949, gentamicin (GEN) in 1963, tobramycin (TOB) in 1967, and sisomycin (SIS) in 1970. [6] These compounds and their semisynthetic derivatives have been the most common class of broad-spectrum antibiotics, and have been successfully used in the management of infectious diseases.

Moreover, newer AGs such as GEN, TOB, and AMK exhibit an improved safety index and pharmacological profile, as well as a broader spectrum of activity, compared with older compounds such as STR and kanamycin (KAN). [7, 8] In some cases, most notably for AMK, these agents are able to overcome antibiotic resistance developed by certain pathogens. [9] Differences in antibacterial activity are associated either with the presence of specific resistance mechanisms that reduce intracellular drug accumulation or activity, or with limited uptake, as observed in Gram-positive bacteria, which present differences in cell envelope structure, and in anaerobic bacteria, which lack the oxygen-dependent, uptake process required for aminoglycoside entry.

Nevertheless, AGs exhibit excellent in-vitro activity against a wide variety of aerobic Gram-negative and some Gram-positive bacilli (see Table 1.1), making them an invaluable resource to treat severe bacterial infections caused by *Escherichia coli, Salmonella spp., Shigella spp., Enterobacter spp., Citrobacter spp., Acinetobacter spp., Proteus spp., Klebsiella spp., Serratia spp., Morganella spp., Pseudomonas spp., Staphylococcus aureus* and some streptococci. [10] AGs represent an important therapeutic option for the treatment of urinary tract infections, [11] visceral leishmaniasis, [12, 13] enterococcal or streptococcal endocarditis, [14, 15] and in all cases of neonatal sepsis. [16]

Pioneering applications of some AGs include the treatment of human genetic disorders due to pathogenic nonsense mutations or premature termination codon mutations, [17–19] cystic fibrosis, [20] and Duchenne muscular dystrophy. [21] Similarly, neamine-based AG was demonstrated to bind to hammerhead ribozyme, [22, 23] the ribozyme from hepatitis delta virus, [24] and group I self-splicing introns, [25, 26] and was shown to inhibit the RNA-protein interaction responsible for the Human Immunodeficiency Virus (HIV) replication cycle. [27, 28]

Despite AGs are among the classes of antibiotics most affected by drug resistance, they still remain indispensable players in the current antibiotics arsenal due to their efficiency

to treat severe bacterial infections, their broad spectrum of activity and rapidity of action. [29, 30]

Although other classes of antimicrobials exhibit a more favorable safety profile, AGs have experienced renewed interest in recent years due to the emergence of MDR pathogens. With the implementation of optimized dosing regimens and careful monitoring of adverse effects, AGs can be used with improved safety while maintaining high antibacterial efficacy. [31, 32]

The continuously improving understanding of the ever-increasing antimicrobial resistance has led to the development of novel AG antibiotics, and formed the basis for further drug optimization. [33] The next generation of AGs will hopefully show superior activity against pathogenic bacteria, as well as an improved safety profile. Moreover, novel applications of AGs based on non-ribosomal RNA interactions provided an important paradigm for the study of RNA molecular recognition, highlighting how an old class of antibiotics can still play an invaluable role in modern medicine and drug discovery.

Aminoglycoside	Source organism	Application
Kanamycin	*S. kanamyceticus*	Short-term treatment of bacterial infections⋆.
Streptomycin	*S. griseus*	Tularemia, tuberculosis, plague.
Paromomycin	*S. krestomuceticus*	Amoebic dysentery, cryptosporidiosis, leishmaniasis.
Gentamicin	*M. purpurea*	Meningitis, pneumonia, sepsis.
Spectinomycin	*S. spectabilis*	Gonorrhœa
Butirosin	*B. circulans*	Pneumonia
Tobramycin	*S. tenebrarius*	Cystic fibrosis, infections from *P. aeruginosa*
Neomycin	*S. fradiæ*	Burns, wounds, ulcers, dermatitis
Amikacin	Deriv. of kanamycin	See Gentamicin
Isepamicin	Deriv. of gentamicin B	Enterococcal endocarditis and Multi-Drug Resistant tuberculosis

Table 1.1 | Aminoglycoside antibiotics, their source organisms and their therapeutic applications. ⋆ active towards one or more of the following pathogens: *E. coli, Proteus, E. aerogenes, K. pneumoniæ, S. mascescens* and *Acinetobacter* species.

AMINOGLICOSIDES: STRUCTURE AND CLASSES

AGs can be categorized into different classes based on their biological origin, chemical structure, and their biosynthesis. The first AGs were isolated from *Streptomyces* (suffix -mycin) species and include kanamycin, apramycin, neomycin and tobramycin, whereas AGs produced by *Micromonospora* species (suffix -micin) include gentamicin and sisomicin. Later on, semisynthetic derivatives were developed to improve the AGs safety, field of applicability,

and antimicrobial resistance. [29, 34–36]

All natural and semisynthetic AGs have a molecular weight between 300 and 600 Da, and share a similar structure, usually consisting of three cyclitol rings, and additional five- or six-membered sugars which are linked via glycosidic bonds. The hallmark of AGs is the presence of at least three amino groups, and multiple hydroxyls conferring the major chemical properties, namely high water solubility, and an anionic, basic character.

The majority of all clinically relevant AGs share the 2-deoxystreptamine (2-DOS) ring as the common structure of their core scaffold. In these compounds, the 2-DOS ring is commonly referred to as ring B (or II). The amino-sugar in position 4 is the Ring A (or I), while the ring in position 5 or 6 is referred as ring C (or III).

These AGs are biosynthetically derived from paromamine and are further divided into two groups: 4,5- and 4,6-disubstituted deoxystreptamines (see Figure 1.1). [37]

The 4,5-disubstituted class includes neomycin (among the oldest AGs that are still in use), ribostamycin, lividomycin, paromomycin and butiromycin. The 4,6-disubstituted constitutes the largest subgroup including kanamycin, tobramycin, and gentamicin, and constitutes the basis for numerous semisynthetic derivatives, like amikacin.

Other classes of AGs with structural moieties different from the 2-DOS ring (see Figure 1.2) are:

Streptomycin and its derivatives based on a disaccharide unit linked to the 4-position of a guanidylated streptamine core with pentose and glucosamine as substituent;

hygromycins which include a spiro ring system;

apramycins a class of 4-monosubstituted 2-DOS compounds that includes a bicyclic pyrano-pyranose sugar moiety.

Other pseudodisaccharides appear to have little or no clinical importance, and will not be discussed here. [38, 39]

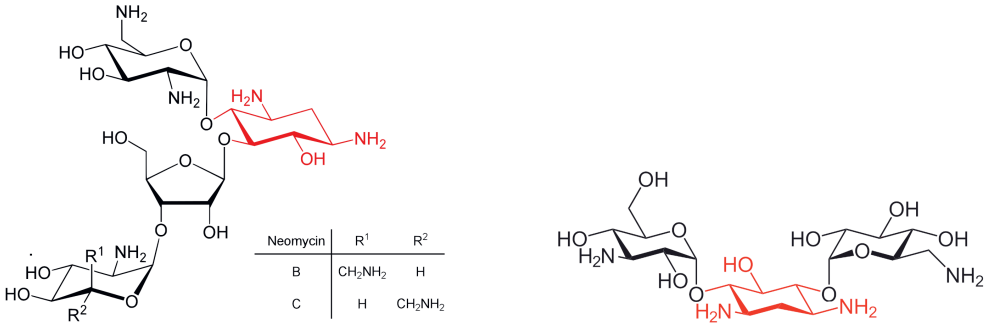


Figure 1.1 | Chemical structures of (a) Neomycin B and C as example of a 4,5-disubstituted AG , and (b) kanamycin A, a 4,6-disubstituted AG . The 2-DOS ring is highlighted in red.

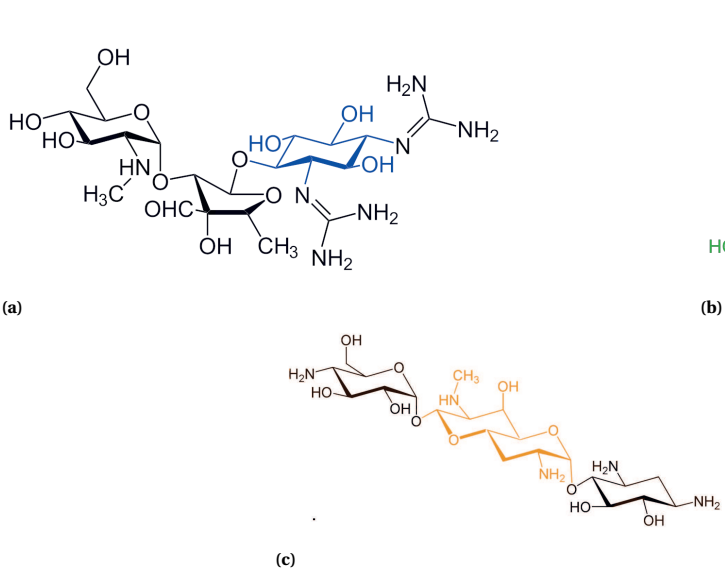


Figure 1.2 | Chemical structures of AGs which do not share the 2-DOS moiety. (a) Streptomycin is based on a deoxystreptamine core, highlighted in blue. (b) Hygromycin presents a spiro ring system highlighted in green, while the bicyclic pyrano-pyranose sugar of apramcinc (c) is represented in orange.

1.2. AMINOGLYCOSIDES MECHANISM OF ACTION

AMINOGLYCOSIDE ACTIVITY

The primary target of AG activity is the 30S subunit of the bacterial ribosome as confirmed by a number of structural studies which have characterized the ribosomal 30S subunit interacting with AGs like streptomycin, spectinomycin, paromomycin, and neomycin. The binding of AGs to the aminoacyl-tRNA recognition site (A-site) leads to protein synthesis inhibition and misreading errors in translation which can lead to mutations and/or truncations, although the precise mechanism how protein synthesis errors lead to cell death is not fully understood. [40, 41]

The main hypotheses that have reached consensus within the scientific community include:

- Insertion of mistranslated membrane proteins leading to a rise in AG permeability of the bacterial membrane, and destabilizing the membrane to the point of breakdown [42]
- positive feedback due to increased aerobic respiratory rate and PMF promotes continuous uptake leading to complete ribosomal inhibition [43]
- oxidative stress from rapid accumulation of reactive oxygen species (ROS) [44, 45]

- dysregulation of membrane potential driven by AG -related metabolic dysfunctions like hyperpolarization of the membrane by ATP synthase working in reverse [46]

Although there is a continuing discussion as to which main mechanism AG exert their activity, there is no disagreement about the importance of AG class of antibiotics.

Indeed, AGs are unique among other protein synthesis inhibitors, and their importance as bactericidal agents can be better appreciated when put in context with all other classes of antibiotics targeting protein synthesis (e.g. chloramphenicol, clindamycin, tetracyclines, macrolides, pleuromutilin, and oxazolidinones) which are all bacteriostatic.

Moreover, the versatility of AGs is fortified by two attractive pharmacodynamic characteristics which have the potential to maximize their antibacterial activity and simultaneously minimize their toxicity: the postantibiotic effect, and a peculiar dose-dependent activity.

The postantibiotic effect of AGs mean that after a short incubation with the drug, it will exert antimicrobial activity even after the compound has been removed. The postantibiotic effect is thought to originate from the AGs irreversible binding to their target, the ribosome. This allows the molecules to continue to exert their bactericidal effect by 0.5-7.5 h despite their depletion in the serum. [47–49]

Additionally, the unique combination of the postantibiotic effect and bacterial uptake contributes to the AGs unique dose-dependent activity. In contrast with other antibiotics, the initial dose at which the bacteria are exposed seems to be more significant than the overall exposure time, or the bacterial inoculum size, [50, 51] and AGs seems to reach an optimum bactericidal activity when the serum concentration reaches tenfold the MIC of the pathogenic bacteria. [52]

Taken together, these two characteristics favor the implementation of a single, daily, high-dose regimen that allows efficient and fast onset of the antimicrobial effect, and minimize the adverse reactions associated with the therapy. [53]

Another significant feature that characterizes AGs is the synergism they show when used in combination with cell wall biosynthesis inhibitors like β-lactams or vancomycin. Enterococci are intrinsically resistant to both AGs and β-lactams and the efficacy of the combination of these two antimicrobial agents is commonly thought to arise from the increased membrane permeability of the bacteria after incubation with cell-wall targeting compounds, and the consequent enhanced uptake of the AGs. [54] The combined use of these two classes of antibiotics results in a valuable asset in the management of some enterococcal and streptococcal infections. [55–57]

ANTIBIOTIC UPTAKE

It has been suggested that AGs uptake happens in three stages. At physiological pH, AGs are polycationic and initially interact electrostatically with anionic components of the bacterial outer membrane, including lipopolysaccharides in Gram-negative bacteria and teichoic acids in Gram-positive bacteria. These interactions displace divalent cations that stabilize lipopolysaccharide cross-bridges, resulting in transient outer-membrane destabilization. This process, often referred to as self-promoted uptake, increases membrane permeability and facilitates aminoglycoside access to the periplasmic space. [58, 59]

The initial electrostatic binding and outer-membrane permeabilization are followed by energy-dependent transport of AGs across the inner membrane. AG uptake across the inner membrane is dependent on an active electron transport chain, as respiratory activity generates the membrane potential required for drug internalization. [60]

This initial energy-dependent phase, commonly referred to as energy-dependent phase I (EDP I), is slow and represents the rate-limiting step of aminoglycoside uptake. Once inside the cytosol, aminoglycosides bind the 30S ribosomal subunit, inducing translational misreading and aberrant protein synthesis. The insertion of mistranslated membrane proteins further disrupts membrane integrity, leading to an accelerated uptake phase known as energy-dependent phase II (EDP II). [61]

Beyond mediating cytoplasmic entry, AG uptake initiates a series of downstream cellular responses that further reinforce antibiotic accumulation and bactericidal activity (Figure 1.3).

Mistranslation induced by ribosomal binding leads to the production of misfolded proteins that can be aberrantly inserted into the cytoplasmic membrane, compromising membrane integrity and promoting an autocatalytic, accelerated uptake of the antibiotic itself. [44, 62]

In parallel, the accumulation of misfolded proteins activates envelope stress response pathways, such as the Arc and Cpx systems, which in turn modulate central carbon metabolism and respiratory activity. [63, 64] AG exposure has also been associated with oxidative stress, whereby hyperactivation of the electron transport chain contributes to iron–sulfur cluster destabilization and the generation of hydroxyl radicals via Fenton chemistry, although the extent and universality of this mechanism remain debated. [65]

Recent research suggests that the bactericidal action of aminoglycosides is driven by metabolic and electrophysiological dysregulation. Inhibition of protein synthesis leads to intracellular ATP accumulation due to decreased ribosomal consumption. This excess ATP can force the F1Fo-ATPase to operate in reverse, hydrolysing ATP to export protons and induce membrane hyperpolarization. [46, 66] While aminoglycosides can enter cells and inhibit translation in the absence of voltage, this hyperpolarization is the critical 'keystone' that triggers lethal ionic fluctuations and bactericide. Furthermore, other mechanisms of ATP synthase disruption, such as inhibition by venturicidin A, can enhance AG uptake by perturbing membrane potential and increasing extracellular proton concentrations. [67] Together, these findings highlight a multifactorial, self-reinforcing cycle where metabolic dysfunction and membrane voltage dysregulation culminate in bacterial death. A schematic overview of these coupled processes is provided in Figure 1.3.

Although no dedicated AG transporter has been conclusively identified, several membrane transport systems, including oligopeptide permease (Opp) components and multidrug efflux or uptake systems such as SbmA/BacA, have been implicated in aminoglycoside sensitivity. Although these systems do not transport aminoglycosides directly, loss-of-function mutations in Opp components have been shown to block the uptake of peptide-like antibiotics, as demonstrated for GE81112 and pacidamycin, where opp mutants exhibit high-level resistance due to impaired transport.[68, 69] Although Opp does not directly import aminoglycosides in *E. coli*, Opp systems in other bacteria influence envelope permeability, which can indirectly modulate AG uptake. Similarly, mutations that alter multidrug efflux pump activity, especially MexXY in *P. aeruginosa*, significantly reduce AG susceptibility by increasing efflux or altering

membrane energetics. [70–73]

STRUCTURAL BASIS OF ANTIBIOTIC ACTIVITY

THE BACTERIAL RIBOSOME

The bacterial ribosome is an RNA-protein complex comprising three RNA molecules and more than 50 proteins, and constitutes one of the main targets of antimicrobial agents. The complex decodes the information, delivered by the mRNA, and provides the platform for the protein synthesis, a process that is highly conserved yet sufficiently distinct between bacteria and eukaryotes to allow selective antimicrobial targeting.

Bacterial protein synthesis involves a coordinated set of factors, and can be divided into four stages: initiation, elongation, termination, and ribosome recycling. During initiation, the 70S ribosome assembles on the messenger RNA (mRNA), positioning the intiator transfer RNA (tRNA) at the peptidyl (P) site.

Each ribosomal subunit (30S and 50S) contains ribosomal RNAs (rRNA) which acts as a structural and functional scaffold during protein synthesis. In particular, the 30S subunit plays a central role in decoding mRNA and constitutes the primary binding site for AG antibiotics. [74]

The large 50S ribosomal subunit comprises two ribosomal RNA molecules, 23S and 5S rRNA, and 33 ribosomal proteins. [75] During translation, transfer RNAs (tRNAs) interact with messenger RNA (mRNA) through codon–anticodon base pairing at the aminoacyl (A) and peptidyl (P) sites formed at the interface of the ribosomal subunits. In the elongation phase, two charged tRNAs sequentially occupy the decoding sites, enabling peptide bond formation at the peptidyl transferase center. Ribosomal translocation then drives the movement of the tRNA carrying the nascent polypeptide chain from the A site to the P site, allowing elongation to proceed until a stop codon is encountered. Recognition of stop codons by class I release factors triggers polypeptide release, followed by dissociation and recycling of the ribosomal complex for subsequent rounds of translation. [76, 77]

Although not all molecular details underlying the high fidelity of ribosomal translation have been fully elucidated, several mechanisms have been proposed. [40, 78, 79] Structural and biochemical studies support a proofreading model in which decoding accuracy is governed by two conserved adenine residues, A1492 and A1493, located within an internal loop of the 16S rRNA at the A site. Upon correct codon–anticodon pairing, these flexible adenines adopt a flipped-out conformation, stabilizing the cognate tRNA within the decoding center and thereby promoting accurate amino acid incorporation. [80]

INHIBITION OF PROTEIN SYNTHESIS

Many details on how AGs bind to the ribosome and inhibit protein synthesis, emerged from recent structural studies on the ribosome, and they are still highly debated subject of discussion. Although the exact binding site is determined by the aminocyclitol ring and may differ slightly among AGs, it is generally recognized that all 4,5- and 4,6 disubstituted AGs bind to the 16S rRNA at the ribosomal decoding site (A site), and share the same mechanism of action. [81]

Upon binding, the AG molecules re-organize the A site, inducing the two sensor adenine

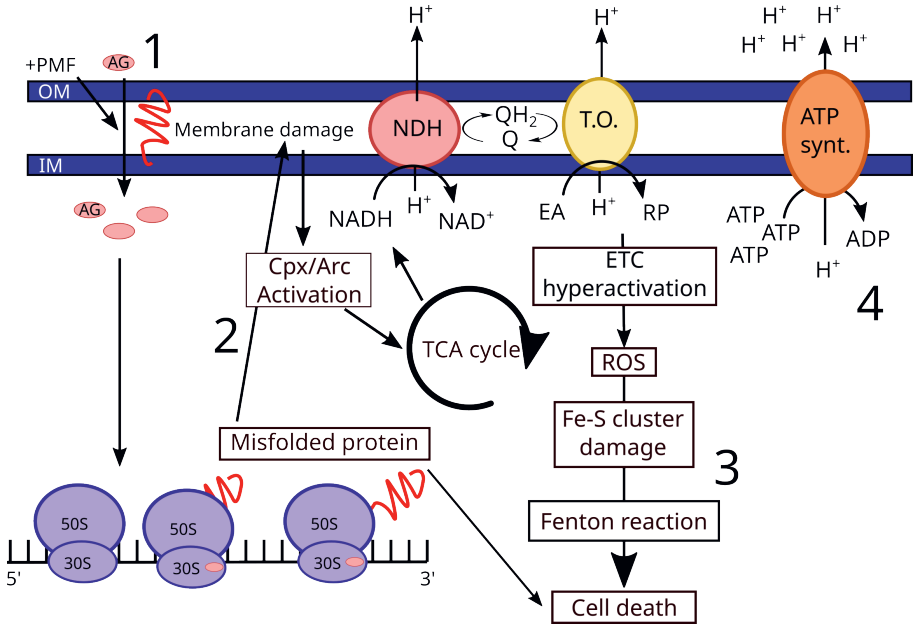


Figure 1.3 | Continuous uptake of AGs (1) generates positive feedback by increasing the aerobic respiratory rate, activating the electron transport chain, and perturbing the tricarboxylic acid (TCA) cycle. Insertion of misfolded proteins (2) into the plasma membrane activates the envelope-responsive (Cpx) and redox-responsive (Arc) two-component systems, altering both cellular metabolism and membrane potential. Oxidative stress and the production of reactive oxygen species (ROS) (3) damage Fe-S clusters, leading to the release of ferrous iron, which subsequently generates DNA-damaging hydroxyl radicals. Hyperpolarization of the membrane (4) occurs through ATP synthase operating in reverse, further affecting membrane potential and cellular energetics. Terminal oxidase (TO) represents the terminal step of the electron transport chain. Depending on growth conditions, different terminal enzymes may operate, using molecular oxygen or alternative electron acceptors (EA) such as nitrate. Abbreviations: reduced product (RP); proton-motive force (PMF); NADH dehydrogenase (NDH); ubiquinone (Q); ubiquinol (QH_2); reactive oxygen species (ROS).

bases into a flipped out conformation which closely resembles the ribosomal state adopted during the mRNA decoding. [82] As a consequence, the discrimination between cognate and non-cognate tRNA-mRNA is diminished together with the proofreading capability of the ribosome, introducing mutations and protein truncation in the growing polypeptide chain. [83] Then, the accumulation of aberrant proteins over time leads to bacterial cell death.

Of note, apramycin (APR) is the only molecule among the AGs that bind to the A-site, whose primary mechanism of action is blocking the ribosome translocation, interrupting the protein syntheses. This unique mode of action is possibly due to the unusual structure of APR that allows it to interact with the protein S12, involved in the translocation process. [84]

1

ADVERSE EFFECTS

Therapeutic use of AGs has long been associated with two main adverse effects: nephrotoxicity [85, 86] and ototoxicity. [87, 88] Other and rarer effects include neuromuscular blockade, and hypersensitivity reactions. [89, 90]. The two main negative effects have been observed in 8-37% of the patients receiving AGs for any period of time, and may worsen in case of prolonged treatment and higher dosage. [91]

Nephrotoxicity has long been recognized as a major complication, and it is usually reversible, in contrast to ototoxicity. [92] In recent years, the implementation of close monitoring strategies of renal function allows an early detection of AG -induced renal damage. [93]

AGs are not metabolized in the human host, and the renal excretion is the only elimination pathway. Nephrotoxicity manifests because of a relatively small amount (~5%) of drugs accumulating in the kidney, causing tubular necrosis. [94] Acute kidney injury is a serious and relatively common complication, and it manifests as a slow rise of serum creatinine concentration, and hyperosmolar urine. Serum creatinine levels are closely related to glomerular damage and is considered a practical marker for renal toxicity, while the urinary excretion of renal tubular cell-derived enzymes is emerging as a highly sensitive and more specific method to detect early tubular renal damage. [95–97]

AG-related ototoxicity is generally irreversible, and it manifests as hear loss at high sound frequencies, when directed to the cochlea, or as vertigo, nausea, and imbalance, when vestibular. [98] Ototoxicity was initially believed to be caused from transiently high drug concentrations in the inner ear, but recent studies, have demonstrated that the drug accumulation in the ear is indeed dose-dependent but saturable, and consider the mitochondrial radical oxygen species (mROS) as a key element for ototoxicity. [99–101]

Genetic predisposition is now recognized as a significant risk factor for aminoglycoside-induced ototoxicity, with genetic analyses revealing strong correlations between hypersensitivity to aminoglycosides and mutations in mitochondrial rRNA genes. [102] Moreover, accumulating experimental evidence suggests that both the peripheral and central auditory systems are involved in circadian regulation, with animal studies indicating greater susceptibility to kanamycin- and gentamicin-induced ototoxicity following nocturnal exposure compared with daytime administration. [103–105]

Importantly, these observations highlight a fundamental dissociation between antibacterial efficacy and host toxicity: while aminoglycoside bactericidal activity is primarily driven by peak concentration, uptake into mammalian cells is limited by saturable transport mechanisms and does not scale linearly with extracellular drug levels. This selectivity arises from fundamental structural differences between bacterial and eukaryotic cytosolic ribosomes, particularly within the decoding center of the small ribosomal subunit, which markedly reduce aminoglycoside binding affinity to eukariotic ribosomes. [106, 107] Consequently, once-daily dosing regimens that achieve high peak concentrations over short exposure times enhance antibacterial killing while minimizing cumulative intracellular drug accumulation in host tissues, thereby reducing toxicity. This pharmacodynamic separation underlies the improved safety index of aminoglycosides observed with extended-interval dosing strategies, bringing their therapeutic profiles closer to those of other widely used broad-spectrum

antibiotics. [108]

1.3. MECHANISMS OF RESISTANCE TO AMINOGLYCOSIDE ANTIBIOTICS

GENERAL OVERVIEW

Generally, antibiotic resistance can be classified into different categories:

Intrinsic resistance is responsible for the naturally low bacterial membrane permeability to AGs and other toxic substances. This resistance mechanism is typically non-specific. [109]

Adaptive resistance causes transient antibiotic tolerance in response to an environmental trigger like sub-inhibitory concentration of antibiotics. [110]

Acquired resistance follows the incorporation of exogenous genetic material or gene mutations. Resistant genes can be transferred during bacterial reproduction (vertically) or by exchanging genetic material horizontally, from one bacterium to another. [111]

We distinguish three major acquired resistance mechanisms bacteria adopt to counteract AGs action: decreased uptake and accumulation; target site modification; enzymatic drug modification (see Figure 1.4).

Decreased uptake and accumulation Intracellular aminoglycoside concentrations can be reduced through diminished uptake and/or enhanced efflux. Reduced uptake may arise not only from decreased outer-membrane permeability, including porin downregulation, but also from alterations in cytoplasmic membrane processes that indirectly affect aminoglycoside internalization. Because aminoglycoside uptake across the inner membrane is driven by membrane potential and respiratory activity rather than a dedicated transporter, mutations that impair energy metabolism, electron transport chain activity, or membrane polarization can substantially limit drug entry.

Well-documented examples include respiratory-deficient mutants and small-colony variants of *Staphylococcus aureus*, in which defects in heme or menaquinone biosynthesis reduce membrane potential and confer decreased susceptibility to aminoglycosides. [112, 113] Similarly, mutations affecting components of the electron transport chain or central metabolism in Gram-negative bacteria have been shown to reduce aminoglycoside uptake by lowering proton motive force. [114]

In parallel, increased drug efflux mediated by multidrug efflux pumps further lowers intracellular drug levels. Although these uptake- and accumulation-related mechanisms are generally considered secondary contributors to resistance, they are frequently observed in combination with other resistance strategies. For instance, enhanced efflux through upregulation of multidrug efflux systems is a common resistance mechanism

in *Pseudomonas aeruginosa*, *Acinetobacter* spp., and *Burkholderia pseudomallei* [115–117]. Moreover, decreased membrane permeability and porin downregulation often occur alongside additional resistance determinants, collectively increasing tolerance to aminoglycosides and other antibiotics [118–120].

Target site modification The modification of the 16S rRNA has been rarely observed, but during the past decade it has become an increasingly common resistance mechanism. In particular, a family of ribosomal methyltransferase enzymes is predominantly observed in *S. aureus* and *E. coli*, and is responsible for the modification of the 23S rRNA, conferring resistance to most AGs together with other chemically unrelated antibiotic classes. [121, 122]

Enzymatic drug modification Although different resistance mechanisms can coexist in the same cell, the primary mechanism for resistance in *Enterobacteriaceae* is the enzymatic alteration of the AGs. The first reports of pathogenic *Enterobacteriaceae* that were able to phosphorylate STR appeared in 1956 in Japan, [123] and in 1963-1964 resistance to KAN and NEO emerged worldwide as a result of a genetically transferable mechanism. [124]

Three families of Aminoglycoside Modifying Enzymes (AMEs) are the major culprit for AG resistance, rendering the enzymatic inactivation of AGs the most prevalent mechanism found in clinical settings. Since different AMEs are encoded in mobile gene fragments such as plasmids, integrons, transposons, resistance genes can be easily exchanged by horizontal gene transfer between different bacterial species. [125, 126]

AMINOGLYCOSIDE MODIFYING ENZYMES

NOMENCLATURE

AMEs catalyze the chemical modification of the -OH and -NH_2 groups present on the AG molecules, and according to the reaction catalyzed, they are grouped into three different classes: N-acetyltransferasess (AACs), which are responsible for the acetylation of primary amines; O-phosphotransferasess (APHs), and O-adenosyltransferases (ANTs), which catalyze the phosphorylation or adenylation of hydroxyl groups, respectively. The genes encoding these enzymes are often part of integrons, transposons, or gene cassette, and mobile elements like plasmids, which contribute to the mobilization of these resistance mechanisms at a molecular or cellular level. Moreover, mutagenesis events contribute to the generation of new enzyme variants which can broad their substrate promiscuity, allowing the bacteria to adapt and counteract the activity of new AGs. [127]

As a consequence, there is an impressive number of genes which encode for AMEs, including putative genes for which there is no additional information other than the annotation.

Two different nomenclatures are used to identify AMEs. The first one identifies the reaction catalyzed by the enzyme with a three-letter abbreviation (AAC for acetylation, APH for phosphorylation, and ANT for adenylation), followed by a parenthesis indicating the modification site on the AG molecule (class). A roman number identifies the resistance profile conferred by the enzyme, and a lowercase letter as an individual identifier. For example, the

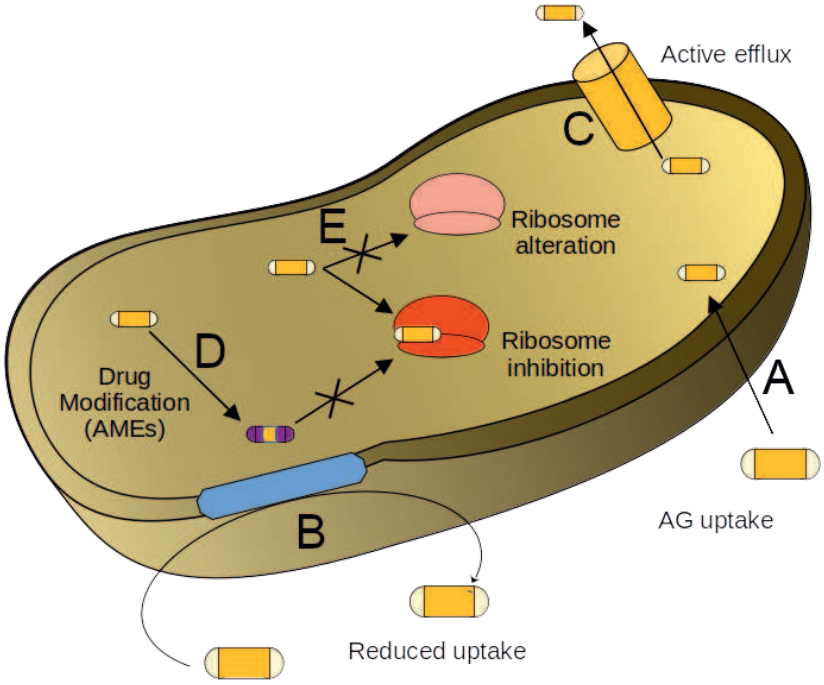


Figure 1.4 | Three major mechanisms by which bacteria counteract AGs. Aminoglycoside uptake (A) can be limited by modifications of the cell envelope or transporter proteins, which reduce drug entry (B), or the antibiotic can be actively removed by a variety of energy-dependent efflux pumps (C). Enzymatic drug modification by aminoglycoside-modifying enzymes (AMEs, D) and ribosomal alterations that prevent drug binding (E) represent the most widespread resistance mechanisms observed in clinical isolates.

enzymes APH(3')Ia and APH(2")Ia represent two enzymes which catalyze the phosphorylation of the -OH group in position 3' and 2", respectively, and they both confer the same resistance profile (type I). Moreover, APH(3')Ia and APH(3')Ib represent two different enzymes (a and b) which are both able to phosphorylate the position 3', and confer the same resistance profile (type I) to their bacterial hosts. The other nomenclature identifies the genes with a lower case three-letter code (aac for AACs, aph for APHs, and aad for ANTs) followed by a capital letter to identify the modification site. A number is then added when there is a need to identify and discriminate among different genes. [128]

AMINOGLYCOSIDE N-ACETYLTRANSFERASES (AACS)

N-acetyltransferases are a class of enzymes responsible for the acetylation of primary amines in AGs, using the acetyl coenzyme A (AcCOA) as donor molecule.

AACs can catalyze the acetylation in position 1, 3, 2' or 6' of 4,5- and 4,6-disubstituted AGs, as summarized in Figure 1.5. The acetylation catalyzed by the AAC(1) and AAC(2') class of enzymes does generally not confer a high resistance profile, and it is rarely found in

clinical isolates. [128] The most common N-acetyltransferases providing for aminoglycoside resistance in clinical isolates are the enzymes that modify the 3 and '6 position. AAC(3) and AAC(6'), were early discovered in *P. aeruginosa* and constitute the main determinant for gentamicin resistance, as well as tobramycin, netilmicin, and kanamycin resistance. [129–131] Table 1.2 summarizes AACs subclasses, known hosts, and resistance profiles.

Although rare, four additional genes encoding bifunctional aminoglycoside-resistance enzymes have been isolated, which possess acetylase activity and are designated as AAC(6')/APH(2"), ANT(3")-Ii/AAC(6')-IId, AAC(3)-Ib/AAC(6')-Ib', and AAC(6')-30/AAC(6')-Ib'. [132]

The early determination of the crystal structures of AAC(3)-Ia from *Serratia marcescens*, and of AAC(6')-Ii from *Enterococcus faecium spp.*, suggested that the fold of this class of enzymes is similar to that of the yeast histone acetyl-transferase HAT1, a member of the ubiquitous GCN5-related N-acetyltransferase (GNAT) superfamily of proteins, which comprises more than 10,000 proteins (see Figure 1.6). [133, 134]

In time, more AACs enzymes have been studied and reviewed, and in some cases the three-dimensional structures have been resolved to provide structural and mechanistic insights. [128, 135, 136]

Of note, eight AACs structures deposited in the Protein Data Bank (PDB) have been lately proposed to form a distinct subgroup of enzymes within the GNAT superfamily (see Table 1.3). These enzymes, although functionally analogous to other members of the GNAT superfamily, display a different folding, and a noncanonical catalytic triad consisting of a glutamic acid, a histidine and the AG as substrate, as summarized in Figure 1.7.

Table 1.2 | Aminoglycoside acetyltransferases (AACs), subclasses, hosts, and resistance profiles.

Class	Subclasses	Hosts	Resistance profile
AAC(1)	–	*Escherichia coli, Actinomycete spp., Campylobacter spp., Methylobacterium spp., Pseudomonas aeruginosa, Salmonella typhimurium, Leptospira spp.*	APR, BUT, LIV, PAR
AAC(3)	Ia, Ib, Ic, Id, Ie	*Serratia marcescens, Salmonella enterica, Salmonella typhimurium, Escherichia coli, Acinetobacter baumannii, Acinetobacter johnsonii, Klebsiella pneumoniae, Klebsiella oxytoca, Pseudomonas aeruginosa, Proteus mirabilis, Enterobacter asburiae, Vibrio fluvialis*	GEN, SIS, FOR
AAC(3)	IIa, IIb, IIc	*Klebsiella pneumoniae, Salmonella spp., Escherichia coli, Alcaligenes faecalis, Serratia marcescens, Pseudomonas aeruginosa*	TOB, NET, 2NET, 6NET, DIB
AAC(3)	IIIa, IIIb, IIIc	*Klebsiella pneumoniae, Pseudomonas aeruginosa*	GEN, KAN, TOB, NEO, APR
AAC(3)	IVa	*Campylobacter jejuni, Pseudomonas stutzeri*	–
AAC(3)	IVb	*Escherichia coli, Campylobacter jejuni, Pseudomonas stutzeri, Salmonella spp., Klebsiella pneumoniae, Proteus mirabilis, Proteus morganii*	–
AAC(3)	VIa	*Escherichia coli, Enterobacter cloacae, Salmonella enterica, Cupriavidus gilardii*	–
AAC(3)	VIIa	*Actinomycetes spp.*	–

Class	Subclasses	Hosts	Resistance profile
AAC(3)	VIIIa	*Streptomyces spp.*	–
AAC(3)	IXa	*Actinomycetes spp.*	–
AAC(3)	X	*Actinomycetes spp.*	–
AAC(2')	Ia, Ib, Ic, Id, Ie	*Providencia stuartii, Mycobacterium fortuitum, Acinetobacter baumannii, Mycobacterium tuberculosis, Mycobacterium bovis, Mycobacterium smegmatis, Mycobacterium leprae*	GEN, TOB, DIB, KAN, NET

Abbreviations: Apramycin (APR), butirosin (BUT), lividomycin (LIV), paromomycin (PAR), gentamicin (GEN), sisomicin (SIS), fortimicin/astromicin (FOR/AST), netilmicin (NET), tobramycin (TOB), 2'-N-ethylnetilmicin (2NET), 6'-N-ethylnetilmicin (6NET), dibekacin (DIB), kanamycin (KAN), neomycin (NEO). This table was adapted from the review of Ramirez & Tolmasky (2010) and updated from `www.uniprot.org` (accessed 17 Nov 2024).

Table 1.3 | AAC(3) enzymes which do not share the typical folding of the GNAT superfamily of proteins, with available UniProt accessions, source organisms, and PDB structures.

Protein	UniProt	Organism	PDB code(s)	Reference
AAC(3)-IIIa	—	*Pseudomonas aeruginosa*	—	This work (see Chapter 2)
AAC(3)-IIIb	Q51405	*Pseudomonas aeruginosa*	6MB4, 6MB5, 6MB6, 6MB7, 6MB8, 6MB9	[137]
AAC(3)-IIIb	A0A059X981	Uncultured bacterium	5HT0, 6MMZ, 6MN0, 7KES	[138]
AAC(3)-IIIb	Q54216	*Streptomyces griseus*	7LAP	—
AAC(3)-IIIb	Q306W4	*Escherichia coli*	6MN3, 6MN4, 6MN5	—
AAC(3)-IIIb	Q01515	*Serratia marcescens*	7LAO	—
AAC(3)-IIIb	O32003	*Bacillus subtilis*	2NYG	[139]
AAC(3)-IIIb	Q0ZQ43	*Streptomyces rubellomurinus*	3SMA	[140]

AMINOGLYCOSIDE O-PHOSPHOTRANSFERASES (APHS)

Aminoglycoside O-phosphotransferases (APHs) catalyze the phosphorylation of hydroxyl groups on AG molecules, thereby altering their charge distribution and introducing steric hindrance that reduces ribosomal binding affinity. Several classes of APHs have been described, including APH(4), APH(6), APH(9), APH(3'), APH(2"), APH(3"), and APH(7") (see Table 1.4).

APH(4)-I and APH(3") mediate resistance exclusively to hygromycin, whereas APH(9) and APH(7") confer resistance to spectinomycin and are only rarely detected in clinical isolates. APH(6) is responsible for streptomycin resistance and is widely distributed among both Gram-negative and Gram-positive bacteria. The specific modification sites of representative APHs on streptomycin and amikacin are illustrated in Figure 1.8.

APH(3') enzymes constitute the largest and most diverse class of APHs and catalyze the phosphorylation of the hydroxyl group at the 3' position of AGs. Notably, APH(3')IIIa exhibits broader substrate specificity and is also capable of phosphorylating the 5" hydroxyl group of neomycin, lividomycin A, and butirosin.

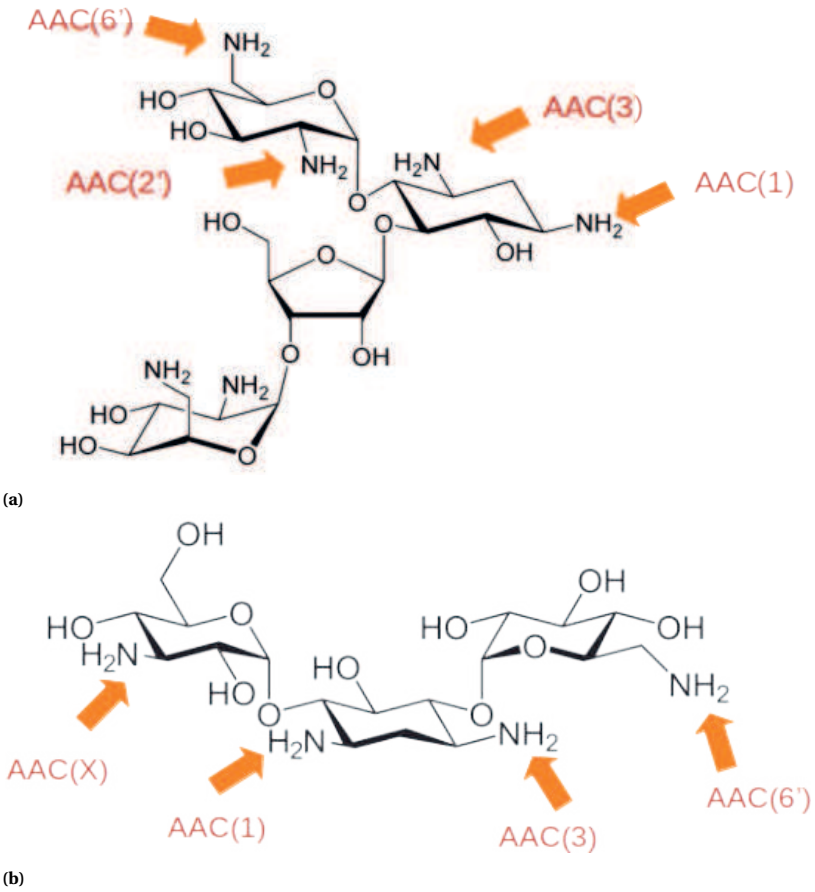


Figure 1.5 | Modification sites of AAC enzymes on (a) neomycin B and (b) kanamycin. AAC(1), AAC(3), AAC(2') and AAC(6') can catalyze the acetylation of position 1, 3, 2', and 6', respectively. In addition to its canonical activity, the AAC(3)-X enzyme is able to additionally acetylate the amino group in position 3".

APH(2") enzymes are commonly encountered among gentamicin-resistant Gram-positive bacteria and frequently occur as part of the bifunctional enzyme AAC(6')/APH(2"), which combines acetyltransferase and phosphotransferase activities within a single polypeptide.

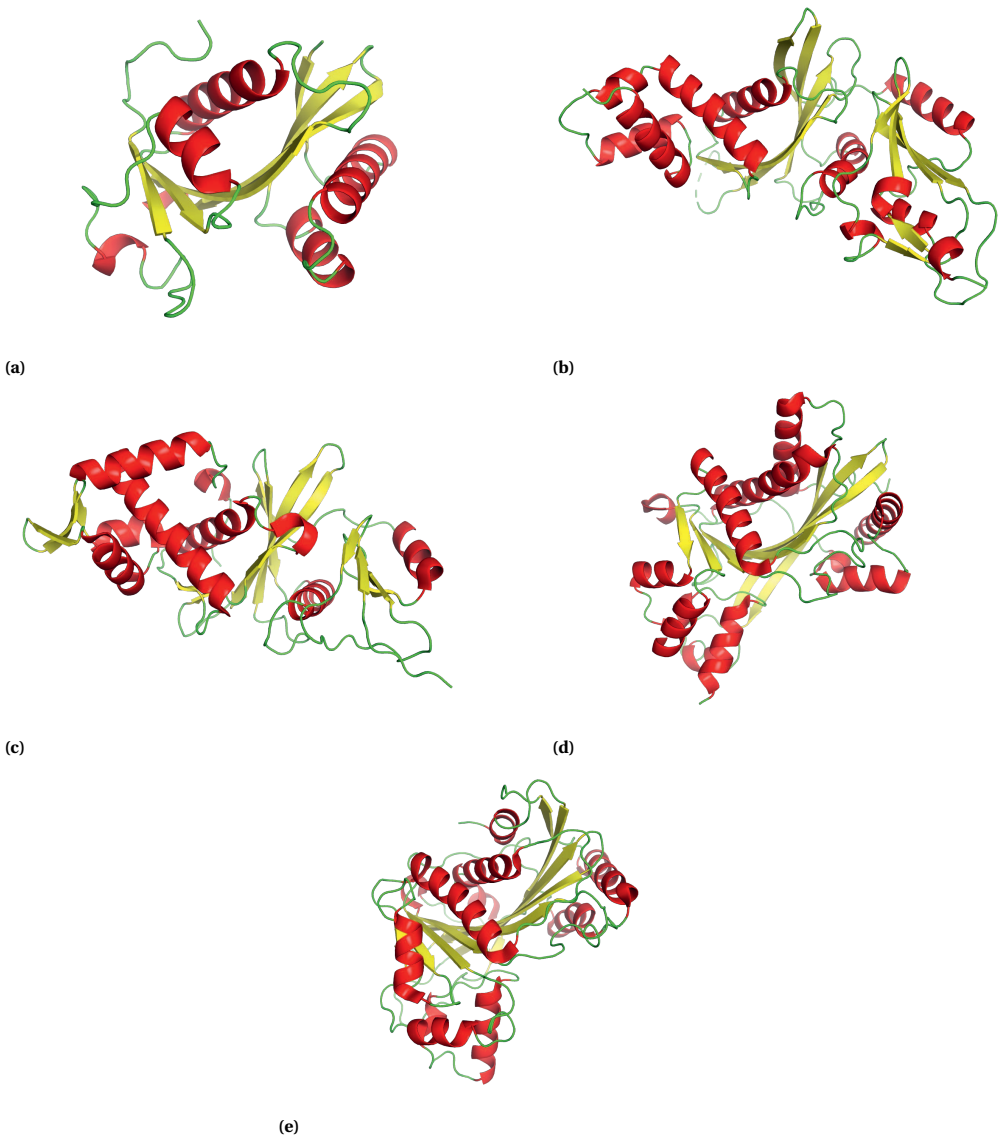


Figure 1.6 | Cartoon representation of histone acetyltransferases (HATs). The conserved structural core consists of a central five-stranded antiparallel β-sheet flanked by three $/alpha$-helices. a) *Tetrahymena thermophila* Gcn5 (PDB: 1QSR); b) *Saccharomyces cerevisiae* Hat1 (PDB: 1BOB); c) *A. Cerevisiae* Esa1 (PDB: 1MJA); d) *Homo sapiens* p300 (PDB: 3BIY); e) *S. cerevisiae* Rtt109 (PDB: 3D35).

1

Class	Subclasses	Hosts	Substrate profile

Table 1.4 | Aminoglycoside phosphotransferases (APHs): subclasses, hosts, substrates, and references.

Class	Subclasses	Hosts	Substrate profile
APH(4)	Ia, Ib	*Escherichia coli, Streptomyces hygroscopicus*	HYG
APH(6)	Ia, Ib, Ic, Id	*Streptomyces griseus, Streptomyces glaucescens, Salmonella enterica, Pseudomonas aeruginosa, Escherichia coli, Klebsiella pneumoniae, Salmonella* spp., *Shigella flexneri, Providencia alcalifaciens, Pseudomonas* spp., *Vibrio cholerae, Edwardsiella tarda, Pasteurella multocida, Aeromonas bestiarum*	STR
APH(9)	Ia, Ib	*Legionella pneumophila, Streptomyces flavopersicus*	SPE
APH(3')	Ia, Ib, Ic	*Escherichia coli, Salmonella enterica, Klebsiella pneumoniae, Acinetobacter baumannii, Serratia marcescens, Corynebacterium* spp., *Photobacterium* spp., *Citrobacter* spp.	KAN, NEO, PAR, RIB, LIV
APH(3')	IIa, IIb, IIc	*Escherichia coli, Pseudomonas aeruginosa, Stenotrophomonas maltophilia*	KAN, NEO, BUT, PAR, RIB
APH(3')	IIIa	*Staphylococcus aureus, Enterococcus* spp.	KAN, NWO, LIV, PAR, LIV, BUT, AMK, ISE
APH(3')	IVa	*Bacillus circulans*	NEO, PAR, RIB
APH(3')	Va, Vb, Vc	*Actinomycetes* spp., *Streptomyces fradiae, Streptomyces ribosidificus, Micromonospora chalcea*	NEO, PAR, RIB
APH(3')	VIa, VIb	*Acinetobacter baumannii, Klebsiella pneumoniae, Serratia marcescens*	KAN, NEO, PAR, RIB, BUT, AMK, ISE
APH(3')	VIIa	*Campylobacter jejuni*	KAN, NEO
APH(2")	Ia, Ie	*Staphylococcus aureus, Clostridioides difficile, Streptococcus mitis, Enterococcus faecium, Enterococcus casseliflavus*	GEN
APH(2")	IIa	*Enterococcus faecium, Escherichia coli*	GEN
APH(3")	Ia, Ib, Ic	*Streptomyces griseus, Enterobacteriaceae, Pseudomonas* spp., *Mycobacterium fortuitum*	STR
APH(7")	Ia	*Streptomyces hygroscopicus*	HYG

Abbreviations: Butirosin (BUT), lividomycin (LIV), paromomycin (PAR), gentamicin (GEN), livostamycin (LIV), isepamicin (ISE), streptomycin (STR), ribostamycin (RIB), hygromycin (HYG), kanamycin (KAN), neomycin (NEO), spectinomycin (SPE). This table was adapted from the review of Ramirez & Tolmasky (2010), and updated from www.uniprot.org (accession date: 17 Nov, 2024).

O-ADENOSYLTRANSFERASES

Genes coding for ANT enzymes are found in plasmids, transposons, and chromosomes. ANTs constitute the smallest family of AMEs, and mediate the adenylylation of AG , catalyzing the transfer of an AMP group from ATP to the hydroxyl group in the AG molecule. There are five classes of ANTs that catalyze the adenylylation in position 6, 9, 4', 2", and 3". For an overview of ANTs subclasses, host organisms and resistance profile, see Table 1.5.

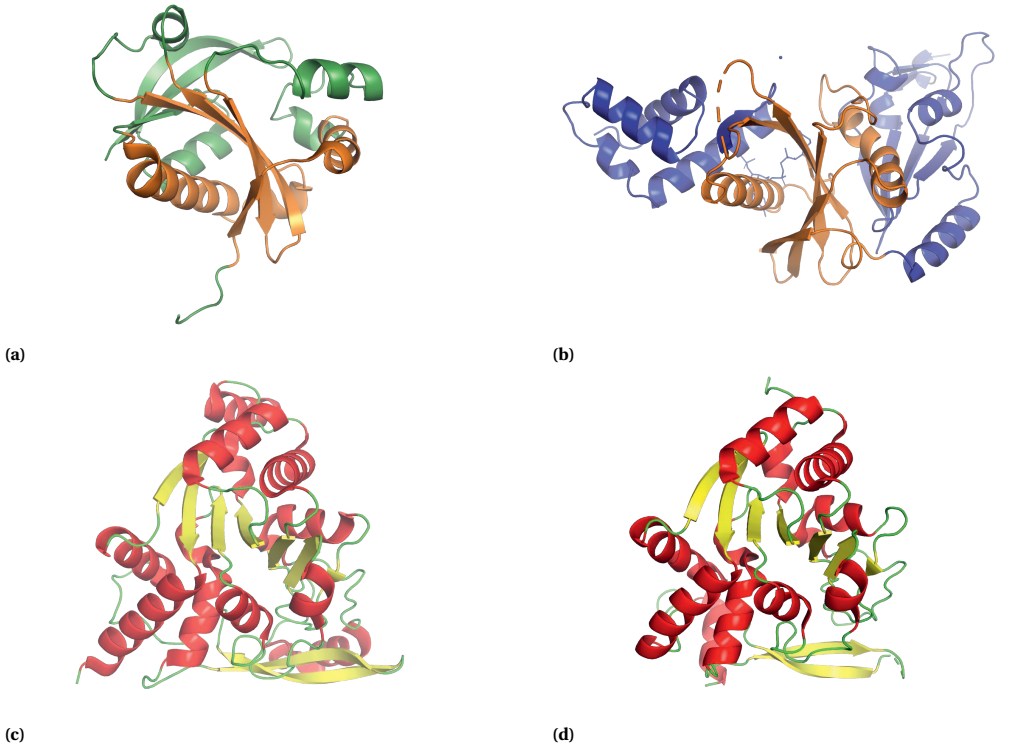


Figure 1.7 | Some AACs like (a) AAC(6')-Ii share the same GNAT fold as Hat1 protein (b). The conserved core common to all GNAT protein fold is here represented in orange. Enzymes like (c) AAC(3)-Xa and (d) AAC(3)-IVa adopt a different fold, and constitute a different group within the GNAT superfamily of proteins.

Table 1.5 | O-adenylyltransferases (ANTs): subclasses, host organisms, and resistance profiles.

Class	Subclasses	Hosts	Substrate profile
ANT(6)	Ia, Ib	*Bacillus subtilis, Staphylococcus epidermidis, Enterococcus faecium, Enterococcus faecalis, Streptococcus suis, Streptococcus mitis, Staphylococcus aureus, Campylobacter jejuni, Streptococcus oralis, Campylobacter fetus* subsp. *fetus*	STR
ANT(9)	Ia, Ib	*Enterococcus avium, Staphylococcus aureus, Enterococcus* spp., *Staphylococcus sciuri, Enterococcus faecalis*	SPE
ANT(4')	Ia	*Pseudomonas aeruginosa, Staphylococcus epidermidis, Staphylococcus aureus, Enterococcus* spp., *Bacillus* spp.	KAN, NEO, TOB, AMK, DIB, ISE, and other aminoglycosides with 4'/4"–OH groups
ANT(4')	IIa, IIb	*Pseudomonas aeruginosa, Enterobacteriaceae*	TOB, AMK, ISE
ANT(2")	Ia	*Pseudomonas aeruginosa, Klebsiella pneumoniae*	GEN, TOB, DIB, SIS, KAN

Class	Subclasses	Hosts	Substrate profile
ANT(3")	Ia	*Enterobacteriaceae, Salmonella* spp., *Acinetobacter baumannii, Pseudomonas aeruginosa, Vibrio cholerae, Klebsiella pneumoniae, Corynebacterium glutamicum, Citrobacter freundii, Aeromonas* spp., *Escherichia coli, Bordetella parapertussis, Kluyvera georgiana, Enterobacter cloacae, Vibrio fluvialis, Salmonella enterica, Bacillus endophyticus, Yersinia enterocolitica, Pasteurella multocida, Aeromonas media*	STR, SPE

*Abbreviations:*Amikacin (AMK), dibekacin (DIB), isepamicin (ISE), gentamicin (GEN), kanamycin (KAN), neomycin (NEO), sisomicin (SIS), tobramycin (TOB), spectinomycin (SPE), streptomycin (STR). This table was adapted from the review of Ramirez & Tolmasky (2010), and updated from www.uniprot.org (accession date: 17 Nov, 2024).

RIBOSOMAL ALTERATION

Generally, ribosomal alteration is a well-known response that can confer resistance to several classes of antibiotics. [141]

One potential mechanism is mutation of the rRNA itself. However, because rRNA is essential for protein biosynthesis and because multiple copies of rRNA genes exist in all organisms, genomic mutations in rRNA are extremely rare.

More commonly, resistance arises through mutations of the ribosomal proteins, as well as post-translational modifications of the ribosome. These mechanisms are not limited to bacteria; similar ribosomal alterations have also been observed in pathogenic yeasts and fungi. For example, mutations in the ribosomal protein L10e confer resistance to sordarins, a class of antibiotics that inhibit protein synthesis by targeting eukaryotic translation elongation factor 2, whereas mutations in L22 confer resistance to erythromycin, a macrolide antibiotic [80, 142].

In bacteria, ribosomal alterations also contribute to resistance against AGs, which is consistent with the strong electrostatic interactions between AGs and nucleic acids. This property underlies the antibacterial activity of AGs, as they bind strongly to prokaryotic rRNA and directly interfere with ribosomal function. In other organisms, AGs can interact with certain structured RNAs, such as the eukaryotic hammerhead ribozyme and group I self-splicing introns, as well as viral RNAs, including the HIV Rev response element (RRE). Importantly, these interactions in eukaryotes do not generally affect eukaryotic ribosomes, which are 80S ribosomes composed of 40S and 60S subunits, unlike bacterial 70S ribosomes composed of 30S and 50S subunits. Moreover, the corresponding rRNA region in eukaryotic ribosomes contains multiple sequence substitutions, adopts a distinct local conformation, and carries bulky post-transcriptional modifications, all of which markedly reduce aminoglycoside binding affinity and prevent translational misreading.[22, 25, 143–145].

Importantly, while AGs can bind a variety of RNA structures, bacterial survival depends on protecting the ribosome itself. Consequently, AG-resistant bacteria often modify the highly conserved rRNA post-translationally via 16S rRNA methyltransferases (16S-RMTases). These enzymes catalyze the transfer of a methyl group from S-adenosyl methionine (SAM) to a

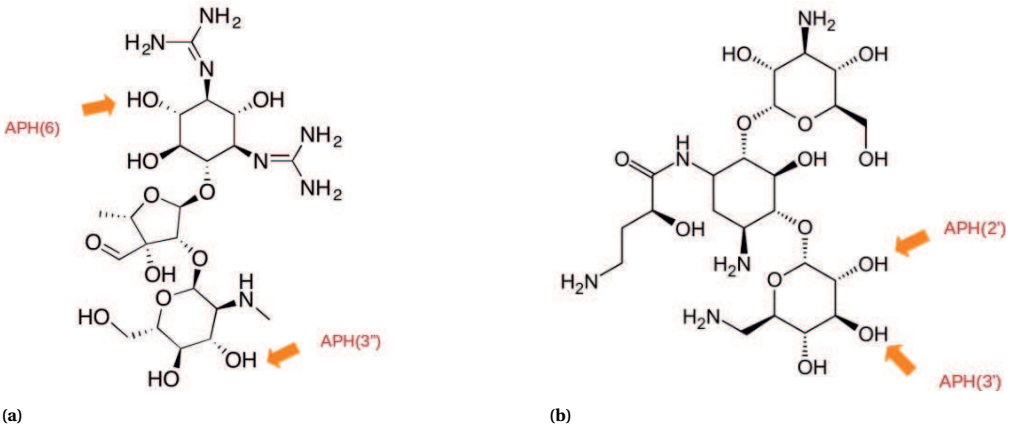


Figure 1.8 | Modification sites of APH(6) and APH(3") enzymes on streptomycin (a) and APH(2')and APH(3') on amikacin (b). In addition to its canonical activity, the bifunctional enzyme AAC(6')/APH(2") is able to additionally acetylate the 6' position.

specific residue at the A site of 16S rRNA. Methylation reduces the binding affinity of AGs to the ribosome, resulting in high-level, clinically relevant resistance to all aminoglycosides used in the clinic.

Eleven genes (armA, rmtA, rmtB, rmtC, rmtD, rmtD2, rmtE, rmtF, rmtG, rmtH, armA, and npmA) have been identified, with armA and rmtB being the most frequently encountered in Enterobacteriaceae [146, 147]

Regarding the enzymatic function of 16S-RMTases, different methyltransferases act on distinct sites of 16S rRNA. For instance, ArmA and RmtA through RmtH methylate N7-G1405 of 16S rRNA, resulting in significant resistance to 4,6-disubstituted 2-DOS. In contrast, NpmA and NpmB methylate N1-A1408 of 16S rRNA and confer resistance to 4,5-disubstituted and 4,6-disubstituted 2-DOS, as well as monosubstituted DOS, while remaining susceptible to streptomycin. Despite differences in target sites, all 16S-RMTases can facilitate high-level resistance to AGs, with particularly efficient action since they modify all copies of 16S rRNA, even when present at low copy number [148, 149].

Originally confined to AG-producing organisms, this resistance mechanism is now rapidly spreading among human pathogens. Reports highlight the widespread dissemination of ArmA and RmtB among Enterobacteriaceae producing both extended-spectrum β-lactamases (ESBLs) and 16S-RMTases across multiple countries, raising concerns about a major therapeutic threat in the near future. Moreover, the presence of transferable genetic elements such as plasmids facilitates horizontal transmission of these resistance genes among pathogens, posing additional challenges for the management of infectious diseases and the control of drug-resistant bacterial infections [150].

ARMA

The 16S rRNA methylase gene *armA* was initially identified in a clinical isolate of *Klebsiella pneumoniae* in France. The strain exhibited multiple antibiotic resistance, including resis-

tance to β-lactams, streptomycin-spectinomycin (due to the presence of *ant(3")-I* gene), and nearly all other aminoglycosides due to the concurrent presence of *aac(3)-II* and *armA* [151].

ArmA shows 37–47

The evolutionary relationship between *armA* and other genes encoding 16S-RMTases has been investigated via phylogenetic analysis. However, the low GC content of *armA* (30

Notably, *armA* is frequently co-located with *rmtB*, resulting in elevated resistance to aminoglycosides, with minimum inhibitory concentrations (MICs) of ≥ 256 μg/mL [152, 153].

Studies indicate that *armA* is often located on transferable plasmids of different Inc types, and mobilization of these resistance genes may involve insertion sequences such as IS26. Furthermore, 16S-RMTase-producing strains frequently carry additional antimicrobial resistance determinants, including $bla_{\text{TEM-1}}$, $bla_{\text{CTX-M}}$, and bla_{NDM}, conferring resistance to β-lactams and carbapenems [154–156].

RMTB

After the presence of the gene was detected initially in *S. marcescens* strains isolated from France in 2004, rmtB is now predominantly found in *E. coli* and *K. pneumoniae* worldwide, resulting in resistance to aminoglycosides with MIC of ≥ 512 μg/mL. In China, rmtB has emerged as the predominant genotype of 16S-RMTase and is often found in combination with armA. [157, 158]

The rmtB gene is commonly situated on transposons within transferable plasmids, often accompanied by insertion sequences such as ISCR1, ISCfr1, and IS26, an arrangement that facilitates transfer and dissemination of rmtB among different strains. [156, 159, 160]

Figure 1.9 provides a representative example illustrating armA and rmtB genes within their genetic context, while in Table 1.6 the MIC values and distribution of the resistance genes are reported.

Table 1.6 | Strains with *armA* and *rmtB* genes, their MIC values and epidemic distributions (2019–2022). Adapted from Yang & Hu (2022) [161]. Abbreviations: amikacin (AMK); gentamicin (GEN); kanamycin (KAN); tobramycin (TOB).

Genotype	MIC (μg/mL)	Subtype	Strain	Isolation year and location
armA	AMK ≥ 256; GEN ≥ 256; TOB ≥ 256; KAN ≥ 256	—	*Klebsiella pneumoniae*	2019–Japan, Brazil, Greece, India
			Escherichia coli	2020–China; 2021–Britain; 2022–China
			Acinetobacter baumannii	2020–India, France; 2021–Britain
			Enterobacter cloacae	2018–China; 2020–Greece, Brazil; 2021–Britain
			Citrobacter freundii	2020–Myanmar; 2021–Britain
			Salmonella enterica	2021–Britain
			Serratia marcescens	2021–China
			Enterobacter xiangfangensis	2020–Turkey
			—	2020–Myanmar

Genotype	MIC (μg/mL)	Subtype	Strain	Isolation year and location
rmtB	AMK ≥ 256; GEN ≥ 256; KAN ≥ 256; TOB ≥ 256	rmtB1	*Escherichia coli*	2019–Japan, Korea; 2020–India, China, France; 2021–China, Britain, Greece, Kenya; 2022–Switzerland
		—	*Klebsiella pneumoniae*	2021–Britain, Brazil, China; 2022–Switzerland
		—	—	2020–China; 2021–China; 2022–China
		—	—	2019–Iran; 2020–China
		—	*Salmonella enterica*	2020–Brazil
		—	*Enterobacter cloacae*	2021–China
		—	*Acinetobacter baumannii*	2021–Britain, Greece
		—	*Citrobacter freundii*	2021–Greece, China
		—	*Providencia stuartii*	2021–China
		rmtB2	*Proteus mirabilis*	2021–America
		rmtB4	*Klebsiella variicola*	2020–Myanmar; 2021–Egypt, Britain, India

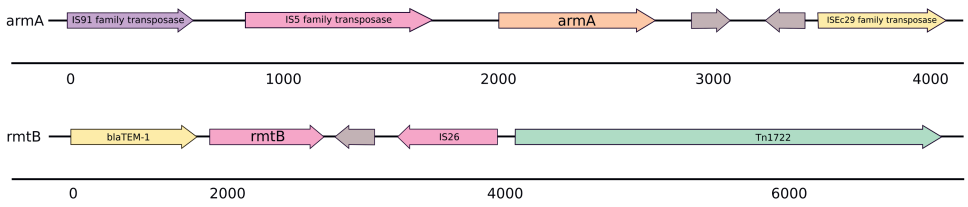


Figure 1.9 | *armA* (GenBank AB083212.2) and *rmtB* (FJ556899.1) gene sequences with their genetic environment. Putative proteins are represented as arrows but not labelled.

1.4. COMMON STRATEGIES ADOPTED TO COUNTERACT THE RESISTANCE

Various approaches have been explored to address the challenges posed by AMEs and RMTs. The development of new AGs, or the enzymatic inhibition of resistant enzymes hold the promise to overcome the resistance mechanisms that have rendered many AGs ineffective, and threatened them to become obsolete. By adopting innovative approaches, we can effectively address the challenges posed by AMEs and RMTs, and pave the way for the development of new treatment options against the rising prevalence of multiresistant pathogens.

SEMI-SYNTHETIC AMINOGLYCOSIDE DERIVATIVES

The continuous emergence of resistance towards the first and second generation of AGs is the driving force towards the identification of antibiotics with similar structure that are not

susceptible to resistance.

The modification of the amino, and hydroxyl groups present on the AG molecules constitutes a simple and straightforward strategy to generate novel compounds, given that the modified functional groups can prevent or alter the binding to the resistance enzymes, but preserve the antibiotic activity when they are not involved in key interactions with the 16S rRNA. [162]

Examples of common synthetic strategies adopted to generate novel AGs are given below.

Deoxygenation of kanamycin related antibiotics Tobramycin and dibekacin are two examples of semi-synthetic aminoglycoside obtained by 3' and 3',4' deoxygenation, respectively. These AGs have proven to be effective against *Staphylococcus* and *Pseudomonas* species, but still amenable of enzymatic modification by ANT(2") and by the bifunctional AAC(6')-APH(2"). Few examples of neomycin-related AG have also been reported. [163]

Derivatization of amino groups Methylation of N-6' and N3" positions of Kanamycin has shown to weaken the antibiotic activity, nevertheless, the derivatives displayed activity against resistant strains. N-1 derivatives of 2-DOS-based AGs, showed to be poorly modified by APH(3') class of enzymes and prompted the generation of several kanamycin and neomycin derivatives like amikacin, and arbekacin, both proven to be a very effective antibiotics, although they perform poorly against some Methicillin-resistant *Staphylococcus aureus* (MRSA) strains. [164, 165]

Modification of N-6', N-2', N'3, ad N'1 deliver a dramatic loss in the enzymatic susceptibility towards most classes of AMEs while retaining the antibacterial activity, like in Plazomycin. [166, 167]

Guanidylation of N-3" of kanamycin proved to have minimal effect on the antibiotic activity, while protecting the derivative against modification by ANT(4'), APH(3') and AAC(6'). [168, 169]

The protecting effects of various derivatization of amino groups is interpreted in terms of steric hindrance with the inactivating enzyme, which does not take place upon binding to the A-site. Moreover, the aminosugar ring in AGs, is the main actor in providing the high affinity for the prokaryotic A-site. Structural studies on 4,5 and 4,6-disubstituted AGs showed that the majority of the antibiotic molecules specifically bind the A-site with several conserved interactions. [170–172] Moreover, the antibiotic molecules present different conformations when bound to the A-site or to the AMEs. [173]

Together, these realizations lead to the exploration of novel aminoglycoside derivatives, and conformationally blocked AGs, with a better prognosis against resistant pathogens than the parent compounds. [174]

Some promising AG derivatives and strategies, but by no means an exhaustive list, are presented in this section.

Synthesis of pyranmycins where the O-5 position of the neamicine moiety is modified with the addition of a pyranose in place of a furanose ring confers low cytotoxicity and high activity against pathogenic strains of *P. aeruginosa* and *S. aureus*. [175]

Aminoglycoside dimers and hybrid antibiotics AG dimers like 5-linked neamine dimers showed enhanced affinity for the rRNA A-site, limited susceptibility to AAC(6')-Ii, APH(3')-IIIa, and AAC(6')-Ie/APH(2")-Ia, and improved antibiotic activity. [176]

Subsequently, various AG homo- and heterodimers were synthesized to further investigate this approach. However, the resistance potential of these novel AG against AMEs has not been evaluated yet, and it will be intriguing to determine their effectiveness. [27, 177, 178]

In addition to AG dimers composed of two distinct AGs, hybrid molecules combining features of NEO or PAR with sisomicin (SIS) exhibited superior activity compared to NEO and demonstrated evasion of APH(3') and ANT(4') activity in *P. aeruginosa* and *S. aureus*, respectively. [179]

Appending diverse chemical functionalities to AGs has been a widely utilized approach as well. While this strategy has yielded significant success, there remain several challenges to overcome, particularly in predicting and achieving target selectivity while preserving potency. [136, 180]

Conformationally restrained AG s Several research groups have made efforts to develop conformational constraints AGs. These molecules aim at selectively binding the A-site rRNA sequence while showing low affinity for AMEs. Modifications like methylene linkers (1- or 3-C) between the 2'-NH and 5"-C positions, rigidified NEO, mimicking the conformation of NEO bound to A-site RNA while deviating from the conformation observed in the ANT(4') active site. [174, 181]

Similarly, PAR analogs were designed by tethering them between the 6-hydroxy and 6"-amino moieties. The design was based on the conformational differences between the PAR bound tot he A-site and NEO bound to APH(3')-IIIa. Unfortunately, these compounds exhibited limited inhibitory effects on the growth of *S. aureus* and *E. coli*, suggesting that specific conformational constraints can affects the binding to the A-site as well. [182]

AME inhibitors Considering that the majority of antibiotic resistance stems from the activity of AMEs, the development of AME inhibitors is an enticing strategy. After all, this approach has proven successful in the case of β-lactams, where the combination of β-lactam antibiotics with inhibitors of β-lactamase enzymes has achieved clinical and commercial accomplishments for over three decades. [183]

Unfortunately, this approach has seen only a modest success in the inhibition of APHs. Of note, the inhibition of APH(3')-IIIa was accomplished through the synthesis of a an ankyrin repeat (AR) protein. This 33-amino acid peptide was chosen from a collection of engineered AR proteins, and showed a more specific binding compared to small molecules. However, the delivery of this therapeutic protein has proven far more complex than that of small molecules. [184, 185]

Adopting a more classical approach to small-molecule chemotherapy, investigations have been conducted to explore the use of previously identified inhibitors of eukaryotic protein kinases as inhibitors of APHs, given that APHs exhibit kinase activity.

Initial studies identified quercetin, along with other known kinase inhibitors, as inhibitors of APH(3')-IIIa and AAC(6')-Ie/APH(2")-Ia. More recently, an inhibitor that competes with ATP for casein kinase 1, was further examined as an inhibitor of APH(3')-IIIa and APH(9)-Ia, showcasing the opportunity for potential development of bacterial kinase inhibitors that selectively target APHs. [186–188]

While APH inhibitors seem promising, the ideal scenario would involve the development of compounds that can inhibit multiple AMEs. Unfortunately, the compounds that have been examined so far either demonstrate poor substrate activity for their intended targets or exhibit limited effectiveness in vivo due to low solubility or inadequate bioavailability. [189–191]

1.5. SCOPE OF THIS THESIS

AGs constitute the most commonly used class of antibiotics that have been used for treating infections caused by pathogenic bacteria. Despite the negative side effects like nephrotoxicity and ototoxicity, and the insurgence of bacterial resistance, several members of this class continue to be employed in clinical setting. The majority of AGs are bactericidal, have predictable pharmacokinetics, lack of allergic reactions, and can act synergistically with other antibiotics, rendering them invaluable tools among the antimicrobial agents. However, between the end of the 20th century and the first decade of the 21st century, the emergence and spread of antibiotic resistance have threatened the efficacy of antibiotic therapy.

However, the recent research developed effective strategies to revive the AGs class of antibiotics, and overcome antimicrobial resistance. Optimal concentrations, modification of the environmental conditions, chemical modification of the antibiotic structures, and combinatorial therapy with active agents are among the multiple approaches adopted to obviate the decline in novel antibiotic discovery, [192, 193] and the possibility that current pathogenic bacteria will adapt to existing antibiotics and evolve resistance. [194, 195]

Chapter 1 provides an introduction to AG antibiotics, including their mode of action, various applications, and the significant mechanisms of resistance employed by bacteria. It also presents an overview of two classes of enzymes, namely AMEs and RMTs, which will be extensively discussed in subsequent chapters. Lastly, the chapter concludes by offering a brief overview of common strategies employed to overcome AG resistance.

Chapter 2 The investigation of alkyl-derivatives of neomycin B and their ability to evade modification by the AAC(3)IIIa enzyme was conducted through the integration of chemical synthesis, biochemistry, and cutting-edge structural biology techniques. The enzymatic characteristics of AAC(3)IIIa were kinetically examined, leading to the proposal of a catalytic mechanism that was subsequently confirmed through X-ray crystallography.

Furthermore, a diverse library of alkylated derivatives of neomycin B was synthesized and tested for their antimicrobial activity. Among these derivatives, one particular com-

pound demonstrated superior performance and was selected for further investigations to unravel the underlying mechanism responsible for its ability to evade enzymatic modification. Intriguingly, the addition of a single methyl group at position 3-N was found to significantly enhance the resistance of neomycin B against modification by AAC(3)IIIa, while still partially preserving its antibiotic activity against a resistant strain.

The impact of neomycin B alkylation on its binding to the ribosome was explored by cryo-electron microscopy (cryo-EM) revealing that the alkylation did not substantially affect the binding of the compound to the ribosome.

Overall, the work presented in this chapter shed light on the previously unknown structure of AAC(3)IIIa, and alkyl-derivatives of neomycin B.

Chapter 3 focuses on the design and characterization of photo-switchable dimeric paromomycin derivatives as a potential solution to combat microbial resistance.

In this study, we employed a combination of two well-established approaches to tackle the challenges associated with aminoglycoside antibiotics: the synthesis of hybrid antibiotics and antibiotic dimers, along with the development of conformationally restrained aminoglycosides. Notably, we introduced a novel element to these strategies by incorporating light-controlled conformational changes.

This approach enabled us to design and synthesize photo-switchable aminoglycoside derivatives that could adopt different conformations upon exposure to light. The ability to modulate the biological activity exploiting different conformations of these compounds would represent a significant advancement in the field.

To evaluate the effectiveness of the compound, we tested its antimicrobial activity against bacterial strains of *E. coli* carrying resistance genes for three different AMEs. Interestingly, we observed a difference in antimicrobial activity between the two isomers. This finding suggests that the controlled conformational changes induced by light can impact the compound's ability to combat bacterial resistance. Moreover, the use of light to modulate the activation and deactivation of the drugs in-situ offers the potential to minimize the development of new resistances: by activating the drugs only when needed, and deactivating them in the external environment, the evolutionary pressure to resistance development can be reduced.

Chapter 4 investigates the impact of stereochemical changes at the C3' position of AGs and their performance against bacterial strains harboring different APH enzymes.

Competition assays, biological activity in vitro, and x-ray crystallography were used to gain insights in the mechanism of action of these compounds. The stereochemical inversion at C3' and the hindrance caused by the presence of an alkyl chain in the equatorial position may potentially impede ATP hydrolysis, laying the groundwork for future investigations, aiming for a comprehensive screening of substituents at the 3'-position, and ultimately develop an effective APH(3') inhibitor.

Chapter 5 presents a conceptual design of inhibitors targeting the 16S rRNA methyltransferase ArmA, responsible for conferring high-level resistance to a wide range of aminoglycosides commonly used in bacterial infection treatment.

To identify potential candidate compounds, we designed a fragment library and performed an in-silico screening against the crystal structure of ArmA. Through the utilization of a genetic algorithm, the top-scoring fragments were evolved to generate lead-like and drug-like compounds. Subsequent manual optimization and rigorous filtering resulted in a series of compounds exhibiting promising predicted characteristics, including anticipated high safety and metabolic stability profiles, and a feasible 2-step synthesis route.

By conducting thorough investigations, we can effectively leverage the emerging AI technology to confront the emergence of new pan-antimicrobial resistance mechanisms. These efforts are crucial in addressing the urgent need for innovative solutions to combat antimicrobial resistance and safeguard the effectiveness of aminoglycoside antibiotics.

Chapter 6 Provides an integrated discussion of all research findings, critically evaluates their scientific and technical significance, and explores broader implications for antimicrobial resistance management. This chapter situates the work within the global context of antibiotic innovation, addresses limitations and reproducibility challenges, and outlines future directions for translational research, and societal impact.

REFERENCES

[1] A. Schatz and K. Robinson, *The true story of the discovery of streptomycin,* Actinomycetes **4**, 27 (1993).

[2] A. Schatz and S. A. Waksman, *Effect of streptomycin and other antibiotic substances upon mycobacterium tuberculosis and related organisms.* Proceedings of the Society for Experimental Biology and Medicine **57**, 244 (1944).

[3] V. Melchionda, H. Wyatt, S. Capocci, R. G. Medina, A. Solamalai, S. Katiri, S. Hopkins, I. Cropley, and M. Lipman, *Amikacin treatment for multidrug resistant tuberculosis: how much monitoring is required?* European Respiratory Journal **42**, 1148 (2013), publisher: Eur Respiratory Soc.

[4] N. Cocco, G. Gargioni, C. Gilpin, L. Gonzalez-Angulo, M. Grzemska, A. Korobitsyn, C. Merle, F. Mirzayev, L. Moja, P. Olliaro, *et al.*, *WHO consolidated guidelines on drug-resistant tuberculosis treatment* (World Health Organization, 2019).

[5] K. A. Cohen, K. E. Stott, V. Munsamy, A. L. Manson, A. M. Earl, and A. S. Pym, *Evidence for expanding the role of streptomycin in the management of drug-resistant mycobacterium tuberculosis,* Antimicrobial agents and chemotherapy **64**, 10 (2020).

[6] W. E. Siegenthaler, A. Bonetti, and R. Luthy, *Aminoglycoside antibiotics in infectious diseases: an overview,* The American journal of medicine **80**, 2 (1986).

[7] G. D. Wright, *Aminoglycoside-modifying enzymes,* Current opinion in microbiology **2**, 499 (1999).

[8] E. Azucena and S. Mobashery, *Aminoglycoside-modifying enzymes: mechanisms of catalytic processes and inhibition,* Drug resistance updates **4**, 106 (2001).

[9] B. A. Cunha, *New uses for older antibiotics: nitrofurantoin, amikacin, colistin, polymyxin b, doxycycline, and minocycline revisited,* Medical Clinics **90**, 1089 (2006).

[10] S. B. Vakulenko and S. Mobashery, *Versatility of aminoglycosides and prospects for their future,* Clinical microbiology reviews **16**, 430 (2003).

[11] N. Poey, F. Madhi, S. Biscardi, S. Béchet, and R. Cohen, *Aminoglycosides monotherapy as first-line treatment for febrile urinary tract infection in children,* The Pediatric Infectious Disease Journal **36**, 1104 (2017).

[12] S. Sundar, T. Jha, C. P. Thakur, P. K. Sinha, and S. K. Bhattacharya, *Injectable paromomycin for visceral leishmaniasis in india,* New England Journal of Medicine **356**, 2571 (2007).

[13] M. Shalev, H. Rozenberg, B. Smolkin, A. Nasereddin, D. Kopelyanskiy, V. Belakhov, T. Schrepfer, J. Schacht, C. L. Jaffe, N. Adir, *et al., Structural basis for selective targeting of leishmanial ribosomes: aminoglycoside derivatives as promising therapeutics,* Nucleic Acids Research **43**, 8601 (2015).

[14] J. Graham and F. Gould, *Role of aminoglycosides in the treatment of bacterial endocarditis,* Journal of Antimicrobial Chemotherapy **49**, 437 (2002).

[15] M. E. Falagas, D. K. Matthaiou, and I. A. Bliziotis, *The role of aminoglycosides in combination with a β-lactam for the treatment of bacterial endocarditis: a meta-analysis of comparative trials,* Journal of Antimicrobial Chemotherapy **57**, 639 (2006).

[16] W. H. Organization, *Pocket book of hospital care for children: guidelines for the management of common childhood illnesses* (World Health Organization, 2013).

[17] L. Zingman, S. Park, T. Olson, A. Alekseev, and A. Terzic, *Aminoglycoside-induced translational read-through in disease: overcoming nonsense mutations by pharmacogenetic therapy,* Clinical pharmacology & therapeutics **81**, 99 (2007).

[18] I. Nudelman, D. Glikin, B. Smolkin, M. Hainrichson, V. Belakhov, and T. Baasov, *Repairing faulty genes by aminoglycosides: development of new derivatives of geneticin (g418) with enhanced suppression of diseases-causing nonsense mutations,* Bioorganic & medicinal chemistry **18**, 3735 (2010).

[19] Z. Bukowy-Bieryllo, M. Dabrowski, M. Witt, and E. Zietkiewicz, *Aminoglycoside-stimulated readthrough of premature termination codons in selected genes involved in primary ciliary dyskinesia,* RNA biology **13**, 1041 (2016).

[20] J. Bhatt, N. Jahnke, and A. R. Smyth, *Once-daily versus multiple-daily dosing with intravenous aminoglycosides for cystic fibrosis,* Cochrane Database of Systematic Reviews (2019).

[21] A. Salmaninejad, Y. Jafari Abarghan, S. Bozorg Qomi, H. Bayat, M. Yousefi, S. Azhdari, S. Talebi, and M. Mojarrad, *Common therapeutic advances for duchenne muscular dystrophy (dmd),* International Journal of Neuroscience **131**, 370 (2021).

[22] Y. Tor, T. Hermann, and E. Westhof, *Deciphering rna recognition: aminoglycoside binding to the hammerhead ribozyme,* Chemistry & biology **5**, R277 (1998).

[23] T. K. Stage, K. J. Hertel, and O. C. Uhlenbeck, *Inhibition of the hammerhead ribozyme by neomycin.* Rna **1**, 95 (1995).

[24] J. Rogers, A. H. Chang, U. von Ahsen, R. Schroeder, and J. Davies, *Inhibition of the self-cleavage reaction of the human hepatitis delta virus ribozyme by antibiotics,* Journal of molecular biology **259**, 916 (1996).

[25] R. Schroeder, C. Waldsich, and H. Wank, *Modulation of rna function by aminoglycoside antibiotics,* The EMBO journal **19**, 1 (2000).

[26] U. von Ahsen, J. Davies, and R. Schroeder, *Non-competitive inhibition of group i intron rna self-splicing by aminoglycoside antibiotics,* Journal of molecular biology **226**, 935 (1992).

[27] E. Riguet, J. Désiré, O. Boden, V. Ludwig, M. Göbel, C. Bailly, and J.-L. Décout, *Neamine dimers targeting the hiv-1 tar rna,* Bioorganic & medicinal chemistry letters **15**, 4651 (2005).

[28] K. Hamasaki and A. Ueno, *Aminoglycoside antibiotics, neamine and its derivatives as potent inhibitors for the rna–protein interactions derived from hiv-1 activators,* Bioorganic & medicinal chemistry letters **11**, 591 (2001).

[29] K. M. Krause, A. W. Serio, T. R. Kane, and L. E. Connolly, *Aminoglycosides: an overview,* Cold Spring Harbor perspectives in medicine **6**, a027029 (2016).

[30] L. Leibovici, L. Vidal, and M. Paul, *Aminoglycoside drugs in clinical practice: an evidence-based approach,* Journal of Antimicrobial Chemotherapy **63**, 246 (2009).

[31] C. D. Freeman, D. Nicolau, P. Belliveau, and C. Nightingale, *Once-daily dosing of aminoglycosides: review and recommendations for clinical practice.* The Journal of antimicrobial chemotherapy **39**, 677 (1997).

[32] W. A. Craig, *Optimizing aminoglycoside use,* Critical care clinics **27**, 107 (2011).

[33] T. Hermann, *Aminoglycoside antibiotics: old drugs and new therapeutic approaches,* Cellular and molecular life sciences **64**, 1841 (2007), publisher: Springer.

[34] S. Jana and J. Deb, *Molecular understanding of aminoglycoside action and resistance,* Applied microbiology and biotechnology **70**, 140 (2006).

[35] M. Tod, C. Padoin, and O. Petitjean, *Clinical pharmacokinetics and pharmacodynamics of isepamicin,* Clinical pharmacokinetics **38**, 205 (2000).

[36] J. B. Aggen, E. S. Armstrong, A. A. Goldblum, P. Dozzo, M. S. Linsell, M. J. Gliedt, D. J. Hildebrandt, L. A. Feeney, A. Kubo, R. D. Matias, *et al.*, *Synthesis and spectrum of the neoglycoside achn-490,* Antimicrobial agents and chemotherapy **54**, 4636 (2010).

[37] W. Piepersberg, K. M. Aboshanab, H. Schmidt-Beißner, and U. F. Wehmeier, *The biochemistry and genetics of aminoglycoside producers,* Aminoglycoside Antibiotics: From Chemical Biology to Drug Discovery , 15 (2007).

[38] B. Becker and M. A. Cooper, *Aminoglycoside antibiotics in the 21st century,* ACS chemical biology **8**, 105 (2013).

[39] S. O'Connor, L. Lam, N. D. Jones, and M. O. Chaney, *Apramycin, a unique aminocyclitol antibiotic,* The Journal of organic chemistry **41**, 2087 (1976).

[40] A. P. Carter, W. M. Clemons, D. E. Brodersen, R. J. Morgan-Warren, B. T. Wimberly, and V. Ramakrishnan, *Functional insights from the structure of the 30s ribosomal subunit and its interactions with antibiotics,* Nature **407**, 340 (2000).

[41] I. Wohlgemuth, R. Garofalo, E. Samatova, A. N. Günenç, C. Lenz, H. Urlaub, and M. V. Rodnina, *Translation error clusters induced by aminoglycoside antibiotics,* Nature communications **12**, 1830 (2021).

[42] B. D. Davis, L. Chen, and P. C. Tai, *Misread protein creates membrane channels: an essential step in the bactericidal action of aminoglycosides.* Proceedings of the National Academy of Sciences **83**, 6164 (1986).

[43] B. Ezraty, A. Vergnes, M. Banzhaf, Y. Duverger, A. Huguenot, A. R. Brochado, S.-Y. Su, L. Espinosa, L. Loiseau, B. Py, *et al.*, *Fe-s cluster biosynthesis controls uptake of aminoglycosides in a ros-less death pathway,* Science **340**, 1583 (2013).

[44] M. A. Kohanski, D. J. Dwyer, J. Wierzbowski, G. Cottarel, and J. J. Collins, *Mistranslation of membrane proteins and two-component system activation trigger antibiotic-mediated cell death,* Cell **135**, 679 (2008).

[45] D. J. Dwyer, J. J. Collins, and G. C. Walker, *Unraveling the physiological complexities of antibiotic lethality,* Annual review of pharmacology and toxicology **55**, 313 (2015).

[46] G. N. Bruni and J. M. Kralj, *Membrane voltage dysregulation driven by metabolic dysfunction underlies bactericidal activity of aminoglycosides,* Elife **9**, e58706 (2020).

[47] Y. Zhuang, W. Chen, F. Yao, Y. Huang, S. Zhou, H. Li, Z. Zhang, C. Cai, Y. Gao, and Q. Peng, *Short-term pretreatment of sub-inhibitory concentrations of gentamycin inhibits the swarming motility of escherichia coli by down-regulating the succinate dehydrogenase gene,* Cellular Physiology and Biochemistry **39**, 1307 (2016).

[48] S. Pagkalis, E. Mantadakis, M. N. Mavros, C. Ammari, and M. E. Falagas, *Pharmacological considerations for the proper clinical use of aminoglycosides,* Drugs **71**, 2277 (2011).

[49] J. A. Roberts and J. Lipman, *Antibacterial dosing in intensive care: pharmacokinetics, degree of disease and pharmacodynamics of sepsis,* Clinical pharmacokinetics **45**, 755 (2006).

[50] R. D. Moore, P. S. Lietman, and C. R. Smith, *Clinical response to aminoglycoside therapy: importance of the ratio of peak concentration to minimal inhibitory concentration,* Journal of Infectious Diseases **155**, 93 (1987).

[51] C. Watanakunakorn, *Effects of inoculum size on the activity of carboxy-and ureido-penicillins and effects of combinations of ureido-penicillins with aminoglycosides against resistant pseudomonas aeruginosa,* Journal of Antimicrobial Chemotherapy **17**, 91 (1986).

[52] M. K. Lacy, D. P. Nicolau, C. H. Nightingale, and R. Quintiliani, *The pharmacodynamics of aminoglycosides,* Clinical infectious diseases **27**, 23 (1998).

[53] A. Forge and J. Schacht, *Aminoglycoside antibiotics,* Audiology and Neurotology **5**, 3 (2000).

[54] J. Rello, L. Campogiani, and V. K. Eshwara, *Understanding resistance in enterococcal infections,* Intensive Care Medicine **46**, 353 (2020), publisher: Springer.

[55] R. C. Moellering, C. Wennersten, and A. N. Weinberg, *Studies on antibiotic synergism against enterococci: I. Bacteriologic studies,* The Journal of laboratory and clinical medicine **77**, 821 (1971), publisher: Elsevier.

[56] R. C. Moellering Jr, C. Wennersten, and A. N. Weinberg, *Synergy of penicillin and gentamicin against enterococci,* Journal of Infectious Diseases **124**, S207 (1971), publisher: The University of Chicago Press.

[57] N. J. Mercuro, S. L. Davis, M. J. Zervos, and E. S. Herc, *Combatting resistant enterococcal infections: a pharmacotherapy review,* Expert opinion on pharmacotherapy **19**, 979 (2018).

[58] N. W. Luedtke, P. Carmichael, and Y. Tor, *Cellular uptake of aminoglycosides, guanidinoglycosides, and poly-arginine,* Journal of the American Chemical Society **125**, 12374 (2003).

[59] L. Bryan and H. Van Den Elzen, *Effects of membrane-energy mutations and cations on streptomycin and gentamicin accumulation by bacteria: a model for entry of streptomycin and gentamicin in susceptible and resistant bacteria,* Antimicrobial agents and chemotherapy **12**, 163 (1977).

[60] R. E. Hancock, *Aminoglycoside uptake and mode of action—with special reference to streptomycin and gentamicin: I. antagonists and mutants,* Journal of Antimicrobial Chemotherapy **8**, 249 (1981).

[61] R. E. Hancock, *Aminoglycoside uptake and mode of action—with special reference to streptomycin and gentamicin: Ii. effects of aminoglycosides on cells,* Journal of Antimicrobial Chemotherapy **8**, 429 (1981).

[62] H. W. Taber, J. P. Mueller, P. F. Miller, and A. Arrow, *Bacterial uptake of aminoglycoside antibiotics,* Microbiological reviews **51**, 439 (1987).

[63] I. Guerrero Montero, K. M. Dolata, R. Schlüter, G. Malherbe, S. Sievers, D. Zühlke, T. Sura, E. Dave, K. Riedel, and C. Robinson, *Comparative proteome analysis in an escherichia coli cydisco strain identifies stress responses related to protein production, oxidative stress and accumulation of misfolded protein,* Microbial Cell Factories **18**, 19 (2019).

[64] E. Ćudić, K. Surmann, G. Panasia, E. Hammer, and S. Hunke, *The role of the two-component systems cpx and arc in protein alterations upon gentamicin treatment in escherichia coli,* BMC microbiology **17**, 197 (2017).

[65] D. J. Dwyer, P. A. Belenky, J. H. Yang, I. C. MacDonald, J. D. Martell, N. Takahashi, C. T. Chan, M. A. Lobritz, D. Braff, E. G. Schwarz, *et al.*, *Antibiotics induce redox-related physiological alterations as part of their lethality,* Proceedings of the National Academy of Sciences **111**, E2100 (2014).

[66] H. W. Taber, J. P. Mueller, P. F. Miller, and A. Arrow, *Bacterial uptake of aminoglycoside antibiotics.* Microbiological reviews **51**, 439 (1987), publisher: American Society for Microbiology (ASM).

[67] V. Yarlagadda, R. Medina, and G. D. Wright, *Venturicidin a, a membrane-active natural product inhibitor of atp synthase potentiates aminoglycoside antibiotics,* Scientific Reports **10**, 8134 (2020).

[68] A. Mistry, M. S. Warren, J. K. Cusick, R. R. Karkhoff-Schweizer, O. Lomovskaya, and H. P. Schweizer, *High-level pacidamycin resistance in pseudomonas aeruginosa is mediated by an opp oligopeptide permease encoded by the opp-fabi operon,* Antimicrobial agents and chemotherapy **57**, 5565 (2013).

[69] A. Maio, L. Brandi, S. Donadio, and C. O. Gualerzi, *The oligopeptide permease opp mediates illicit transport of the bacterial p-site decoding inhibitor ge81112,* Antibiotics **5**, 17 (2016).

[70] Y. Ge, J. H. Lee, B. Hu, and Y. Zhao, *Loss-of-function mutations in the dpp and opp permeases render erwinia amylovora resistant to kasugamycin and blasticidin s,* Molecular Plant-Microbe Interactions **31**, 823 (2018).

[71] E. H. Nakamatsu, E. Fujihira, R. C. Ferreira, A. Balan, S. O. Costa, and L. C. Ferreira, *Oligopeptide uptake and aminoglycoside resistance in escherichia coli k12,* FEMS microbiology letters **269**, 229 (2007).

[72] A. Thacharodi and I. L. Lamont, *Gene–gene interactions reduce aminoglycoside susceptibility of pseudomonas aeruginosa through efflux pump-dependent and-independent mechanisms,* Antibiotics **12**, 152 (2023).

[73] A. Seupt, M. Schniederjans, J. Tomasch, and S. Häussler, *Expression of the mexxy aminoglycoside efflux pump and presence of an aminoglycoside-modifying enzyme in clinical pseudomonas aeruginosa isolates are highly correlated,* Antimicrobial Agents and Chemotherapy **65**, 10 (2020).

[74] Z. Shajani, M. T. Sykes, and J. R. Williamson, *Assembly of bacterial ribosomes,* Annual review of biochemistry **80**, 501 (2011).

[75] B. S. Laursen, H. P. Sørensen, K. K. Mortensen, and H. U. Sperling-Petersen, *Initiation of protein synthesis in bacteria,* Microbiology and molecular biology reviews **69**, 101 (2005).

[76] R. Green and H. F. Noller, *Ribosomes and translation,* Annual review of biochemistry **66**, 679 (1997), publisher: Annual Reviews.

[77] V. Ramakrishnan, *Ribosome structure and the mechanism of translation,* Cell **108**, 557 (2002), publisher: Elsevier.

[78] D. N. Wilson, *Ribosome-targeting antibiotics and mechanisms of bacterial resistance,* Nature Reviews Microbiology **12**, 35 (2014).

[79] A. Yonath, *Antibiotics targeting ribosomes: resistance, selectivity, synergism, and cellular regulation,* Annu. Rev. Biochem. **74**, 649 (2005).

[80] L. P. Kotra, J. Haddad, and S. Mobashery, *Aminoglycosides: perspectives on mechanisms of action and resistance and strategies to counter resistance,* Antimicrobial agents and chemotherapy **44**, 3249 (2000).

[81] T. Hermann, *Drugs targeting the ribosome,* Current opinion in structural biology **15**, 355 (2005), publisher: Elsevier.

[82] S. Shandrick, Q. Zhao, Q. Han, B. K. Ayida, M. Takahashi, G. C. Winters, K. B. Simonsen, D. Vourloumis, and T. Hermann, *Monitoring molecular recognition of the ribosomal decoding site,* Angewandte Chemie International Edition **43**, 3177 (2004), publisher: Wiley Online Library.

[83] J. M. Ogle, D. E. Brodersen, W. M. Clemons, M. J. Tarry, A. P. Carter, and V. Ramakrishnan, *Recognition of cognate transfer RNA by the 30S ribosomal subunit,* Science **292**, 897 (2001), publisher: American Association for the Advancement of Science.

[84] Q. Han, Q. Zhao, S. Fish, K. B. Simonsen, D. Vourloumis, J. M. Froelich, D. Wall, and T. Hermann, *Molecular recognition by glycoside pseudo base pairs and triples in an apramycin–RNA complex,* Angewandte Chemie **117**, 2754 (2005), publisher: Wiley Online Library.

[85] R. J. Walker and G. G. Duggin, *Drug nephrotoxicity,* Annual Review of Pharmacology and Toxicology **28**, 331 (1988).

[86] M.-P. Mingeot-Leclercq and P. M. Tulkens, *Aminoglycosides: nephrotoxicity,* Antimicrobial agents and chemotherapy **43**, 1003 (1999).

[87] P. De Jager and R. Van Altena, *Hearing loss and nephrotoxicity in long-term aminoglycoside treatment in patients with tuberculosis,* The International Journal of Tuberculosis and Lung Disease **6**, 622 (2002).

[88] C. Lanvers-Kaminsky and G. Ciarimboli, *Pharmacogenetics of drug-induced ototoxicity caused by aminoglycosides and cisplatin,* Pharmacogenomics **18**, 1683 (2017).

[89] E. Del Pozo and J. Baeyens, *Effects of calcium channel blockers on neuromuscular blockade induced by aminoglycoside antibiotics,* European journal of pharmacology **128**, 49 (1986).

[90] L. M. Childs-Kean, K. M. Shaeer, S. Varghese Gupta, and J. C. Cho, *Aminoglycoside allergic reactions,* Pharmacy **7**, 124 (2019).

[91] C. A. Peloquin, *Therapeutic drug monitoring in the treatment of tuberculosis,* Drugs **62**, 2169 (2002).

[92] G. J. Kaloyanides and E. Pastoriza-Munoz, *Aminoglycoside nephrotoxicity,* Kidney international **18**, 571 (1980).

[93] U. S. GONZALEZ III and J. P. Spencer, *Aminoglycosides: a practical review,* American family physician **58**, 1811 (1998).

[94] C. Martinez-Salgado, F. J. López-Hernández, and J. M. López-Novoa, *Glomerular nephrotoxicity of aminoglycosides,* Toxicology and applied pharmacology **223**, 86 (2007).

[95] J. Cabrera, V. Arroyo, A. M. Ballesta, A. Rimola, J. Gual, M. Elena, and J. Rodes, *Aminoglycoside nephrotoxicity in cirrhosis: value of urinary β2-microglobulin to discriminate functional renal failure from acute tubular damage,* Gastroenterology **82**, 97 (1982).

[96] F. Rougier, D. Claude, M. Maurin, and P. Maire, *Aminoglycoside nephrotoxicity,* Current Drug Targets-Infectious Disorders **4**, 153 (2004).

[97] S. J. McWilliam, D. J. Antoine, A. L. Jorgensen, R. L. Smyth, and M. Pirmohamed, *Urinary biomarkers of aminoglycoside-induced nephrotoxicity in cystic fibrosis: kidney injury molecule-1 and neutrophil gelatinase-associated lipocalin,* Scientific reports **8**, 1 (2018).

[98] J. Xie, A. E. Talaska, and J. Schacht, *New developments in aminoglycoside therapy and ototoxicity,* Hearing research **281**, 28 (2011), publisher: Elsevier.

[99] K. M. Olsen, M. I. Rudis, J. A. Rebuck, J. Hara, D. Gelmont, R. Mehdian, C. Nelson, and M. E. Rupp, *Effect of once-daily dosing vs. multiple daily dosing of tobramycin on enzyme markers of nephrotoxicity,* Critical care medicine **32**, 1678 (2004).

[100] L. Rybak and V. Ramkumar, *Ototoxicity,* Kidney international **72**, 931 (2007).

[101] M. A. Kohanski, D. J. Dwyer, B. Hayete, C. A. Lawrence, and J. J. Collins, *A common mechanism of cellular death induced by bactericidal antibiotics,* Cell **130**, 797 (2007).

[102] S.-i. Usami, S. Abe, J. Akita, A. Namba, H. Shinkawa, M. Ishii, S. Iwasaki, T. Hoshino, J. Ito, K. Doi, *et al., Prevalence of mitochondrial gene mutations among hearing impaired patients,* Journal of medical genetics **37**, 38 (2000).

[103] C. Cederroth, F. Gachon, and B. Canlon, *Time to listen: circadian impact on auditory research,* Current Opinion in Physiology **18**, 95 (2020).

[104] A. Yonovitz and J. E. Fisch, *Circadian rhythm dependent kanamycin-induced hearing loss in rodents assessed by auditory brainstem responses,* Acta oto-laryngologica **111**, 1006 (1991).

[105] G. Soulban, M. H. Smolensky, and A. Yonovitz, *Gentamicin-induced chronotoxicity: use of body temperature as a orcadian marker rhythm,* Chronobiology international **7**, 393 (1990).

[106] M.-P. Mingeot-Leclercq, Y. Glupczynski, and P. M. Tulkens, *Aminoglycosides: activity and resistance,* Antimicrobial agents and chemotherapy **43**, 727 (1999).

[107] E. Durante-Mangoni, A. Grammatikos, R. Utili, and M. E. Falagas, *Do we still need the aminoglycosides?* International journal of antimicrobial agents **33**, 201 (2009).

[108] E. C. Böttger and D. Crich, *Aminoglycosides: time for the resurrection of a neglected class of antibacterials?* ACS infectious diseases **6**, 168 (2019).

[109] J. M. Blair, M. A. Webber, A. J. Baylay, D. O. Ogbolu, and L. J. Piddock, *Molecular mechanisms of antibiotic resistance,* Nature reviews microbiology **13**, 42 (2015).

[110] L. Fernández, E. B. Breidenstein, and R. E. Hancock, *Creeping baselines and adaptive resistance to antibiotics,* Drug Resistance Updates **14**, 1 (2011).

[111] A. H. Van Hoek, D. Mevius, B. Guerra, P. Mullany, A. P. Roberts, and H. J. Aarts, *Acquired antibiotic resistance genes: an overview,* Frontiers in microbiology **2**, 203 (2011).

[112] C. A. Wakeman, N. D. Hammer, D. L. Stauff, A. S. Attia, L. L. Anzaldi, S. I. Dikalov, M. W. Calcutt, and E. P. Skaar, *Menaquinone biosynthesis potentiates haem toxicity in s taphylococcus aureus,* Molecular microbiology **86**, 1376 (2012).

[113] M. Vestergaard, K. Nøhr-Meldgaard, and H. Ingmer, *Multiple pathways towards reduced membrane potential and concomitant reduction in aminoglycoside susceptibility in staphylococcus aureus,* International Journal of Antimicrobial Agents **51**, 132 (2018).

[114] X. Zhao, Y. Jin, F. Bai, Z. Cheng, W. Wu, and X. Pan, *Pseudomonas aeruginosa phosphate transporter pita (pa4292) controls susceptibility to aminoglycoside antibiotics by regulating the proton motive force,* Antimicrobial Agents and Chemotherapy **66**, e00992 (2022).

[115] R. A. Moore, D. DeShazer, S. Reckseidler, A. Weissman, and D. E. Woods, *Efflux-mediated aminoglycoside and macrolide resistance in burkholderia pseudomallei,* Antimicrobial agents and chemotherapy **43**, 465 (1999).

[116] J. R. Aires, T. Kohler, H. Nikaido, and P. Plésiat, *Involvement of an active efflux system in the natural resistance of pseudomonas aeruginosa to aminoglycosides,* Antimicrobial agents and chemotherapy **43**, 2624 (1999).

[117] S. Westbrock-Wadman, D. R. Sherman, M. J. Hickey, S. N. Coulter, Y. Q. Zhu, P. Warrener, L. Y. Nguyen, R. M. Shawar, K. R. Folger, and C. K. Stover, *Characterization of a pseudomonas aeruginosa efflux pump contributing to aminoglycoside impermeability,* Antimicrobial agents and chemotherapy **43**, 2975 (1999).

[118] I. Phillips, A. King, and K. Shannon, *Prevalence and mechanisms of aminoglycoside resistance: a ten-year study,* The American journal of medicine **80**, 48 (1986).

[119] R. Hancock, *Intrinsic antibiotic resistance of pseudomonas aeruginosa,* Journal of Antimicrobial Chemotherapy **18**, 653 (1986).

[120] L. Bryan, *Two forms of antimicrobial resistance: bacterial persistence and positive function resistance,* Journal of Antimicrobial Chemotherapy **23**, 817 (1989).

[121] J. Poehlsgaard and S. Douthwaite, *The bacterial ribosome as a target for antibiotics,* Nature Reviews Microbiology **3**, 870 (2005).

[122] K. S. Long, J. Poehlsgaard, C. Kehrenberg, S. Schwarz, and B. Vester, *The cfr rrna methyltransferase confers resistance to phenicols, lincosamides, oxazolidinones, pleuromutilins, and streptogramin a antibiotics,* Antimicrobial agents and chemotherapy **50**, 2500 (2006).

[123] H. Umezawa, M. Okanishi, S. Kondo, K. Hamana, R. Utahara, K. Maeda, and S. Mitsuhashi, *Phosphorylative inactivation of aminoglycosidic antibiotics by escherichia coli carrying r factor,* Science **157**, 1559 (1967).

[124] J. Davies and G. D. Wright, *Bacterial resistance to aminoglycoside antibiotics,* Trends in microbiology **5**, 234 (1997).

[125] S. Magnet, T.-A. Smith, R. Zheng, P. Nordmann, and J. S. Blanchard, *Aminoglycoside resistance resulting from tight drug binding to an altered aminoglycoside acetyltransferase,* Antimicrobial agents and chemotherapy **47**, 1577 (2003).

[126] S. Magnet and J. S. Blanchard, *Molecular insights into aminoglycoside action and resistance,* Chemical reviews **105**, 477 (2005).

[127] M. E. Tolmasky, *Aminoglycoside-modifying enzymes: Characteristics, localization, and dissemination,* Enzyme-Mediated Resistance to Antibiotics: Mechanisms, Dissemination, and Prospects for Inhibition , 35 (2007).

[128] M. S. Ramirez and M. E. Tolmasky, *Aminoglycoside modifying enzymes,* Drug resistance updates **13**, 151 (2010).

[129] H. Sagai, V. Krcmery, K. Hasuda, S. Iyobe, H. Knothe, and S. Mitsuhashi, *R factor-mediated resistance to aminoglycoside antibiotics in pseudomonas aeruginosa,* Japanese Journal of Microbiology **19**, 427 (1975).

[130] S. Biddlecome, M. Haas, J. Davies, G. Miller, D. Rane, and P. Daniels, *Enzymatic modification of aminoglycoside antibiotics: a new 3-n-acetylating enzyme from a pseudomonas aeruginosa isolate,* Antimicrobial agents and chemotherapy **9**, 951 (1976).

[131] K. Poole, *Aminoglycoside resistance in pseudomonas aeruginosa,* Antimicrobial agents and Chemotherapy **49**, 479 (2005).

[132] W. Zhang, J. F. Fisher, and S. Mobashery, *The bifunctional enzymes of antibiotic resistance,* Current opinion in microbiology **12**, 505 (2009).

[133] A. I. M. Salah Ud-Din, A. Tikhomirova, and A. Roujeinikova, *Structure and functional diversity of gcn5-related n-acetyltransferases (gnat),* International journal of molecular sciences **17**, 1018 (2016).

[134] Y. Costa, M. Galimand, R. Leclercq, J. Duval, and P. Courvalin, *Characterization of the chromosomal aac (6')-ii gene specific for enterococcus faecium,* Antimicrobial Agents and Chemotherapy **37**, 1896 (1993).

[135] E. Azucena and S. Mobashery, *Aminoglycoside-modifying enzymes: mechanisms of catalytic processes and inhibition,* Drug Resistance Updates **4**, 106 (2001), publisher: Elsevier.

[136] J. L. Houghton, K. D. Green, W. Chen, and S. Garneau-Tsodikova, *The future of aminoglycosides: the end or renaissance?* ChemBioChem **11**, 880 (2010), publisher: Wiley Online Library.

[137] P. Kumar, B. Selvaraj, E. H. Serpersu, and M. J. Cuneo, *Encoding of promiscuity in an aminoglycoside acetyltransferase,* Journal of medicinal chemistry **61**, 10218 (2018), publisher: ACS Publications.

[138] P. J. Stogios, E. Bordeleau, Z. Xu, T. Skarina, E. Evdokimova, S. Chou, L. Diorio-Toth, A. W. D'Souza, S. Patel, G. Dantas, *et al.*, *Structural and molecular rationale for the diversification of resistance mediated by the antibiotic_nat family,* Communications biology **5**, 1 (2022).

[139] F. van den Ent and J. Löwe, *Crystal structure of the ubiquitin-like protein yukd from bacillus subtilis,* FEBS letters **579**, 3837 (2005).

[140] B. Bae, R. E. Cobb, M. A. DeSieno, H. Zhao, and S. K. Nair, *New n-acetyltransferase fold in the structure and mechanism of the phosphonate biosynthetic enzyme frbf,* Journal of Biological Chemistry **286**, 36132 (2011).

[141] M. C. Justice, T. Ku, M.-J. Hsu, K. Carniol, D. Schmatz, and J. Nielsen, *Mutations in ribosomal protein l10e confer resistance to the fungal-specific eukaryotic elongation factor 2 inhibitor sordarin,* Journal of Biological Chemistry **274**, 4869 (1999).

[142] J. Unge, S. Al-Kharadaghi, A. Nikulin, S. Nikonov, N. Davydova, N. Nevskaya, M. Garber, A. Liljas, *et al., The crystal structure of ribosomal protein l22 from thermus thermophilus: insights into the mechanism of erythromycin resistance,* Structure **6**, 1577 (1998).

[143] N. M. Lowden, L. Yeruva, C. M. Johnson, A. K. Bowlin, and D. J. Fisher, *Use of aminoglycoside 3' adenyltransferase as a selection marker for chlamydia trachomatis intron-mutagenesis and in vivo intron stability,* BMC research notes **8**, 570 (2015).

[144] J. B.-H. Tok, L. J. Dunn, and R. C. Des Jean, *Binding of dimeric aminoglycosides to the hiv-1 rev responsive element (rre) rna construct,* Bioorganic & medicinal chemistry letters **11**, 1127 (2001).

[145] N. W. Luedtke, *RNA affinity and specificity of modified aminoglycosides, metal complexes, and intercalating agents that target the HIV-1 Rev response element* (University of California, San Diego, 2003).

[146] M. Galimand, P. Courvalin, and T. Lambert, *Plasmid-mediated high-level resistance to aminoglycosides in enterobacteriaceae due to 16s rrna methylation,* Antimicrobial agents and chemotherapy **47**, 2565 (2003).

[147] A. Ayad, M. Drissi, C. de Curraize, C. Dupont, A. Hartmann, S. Solanas, E. Siebor, L. Amoureux, and C. Neuwirth, *Occurence of arma and rmtb aminoglycoside resistance 16s rrna methylases in extended-spectrum β-lactamases producing escherichia coli in algerian hospitals,* Frontiers in Microbiology **7**, 1409 (2016).

[148] E. F. Azucena Jr, *Study of aminoglycoside resistance mechanism in bacteria* (Wayne State University, 2001).

[149] I. Padilla and L. Burgos, *Aminoglycoside antibiotics: structure, functions and effects on in vitro plant culture and genetic transformation protocols,* Plant cell reports **29**, 1203 (2010).

[150] J.-I. Wachino, Y. Doi, and Y. Arakawa, *Aminoglycoside resistance: updates with a focus on acquired 16s ribosomal rna methyltransferases,* Infectious Disease Clinics **34**, 887 (2020).

[151] P. Courvalin, *New plasmid-mediated resistances to antimicrobial agents,* Archives of microbiology **189**, 289 (2008).

[152] B. González-Zorn, T. Teshager, M. Casas, M. C. Porrero, M. A. Moreno, P. Courvalin, and L. Domínguez, *arma and aminoglycoside resistance in escherichia coli,* Emerging infectious diseases **11**, 954 (2005).

[153] A. Hasani, V. Sheikhalizadeh, M. Ahangarzadeh Rezaee, M. Rahmati-Yamchi, A. Hasani, R. Ghotaslou, and H. R. Goli, *Frequency of aminoglycoside-modifying enzymes and arma among different sequence groups of acinetobacter baumannii in iran,* Microbial Drug Resistance **22**, 347 (2016).

[154] M. Galimand, S. Sabtcheva, P. Courvalin, and T. Lambert, *Worldwide disseminated arma aminoglycoside resistance methylase gene is borne by composite transposon tn 1548,* Antimicrobial agents and chemotherapy **49**, 2949 (2005).

[155] L. Poirel, J. Goutines, M. Aires-de Sousa, and P. Nordmann, *High rate of association of 16s rrna methylases and carbapenemases in enterobacteriaceae recovered from hospitalized children in angola,* Antimicrobial agents and chemotherapy **62**, e00021 (2018).

[156] L. Poirel, A. Ros, A. Carricajo, P. Berthelot, B. Pozzetto, S. Bernabeu, and P. Nordmann, *Extremely drug-resistant citrobacter freundii isolate producing ndm-1 and other carbapenemases identified in a patient returning from india,* Antimicrobial agents and chemotherapy **55**, 447 (2011).

[157] H. Tate, J. P. Folster, C.-H. Hsu, J. Chen, M. Hoffmann, C. Li, C. Morales, G. H. Tyson, S. Mukherjee, A. C. Brown, *et al.*, *Comparative analysis of extended-spectrum-β-lactamase ctx-m-65-producing salmonella enterica serovar infantis isolates from humans, food animals, and retail chickens in the united states,* Antimicrobial Agents and Chemotherapy **61**, e00488 (2017).

[158] A. Adler, D. E. Katz, and D. Marchaim, *The continuing plague of extended-spectrum β-lactamase–producing enterobacteriaceae infections,* Infectious Disease Clinics **30**, 347 (2016).

[159] Y. Doi, J. M. Adams-Haduch, and D. L. Paterson, *Escherichia coli isolate coproducing 16s rrna methylase and ctx-m-type extended-spectrum β-lactamase isolated from an outpatient in the united states,* Antimicrobial agents and chemotherapy **52**, 1204 (2008).

[160] V. R. Gajamer, A. Bhattacharjee, D. Paul, B. Ingti, A. Sarkar, J. Kapil, A. K. Singh, N. Pradhan, and H. K. Tiwari, *High prevalence of carbapenemase, ampc β-lactamase and aminoglycoside resistance genes in extended-spectrum β-lactamase-positive uropathogens from northern india,* Journal of global antimicrobial resistance **20**, 197 (2020).

[161] W. Yang and F. Hu, *Research updates of plasmid-mediated aminoglycoside resistance 16s rrna methyltransferase,* Antibiotics **11**, 906 (2022).

[162] S. G. Zárate, M. L. De la Cruz Claure, R. Benito-Arenas, J. Revuelta, A. G. Santana, and A. Bastida, *Overcoming aminoglycoside enzymatic resistance: design of novel antibiotics and inhibitors,* Molecules **23**, 284 (2018).

[163] J. Wang and C.-W. T. Chang, *Design, chemical synthesis, and antibacterial activity of kanamycin and neomycin class aminoglycoside antibiotics,* Aminoglycoside Antibiotics: From Chemical Biology to Drug Discovery , 141 (2007).

[164] S. Umezawa, *Recent advances in the synthesis of aminoglycoside antibiotics,* Pure and Applied Chemistry **50**, 1453 (1978).

[165] R.-B. Yan, M. Yuan, Y. Wu, X. You, and X.-S. Ye, *Rational design and synthesis of potent aminoglycoside antibiotics against resistant bacterial strains,* Bioorganic & medicinal chemistry **19**, 30 (2011).

[166] G. Cox, L. Ejim, P. J. Stogios, K. Koteva, E. Bordeleau, E. Evdokimova, A. O. Sieron, A. Savchenko, A. W. Serio, K. M. Krause, *et al.*, *Plazomicin retains antibiotic activity against most aminoglycoside modifying enzymes,* ACS infectious diseases **4**, 980 (2018).

[167] K. M. Shaeer, M. T. Zmarlicka, E. B. Chahine, N. Piccicacco, and J. C. Cho, *Plazomicin: a next-generation aminoglycoside,* Pharmacotherapy: The Journal of Human Pharmacology and Drug Therapy **39**, 77 (2019).

[168] S. Bera, G. G. Zhanel, and F. Schweizer, *Antibacterial activity of guanidinylated neomycin b-and kanamycin a-derived amphiphilic lipid conjugates,* Journal of Antimicrobial Chemotherapy **65**, 1224 (2010).

[169] N. W. Luedtke, T. J. Baker, M. Goodman, and Y. Tor, *Guanidinoglycosides: a novel family of rna ligands,* Journal of the American Chemical Society **122**, 12035 (2000).

[170] S. N. Hobbie, P. Pfister, C. Brüll, E. Westhof, and E. C. Böttger, *Analysis of the contribution of individual substituents in 4, 6-aminoglycoside-ribosome interaction,* Antimicrobial agents and chemotherapy **49**, 5112 (2005).

[171] T. Vacas, F. Corzana, G. Jimenez-Oses, C. Gonzalez, A. M. Gomez, A. Bastida, J. Revuelta, and J. L. Asensio, *Role of aromatic rings in the molecular recognition of aminoglycoside antibiotics: implications for drug design,* Journal of the American Chemical Society **132**, 12074 (2010).

[172] J. Revuelta, T. Vacas, F. Corzana, C. Gonzalez, A. Bastida, and J. L. Asensio, *Structure-based design of highly crowded ribostamycin/kanamycin hybrids as a new family of antibiotics,* Chemistry–A European Journal **16**, 2986 (2010).

[173] K. F. Blount, F. Zhao, T. Hermann, and Y. Tor, *Conformational constraint as a means for understanding rna-aminoglycoside specificity,* Journal of the American Chemical Society **127**, 9818 (2005).

[174] J. L. Asensio, A. Hidalgo, A. Bastida, M. Torrado, F. Corzana, J. L. Chiara, E. García-Junceda, J. Cañada, and J. Jiménez-Barbero, *A simple structural-based approach to prevent aminoglycoside inactivation by bacterial defense proteins. conformational restriction provides effective protection against neomycin-b nucleotidylation by ant4,* Journal of the American Chemical Society **127**, 8278 (2005).

[175] C.-W. T. Chang, Y. Hui, B. Elchert, J. Wang, J. Li, and R. Rai, *Pyranmycins, a novel class of aminoglycosides with improved acid stability: the sar of d-pyranoses on ring iii of pyranmycin,* Organic Letters **4**, 4603 (2002).

[176] J. B.-H. Tok and G. R. Huffman, *Enhanced binding of aminoglycoside dimers to a "dimerized" a-site 16s rrna construct,* Bioorganic & medicinal chemistry letters **10**, 1593 (2000).

[177] F. Agnelli, S. J. Sucheck, K. A. Marby, D. Rabuka, S.-L. Yao, P. S. Sears, F.-S. Liang, and C.-H. Wong, *Dimeric aminoglycosides as antibiotics,* Angewandte Chemie International Edition **43**, 1562 (2004).

[178] S. Freisz, K. Lang, R. Micura, P. Dumas, and E. Ennifar, *Binding of aminoglycoside antibiotics to the duplex form of the hiv-1 genomic rna dimerization initiation site,* Angewandte Chemie International Edition **47**, 4110 (2008).

[179] S. Hanessian, J. P. Maianti, R. D. Matias, L. A. Feeney, and E. S. Armstrong, *Hybrid aminoglycoside antibiotics via tsuji palladium-catalyzed allylic deoxygenation,* Organic letters **13**, 6476 (2011).

[180] M. Carriere, V. Vijayabaskar, D. Applefield, I. Harvey, P. Garneau, J. Lorsch, A. Lapidot, and J. Pelletier, *Inhibition of protein synthesis by aminoglycoside–arginine conjugates,* RNA **8**, 1267 (2002).

[181] K. J. Labby and S. Garneau-Tsodikova, *Strategies to overcome the action of aminoglycoside-modifying enzymes for treating resistant bacterial infections,* Future medicinal chemistry **5**, 1285 (2013).

[182] S. Hanessian, J. Szychowski, N. B. C.-R. Pineda, A. Furtos, and J. W. Keillor, *6-hydroxy to 6"'-amino tethered ring-to-ring macrocyclic aminoglycosides as probes for aph (3')-iiia kinase,* Bioorganic & medicinal chemistry letters **17**, 3221 (2007).

[183] F. J. Perez-Llarena and G. Bou, *β-lactamase inhibitors: the story so far,* Current medicinal chemistry **16**, 3740 (2009).

[184] P. Amstutz, H. K. Binz, P. Parizek, M. T. Stumpp, A. Kohl, M. G. Grutter, P. Forrer, and A. Pluckthun, *Intracellular kinase inhibitors selected from combinatorial libraries of designed ankyrin repeat proteins,* Journal of Biological Chemistry **280**, 24715 (2005).

[185] A. Kohl, P. Amstutz, P. Parizek, H. K. Binz, C. Briand, G. Capitani, P. Forrer, A. Plückthun, and M. G. Grütter, *Allosteric inhibition of aminoglycoside phosphotransferase by a designed ankyrin repeat protein,* Structure **13**, 1131 (2005).

[186] C. El-Khoury, E. Mansour, Y. Yuliandra, F. Lai, B. A. Hawkins, J. J. Du, E. J. Sundberg, N. Sluis-Cremer, D. E. Hibbs, and P. W. Groundwater, *The role of adjuvants in overcoming antibacterial resistance due to enzymatic drug modification,* RSC Medicinal Chemistry **13**, 1276 (2022).

[187] G. Dhanda, Y. Acharya, and J. Haldar, *Antibiotic adjuvants: A versatile approach to combat antibiotic resistance,* ACS omega **8**, 10757 (2023).

[188] D. M. Daigle, G. A. McKay, and G. D. Wright, *Inhibition of aminoglycoside antibiotic resistance enzymes by protein kinase inhibitors,* Journal of Biological Chemistry **272**, 24755 (1997).

[189] P. J. Stogios, P. Spanogiannopoulos, E. Evdokimova, O. Egorova, T. Shakya, N. Todorovic, A. Capretta, G. D. Wright, and A. Savchenko, *Structure-guided optimization of protein kinase inhibitors reverses aminoglycoside antibiotic resistance,* Biochemical Journal **454**, 191 (2013).

[190] D. L. Burk and A. M. Berghuis, *Protein kinase inhibitors and antibiotic resistance,* Pharmacology & therapeutics **93**, 283 (2002).

[191] K. Shi, S. J. Caldwell, D. H. Fong, and A. M. Berghuis, *Prospects for circumventing aminoglycoside kinase mediated antibiotic resistance,* Frontiers in cellular and infection microbiology **3**, 22 (2013).

[192] J. H. Lee, S. H. Jeong, S.-S. Cha, and S. H. Lee, *A lack of drugs for antibiotic-resistant gram-negative bacteria,* Nature Reviews Drug Discovery **6**, 938 (2007).

[193] L. Freire-Moran, B. Aronsson, C. Manz, I. C. Gyssens, A. D. So, D. L. Monnet, O. Cars, E.-E. working group, *et al., Critical shortage of new antibiotics in development against multidrug-resistant bacteria—time to react is now,* Drug resistance updates **14**, 118 (2011).

[194] B. Spellberg, J. H. Powers, E. P. Brass, L. G. Miller, and J. E. Edwards Jr, *Trends in antimicrobial drug development: implications for the future,* Clinical infectious diseases **38**, 1279 (2004).

[195] J. H. Lee, S. H. Jeong, S.-S. Cha, and S. H. Lee, *New disturbing trend in antimicrobial resistance of gram-negative pathogens,* PLoS pathogens **5**, e1000221 (2009).

2

3-N-ALKYLATION IN AMINOGLYCOSIDE ANTIBIOTIC NEOMYCIN B OVERCOMES BACTERIAL RESISTANCE MEDIATED BY ACETYLTRANSFERASE (3) IIIA

Nicola PONTILLO, Eliza M. WARSZAWIK, Michele PARTIPILO, Artem STETSENKO, Mark LOZNIK, Xintong YANG, Dirk J. SLOTBOOM, Albert GUSKOV and Andreas HERRMANN

"In the battle against resistance, every atom counts
and sometimes, a single methyl group can tip the scales."

— Medicinal chemistry principle
(or it should be)

2

ABSTRACT

Aminoglycosides are potent, broad-spectrum bactericidal antibiotics, yet their clinical efficacy has been significantly hampered by the rise of antimicrobial resistance. Among the resistance mechanisms, the AAC(3)-IIIa enzyme is notably promiscuous, mediating the inactivation of neomycin, kanamycin, gentamicin, and paromomycin. This study investigates the structural and catalytic characteristics of AAC(3)-IIIa while proposing a novel approach to counter its activity. Recognizing the critical role of the amine at position 3 of neomycin B, we designed a series of alkyl derivatives to circumvent AAC(3)-IIIa-mediated resistance while preserving bactericidal potency. Three newly synthesized mono-N-alkylated derivatives demonstrated cytotoxic activity against an E. coli strain expressing AAC(3)-IIIa, which resists unmodified neomycin B. Remarkably, 3-N-methyl-neomycin B, differing from the parent compound by a single methyl group, exhibited superior performance. Crystallographic analysis revealed that its resistance to enzymatic modification stems from an unanticipated binding conformation. Furthermore, cryo-EM analysis of the ribosome confirmed that 3-N-methyl-neomycin B maintains its binding to the A-site, unaffected by the methylation. This work represents the first demonstration of successful 3-position modification in neomycin B to overcome N-acetyltransferases (3) type IIIa (AAC(3)-IIIa) resistance, paving the way for further optimization to restore the therapeutic efficacy of aminoglycosides.

2.1. INTRODUCTION

Antimicrobial resistance is increasingly undermining the efficacy of many antimicrobial drugs, including aminoglycosidess (AGs), which are becoming less effective in treating infectious diseases.[1, 2] As one of the three major classes of antibiotics and the only one known to interfere with protein translation,[3–5] AGs have been highlighted in reports by the World Health Organization (WHO) and the European Union (EU), which emphasize the urgent need for new antimicrobial compounds and strategies to curb the spread of antibiotic resistance.[6, 7]

AGs are highly effective natural and semi-synthetic bactericidal antibiotics with a broad spectrum of activity against aerobic Gram-negative bacteria, certain Gram-positive species, and Mycobacteria.[8–11] Despite their severe and sometimes irreversible side effects, AGs remain invaluable in treating severe infections such as sepsis, endocarditis, pneumonia, urinary tract infections, and multidrug-resistant tuberculosis.[12–14] Their well-established mode of action, known dosing regimens, and modifiable chemical structure provide a robust foundation for the development of next-generation aminoglycosides to overcome resistance and address pressing clinical challenges.

AGs exert their bactericidal effects by interacting with the decoding site (A-site) of 16S rRNA in the 30S ribosomal subunit. It is commonly understood that this interaction disrupts protein biosynthesis by inducing translational inhibition and mRNA misreading, ultimately leading to rapid cell death.[15, 16]

Most clinically significant aminoglycosides are derived from the neamine moiety,[17] a highly conserved core structure critical for sequence recognition and binding to the conserved A-site.[18–20] The neamine unit is further linked to additional amino-sugar rings at position 6 of the aminocyclitol ring (ring II) in compounds such as tobramycin, gentamicin, and amikacin, or at position 5 in neomycin (NEO) B (NEO B) and paromomycin (PAR) (Figure 2.1).[21]

Bacteria have evolved various mechanisms to counteract the bactericidal effects of AGs, including reduced membrane permeability,[22, 23] efflux pump expression,[24] ribosome alteration,[25, 26] and chemical modification by Aminoglycoside Modifying Enzymes (AMEs).[27] Among these, AMEs play a central role by catalyzing the chemical modification of hydroxyl or amino groups in AGs. Such modifications reduce AG affinity for their biological target, leading to decreased antimicrobial efficacy.[28–30]

AMEs are encoded by mobile genetic elements, including plasmids, integrons, and transposons, facilitating horizontal gene transfer between bacterial species and contributing to the accumulation of resistance genes. [31, 32] This is particularly concerning in Multi-Drug Resistant (MDR) bacteria within the ESKAPE panel (*E. faecium, S. aureus, K. pneumoniae, A. baumannii, P. aeruginosa*, and *Enterobacter spp.*).[33, 34] Among AMEs, N-acetyltransferasess (AACs) acetylate primary amines using acetyl coenzyme A (AcCOA) as a cofactor.[28] AAC(3) enzymes specifically modify the 3-C amine on the 2-deoxystreptamine (2-DOS) ring of AGs, disrupting the electrostatic and hydrogen bond interactions essential for binding to the ribosomal A-site and causing steric hindrance.[35]

Despite the synthetic challenges associated with modifying AGs, site-selective alterations have proven effective in restoring antimicrobial activity against AME-expressing pathogens.

For example, the introduction of an L-hydroxyamino butyric acid moiety at the 1-C position of kanamycin (KAN) led to the development of amikacin (AMK), while combining this modification with a 2-hydroxyethyl group at the 6'-N position of sisomycin (SIS) yielded plazomycin (PLZ), a third-generation AG recently approved for clinical use.[36, 37] However, modifications of the 3-C position in NEO have remained largely unexplored, possibly due to the difficulty of achieving selective synthesis in the presence of multiple reactive groups.[38, 39]

To address this, we employed a previously established regioselective diazo transfer methodology for unprotected AGs, enabling efficient modification of the 3-C amine.[40] Using this approach, we synthesized a library of 3-N-alkylated neomycin B derivatives and evaluated their antimicrobial activity against an MDR strain of *E. coli* expressing N-acetyltransferases (3) type IIIa (AAC(3)-IIIa). Among these derivatives, the 3-N-methyl Neomycin B, also known as compound **8** (Neo-CH_3) demonstrated superior activity, effectively overcoming AAC(3)-IIIa-mediated resistance while maintaining strong binding to the ribosomal A-site.

Structural analysis of AAC(3)-IIIa revealed a high degree of substrate promiscuity and a catalytic mechanism consistent with other members of the GCN5-related N-acetyltransferase (GNAT) superfamily. Despite low sequence similarity among AACs, their conserved fold and structural features underscore the need for detailed investigation of individual variants to enable rational drug design. Interestingly, the methyl substitution at the 3-C position induces an unexpected binding mode to AAC(3)-IIIa while leaving ribosomal binding unaffected. This highlights the potential of small, basic, and flexible moieties to enhance AG activity against resistant pathogens.

Our findings establish 3-C alkylation as a promising strategy for overcoming AAC(3)-IIIa-mediated resistance, paving the way for further development of aminoglycosides with improved therapeutic profiles.

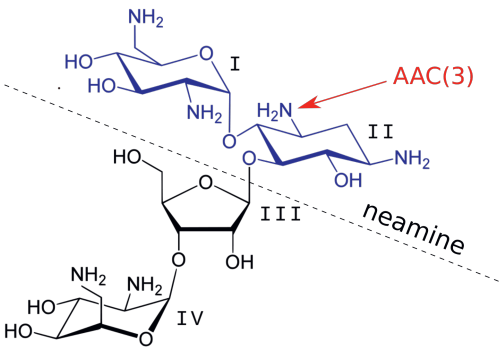


Figure 2.1 | Chemical structure of NEO B, a 4,5-disubstituted aminoglycoside. The neamine unit is highlighted in blue while the red arrow indicates the 3-N amine, targeted by the AAC(3) class of enzymes. Roman numerals identify the different rings in the structure.

2.2. RESULTS AND DISCUSSION

THE CRYSTAL STRUCTURE OF AAC(3)-IIIA REVEALS A UNIQUE FOLD AMONG ACETYLTRANSFERASES

In this work, two crystal structures of AAC(3)-IIIa in complex with AcCOA and NEO B have been determined, along with a structure of the ternary complex AAC(3)-IIIa-AcCOA-NEO B. All crystals belonged to the orthorhombic space group $P2_12_122$ and diffracted to high resolution (1.8–2.4 Å). The quality of the electron density maps allowed for the building and refinement of a model comprising residues 22 to 286. Crystallographic data and refinement statistics for each structure are summarized in Table 2.2.

AAC(3)-IIIa shares 29–47% sequence identity with seven other proteins deposited in the Protein Data Bank (PDB). While these proteins are functionally analogous as members of the GNAT superfamily, AAC(3)-IIIa exhibits a distinct fold and architecture, branching out as a unique subgroup of AACs. This divergence underscores the functional and structural variability within the GNAT family.

AAC(3)-IIIa forms a homodimer, with each protomer consisting of two domains. The interface between these domains forms a major groove on the protein surface, which constitutes the active site and houses the binding pockets for AcCOA and NEO B. The larger domain, responsible for coenzyme A binding, contains two pairs of three antiparallel β-sheets with the inner strands running parallel. These β-sheets are flanked by clusters of α-helices on both sides. The pantetheine moiety of AcCOA is coordinated via polar interactions with the backbone and side chains of Ala52 and His51.

Adjacent to the AcCOA binding pocket lies the NEO B binding site, located within the smaller domain. This domain comprises two antiparallel β-sheets and two short α-helices, which collectively coordinate NEO B binding. Key interactions involve the side chains of Tyr84, Tyr166, and Glu143, which coordinate the amine at position 1 of ring II.

Comparison of the binary and ternary complexes reveals differences in NEO B binding. In the binary complex, His196 directly coordinates the 3-C amine of NEO B, resulting in well-resolved electron density for rings I, II, and III, indicative of strong interactions. Conversely, ring IV exhibits higher B-factors, suggesting weaker interactions and increased flexibility. In the ternary complex, the acetyl group of AcCOA coordinates with His196, causing the 3-C amino group to withdraw and inducing a slight conformational change in ring IV.

An additional feature of the ternary complex is the interaction of Arg121 from chain A, which stacks with the adenine base of AcCOA in chain B. This interaction appears to stabilize the quaternary structure, contributing to the overall assembly's robustness.

THE CATALYTIC MECHANISM FEATURES A NON-CANONICAL CATALYTIC TRIAD

The hydrogen-bonding network between AAC(3)-IIIa and its substrates reveals a non-canonical catalytic triad that facilitates acetyl transfer without forming a covalent intermediate with the protein. This triad involves two key residues, His196 and Glu199, which enable the NEO B molecule to act as a nucleophile and directly attack the acetyl group of AcCOA. For details, see Figure 2.3

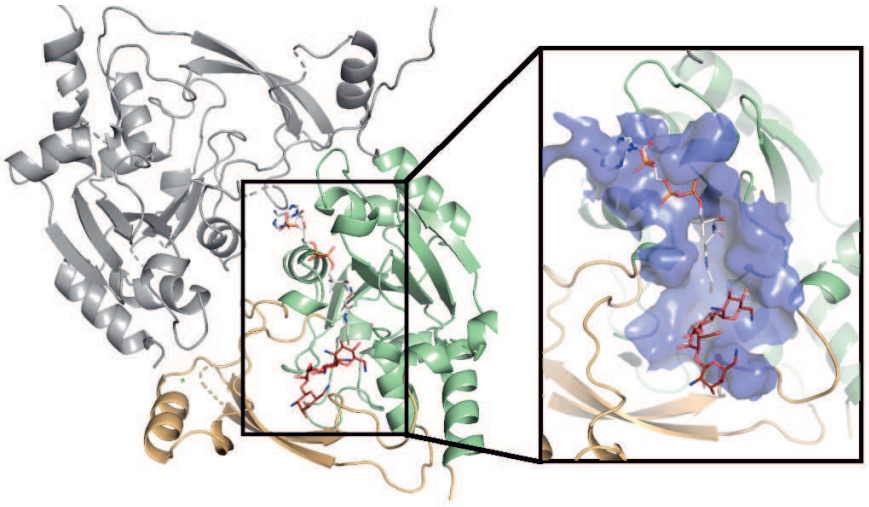


Figure 2.2 | Cartoon representation of the dimeric AAC(3)-IIIa oriented along the twofold axis. The dimer is found in the crystal structure and represents the most stable calculated assembly in solution (according to PISA [41]). On one monomer the two major domains are highlighted in green and yellow. The inset shows the major groove present on the protein surface (blue) where the binding pockets of AcCOA (grey) and NEO B (red) are located.

Specifically, the $O^{\epsilon 1}$ atom of Glu199 forms a hydrogen bond (2.8 Å) with the N^{δ} atom of His196, enhancing the nucleophilicity of His196's N^{ϵ}. This activated N^{ϵ} is optimally positioned (2.7 Å) to abstract a proton from the amine at the 3-C position of NEO B. The deprotonated amine then attacks the carbonyl group of AcCOA, forming a tetrahedral intermediate.

Thr193 plays a critical role in coordinating the mercapto-ethanolamine group of AcCOA. This residue likely aids in the correct positioning of the acetyl group and stabilizes the reaction intermediate, ensuring efficient catalysis.

From the tetrahedral intermediate, a proton is transferred from His196 to the thiolate of CoA, regenerating the active site and facilitating the release of the acetylated NEO B and CoA as products.

KINETIC CHARACTERIZATION AND SUBSTRATE PROMISCUITY OF AAC(3)-IIIA

The enzymatic activity of purified AAC(3)-IIIa was assessed spectrophotometrically, as described in Section 2.6. At a fixed AcCOA concentration of 100 μM, the K_M for NEO B was determined to be 11.3 ± 1.2 μM. Conversely, at a NEO B concentration of 100 μM, the K_M for AcCOA was 10.7 ± 2.9 μM.

These kinetic parameters are consistent with those reported for other members of the AAC(3) family. For example, AAC(3)-IIIb from *P. aeruginosa* and AAC(3)-IV from *E. coli*, which share 47% and 32% sequence dentity with AAC(3)-IIIa, exhibit K_M values for AcCOA of 17.0 μM and 9.2 μM, respectively.[42, 43] While the affinity constants for NEO B in these homologues

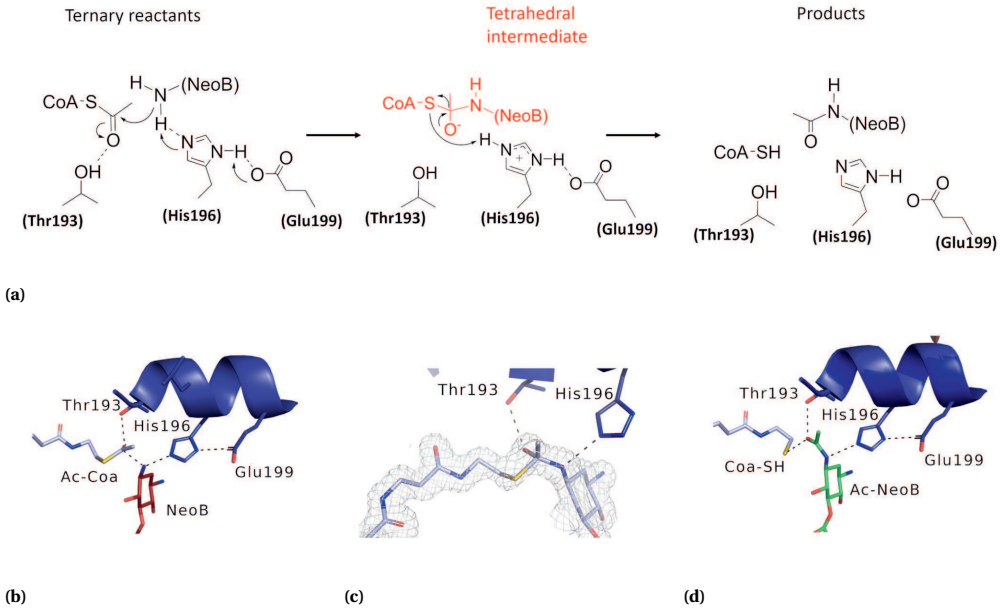


Figure 2.3 | (a) Catalytic mechanism proposed for the acetylation of NEO B by AAC(3)-IIIa based on the obtained crystal structure of the complex. (b) Cartoon and stick representation of the AcCOA (gray) and NEO B (red) bound to AAC(3)-IIIa. (c) Stick representation and Omit map (3σ) of the tetrahedral intermediate. (d) Stick representation of the acetylated NEO B (green) and CoA-SH.

are slightly lower (1.2 μM for AAC(3)-IIIb and 0. μM for AAC(3)-IV),[44] all values remain in the micromolar range, underscoring similarities in substrate binding across this enzyme class.

AAC(3)-IIIa exhibits a low turnover number ($k_{cat} = 0.04\ s^{-1}$), resulting in a catalytic efficiency of $3.54 \times 10^3\ s^{-1}M^{-1}$. Such low turnover rates are not uncommon among AACs, and significant variations in k_{cat} have been documented within this enzyme family.[45]

In addition to NEO B, AAC(3)-IIIa demonstrates substrate promiscuity, transferring the acetyl group from AcCOA to other aminoglycosides, including gentamicin (GEN), KAN(KAN), and PAR, but not to AMK (see Figure 2.4). The acetylation of GEN occurs 1.3 times faster than that of NEO B, whereas the reactions with KAN and PAR are comparatively slower. These findings align with the pioneering work of Vliegenthart et al.,[46] who first identified the AAC(3)-IIIa gene *in vivo* and characterized its enzymatic function in cell-free lysates.

SYNTHESIS OF 3-C MODIFIED NEO B DERIVATIVES

To synthesize the 3-*N*-alkylated derivatives, NEO B was first transformed into 3-*C*-azido-neomycin B (**1**) using a previously established methodology. [40] Following this, the remaining amines were protected with carboxybenzyl (Cbz) groups. compound **1** was then reacted with an excess (18 equivalents) of *N*-(benzyloxycarbonoxy)succinimide in H_2O–THF

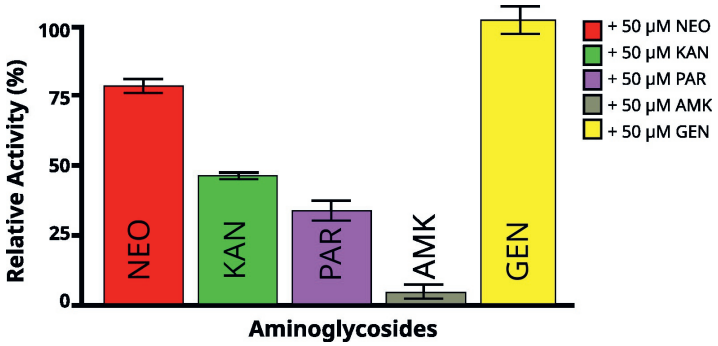


Figure 2.4 | Acetylation rates of AAC(3)-IIIa towards different AGs. The activity is defined as the linear acetylation rate in the presence of 100 μM AcCOA. The acetylation activity is highest with GEN (arbitrarily set at 100%) as substrate when compared to the other tested AGs, followed by NEO B . KAN and PAR were identified as substrates too, although with roughly half of the activity of NEO B. AMK is the only AG not to be acetylated by AAC(3)-IIIa.

in the presence of K_2CO_3 at room temperature for 36 h. Purification yielded 3-*C*-azido-1,2′,2‴,6′,6‴(Cbz)$_5$-neomycin B (**2**) in 58% yield.

Reduction of the azido group in compound **2** to an amine was achieved using the Staudinger reaction. Refluxing with trimethylphosphine (PMe_3) in 1.0 M NaOH produced 1,2′,2‴,6′,6‴(Cbz)$_5$-neomycin B (**3**) in 46% yield. The presence of a single unprotected amine at the C-3 position of **3** enabled subsequent mono-*N* and di-*N,N* alkylation reactions.

Mono- and Dimethylation. Mono-methylation of the C-3 position was performed by treating compound **3** with trifluoromethanesulfonate (1.5 equivalents) in hexafluoroisopropanol under an inert argon atmosphere for 2 h, following the method of Lebleu *et al.*[47] Purification yielded 3-*N*-methyl-1,2′,2‴,6′,6‴(Cbz)$_5$-neomycin B (**4**) as a pentafluoroacetate salt, with a 78% yield.

To generate 3-*N,N*-dimethyl-1,2′,2‴,6′,6‴(Cbz)$_5$-neomycin B (**5**), reductive alkylation was carried out using an excess of formaldehyde (10 equivalents) and sodium cyanoborohydride ($NaBH_3CN$, 3 equivalents) in the presence of catalytic glacial acetic acid for 3 h, resulting in a 90% yield.

Propyl- and Hexylation. For 3-*N*-propylation, compound **3** was reacted with propanal (1 equivalent) and $NaBH_3CN$ (1 equivalent), affording 3-*N*-propyl-1,2′,2‴,6′,6‴(Cbz)$_5$-neomycin B (**6**) in a 96% yield. Similarly, reaction with hexanal (1 equivalent) under the same conditions produced 3-*N*-hexyl-1,2′,2‴,6′,6‴(Cbz)$_5$-neomycin B (**7**) with a yield of 44%.

Final Deprotection. Catalytic hydrogenation of compounds **4**–**7** with Pd/C in the presence of acetic acid (24–48 h) removed the Cbz protecting groups, yielding the final derivatives: 3-*N*-methyl-neomycin B (**8**), 3-*N,N*-dimethyl-neomycin B (**9**), 3-*N*-propyl-neomycin B (**10**), and 3-*N*-hexyl-neomycin B (**11**). The synthetic pathway for these derivatives is outlined in Figure 2.5.

Structural Confirmation. The structures of all derivatives were confirmed using ^{1}H NMR, ^{13}C NMR, 2D NMR, heteronuclear single quantum coherence (HSQC), and high-resolution mass spectrometry (HRMS). Total correlation spectroscopy (TOCSY) and correlation spectroscopy (COSY) were also performed to assign NMR signals.

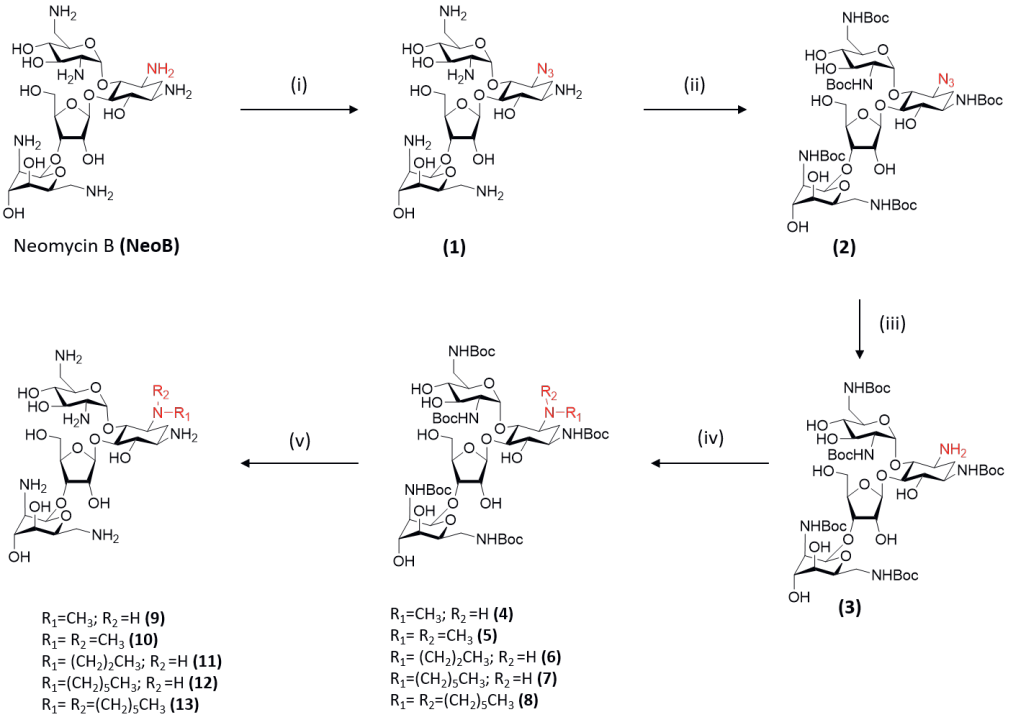


Figure 2.5 | Synthetic pathway of 3-N- and 3-N,N-alkylated aminoglycosides. Reagents, reactions conditions, and isolated yields: i) imidazole sulfonyl-1-azide·xHCl, H_2O, pH=6.8, RT, 40h, 70%; ii) N-(benzyloxycarbonyloxy)succinimide, THF/H_2O, RT, 48h, 58%; iii) $P(CH_3)_3$, THF/H_2O, NaOH, reflux, 2h, 46%; iv-a) methyl-trifluoromethanesulphonate, hexafluoroisopropanol, RT, 2h, 78%; iv-b) formaldehyde, $NaBH_3CN$, acetic acid (cat.), RT, 3h, 90%; iv-c) propanal, $NaBH_3CN$, acetic acid (cat.), RT, 2h, 96%; iv-d) hexanal, $NaBH_3CN$, acetic acid (cat.), RT, 2h, 44%; v) H_2, Pd/C (20% wt), CH_3COOH (cat.), RT, 24-72h, quantitatively.

EVALUATION OF THE ANTIBACTERIAL ACTIVITY OF NEO B DERIVATIVES

The antibacterial activity of NEO B and its alkylated analogues was assessed by estimating their Minimal Inhibitory Concentrations (MICs)against *E. coli* ATCC25922 (non-resistant strain) and the same strain overexpressing the gene encoding AAC(3)-IIIa. MICs were determined from bacterial growth curves recorded in the presence of varying concentrations of each compound.

As summarized in Table 2.1, all alkylated derivatives exhibited reduced activity against the non-resistant strain compared to the parent compound. NEO B displayed an MIC of 8 μM,

whereas the mono-methylated, mono-propylated, and mono-hexylated derivatives showed MICs of 32μM, 128μM, and 256μM, respectively. The N,N-dimethylated derivative failed to inhibit bacterial growth within the tested concentration range.

These results underscore the critical role of the 3-C amine in NEO B's antimicrobial activity. Furthermore, the observed trend indicates that longer alkyl chains negatively impact antibacterial efficacy, likely due to increased steric hindrance, which may reduce binding affinity to the ribosome.

In contrast to the non-resistant strain, NEO B was unable to inhibit bacterial growth in the resistant strain overexpressing AAC(3)-IIIa within the tested concentration range. However, all N-alkylated derivatives demonstrated improved activity compared to the parent compound. Notably, the MICs of the derivatives were unaffected by the expression of AAC(3)-IIIa, suggesting resistance to enzymatic inactivation.

Among the derivatives, compound 8 exhibited the most potent activity, fully inhibiting bacterial growth at a concentration of 32μM. The 3-N-propylated (**10**) and 3-N-hexylated (**11**) derivatives displayed MICs of 128μM and 256μM, respectively. These findings indicate that derivatives **8**, **10**, and **11** retain the ability to bind the bacterial ribosome while evading AAC(3)-IIIa-mediated inactivation.

Given its superior performance, compound **8** was selected for further investigation.

Table 2.1 | Antimicrobial activity of NEO B and 3-N-modified derivatives against *E. coli* ATCC 25922 and the same strain expressing AAC(3)-IIIa. Antimicrobial susceptibility was determined in liquid culture, and MIC values are reported in μM.

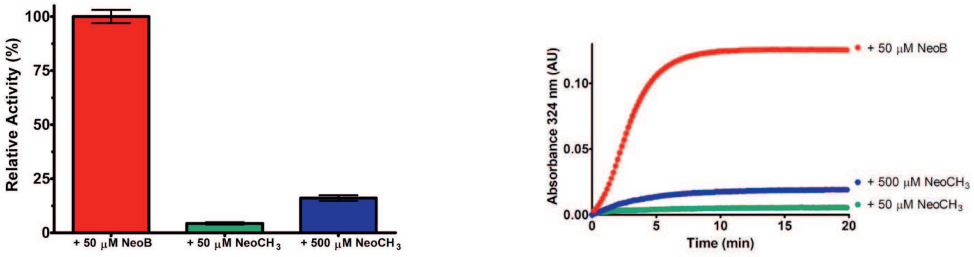
Compound	***E. coli* (no resistance)**	***E. coli* (AAC(3)-IIIa)**
Neomycin B (NEO B)	8	> 512
3-C-azido NEO B **(1)**	> 512	> 512
3-N-methyl NEO B **(8)**	32	32
3-N,N-dimethyl NEO B **(9)**	> 512	> 512
3-N-propyl NEO B **(10)**	128	128
3-N-hexyl NEO B **(11)**	256	256

3-N-METHYLATION OF NEO B DRAMATICALLY REDUCES AAC(3)-IIIA CATALYSIS WHILE RETAINING RIBOSOMAL BINDING

As shown in Figure 2.6, the acetyltransferase activity of AAC(3)-IIIa with 3-N-methyl NEO B (compound **8**) is significantly reduced, achieving only 4% of the conversion observed with NEO B at a concentration of 50 μM. Increasing the concentration of compound **8** by tenfold results in only a marginal increase in conversion, confirming that this derivative is a very poor substrate for the enzyme. Consequently, the estimation of its kinetic parameters is inaccurate.

The structural basis for this reduced activity was elucidated through the crystal structure of AAC(3)-IIIa co-crystallized with compound **8**. Despite differing from NEO B by only a single methyl group at position 3-C, compound **8** adopts a distinct binding orientation within the enzyme's active site. Specifically, the derivative is rotated by 90° compared to NEO B, as

illustrated in Figure 2.7. This rotation repositions ring I of the methylated derivative to occupy the space where ring II of NEO B would typically bind.



(a) (b)

Figure 2.6 | NEO and Neo-CH_3 as substrates of AAC(3)-IIIa. (a) The acetyltransferase activity is monitored after the addition of 50 μM NEO (red), 50 μM (green), or 500 μM (blue) Neo-CH_3. (b) Time course of the reaction, with all other components fixed; the reported values correspond to the end-point measurements.

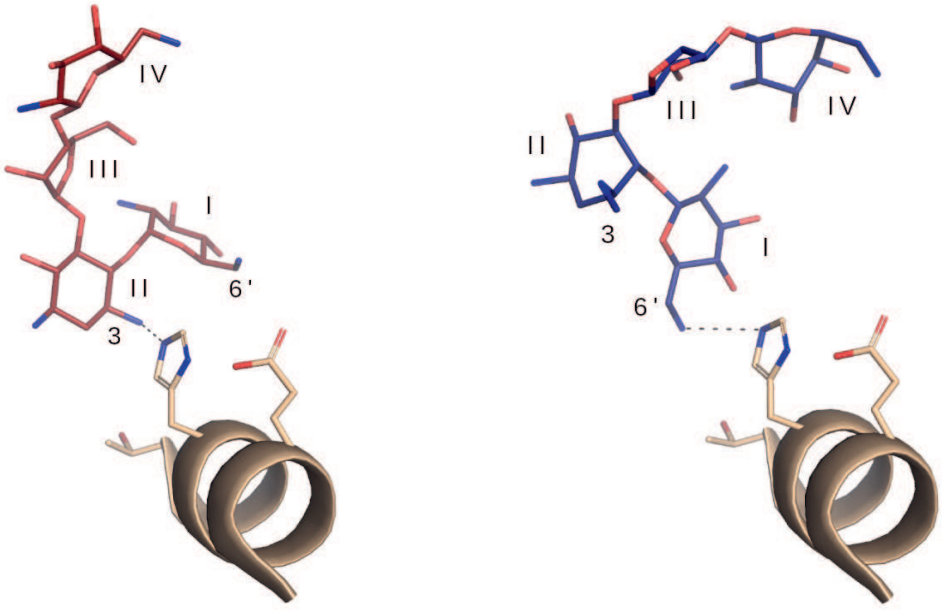
In this unique conformation, the methylated 3-N group is positioned far from the active site, rendering acetylation at this position impossible. This structural insight explains why compound **8** exhibits poor substrate characteristics while highlighting its potential to evade AAC(3)-IIIa-mediated inactivation.

The amine attached to position 6' in compound **8** coordinates with the N^{ϵ} atom of His196, suggesting that the residual catalytic activity observed for this derivative may be attributed to the acetylation of this group. This dramatic effect on binding is surprising given the small structural difference between compound **8** and its parent NEO B. It is likely a consequence of AAC(3)-IIIa's inherent ability to accommodate structurally diverse substrates, a characteristic shared with other members of this enzyme class [45, 48].

The capacity of AAC(3)-IIIa to bind and modify structurally distinct AGs with minimal reorganization of its binding pocket appears to facilitate the accommodation of compound **8** in the active site. To our knowledge, this represents the first documented case of a significant reorientation of anAGderivative within the active site of AMEs, highlighting the remarkable structural adaptability of AAC(3)-IIIa.

To further investigate the mechanism of action of compound **8**, we examined whether the addition of the methyl group at the 3-C position affects its binding to the ribosome. A Cryo-EM structure of the *E. coli* 70S ribosome in complex with compound **8** reveals that the methylation does not disrupt ribosomal binding (Figure 2.8). Only minimal differences are observed in the positioning of rings I and IV, with the methyl group projecting outward from the A-site. This configuration allows the ribosome to accommodate the modification without disrupting the interaction network within the binding site.

Compound **8** binds the 30S ribosomal A-site in a manner similar to NEO B, inducing the "flipped-out" conformation of the "sensor" residues A1492 and A1493, mimicking the state observed during mRNA decoding (Figure 2.9) [49]. These findings suggest that the ribosome can likely accommodate other alkyl substitutions at the 3-C position. Further studies are



(a) (b)

Figure 2.7 | (a) Cartoon and stick representation of NEO B (red) binding to the active site of AAC(3)-IIIa. (b) When compared to NEO B, 3-N-methyl NEO B (blue) binds AAC(3)-IIIa with a 90° rotation and exposes the 6′-N-amino group (3.5 Å) on the ring I to His196 while the methylated amine in position 3 is positioned away from the active site.

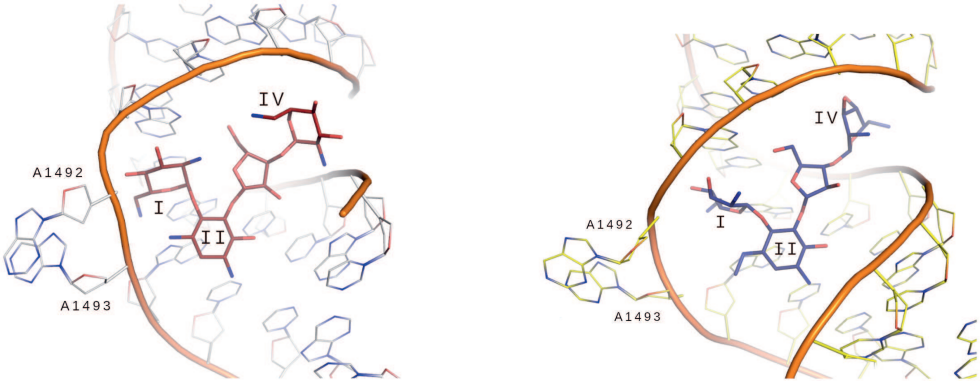
warranted to determine whether such modifications influence the aminoglycoside uptake mechanism.

2.3. CONCLUSION

The crystal structures of the aminoacyltransferase AAC(3)-IIIa and its complexes with NEO B and AcCOA have been successfully resolved. These structures provide insights into the enzyme's catalytic mechanism, which involves the transfer of an acetyl group from AcCOA to the amine at the 3-C position of NEO B. This process is mediated by a non-canonical catalytic triad comprising His196, Glu199, and the aminoglycoside (AG) substrate.

Biochemical assays identified NEO B and AcCOA as natural substrates of AAC(3)-IIIa, with affinities in the micromolar range. Additionally, AAC(3)-IIIa demonstrated substrate promiscuity, efficiently modifying several AGs, consistent with the behavior of other AAC enzymes. Among the tested AGs, GEN exhibited the highest reactivity, followed by NEO B, KAN, and PAR.

In contrast, AMK was not identified as a cognate substrate for AAC(3)-IIIa. Utilizing



(a) (b)

Figure 2.8 | (a) Cartoon and stick representation of the Cryo-EM structure of the *E. coli* 70S ribosome in complex with NEO B (red, PDB code 4V52). (b) Like its parent compound, 3-N-methyl NEO B (blue) binds the ribosome at the A-site with minimal differences in the positioning of rings I and IV.

our previously established methodology to selectively modify the 3-N position in AGs, we synthesized and evaluated a library of 3-N-alkylated and 3-N,N-dialkylated NEO B derivatives. All derivatives exhibited reduced antimicrobial activity compared to the parent compound NEO B. Among them, 3-N-methyl NEO B demonstrated a relatively modest 4-fold reduction in MIC against the non-resistant strain compared to unmodified NEO B, highlighting its potential as a viable candidate for further optimization.

N-alkylated derivatives **8**, **10**, and **11** demonstrated improved activity against the resistant strain. Notably, the mono-methylation of NEO B (compound 8) revealed how a minimal structural modification could significantly reduce substrate affinity for AAC(3)-IIIa. This derivative evaded enzymatic catalysis, showing only 4% to 1% acetylation across the tested concentration range.

This reduced enzymatic activity is attributed to an unexpected change in the substrate's binding orientation within AAC(3)-IIIa. The reoriented binding exposed a different molecular surface to the active site, thereby lowering the catalytic efficiency. Such reorientation likely stems from the inherent substrate promiscuity of AACs and AMEs in general.

As hypothesized, the methylation at the 3-C position did not affect the ability of NEO B to bind the ribosome, as confirmed by the Cryo-EM structure. These findings establish compound **8** as a promising lead for further drug optimization, offering a potential strategy to overcome AAC(3)-IIIa-mediated resistance while retaining ribosomal targeting.

Although sparsely investigated, the modification of the 3-C position in 4,5-disubstituted AGs presents a promising strategy for the design of novel AGs. This study has demonstrated that chemical alkylation at the 3-C position can be achieved with minimal synthetic effort, requiring only five steps.

The successful 3-N-methylation of NEO B allowed us to overcome AAC(3)-IIIa-mediated antimicrobial resistance, showcasing the potential of this approach to produce novel, active compounds. These findings provide a foundation for expanding the repertoire of effective

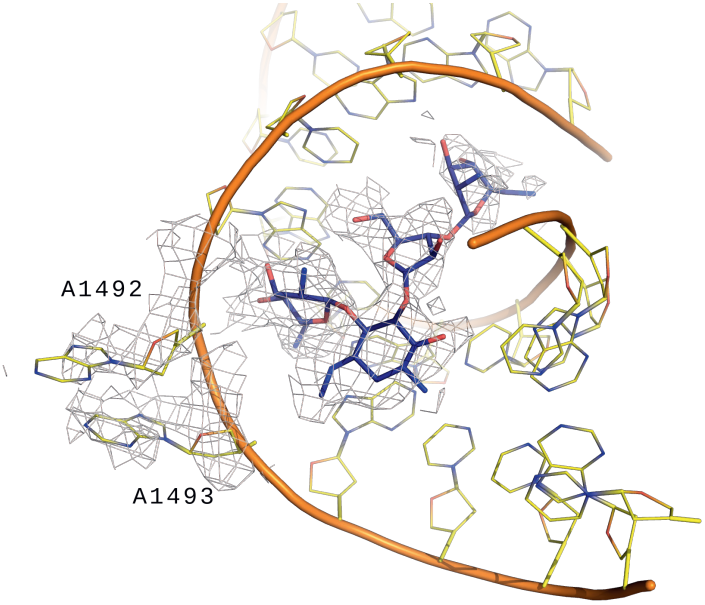


Figure 2.9 | Cryo-EM map (2.8σ) of the 3-N-methyl neomycin B (blue) bound to the A-site (yellow) of the *E. coli* 30S ribosomal subunit.

antibiotics and addressing the growing challenge of drug-resistant bacterial infections.

2.4. METHODS

PROTEIN EXPRESSION AND PURIFICATION

CLONING OF PET28B(+)-AAC(3)-IIIA

The Open Reading Frame (ORF) of the gene encoding AAC(3)-IIIa was codon-optimized for *E. coli* expression and synthesized by IDT Technologies (Belgium). NdeI and HindIII restriction sites were added to the 5′ and 3′ ends, respectively. The synthesized gene was initially ligated into the pJET1.2/blunt vector (Thermo Fisher) using a blunt-end ligation approach and subsequently transformed into chemically competent *E. coli* DH5α cells (Invitrogen) for propagation.

The target gene was excised from the pJET1.2/blunt vector using NdeI and HindIII restriction enzymes (NEB) and subcloned into the pET28b(+) vector (Merck). This construct, named pET28b(+)-*aac3*, encodes AAC(3)-IIIa with an N-terminal His-tag containing a thrombin cleavage site. The resulting plasmid was transformed into *E. coli* BL21 (DE3) cells (Merck) for overexpression of the recombinant protein.

OVEREXPRESSION AND PURIFICATION

The AAC(3)-IIIa protein was overexpressed using standard protocols. Briefly, *E. coli* BL21 (DE3) cells transformed with pET28b(+)-*aac3* were grown in LB medium supplemented with 50 μg/mLKAN A sulfate (Thermo Fisher) at 37 °C. Protein overexpression was induced by adding 1 mM IPTG (Thermo Fisher) once the culture reached an OD_{600} of 0.6. After induction, the cells were incubated for 16 h at 22 °C.

Cells were harvested by centrifugation at 7460 × *g* for 10 min at 4 °C and washed once with 50 mM K_3PO_4 buffer (pH 7.5). The cell pellet was then resuspended in lysis buffer containing 50 mM K_3PO_4, 500 mM NaCl, 1 mM $MgSO_4$, 10 mM imidazole, and 1 mM PMSF protease inhibitor (pH 7.5). Pancreatic bovine DNase (50 μg) was added to the suspension to degrade nucleic acids.

Cells were lysed using a constant cell disruptor (Constant Systems Ltd.) at a pressure of 25 kpsi. The resulting lysate was cleared of cell debris and membrane fractions by ultracentrifugation at 186,000 × *g* for 60 min at 4 °C. The supernatant containing soluble AAC(3)-IIIa protein was collected for further purification.

The cleared supernatant was loaded onto a 5 mL Ni-Sepharose column (GE Healthcare) pre-equilibrated with wash buffer containing 50 mM K_3PO_4, 500 mM NaCl, 30 mM imidazole, 5 mM $MgCl_2$, pH 7.5. To remove any acetyl coenzyme A (Ac-CoA) bound to the active site, the protein was chemically denatured while bound to the column.

The column was washed sequentially with four column volumes (CV) of wash buffer supplemented with varying concentrations of guanidinium chloride (4.0 M, 2.0 M, 1.0 M, and 0.5 M). A final wash step was performed using 8 CV of wash buffer without guanidinium chloride to remove residual contaminants.

The apo-protein was eluted using an elution buffer containing 50 mM K_3PO_4, 500 mM NaCl, 300 mM imidazole, 5 mM $MgCl_2$, and 20% glycerol (pH 7.5). Elution fractions containing the target protein were pooled, flash-frozen in liquid nitrogen, and stored for further use.

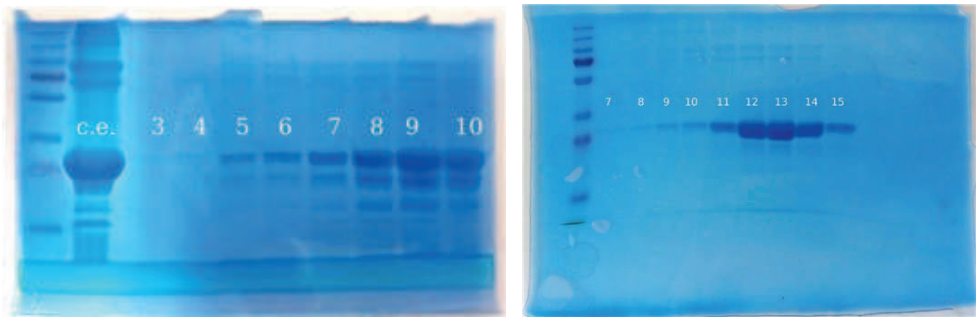
FURTHER PURIFICATION BY SIZE-EXCLUSION CHROMATOGRAPHY

The target protein was further purified by Size-Exclusion Chromatography (SEC) using a Superdex 200 10/300 GL gel filtration column (GE Healthcare). The column was equilibrated with elution buffer consisting of 20 mM HEPES, 100 mM NaCl, and 1 mM $MgCl_2$, pH 7.0.

Eluted fractions were analyzed by SDS–PAGE to confirm the purity of the protein (see Figure 2.10). Fractions containing the purified target protein were collected for downstream applications.

When required, peak fractions were concentrated to 20 mg/mL using a Vivaspin 10 kDa molecular weight cut-off concentrator (GE Healthcare). Protein concentration was determined spectrophotometrically.

The oligomeric state of AAC(3)-IIIa was assessed by SEC coupled with SEC (see Figure 2.11). The combined approach provided insights into the quaternary structure and molecular weight of the protein in solution.



(a) **(b)**

Figure 2.10 | (a) Coomassie blue-stained 15% Tris-HCl SDS-PAGE gel showing the cell lysate (c.e.), and diffferent aliquotes (3-10) of the purified AAC(3)-IIIa eluting from the IMAC (b) SDS-PAGE gel showing the purified AAC(3)-IIIa. Lanes 7-15 corresponds to the different aliquotes eluting from the SEC.

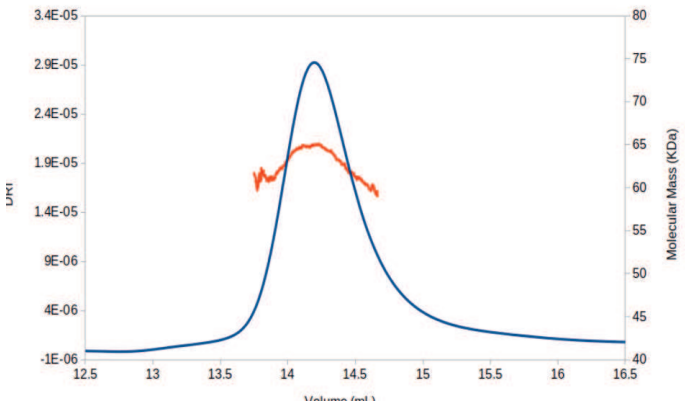


Figure 2.11 | SEC-LS analysis of AAC(3)-IIIa. The column was equilibrated with 20 mM HEPES/KOH, 150 mM NaCl (pH 7.1), and the protein was dissolved in the same buffer. The chromatogram shows the detector readings of the LS and Differential Refractive Index (DRI) in red and blue, respectively. The molecular mass (scale on the right-hand axis) of AAC(3)-IIIa reveals a dimeric assembly of the protein in solution.

2.5. AAC(3)-IIIA STRUCTURAL CHARACTERIZATION

CRYSTALLIZATION

AAC(3)-IIIa was crystallized using the hanging-drop vapor diffusion technique. Equal volumes (1 μL each) of apo-protein solution (10–20 mg/mL) and crystallization solution (7–14% PEG 10,000, 0.1 M sodium acetate, and 0.1 M Bis-Tris, pH 5.5) were mixed and allowed to equilibrate at room temperature. Crystals appeared within a week and ceased growing after two weeks.

NEO B and Neo-CH_3 were pre-treated by stirring overnight with ion-exchange resin Amberlite CG-50 type 1 (Acros Organics), followed by filtration and lyophilization to ensure purity for crystallographic studies. The different AAC(3)-IIIa complexes were prepared by soaking crystals in the mother liquor, adjusted to a final concentration of 5 mM of the respective compound, for 1–2 hours. The ternary AAC(3)-IIIa–NEO–AcCOA complex was obtained by soaking pre-formed AAC(3)-IIIa–NEO crystals in mother liquor supplemented with 5 mM NEO B and 5 mM AcCOA. Stock solutions of the ligands were prepared in water.

DATA COLLECTION, MODEL BUILDING AND REFINEMENT

X-ray diffraction data for AAC(3)-IIIa crystals soaked with Neo-CH_3 were collected *in-house* using an ENRAF–Nonius CuKα rotating anode generator equipped with a Mac–Science DIP2030 image plate detector. Data for the AAC(3)-IIIa–AcCOA complex were collected at the EPFL/PSI X-Treme beamline at the Swiss Light Source (Paul Scherrer Institute, Villigen, Switzerland). Additional diffraction data for other complexes were collected at the PETRA III P13 and P14 photon beamlines at DESY (Hamburg, Germany).

All datasets were processed using XDS. Initial models were obtained using the BALBES pipeline and subsequently refined using the program PHASER for molecular replacement (MR).

All crystals were confirmed to belong to the space group $P2_12_12$, as determined by POINTLESS. The electron density maps were unambiguous, allowing for the modeling of residues starting from position 22. Models were built using COOT, with refinement and validation steps performed in PHENIX. Non-crystallographic symmetry (NCS) restraints were not applied during refinement. Data collection and refinemnet statistics are listed in Table 2.2.

Table 2.2 | Data collection and refinement statistics. Statistics for the highest-resolution shell are shown in parentheses.

Ligand	**NEO B**	**AcCOA**	**Neo-CH_3 (1)**	**Neo-CH_3 (2)**	**NEO+AcCOA**
PDB code	–	–	–	–	–
Wavelength	0.99	0.99	CuKα	CuKα	0.99
Space group	P 21 21 2	P 21 2 21	P 2 21 21	P 21 21 2	P 21 2 21
Z	2	4	2	2	4
Unit cell (Å)					
a	89.279	91.037	64.59	89.004	90.957
b	103.047	100.803	89.235	103.122	100.489
c	65.244	132.206	103.248	64.555	131.908
$\alpha = \beta = \gamma$	90°	90°	90°	90°	90°
Total reflections	189,248 (13,687)	184,795 (18,126)	309,057 (17,054)	400,648 (31,072)	738,242 (71,860)
Unique reflections	102,050 (8,356)	93,200 (9,196)	43,209 (3,999)	53,217 (4,801)	219,293 (21,854)
Multiplicity	1.9 (1.6)	2.0 (2.0)	7.2 (4.3)	7.5 (6.5)	3.4 (3.3)
Completeness (%)	95.26 (79.25)	99.54 (98.42)	99.13 (93.41)	98.20 (88.71)	98.50 (98.90)
$\langle I \rangle / \sigma(I)$	14.74 (0.92)	6.00 (0.54)	8.04 (1.05)	5.72 (0.61)	11.90 (0.87)
Wilson *B* factor	22.59	37.94	29.50	26.87	20.28
R-merge	0.02061 (0.7824)	0.1315 (1.496)	0.1743 (1.022)	0.2592 (1.628)	0.0497 (1.398)
R-meas	0.02915 (1.106)	0.186 (2.116)	0.1878 (1.157)	0.2782 (1.768)	0.05888 (1.67)
R-pim	0.02061 (0.7824)	0.1315 (1.496)	0.06882 (0.5267)	0.09973 (0.6739)	0.031 (0.8962)
$CC_{1/2}$	0.999 (0.474)	0.972 (0.198)	0.996 (0.551)	0.990 (0.287)	0.999 (0.385)
CC*	1 (0.802)	0.993 (0.575)	0.999 (0.843)	0.997 (0.668)	1 (0.746)
No. reflections	102,027 (8,346)	93,012 (9,087)	43,185 (3,998)	53,030 (4,706)	219,125 (21,801)
No. reflections (R-free)	5,014 (402)	4,675 (453)	2,133 (207)	2,619 (220)	10,949 (1,112)
R-work	0.1805 (0.4207)	0.2433 (0.4621)	0.1917 (0.3295)	0.1948 (0.3321)	0.1816 (0.4036)
R-free	0.2117 (0.4567)	0.2920 (0.4907)	0.2324 (0.3432)	0.2338 (0.3706)	0.2070 (0.4093)
CC(work)	0.969 (0.721)	0.956 (0.518)	0.967 (0.713)	0.962 (0.651)	0.970 (0.681)
CC(free)	0.949 (0.628)	0.927 (0.445)	0.941 (0.628)	0.949 (0.647)	0.959 (0.668)
No. non-H atoms	4,830	8,698	4,688	4,710	9,898
macromolecules	4,152	8,102	4,125	4,106	8,341
ligands	166	329	69	105	414
solvent	512	267	494	499	1,143
Protein residues	530	1,044	527	528	1,059

Table 2.2 (continued): Data collection and refinement statistics.

Ligand	**NEO B**	**AcCOA**	**Neo-CH_3 (1)**	**Neo-CH_3 (2)**	**NEO B+AcCOA**
RMS (bonds)	0.007	0.012	0.039	0.010	0.006
RMS (angles)	0.92	1.40	1.39	1.17	0.80
Ramachandran					
favored (%)	98.10	96.62	97.13	97.51	97.43
allowed (%)	1.90	2.99	2.68	2.30	2.38
outliers (%)	0.00	0.39	0.19	0.19	0.19
Rotamer outliers (%)	0.00	0.73	0.18	1.43	0.23
Clashscore	3.96	5.22	2.42	3.37	1.64
Av. *B*-factor	30.37	45.78	30.32	31.09	25.45
macromolecules	28.59	45.38	30.29	29.85	23.77
ligands	47.59	55.05	30.65	52.52	34.16
solvent	39.28	46.44	39.54	36.78	34.51
No. of TLS groups	13	21	13	14	–

2.6. ENZYMATIC ASSAY

PROTEIN PURIFICATION

To assess the enzymatic activity of AAC(3)-IIIa, the protein was purified without the denaturation/renaturation step using guanidinium chloride. Following the Ni-Sepharose column purification described earlier, the cell lysate was loaded onto the column and washed with washing buffer. The target protein was eluted using elution buffer, and the eluted fractions were pooled and flash-frozen in liquid nitrogen. The protein was further purified by SEC, as previously detailed.

ENZYMATIC ASSAYS OF AAC(3)-IIIA

The acetyltransferase activity of AAC(3)-IIIa was monitored by coupling the formation of CoA–SH with the DTDP assay ($\varepsilon = 1.98 \times 10^4\ \mathrm{M^{-1}cm^{-1}}$). The reaction product, 4-thiopyridone, enabled real-time monitoring via absorbance measurement at 324 nm. All enzymatic and kinetic assays were performed at 30 °C using a Spark 10M microplate reader (Tecan). Freshly prepared DTDP was used for each assay to ensure accurate and reliable results.

DETERMINATION OF KINETIC PARAMETERS

For determining the kinetic parameters of NEO B, reaction mixtures were prepared containing 100 μM AcCOA, 340 nM AAC(3)-IIIa, and 0.2 mM DTDP in activity buffer, with a total reaction volume of 200 μL. The assays were initiated by adding variable concentrations of aminoglycoside (0.5–200 μM). The reaction velocity increased with NEO B concentration similar to Michaelis–Menten behavior at low concentrations, but at higher concentrations the velocity decreased, indicating substrate inhibition. Kinetic parameters were fitted using a substrate inhibition model:

$$v = \frac{V_{\max}[S]}{K_{\mathrm{m}} + [S]\left(1 + \frac{[S]}{K_i}\right)} \tag{2.1}$$

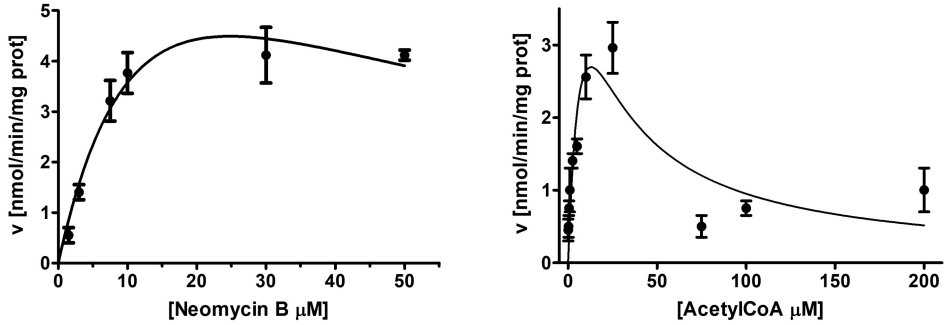
Equation | 2.1 where $[S]$ is the NEO B concentration, $V_{\max}$ is the maximal velocity, K_{m} is the Michaelis constant, and K_i is the inhibition constant.

For AcCOA kinetics, NEO B was included at a fixed concentration of 200 μM, while the AcCOA concentration was varied (0.3–200 μM). The reaction velocity initially increased with AcCOA concentration, reached a peak, and then rapidly decreased at higher concentrations, consistent with a mixed inhibition effect. Kinetic parameters were estimated using a mixed inhibition model:

$$v = \frac{V_{\max}[S]}{K_{\mathrm{m}}\left(1 + \frac{[I]}{K_i}\right) + [S]\left(1 + \frac{[I]}{K_i'}\right)} \tag{2.2}$$

Equation | 2.2 where $[S]$ is the AcCOA concentration, $[I]$ represents an inhibitory effect from high substrate concentration, $V_{\max}$ is the maximal velocity, K_{m} is the Michaelis constant, and K_i and K_i' are inhibition constants.

All kinetic parameters were estimated from two independent protein purification batches (see Figure 2.12).
When comparing pristine NEO B to its derivatives or assessing activity with other natural antibiotics, reaction mixtures contained 100 μM AcCOA, 1.7 μM AAC(3)-IIIa, 0.2 mM DTDP, 10 mM HEPES, and 100 mM NaCl at pH 7.1. These assays were initiated by adding 50 μM aminoglycoside unless specified otherwise.



(a) (b)

Figure 2.12 | Kinetics of AAC(3)-IIIa-IIIa for neomycin B (a) and acetyl coenzyme A (b). (a) Reaction velocity as a function of NEO B concentration shows substrate inhibition: the velocity increases at low concentrations but decreases at higher concentrations. Data were fitted to a substrate inhibition model (Equation 2.1). (b) Reaction velocity as a function of AcCOA concentration. Data were fitted to a mixed inhibition model (Equation 2.2). All data represent two independent protein purification batches.

CLONING OF *pBluescript-aacC3*

The ORF encoding the AAC(3)-IIIa from *Pseudomonas aeruginosa* PST-I was codon-optimized for expression in *Escherichia coli* under the control of a constitutive synthetic lipoprotein promoter and positioned upstream of the *rrnC* transcription terminator. The gene was synthesized by IDT Technologies (Belgium) and initially subcloned into the pJET1.2/blunt vector (Thermo Fisher), yielding pJET-*aacC3*.
The pJET-*aacC3* plasmid was digested with restriction endonucleases *EcoRI* and *PstI*, and the insert was subcloned into the pBluescript SK plasmid, forming pBlue-*aacC3*. The construct was sequenced to confirm the correct reading frame. The resulting plasmid was transformed into *E. coli* strain ATCC 25922, which was grown in LB Lennox broth (Sigma–Aldrich).

MIC DETERMINATION

Pre-cultures of *E. coli* ATCC 25922 and *E. coli* harboring the pBlue-*aacC3* plasmid encoding the aminoglycoside resistance gene were prepared from frozen stocks. These cultures were grown in Mueller–Hinton Broth 2 (Sigma–Aldrich) at 37 °C and 220 rpm.
The cultures were diluted with fresh medium to an optical density at 600 nm (OD_{600}) of 0.05,

and 200 μL aliquots were added to 2 mL DeepWell 96-well plates (Nunc) containing serial twofold dilutions of NEO B and derivatives **8**–**11**. The concentrations ranged from 512 μM to 0.5 μM. Control wells without aminoglycosides were included.
All tests were performed in triplicate. Following overnight incubation at 37 °C and 220 rpm, 200 μL of each culture was transferred to 96-well microplates, and the OD_{600} was measured using a SpectraMax M3 microplate reader (Molecular Devices).

2.7. CRYO-EM STRUCTURE OF THE 70S *E. coli* RIBOSOME

SAMPLE PREPARATION AND DATA COLLECTION

The 70S ribosome from *E. coli* was obtained from BioKe (P0763S). The ribosome–Neo-CH_3 complex was prepared by diluting the ribosome (1 g/L) in blotting buffer (10 mM Tris, 20 mM magnesium acetate, 20 mM ammonium acetate, 100 mM KCl, 6 mM β-mercaptoethanol, pH 7.0) in the presence of Neo-CH_3 at a 1:100 molar ratio.
Aliquots of 2.7 μL of the prepared sample were applied to freshly glow-discharged holey carbon grids (Quantifoil Cu R1.2/1.3 with carbon support, 200 mesh). Excess liquid was blotted for 3–5 s using an FEI Vitrobot Mark IV, and the grids were plunge-frozen in liquid ethane at approximately 100 K.
The frozen grids were transferred into a Titan Talos Arctica 200 keV microscope (Thermo Fisher) equipped with a K2 direct-electron detector (Gatan). Zero-loss images were recorded semi-automatically using the UCSF Image script. The GIF-quantum energy filter slit width was set to 20 eV. Images were collected at a nominal magnification of 130,000×, yielding a pixel size of 1.012 Å, with a defocus range of −0.5 to −3.0 μm. A total of 927 movie images were collected, with 60 frAMEs dose-fractionated over 40 s.

DATA PROCESSING AND RECONSTRUCTION

- **Motion correction and CTF estimation:** Performed using CRYOSPARC.
- **Particle picking and classification:** Template-based particle picking, 2D classification, *ab initio* volume generation, and non-uniform 3D refinement were performed in CRYOSPARC. No symmetry was applied unless stated otherwise.
- **Map sharpening:** Maps were sharpened using the AUTOSHARPEN MAP procedure in PHENIX.
- **Model building:** Sharpened maps were used for manual model building in COOT. Coordinates were refined using the Real Space Refine module in PHENIX.

Figure 2.13 illustrates the steps involved in the reconstruction of the 70S ribosome. Data collection and refinement statistics are summarized in Table 2.3.

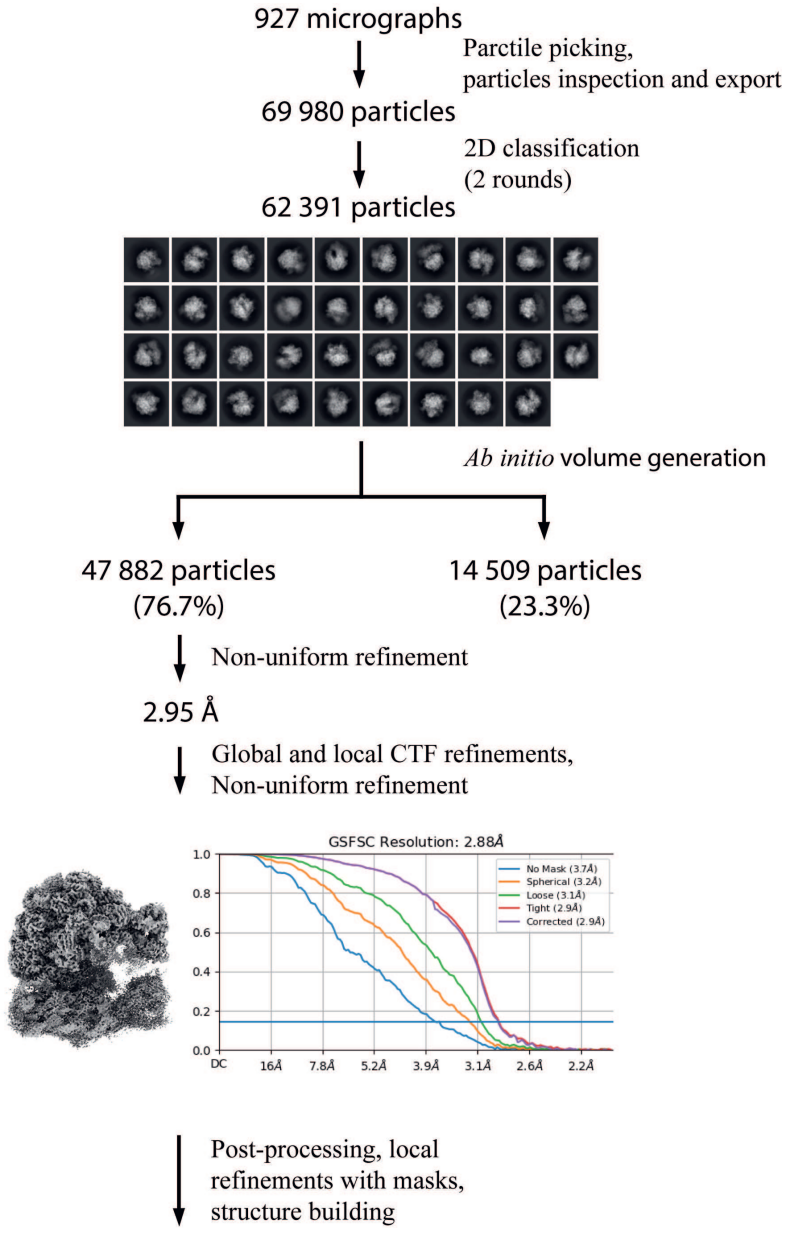


Figure 2.13 | Cryo-EM reconstruction of the 70S *E. coli* ribosome.

Table 2.3 | Data collection and refinement statistics relative to the cryo-EM structure of the 30S ribosomal subunit.

Data collection	
Microscope	Titan Talos Arctica
Detector	k2-detector
Voltage	200 kV
Pixel size (Å)	1.012
Micrographs collected	927
Electron exposure ($e^- \cdot Å^{-2}$)	53.6
Defocus range	-0.5 -0.3
Symmetry imposed	C1
Refinement	
Particles	47,882
Resolution (Å; at FSC=0.143)	2.88
CC (model to map fit)	0.7267
RMS deviations	
Bonds (Å) (# > 4σ)	0.004
Angles (°)	(# > 4σ) 0.649
Validation	
Clashscore	16.91
Ramachandran favored (%)	88.67
Ramachandran allowed (%)	10.21
Ramachandran outliers (%)	1.12

2.8. SYNTHESIS OF 3-*N*-ALKYLATED NEOMYCIN B DERIVATIVES

GENERAL METHODS

All reagents and solvents were obtained from commercial suppliers (Sigma–Aldrich, Acros, TCI) and used without further purification. Argon and hydrogen gases were purchased from Linde. Reaction buffer pH adjustments were performed using a Hanna Instruments pH 209 meter equipped with a glass combination electrode.
Thin-layer chromatography (TLC) was conducted on silica gel 60 F254 pre-coated plates (0.25 mm, Merck). Compound visualization was achieved by staining with a 2% ninhydrin solution in methanol, followed by heating. Column chromatography was carried out using silica gel (60–120 mesh) for purification.
Automated flash chromatography was performed on a Grace Reveleris R Prep purification system equipped with ELSD laser and UV detectors (path lengths: 0.1, 0.3, 0.6, and 1.3 mm). Various Reveleris R silica, C18, and amine columns (ranging from 4 to 24 g) were employed based on purification requirements.
The detailed synthesis procedures for all compounds are provided in Appendix A at the end of this chapter.

NUCLEAR MAGNETIC RESONANCE (NMR) SPECTROSCOPY

NMR spectra were recorded at 25 °C on the following instruments:

- Bruker (600 MHz for ^{1}H–NMR and 152 MHz for ^{13}C–NMR),
- Varian Unity Inova (500 MHz for ^{1}H–NMR and 125.7 MHz for ^{13}C–NMR),
- Varian AMX400 (400 MHz for ^{1}H–NMR and 100.59 MHz for ^{13}C–NMR).

Additional experiments such as Attached Proton Test (APT), Total Correlation Spectroscopy (TOCSY), Correlation Spectroscopy (COSY), and Heteronuclear Single Quantum Coherence (HSQC) were performed to assist in signal assignments.
NMR experiments were conducted using MeOD-d_4 or D_2O as solvents. Chemical shifts (δ) are reported in ppm relative to the solvent resonance as the internal standard:

- MeOD-d_4: δ 3.31 (^{1}H), δ 49.2 (^{13}C),
- D_2O: δ 4.80 (^{1}H).

Data are reported as follows: chemical shift (δ), multiplicity (s = singlet, s(br) = broad singlet, d = doublet, t = triplet, q = quartet, m = multiplet), coupling constants (J in Hz), integration, and signal assignment.

HIGH-RESOLUTION MASS SPECTROMETRY (HRMS)

HRMS analysis was carried out using an LTQ Orbitrap XL instrument (Thermo Scientific) equipped with electrospray ionization in positive or negative ion modes (ESI^+/ESI^-).

LIQUID CHROMATOGRAPHY–MASS SPECTROMETRY (LC–MS)

LC–MS analysis of selected samples was performed using a Waters AQUITY H-class UPLC system equipped with a TUV detector and a Xevo G2 TOF mass detector (Waters Chromatography BV). The separations were carried out on an AQUITY UPLC C18 column with a particle size of 1.7 μm. The column temperature was maintained at 35 °C, and samples were eluted at a flow rate of 0.3 mL/min using a linear gradient of buffer A to buffer B:

- Buffer A: 95% water containing 100 mM trifluoroacetic acid (TFA), 5% acetonitrile,
- Buffer B: 95% acetonitrile, 5% water containing 100 mM TFA.

The gradient transitioned from 95% buffer A to 5% buffer A over the course of the analysis.

HIGH-RESOLUTION CHROMATOGRAPHIC SEPARATIONS

High-resolution chromatographic separations (HRMS) were carried out using a Shimadzu VP series High-Performance Liquid Chromatography (HPLC) modular system. The system included the following components:

- DGU-14A3 online vacuum degasser,
- Two LC-20AT pumps,
- SIL-20A autosampler,
- CTP-20A column oven,
- RID-10 refractive index detector,
- FRC-10 fraction collector.

All operations were managed using Shimadzu LCsolution software.

HPLC PURIFICATION

HPLC purifications were performed on a Gemini NX–C18 semi-preparative column (250 × 10 mm) with spherical particles of 5 μm and 110 Å pore size. Isocratic elution was employed using a mobile phase of water/acetone (1/0.9) containing 12.4 mM heptafluorobutyric acid (HFBA). The flow rate was set to 4 mL/min, and the column temperature was maintained at 40 °C.

ACKNOWLEDGEMENTS

The authors thank Dr. C. Piamonteze for assistance with data collection at the EPFL/PSI X-Treme beamline at the Swiss Light Source (Paul Scherrer Institut, Villigen, Switzerland); Dr. P. Saravanan for support at the PETRA III photon beamlines P13 and P14 at DESY (Hamburg, Germany); Dr. J. S. H. C. Rheinberger for help with cryo-EM data collection; and Dr. I. van 't Land–Kuper for her assistance with kinetic assays.

FUNDING

This project received funding from the European Union's Horizon 2020 research and innovation programme under the Marie Skłodowska–Curie grant agreement No. 713482, and from the European Research Council Advanced Grant *Suprabiotics* (No. 694610). M. P. and D. J. S. were supported by the Netherlands Organization for Scientific Research (NWO/OCW) through the BaSyC—*Building a Synthetic Cell* Gravitation grant (024.003.019).

AUTHOR CONTRIBUTIONS

N.P., E.M.W., D.J.S., A.G., and A.H. designed the research. N.P and E.M.W. contributed equally to this work. Experimental work was carried out by the following contributors:

- N.P.: Cloning, protein expression and purification, X-ray crystallography data collection, analysis, and structure determination; Cryo-EM structure determination.
- E.M.W.: Synthesis and characterization of compounds.
- M.P.: Enzymatic activity and kinetic assays.
- A.S.: Cryo-EM data analysis.
- M.L.: Cloning and MIC determination.
- X.Y.: Synthesis.

2.9. SUPPORTING INFORMATION

SYNTHESIS OF IMIDAZOLE-1-SULFONYL AZIDE

2

An ice-cooled suspension of sodium azide (11.2 g, 170 mmol, 1 equiv.) in acetonitrile (170 mL) was prepared. Sulfuryl chloride (13.7 mL, 170 mmol, 1 equiv.) was added dropwise to the suspension with constant stirring. The resulting slurry was stirred overnight (15 h) at room temperature.
After completion, the mixture was cooled in an ice bath, and imidazole (26.3 g, 323 mmol, 1.9 equiv.) was added portionwise. Stirring was continued for an additional 3 h at room temperature. The reaction mixture was diluted with ethyl acetate (350 mL) and washed twice with saturated aqueous $NaHCO_3$ solution (350 mL). The organic layer was separated, dried over $MgSO_4$, and filtered.
To precipitate the product, 6 M HCl solution (43 mL) was added to the filtrate while cooling in an ice bath. The resulting solid was washed three times with ethyl acetate (86 mL) and isolated as a white solid.
Yield: 22.8 g (108.7 mmol, 64%).

CHARACTERIZATION

^{1}**H NMR** (600 MHz, D_2O): $\delta = 9.51$ (s, 1H, H-2), 8.08 (s, 1H, H-5), 7.68 (s, 1H, H-4) ppm.
^{13}**C NMR** (151 MHz, D_2O, TMS): $\delta = 137.66, 122.95, 120.21$ ppm.
HRMS (ESI$^-$): Calculated for $C_3H_4N_5O_2S$ $[M–HCl]^-$: $m/z = 174.008$. Found: 174.008.

Note: Data are consistent with reported literature values [50].

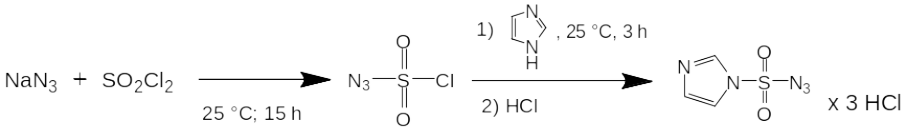


Figure 2.14 | Synthetic pathway for the synthesis of imidazole-1-sulfonyl azide.

2.10. SYNTHESIS OF 3-C-AZIDO NEOMYCIN B (COMPOUND 1)

PROCEDURE

A solution of NEO B trisulfate (5 g, 5.5 mmol, 1 equiv.) in water (250 mL) was prepared and combined with a solution of imidazole-1-sulfonyl azide hydrochloride (9.18 g, 44 mmol, 8 equiv.) in water (250 mL). The pH of the reaction mixture was adjusted to 6.6 using 2 M NaOH. The reaction was stirred at room temperature for 40 hours.
After completion, the reaction was quenched by washing the mixture three times with

dichloromethane (DCM, 500 mL per wash). The aqueous layer was separated and concentrated under reduced pressure. The crude product was subjected to column chromatography, eluting with a gradient of DCM/MeOH/NH_4OH_{aq} (2:2:75 to 2:2:1 v/v/v).
The purified product was concentrated, dissolved in water, filtered through a PTFE syringe filter (0.2 μm membrane), and lyophilized to yield compound 1 as a slightly yellowish solid.
Yield: 3.5 g (5.7 mmol, 70%).

CHARACTERIZATION

TLC (2:2:1 v/v/v of DCM/MeOH/NH_4OHaq) Rf =0.4.

1H NMR (600 MHz, D_2O) δ 5.64 (d, J = 3.9 Hz, ^{1}H, 1′-H), 5.41 (d, J = 1.8 Hz, ^{1}H, 1″-H), 5.03 (d, J = 1.8 Hz, ^{1}H, 1‴-H), 4.51 – 4.47 (m, ^{1}H, 3″-H), 4.38 (dd, J = 4.8, 1.9 Hz, ^{1}H,2″-H), 4.20 – 4.14 (m, ^{1}H, 4″-H), 4.14 – 4.05 (m, 2H, 3‴-H;5‴-H), 3.92 (dd, J = 12.6, 3.1 Hz, ^{1}H,5″-Ha), 3.79 – 3.66 (m, 7H, 5′-H; 4-H; 3′-H; 5′-H; 4‴-H; 3-H; 5″-Hb), 3.42 – 3.35 (m, ^{1}H, 5′-H), 3.33 – 3.19 (m, 3H, 6′-Ha; 6-H; 6′-Hb), 3.16 – 3.08 (m, ^{1}H, 6‴-Hb), 3.11 – 3.08 (m, ^{1}H, 2‴-H), 3.04 (dd, J = 13.7, 7.1 Hz, ^{1}H, 6‴-Ha), 2.85 (dd, J = 10.4, 3.8 Hz, ^{1}H, 2′-H), 2.83 – 2.77 (m, ^{1}H, 1-H), 2.26 (dt, J = 12.9, ^{1}H, 2-Heq), 1.48 – 1.36 (m, ^{1}H, 2-Hax) ppm. ATP (151 MHz, D_2O) δ = 109.06 (C1″), 98.79 (C1‴), 97.7 (C1′), 84.83 (C5), 81.21 (C4″), 76.90 (C4), 76.85 (C6), 75.48 (C3″), 73.50 (C2″), 73.07 (C5‴), 72.69 (C3′), 71.23 (C5′), 71.08 (C4′), 70.33 (C3‴), 68.50 (C4‴), 60.73 (C5″), 60.40 (C3), 50.00 (C2′), 52.40 (C2‴), 49.70 (C1), 41.06 (C6‴), 40.87 (C6′), 33.17 (C2) ppm.

HRMS (ESI+) (m/z) calculated for $C_{23}H_{44}N_8O_{13}$ $[M+H]^+$ 641.310, found 641.310.

Spectroscopic data matches the literature.[40]

2.11. SYNTHESIS OF 1,2',2",6',6"-*N*-PENTA-CBZ-3-C-AZIDO-NEOMYCIN B (COMPOUND 2)

PROCEDURE

Compound **1** (1.43 g, 2.23 mmol, 1 equiv.) was dissolved in water (7.7 mL), and a solution of potassium carbonate (1.08 g, 7.86 mmol, 3.5 equiv.) in water (12.4 mL) was added. The mixture was diluted with THF (10.7 mL). A solution of N-(benzyloxycarbonyloxy)succinimide (5.02 g, 20.16 mmol, 9 equiv.) in THF (9.2 mL) was then added, and the reaction mixture was stirred vigorously for 18 hours.
Reaction progress was monitored using TLC and LC-MS. An additional portion of N-(benzyloxycarbonyloxy)succinimide (5.02 g, 20.16 mmol, 9 equiv.) in THF (9.2 mL) was added, and stirring continued for another 18 hours.
Upon reaction completion, 3-dimethylaminopropylamine (5 mL, 40 mmol, 18 equiv.) was added, followed by dilution with ethyl acetate (4.3 mL) and water (5.4 mL). The organic layer was separated and washed with:

- A 1:1 mixture of an aqueous 20% (wt/wt) citric acid solution (5.4 mL) and brine (5.4 mL).

- A 1:1 mixture of a saturated aqueous solution of $NaHCO_3$ (5.4 mL) and water (5.4 mL).

The organic layer was then separated, and ethyl acetate (10.7 mL) was added. The solvent was evaporated under reduced pressure to remove THF residues. This procedure was repeated twice until all solvents were removed.
The crude product was re-dissolved in DCM and purified via column chromatography using a DCM/MeOH (19:1 v/v) eluent. Fractions containing the product were combined, and solvents were removed under reduced pressure to yield the title compound as a white solid.
Yield: 0.79 g (0.603 mmol, 58%).

CHARACTERIZATION

TLC (DCM/MeOH 19:1 v/v) Rf= 0.33.

1H NMR (400 MHz, CD3OD) δ 7.73 – 6.78 (m, 25H, Ar-H), 5.27 – 4.93 (m, 12H, 1′-H; 1″-H; Ar-CH_2), 4.74 (s, ^{1}H, 1‴-H), 3.99 – 3.25 (m, 20H, 2″-H; 5‴-H; 3‴-H; 3″-H;4″-H;3-H; 5″-Ha; 5′-H; 6′-Ha;2‴-H; 5″-Hb;3′-H; H-5; 4‴-H; H-4; 1-H; 6‴-Ha+b; 2′-H; 6′-Hb);3.18 (m, 2H; 6-H; 4′-H), 2.03 (d, J = 8.0 Hz, ^{1}H, 2-Heq), 1.27 – 1.17 (m, ^{1}H, 2-Hax).

13C NMR (101 MHz, CD3OD) δ159.2 (C=O), 159.2 (C=O), 159.0 (C=O), 158.9 (C=O), 158.7 (C=O),138.2 (C(Ar), 138.12 (C(Ar), 137.8 (C(Ar), 129.6 (Ar-H), 129.6 (Ar-H), 129.5 (Ar-H), 129.5 (Ar-H), 129.2 (Ar-H), 129.1 (Ar-H), 129.0 (Ar-H), 128.9 (Ar-H), 128.9(Ar-H), 128.7(Ar-H), 110.3 (C1″), 100.23 (C1′), 99.8 (C1‴), 86.4 (C5), 83.5 (C4″), 80.5 (C4), 77.9 (C3″), 75.4(C2″), 75.3 (C5‴), 74.5 (C6), 73.0 (C5‴), 72.4 (C4′), 71.5(C5′), 69.1 (C3′), 68.1(C3‴), 69.1 (C4‴), 67.7 (Ar-CH_2), 67.7 (Ar-CH_2), 63.0 (C5″), 62.2 (C2′), 57.5 (C2‴), 54,0 (C3), 52.0 (C1), 43.01 (C6′), 42.5 (C6‴), 34.0 (C2).

HRMS (ESI+): m/z calculated for $C_{63}H_{75}N_8O_{23}$ $[M+H]^+$ 1311.50., found: 1311.50.

2.12. SYNTHESIS OF 1,2',2",6',6"-*N*-PENTA-CBZ-NEOMYCIN B (COMPOUND 3)

PROCEDURE

In a round-bottom flask equipped with a reflux condenser, a solution of compound **2** (0.876 g, 0.77 mmol, 1 equiv.) in THF (12 mL) was combined with 0.1 M NaOH aqueous solution (2 mL). A 1 M solution of trimethylphosphine (PMe_3) in THF (3.3 mmol, 5 equiv.) was added, and the reaction mixture was refluxed at 50 °C for 2 hours.
After cooling, the reaction mixture was diluted with ethyl acetate (200 mL) and washed three times with water (3 × 200 mL). The organic layer was separated, dried over $MgSO_4$, and filtered. The solvents were removed under reduced pressure, and the crude product was purified by column chromatography using a DCM/MeOH gradient from 19:1 (v/v) to 9:1 (v/v). Fractions containing the product were combined, and the solvents were removed under vacuum to yield the title compound as a white solid.
Yield: 0.455 g (0.35 mmol, 46%).

CHARACTERIZATION

TLC (DCM/MeOH, 19:1 v/v) Rf= 0.2.

1H NMR (400 MHz, CD3OH) δ 7.73 – 6.78 (m, 25H, Ar-H), 5.27 – 4.93 (m, 12H, 1′-H; 1″-H; Ar-CH_2), 4.74 (s, ^{1}H, 1‴-H), 3.99 – 3.25 (m, 20H, 5‴-H; 4‴-H; 3‴-H; 2″-H; 3″-H; 4″-H; 3-H; 5″-Ha; 5′-H; 6′-Ha ;2‴-H; 5″-Hb; 3′-H; 5-H; 4-H; 1-H, 6‴-Ha+b; 2′-H; 6′-Hb); 3.18 (m, 2H, 6-H; 4′-H), 2.03 (d, J = 8.0 Hz, ^{1}H, 2-Heq), 1.27 – 1.17 (m, ^{1}H, 2-Hax).

13C NMR (126 MHz, CD3OD) δ 159.3 (C=O), 159.2 (C=O), 159.0, (C=O) 158.7 (C=O), 158.4 (C=O), 138.3 (C(Ar), 138.1 (C(Ar), 129.8 (Ar-H), 129.6 (Ar-H), 129.2 (Ar-H), 128.9 (Ar-H), 128.8 (Ar-H), 110.7 (C1″), 101.9 (C1′), 100.7 (C1‴), 87.9 (C5), 86.1 (C4″), 83.8 (C3″), 76.3 (C4), 74.7 (C6), 74.4 (C3′), 73.9 (C2″), 73.2 (C5‴), 72.0 (C4′), 71.5 (C5′), 69.0 (Ar-CH_2), 68.2 (C3‴), 67.7 (C4‴), 67.5 (C5″), 62.7 (C2′), 57.8 (C2‴), 53.8 (C1), 53.8 (C3) 52.4, 43.2 (C6′), 42.7 (C6‴), 35.0 (C2).

HRMS (ESI+) (m/z) calculated $C_{63}H_{77}N_6O_{23}$ $[M+H]^+$ 1285.50, found 1285.51.

2.13. SYNTHESIS OF 1,2',2",6',6"-*N*-PENTA-CBZ-3-*N*-METHYL-NEOMYCIN B (COMPOUND 4) AS 5×TFA SALT

PROCEDURE

Compound 3 (307 mg, 0.239 mmol, 1 equiv.) was dissolved in hexafluoroisopropanol (HFIP, 3.5 mL). Methyl trifluoromethanesulfonate (38.8 μL, 0.359 mmol, 1.5 equiv.) was added, and the reaction mixture was stirred at room temperature for 24 hours under an argon atmosphere. The reaction was quenched by adding 1 M HCl (350 μL), and the solvent was evaporated under reduced pressure. The crude product was purified by automated flash chromatography (reverse-phase chromatography, RPC), using a linear gradient from 0% to 100% buffer B in buffer A.

Buffers:

- Buffer A: Water with 0.1% trifluoroacetic acid (TFA).
- Buffer B: Acetonitrile with 0.1% TFA.

The purified product was isolated as a white solid in its 5×TFA salt form.
Yield: 245 mg (0.18 mmol, 78%).

CHARACTERIZATION

TLC (MeOH/EtOAc 1/10 v/v) Rf= 0.2.

1H NMR (400 MHz, Methanol-d4) δ 7.49 – 7.17 (m, 25H, Ar-H), 5.40 – 4.88 (m, 12H, 1′-H; 1″-H; Ar-CH_2), 4.67 (s, ^{1}H, 1‴-H), 3.96 – 3.32 (m, 22H, 5‴-H; 4‴-H; 3‴-H; 2″-H; 3″-H; 4″-H; 5″-Ha; 5′-H; 6′-Ha; 3-H, 2‴-H; 5″-Hb; 3′-H; H-5; 4-H; 1-H, 6‴-Ha+b; 2′-H; 6′-Hb; 6-H; 4′-H), 2.68 (s, 3H, CH_3), 2.29 – 2.13 (m, ^{1}H, 2-Heq), 1.51 – 1.39 (m, ^{1}H, 2-Hax).

13C NMR (126 MHz, MeOD) δ 162.8 (TFA) 159.3(C=O), 159.2(C=O), 158.7(C=O), 158.5 (C=O), 138.5 (C(Ar), 138.4, 137.7 (C(Ar), 129.8 (Ar-H), 129.7 (Ar-H), 129.6 (Ar-H), 129.4 (Ar-H), 129.2 (Ar-H), 129.0 (Ar-H), 116.9 (TFA) 110.6 (C1″), 101.9(C1′), 100.9(C1‴), 85.2(C5), 84.1, 77.4, 75.3, 75.0, 74.6, 73.0, 72.8, 71.7, 69.3, 68.5, 67.8, 62.8, 62.6, 59.7, 57.1, 54.1, 52.1, 43.3 (C6′), 42.8 (C6‴), 31.4 (CH_3), 29.1(C2).

HRMS (ESI+): m/z calculated for $C_{64}H_{79}N_6O_{23}$ $[M+H]^+$ 1299.51 found $[M+H]^+$ 1299.52.

2.14. SYNTHESIS OF 1,2',2",6',6"-*N*-PENTA-CBZ-3-*N*,*N*-DIMETHYL-NEOMYCIN B (COMPOUND 5) AS 5×TFA SALT

PROCEDURE

The synthesis of the title compound was performed using the general procedure for reductive amination. Compound 3 (1 g, 0.78 mmol, 1 equiv.) was reacted with formaldehyde (620 μL, 7.8 mmol, 10 equiv.) and sodium cyanoborohydride ($NaBH_3CN$, 150 mg, 2.3 mmol, 3 equiv.) at room temperature for 3 hours.
The reaction mixture was purified by flash chromatography, using a gradient of ethyl acetate (EtOAc) and methanol (MeOH) from 19:1 to 9:1 (v/v).
The purified product was obtained as a white solid in its 5×TFA salt form.
Yield: 920 mg (0.7 mmol, 90%).

CHARACTERIZATION

TLC (EtOAc/MeOH 1:13.5 v/v) Rf=0.39.

1H NMR (400 MHz, MeOD) δ 7.37 – 7.28 (m, 25H, Ar-H), 5.22 – 5.05 (m, 12H, 1-H′; 1-H″; Ar-CH_2), 4.85 (1‴-H (overlap with the solvent peak), 4.09 (s, 2H, 3″-H; 2″-H), 4.05 – 3.98 (m, ^{1}H, 5‴-H), 3.95 – 3.89 (m, 3H, 4″-H; 3′-H; 3‴-H), 3.84 (s, ^{1}H, 2‴-H), 3.78 – 3.68 (m, 2H, 5″-Ha; 5′-H), 3.67 – 3.46 (m, 7H, 5-H″b ; 2-H′; 5-H; 4-H‴; 6-H′a ; 4-H, 3-H), 3.40 – 3.33 (m, 5H, 6-H; 6-H‴a+b ; 6′-Hb; 1-H), 3.24 (t, J = 9.4 Hz, ^{1}H, 4′-H), 2.14 (s, 6H, CH_3), 1.93 – 1.85 (m, ^{1}H, 2-Heq), 1.19 – 1.07 (m, ^{1}H, 2-Hax).

13C NMR (151 MHz, CD3OD) 159.3 (C=O), 159.2 (C=O), 159.0, (C=O) 158.7 (C=O), 158.4 (C=O), 138.3 (C(Ar), 138.1 (C(Ar), 129.8 (Ar-H), 129.6 (Ar-H), 129.2 (Ar-H), 128.9 (Ar-H), 128.8 (Ar-H), 108.8 (C1″), 100.2 (C1′), 99.4 (C1‴), 87.8 (C5), 84.6 (C4″),79.6 (C4), 79.3 (C3″), 78.3, 77.0, 76.8 75.9 (C6), 74.5 (C3′), 73.6 (C2″), 72.8 (C5‴), 72.4 (C4′), 70.4 (C5′), 68.9 (Ar-CH_2), 64.0 (C5″), 58.9 (C2′), 55.3 (C2‴), 55.3, 54.3 (C1), 44.5 (C6‴), 43.8 (C6′), 42.1
(CH_3), 31.9 (C2).

HRMS (ESI+): m/z calculated for $C_{65}H_{81}N_6O_{23}$ $[M+H]^+$ 1313.53, found $[M+H]^+$1313.53.

2.15. SYNTHESIS OF 1,2',2",6',6"-*N*-PENTA-CBZ-3-*N*-PROPYL-NEOMYCIN B (COMPOUND 6)

PROCEDURE

The synthesis of the title compound followed the general procedure for reductive amination. Compound 3 (300 mg, 0.23 mmol, 1 equiv.) was reacted with propanal (17 μL, 0.23 mmol, 1 equiv.) and sodium cyanoborohydride ($NaBH_3CN$, 3.55 mg, 0.23 mmol, 1 equiv.) in the presence of acetic acid (12 μL) at room temperature for 2 hours.
The reaction mixture was processed, and the product was isolated as a white solid.
Yield: 298 mg (0.22 mmol, 96%).

CHARACTERIZATION

TLC (EtOAc/MeOH 1:13.5 v/v) Rf=0.49.

1H NMR (600 MHz, MeOD) δ 7.52 – 7.15 (m, 25H, Ar-H), 5.25 – 4.95 (m, 13H, 1′-H; 1″-H; 1‴-H; Ar-CH_2), 3.97 – 3.36 (m, 22H, 5‴-H; 4‴-H; 3‴-H; 2″-H; 3″-H; 4″-H; 3-H; 5″-Ha; 5′-H; 6′-Ha; 2‴-H; 5″-Hb; 3′-H; H-5; H-4; 1-H, 6‴-Ha+b; 2′-H; 6′-Hb; 6-H; 4′-H), 3.07 (m, ^{1}H, NH-CH_2), 2.93 (m, ^{1}H, NH-CH_2), 2.28 (d, J = 12.0 Hz, ^{1}H, 2-Heq), 1.72 (s, 2H, CH_2CH_3), 1.54 (m, ^{1}H, 2-Hax), 0.99 (t, J = 7.3 Hz, 3H, CH_3).

13C NMR (151 MHz, CD3OH) δ 159.6 (C=O), 159.5 (C=O), 159.3 (C=O), 158.9 (C=O), 158.7 (C=O), 138.4 (C(Ar), 137.8 (C(Ar), 130.0 (Ar-H), 129.8 (Ar-H), 129.5 (Ar-H), 129.3 (Ar-H), 129.1 (Ar-H), 110.5 (C1″), 101.7 (C1′), 100.9 (C1‴), 85.4 (C5), 84.1 (C4″), 80.7 (C4), 77.5 (C3″), 75.5 (3′), 75.2 (2″), 75.1 (C6), 74.7 (C5‴), 72.9 (C4′), 71.8 (C5′), 69.3 (C3‴), 68.6 (C4‴), 68.0 (Ar-CH_2), 67.9 (Ar-CH_2), 65.5 (C5″), 58.6 (C3), 57.2 (C2′), 54.2 (C2‴), 52.3 (C1), 47. 5 (NH-CH_2) , 43.6 (C6′), 42.9 (C6‴), 29.6 (C2), 21.4 (CH_2-CH_3), 11.5 (CH_3).

HRMS (ESI+): m/z calculated for $C_{66}H_{83}N_6O_{23}$ $[M+H]^+$ 1327.54 found $[M+H]^+$ 1327.55.

2.16. SYNTHESIS OF 1,2',2",6',6"-*N*-PENTA-CBZ-3-*N*-HEXYL-NEOMYCIN B (COMPOUND 7) AS 5×TFA SALT

PROCEDURE

The synthesis of the title compound followed the general procedure for reductive amination. Compound 3 (300 mg, 0.23 mmol, 1 equiv.) was reacted with hexanal (29 μL, 0.23 mmol, 1 equiv.) and sodium cyanoborohydride ($NaBH_3CN$, 3.55 mg, 0.23 mmol, 1 equiv.) in the presence of acetic acid (12 μL) at room temperature for 2 hours.
The crude product was purified by reverse-phase chromatography (RPC) using a gradient from 0% to 100% buffer B in buffer A.
Buffers:

- Buffer A: Water with 0.1% trifluoroacetic acid (TFA).

- Buffer B: Acetonitrile with 0.1% TFA.

The purified product was obtained as a white solid in its 5×TFA salt form.
Yield: 200 mg (0.1 mmol, 44%).

CHARACTERIZATION

TLC (EtOAc/MeOH 1:13.5 v/v) Rf=0.6.

1H NMR (500 MHz, CD3OD) δ 7.48 – 7.21 (m, 25H, Ar-H), 5.22 – 5.03 (m, 12H, 1′-H; 1″-H; Ar-CH_2), 4.75 (d, J = 10.1 Hz, ^{1}H, 1‴-H), 3.94 (s (br), 2H, 3″-H;2″-H), 3.90 – 3.44 (m, 17H, 5‴-H; 4″-H; 3′-H; 3‴-H; 2‴-H; 5″-Ha; 5′-H; 5-H″b ; 2-H′; 5-H; 4-H‴; 6-H′a ; 4-H; 6-H; 6-H‴a+b ; 6′-Hb;), 3.37 (s, 4H, 3-H; 2‴-H; 1-H ;4′-H,), 3.13 (s, ^{1}H, NH-CH_2), 2.99 (s, ^{1}H, NH-CH_2), 2.30 (d, J = 12.0 Hz, ^{1}H, 2-Heq), 1.76 – 1.62 (m, 2H, CH_2), 1.59 – 1.47 (m, ^{1}H, 2-Hax), 1.44 – 1.35 (m, 6H, CH_2CH_3), 0.96 – 0.89 (m, 3H, CH_3).

13C NMR (126 MHz, CD3OD) δ 162.8 (TFA) 159.1 (C=O) , 159.0 (C=O), 158.8 (C=O), 158.4 (C=O), 138.2 (C(Ar), 138.1 (C(Ar), 129.6 (Ar-H), 129.4 (Ar-H), 129.3 (Ar-H), 128.9 (Ar-H), 128.7 (Ar-H), 128.5 (Ar-H), 116.7 (TFA), 110.3 (C1″), 100.5 (C1′), 99.6 (C1‴), 85.0 (C5), 83.7 (C4″), 80.7 (C4), 77.1(C3‴), 75.2 (C3′), 74.9 (C2″), 74.8 (C3″), 73.1 (C4′) 72.6 (C6), 71.4 (C3‴), 71.3 (C5′), 68.9 (C4‴), 67.5 (Ar-CH_2), 62.3 (C5″), 58.2 (C3), 56.7 (C2′), 53.8 (C2‴), 51.9 (C1), 47.7 (NH-CH_2), 43.5 (C6′), 42.4 (C6‴), 29.2 (C2), 27.5 (CH_2), 27.0 (CH_2), 23.3 (CH_2), 20.6 (CH_2-CH_3), 14.1 (CH_3), 9.0.

HRMS (ESI+): m/z calculated for $C_{69}H_{89}N_6O_{23}$ $[M+H]^+$ 1369.59 found $[M+H]^+$ 1370.11.

2.17. GENERAL PROCEDURE FOR AMINE DEPROTECTION

Reactions were carried out using Schlenk techniques under an argon (Ar) atmosphere. Solvents were degassed by sonication for 2 hours and purged with Ar (3 × 10 min) prior to use. A solution of Cbz-protected aminoglycoside in a mixture of methanol, water, and acetic acid (MeOH/H_2O/AcOH, 36:3:1 v/v/v) was placed in a round-bottom flask equipped with a stirring bar. Pd/C (20% wt) was added to the reaction mixture.
The flask was purged with Ar for 30 minutes and the reaction mixture was stirred under a hydrogen atmosphere (balloon) for 24–72 hours. Progress of the reaction was monitored using TLC and LC-MS. Upon completion, the mixture was filtered through a Celite pad and washed.

2.18. SYNTHESIS OF 3-*N*-METHYL-NEOMYCIN B (COMPOUND 8) AS 5×HFBA SALT

PROCEDURE

The title compound was synthesized following the general amine deprotection procedure, starting with compound **4** (100 mg, 0.053 mmol). After deprotection, the product was dis-

solved in water and purified by HPLC. Fractions containing the product were combined, and acetone was removed under reduced pressure. The product was then lyophilized to yield compound **8** as a yellowish solid in its 5×HFBA salt form.
Yield: 55 mg (0.03 mmol, 57%).

NMR ANALYSIS

- ^{1}H-NMR: Reported in Figure 2.15a.
- ^{13}C-NMR: Reported in Figure 2.15b.
- HSQC-NMR: Reported in Figure 2.16.

TLC (DCM/MeOH/NH4OH 2:2:1 (v/v/v) Rf=0.1.

1H NMR (400 MHz, D_2O) δ 6.15 – 6.10 (m, ^{1}H, 1′-H), 5.47 (s, ^{1}H, 1″-H), 5.32 (s, ^{1}H, 1‴-H), 4.56 – 4.48 (m, ^{1}H, 3″-H), 4.45 – 4.39 (m, ^{1}H, 2″-H;4-H), 4.38 – 4.32 (m, ^{1}H, 5‴-H), 4.32 – 4.24 (m, 2H, 3‴-H; 4″-H), 4.21 (t, J = 9.7 Hz, ^{1}H, 4-H), 4.14 – 3.90 (m, 4H, 4‴-H; 5-H; 3′-H; 5″-Hb), 3.86 (s, ^{1}H, 5′-H), 3.83 – 3.69 (m, 2H, 5″-Ha; 6-H), 3.70 – 3.60 (m, ^{1}H, 3-H), 3.59 – 3.24 (m, 8H, 2‴-H; 4′-H; 2′-H; 6′-Ha+b ;1-H; 6‴-Ha+b), 2.82 (s, 3H, CH_3), 2.65 – 2.55 (m, ^{1}H, 2-Heq), 1.85 (q, J = 12.1, 11.7 Hz, ^{1}H, 2-Hax).

13C NMR (101 MHz, D_2O) δ 164.0 (HFBA), 119.5 (HFBA) , 117.2 (HFBA), 112.6 (C1″), 109.1 (HFBA), 98.2 (C1′), 98.0 (C1‴), 87.4 (C5), 84.3 (C4″), 78.1 (C3″), 76.9 (C4), 76.3 (C2″), 75.0 (C6), 72.9 (C4′),72.7 (C5‴), 72.2 (C3′), 70.4 (C4‴), 70.0 (C3‴), 70.0 (C5′), 62.9 (C5″), 59.4 (C3), 57.5 (C2′), 56.0 (C2‴), 52.4 (C1), 42.7(C6′), 42.5 (C6‴), 32.7 (CH_3), 27.5 (C2).

HRMS (ESI+): m/z calculated for $C_{24}H_{48}N_6O_{13}$ $[M+H]^+$ 629.335, found: 629.334.

2.19. SYNTHESIS OF 3-*N,N*-DIMETHYL-NEOMYCIN B (COMPOUND 9) AS 5×HFBA SALT

PROCEDURE

The title compound was synthesized following the general amine deprotection procedure, starting with compound **5** (136 mg, 0.1 mmol). After deprotection, the product was dissolved in water and purified by HPLC. Fractions containing the product were combined, and acetone was removed under reduced pressure. The product was then lyophilized to yield compound **9** as a yellowish solid in its 5×HFBA salt form.
Yield: 124 mg (0.072 mmol, 72%).

NMR ANALYSIS

- ^{1}H-NMR: Reported in Figure 2.17a.

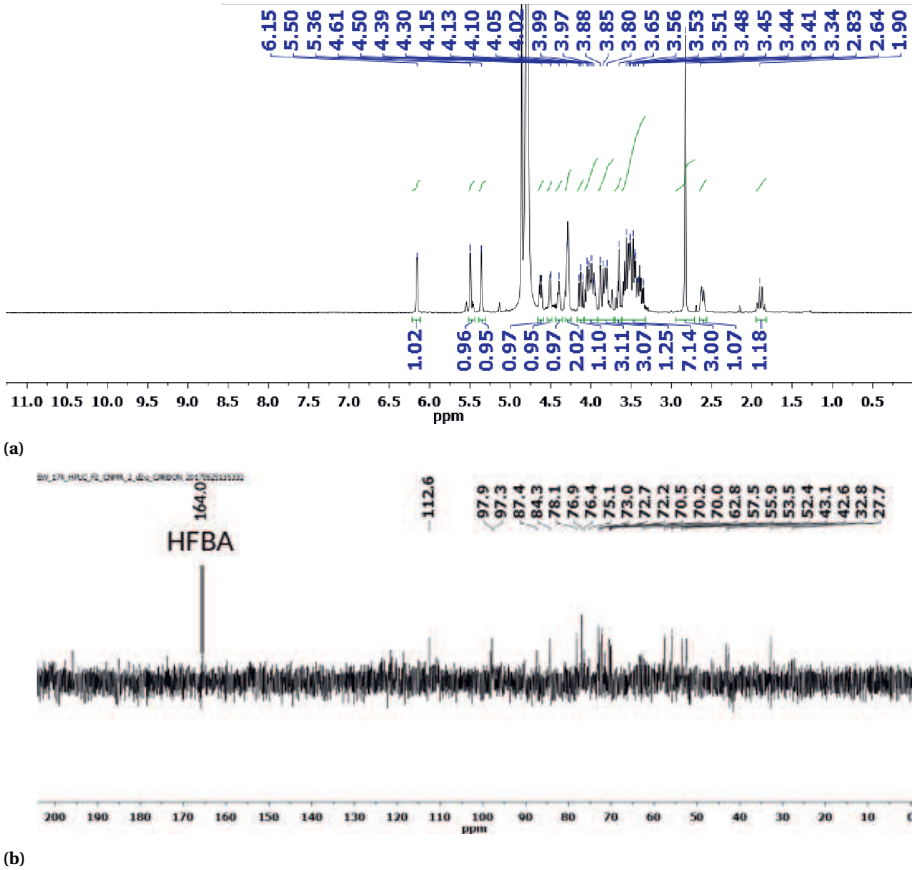


Figure 2.15 | (a) 1H NMR (400MHz, D_2O) spectrum of 3-N-methyl neomycin B (x 5HFBA). (b) 13C NMR ATP(101MHz, D_2O) spectrum of 3-N-methyl neomycin B (x 5HFBA).

- ^{13}C-NMR: Reported in Figure 2.17b.
- HSQC-NMR: Reported in Figure 2.18.

TLC (DCM/MeOH/NH_4OH 2:1:1 v/v/v) Rf=0.13.

1H NMR (400 MHz, D_2O) δ 6.12 (d, J = 4.1 Hz, ^{1}H, 1′-H), 5.49 (d, J = 2.3 Hz, ^{1}H, 1″-H), 5.33 (d, J = 1.8 Hz, ^{1}H, 1‴-H), 4.56 (dd, J = 6.6, 4.9 Hz, ^{1}H, 3″-H), 4.50 – 4.43 (m, 2H, 2″-H;4-H), 4.35 (t, J = 5.2 Hz, ^{1}H, 5‴-H), 4.27 (m, 2H, 3‴-H;4″-H), 4.13 (dd, J = 10.6, 8.7 Hz, ^{1}H, 4‴-H), 4.08 – 3.89 (m, 3H, 5″-Ha; 3′-H; 5-H), 3.86 (d, J = 3.4 Hz, ^{1}H, 5′-H), 3.84 – 3.66 (m, 3H, 5″-Hb; 3-H; 6-H), 3.64 – 3.56 (m, 2H, 2″-H; 4′-H), 3.66 – 3.26 (m, 5H, 6′-Ha+b;6‴-Hb; 2′-H; 1-H), 3.32 (dd, J = 13.9, 4.1 Hz, ^{1}H, 6′-Ha), 3.01 (s, 6H, CH_3), 2.60 – 2.49 (m, ^{1}H, 2-Heq), 1.95 (q, J = 12.6 Hz, ^{1}H, 2-Hax).

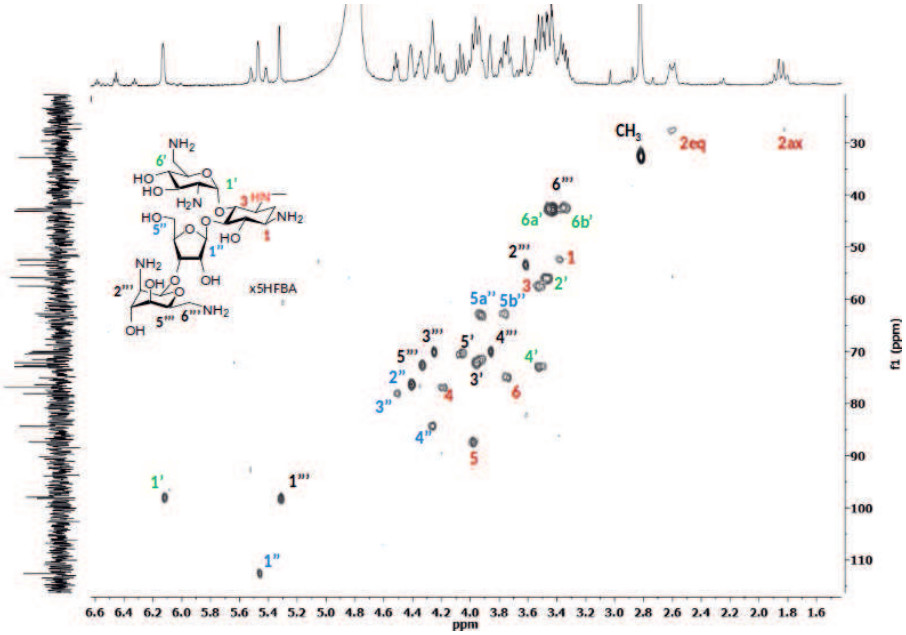


Figure 2.16 | HSQC-NMR spectrum of 3-N-methyl neomycin B x 5HFBA with peak assignment.

13C NMR (101 MHz, D_2O) δ 164.0 (HFBA), 119.5 (HFBA) , 117.2 (HFBA), 112.0 (C1″), 109.1 (HFBA), 98.0 (C1‴), 97.6 (C1′), 86.8 (C5), 83.9 (C4″), 77.7 (C3″), 75.6 (C2″),75.6 (C4), 74.8 (C6), 72.4 (C5‴), 72.1 (C3′), 71.9 (C4′), 70.1 (C4‴), 70.1 (C3‴), 69.9 (C5′), 63.3 (C3), 62.5 (C5″), 55.7(C2′), 53.5 (C2‴), 52.4 (C1), 45.6 (CH_3); 43.1 (C6‴), 41.8 (C6′), 37.6 (CH_3), 24.1 (C2).

HRMS (ESI+): m/z calculated for $C_{25}H_{51}N_6O_{13}$ $[M+H]^+$ 643.351, found: 643.350.

2.20. SYNTHESIS OF 3-*N*-PROPYL-NEOMYCIN B (COMPOUND 10) AS 5×HFBA SALT

PROCEDURE

The title compound was synthesized following the general amine deprotection procedure, starting with 300 mg of compound **6** (as a 5×TFA salt). The product was re-dissolved in water, filtered through a PTFE syringe filter (0.2 μm membrane), and lyophilized.
The lyophilized product was further dissolved in water and purified by HPLC. Fractions containing the product were combined, and acetone was removed under reduced pressure. The purified product was lyophilized to yield compound **10** as a yellowish solid in its 5×HFBA salt form.

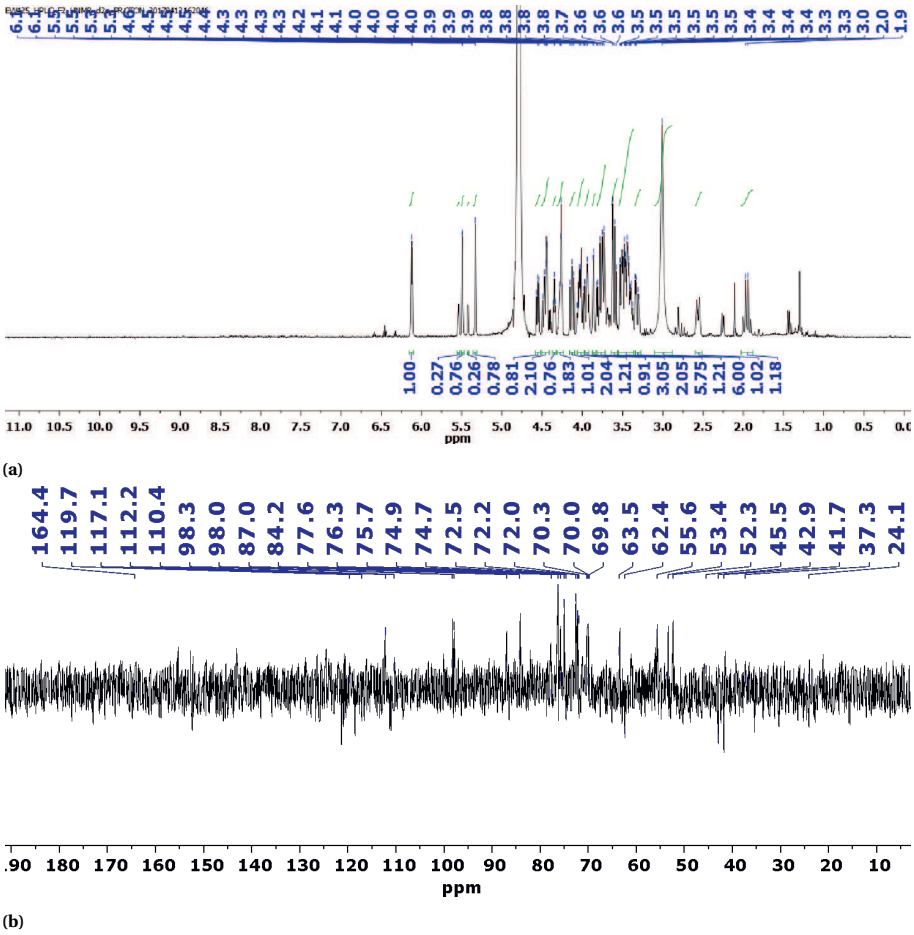


Figure 2.17 | (a) 1H NMR (400MHz, D_2O) spectrum of 3-N,N-dimethyl neomycin B (x 5HFBA). (b) 13C NMR ATP(101MHz, D_2O) spectrum of 3-N,N-dimethyl neomycin B (x 5HFBA).

Yield: 220 mg (0.127 mmol, 80%).

NMR ANALYSIS

- ^{1}H-NMR: Reported in Figure 2.19a.
- ^{13}C-NMR: Reported in Figure 2.19b.
- HSQC-NMR: Reported in Figure 2.20.

TLC (DCM/MeOH/NH_4OH 1:1:0.75 v/v/v) Rf=0.16.

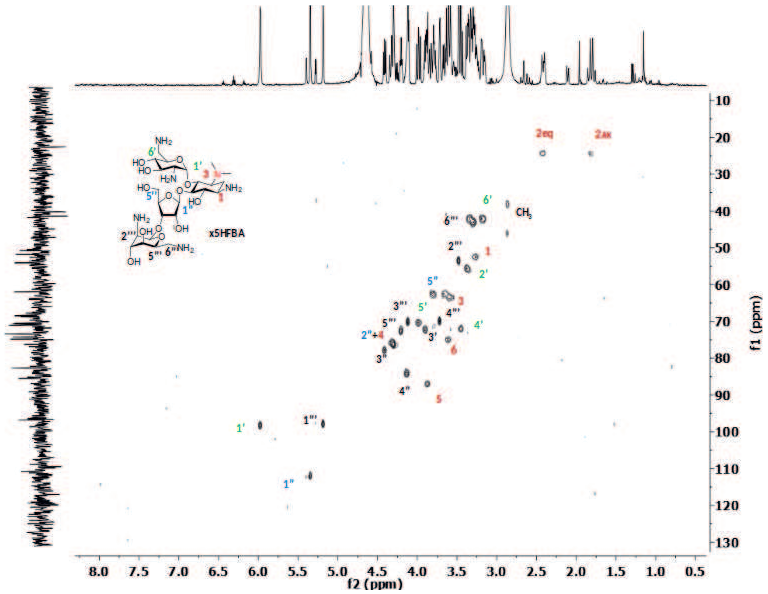


Figure 2.18 | HSQC-NMR spectrum of 3-N,N-dimethyl neomycin B x 5HFBA with peak assignment.

1H NMR (500 MHz, D_2O) δ 6.07 (d, J = 3.9 Hz, ^{1}H,1′-H), 5.44 (d, J = 2.1 Hz, ^{1}H, 1″-H), 5.29 (s, ^{1}H,1‴-H), 4.49 (s, ^{1}H, 3″-H), 4.39 (dd, J = 4.9, 2.2 Hz, ^{1}H, 2″-H), 4.37 – 4.28 (m, ^{1}H, 5‴-H), 4.27 – 4.22 (m, 2H, 3‴-H; 4″-H), 4.19 (t, J = 9.7 Hz, ^{1}H, 4-H), 4.05 (dd, J = 10.8, 8.8 Hz, ^{1}H, 4‴-H), 4.0-3.8 (m, 4H, 5″-Ha; 5-H; 5′-H; 3′-H), 3.8 – 3.7 (m, 2H; 5″-Hb; 6-H), 3.6-3.2(m, 9H, 6‴-Ha+b;6′-Ha+b;1-H; 2′-H; 4′-H; 2‴-H; 3-H), 3.16 (td, J = 11.1, 5.5 Hz, ^{1}H, NH-CH_2), 3.03 (td, J = 12.2, 11.6, 5.6 Hz, ^{1}H, NH-CH_2), 2.65 – 2.54 (m, ^{1}H, 2-Heq), 1.87 (q, J = 12.4 Hz, ^{1}H, 2-Hax), 1.80 – 1.60 (m, 2H, CH_2CH_3), 0.98 (t, J = 7.4 Hz, 3H,CH_3).

13C NMR (126 MHz, D_2O) δ 164.0 (HFBA), 119.5 (HFBA) , 117.2 (HFBA), 109.3(C1″), 109.1 (HFBA), 96.4(C1′), 96.3(C1‴), 85.4 (C5), 82.6 (C4″), 76.4 (C3″), 75.7 (C4),74.6 (C2″), 73.1 (C6), 70.9 (C5‴), 70.7 (C3′), 70.4 (C4′), 68.8 (C4‴), 68.4 (C3‴),68.2 (C5′), 60.9 (C5″), 54.7(C2‴), 54.1(C2′), 51.7 (C3), 50.7 (C1), 46.9 ($NHCH_2CH_2$), 41.3 (C6‴), 40.1 (C6′), 26.2 (C2), 20.0 (CH_2CH_3), 10.9 (CH_3).

HRMS (ESI+): m/z calculated for $C_{26}H_{52}N_6O_{13}$ $[M+H]^+$ 657.367, found: 657.367.

2.21. SYNTHESIS OF 3-*N*-HEXYL-NEOMYCIN B (COMPOUND 11)

PROCEDURE

The title compound was synthesized following the general amine deprotection procedure, starting with 200 mg (0.1 mmol) of compound **7** (as a 5×TFA salt). The crude reaction mixture

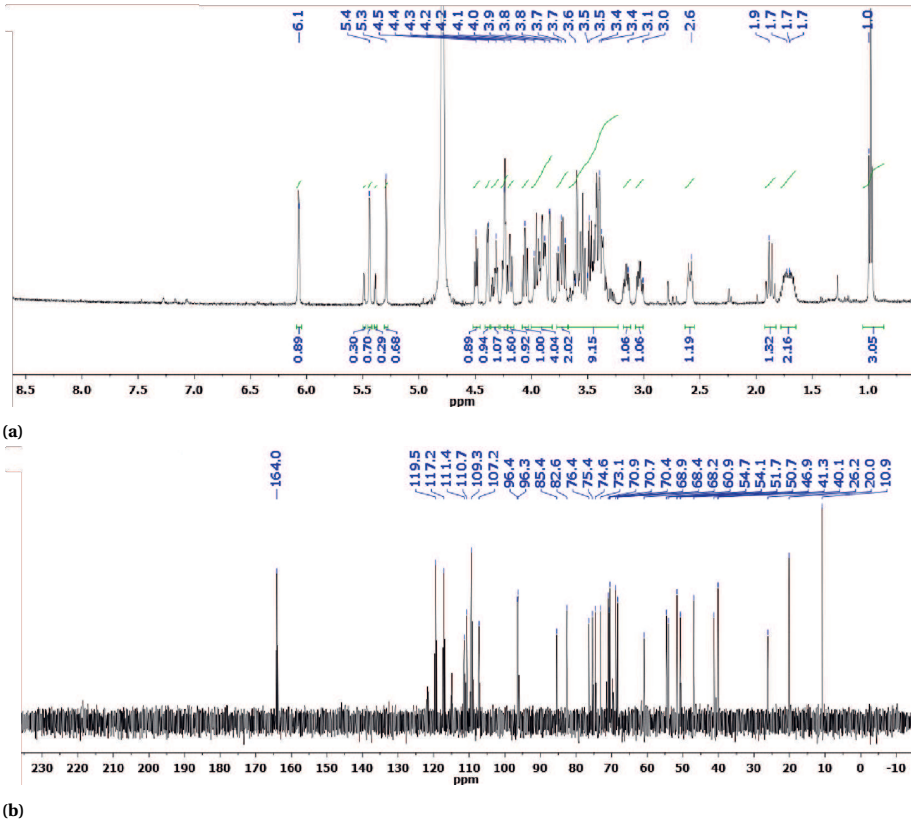


Figure 2.19 | (a) 1H NMR (400MHz, D_2O) spectrum of 3-N-propyl neomycin B (x 5HFBA). (b) 13C NMR ATP(101MHz, D_2O) spectrum of 3-N-propyl neomycin B (x 5HFBA).

was re-dissolved in water and purified by flash chromatography. The elution was carried out using a gradient of dichloromethane (DCM), methanol (MeOH), and aqueous ammonium hydroxide (NH_4OH_{aq}) in a ratio of 2:2:0.75 (v/v/v).
Fractions containing the desired product were combined, and solvents were removed under reduced pressure. The resulting product was re-dissolved in water, filtered through a PTFE syringe filter (0.2 μm membrane), and lyophilized to yield the title compound as a yellow solid.
Yield: 54 mg (0.077 mmol, 77%).

NMR ANALYSIS

- ^{1}H-NMR: Reported in Figure 2.21a.
- ^{13}C-NMR: Reported in Figure 2.21b.

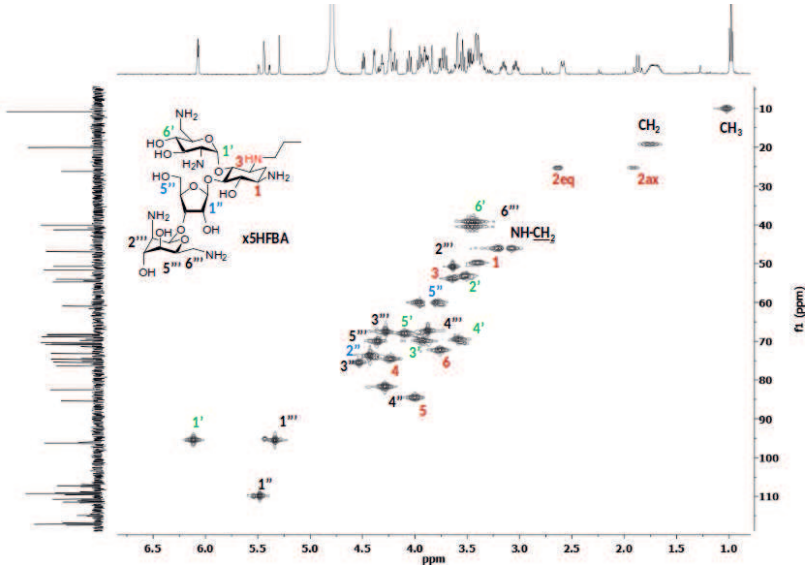


Figure 2.20 | HSQC-NMR spectrum of 3-N-propyl neomycin B x 5HFBA with peak assignment.

- HSQC-NMR: Reported in Figure 2.22.

TLC (DCM/MeOH/NH_4OH 1:1:0.75 v/v/v) Rf=0.3.

1H NMR (500 MHz, D_2O) δ 6.08 (d, J = 4.1 Hz, ^{1}H,1′-H), 5.44 (d, J = 2.1 Hz, ^{1}H, 1″-H), 5.29 (s, ^{1}H,1‴-H), 4.49 (s, ^{1}H,3″-H), 4.39 (dd, J = 4.9, 2.2 Hz, ^{1}H, 2″-H), 4.34 – 4.30 (m, ^{1}H, 5‴-H), 4.27 – 4.18 (m, 3H, 3‴-H; 4″-H, 4-H), 4.07 (t, J = 9.8 Hz, ^{1}H, 5′-H), 4.00 – 3.86 (m, 3H, 5″-Ha; 3′-H; 5-H), 3.84 (dt, J = 3.1, 1.3 Hz, ^{1}H,4‴-H), 3.78 – 3.71 (m, 2H, 5″-Hb; 6-H), 3.66 – 3.52 (m, 3H,3-H; 2‴-H;4′-H), 3.50 – 3.32 (m, 6H, 2′-H; 6‴-Ha+b; 6′-Ha+b;1-H), 3.19 – 3.15 (m, ^{1}H, NH-CH_2), 3.09 – 3.03 (m, ^{1}H, NH-CH_2), 2.63 – 2.56 (m, ^{1}H, 2-Heq), 1.88 (q, J = 12.6 Hz, ^{1}H, 2-Hax), 1.42 – 1.34 (m, 2H, CH_2), 1.32 – 1.28 (m, 6H, CH_2; CH_2; CH_2), 0.88 – 0.83 (m, 3H, CH_3).

13C NMR (126 MHz, D_2O) δ 109.8 (C1″), 95.5 (C1′), 95.45 (C1‴), 84.5 (C5), 81.7(C4″), 75.5 (C3″), 74.6 (C4), 73.7(C2″), 72.3(C6), 70.0(C3′), 69.8(C5‴), 69.6(C4′), 68.0(C5′), 67.6(C3‴), 67.4(C4‴), 60.1 (C5‴), 53.9(C3), 53.2(C2′), 50.9(C2‴), 49.8 (C1), 46.7, 44.8 (NH-CH_2), 40.4(C6′), 39.2(C6‴), 30.4(CH_2), 25.5(C2), 25.4(CH_2), 21.7 (CH_2CH_3), 13.1 (CH_3), 8.18.

HRMS (ESI+): m/z calculated for $C_{29}H_{58}N_6O_{13}$ $[M+H]^+$ 699.413, found: 699.414.

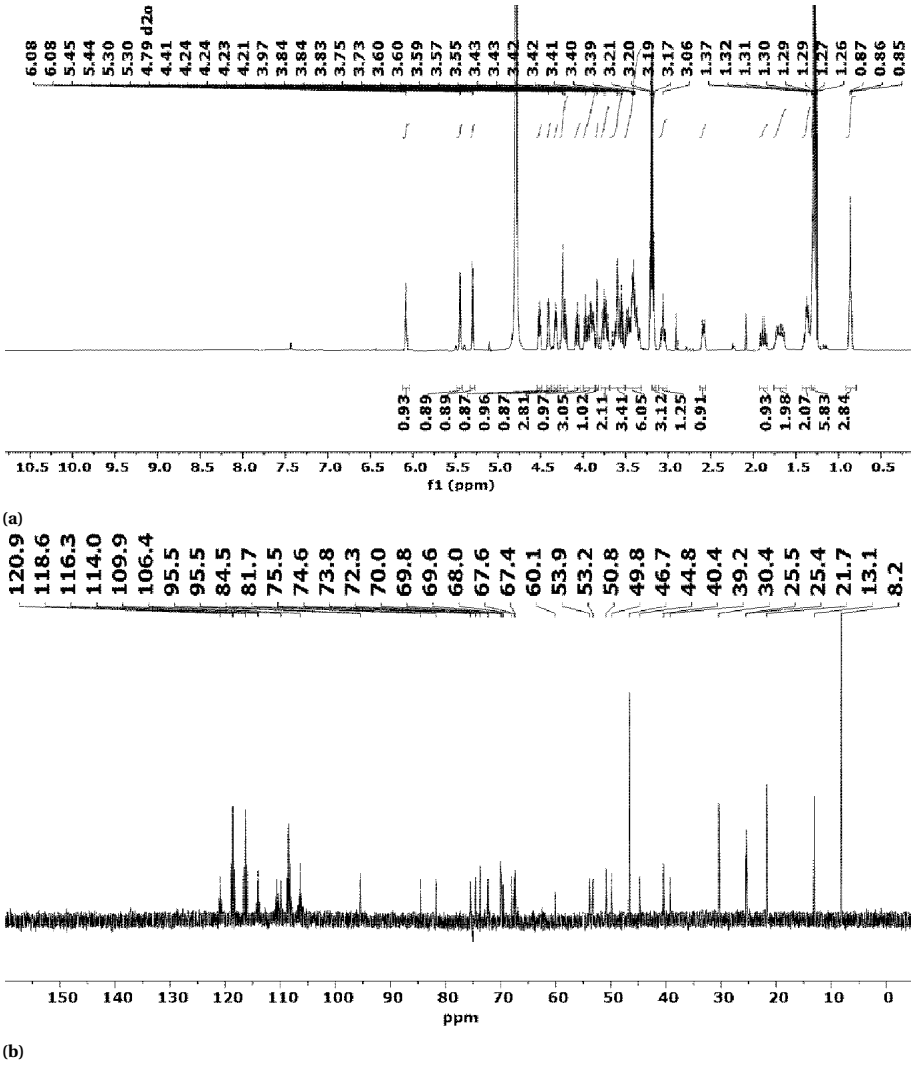


Figure 2.21 | (a) 1H NMR (400MHz, D_2O) spectrum of 3-N-propyl neomycin B (x 5HFBA). (b) 13C NMR ATP(101MHz, D_2O) spectrum of 3-N-propyl neomycin B (x 5HFBA).

REFERENCES

[1] J. Davies, *Inactivation of antibiotics and the dissemination of resistance genes,* Science **264**, 375 (1994), publisher: American Association for the Advancement of Science.

[2] D. L. Mayers, J. D. Sobel, M. Ouellette, K. S. Kaye, and D. Marchaim, *Antimicrobial Drug Resistance: Clinical and Epidemiological Aspects, Volume 2*, Vol. 2 (Springer, 2017).

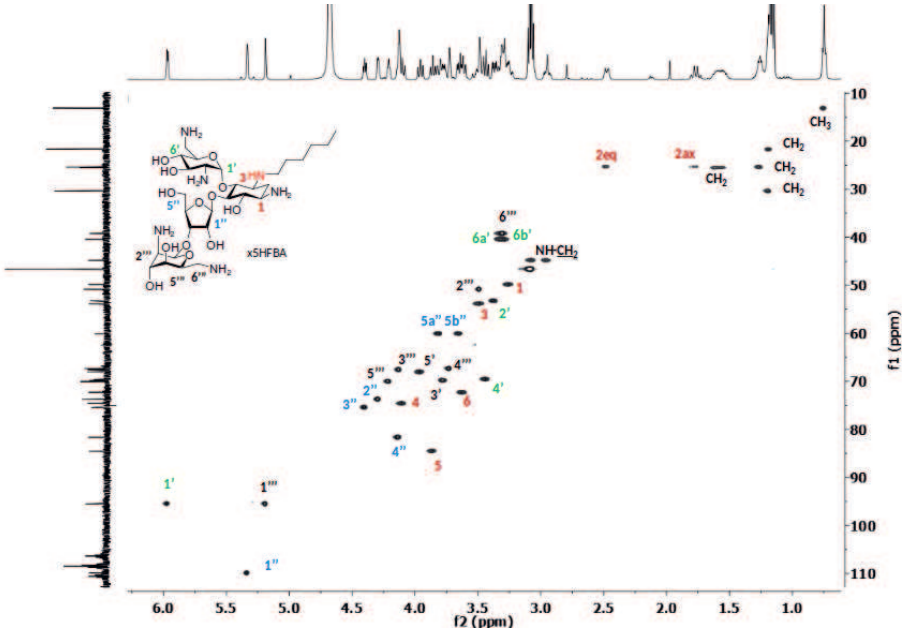


Figure 2.22 | HSQC-NMR spectrum of 3-N-propyl neomycin B x 5HFBA with peak assignment.

[3] C. Walsh, *Where will new antibiotics come from?* Nature Reviews Microbiology **1**, 65 (2003), publisher: Nature Publishing Group.

[4] T. Weisenburg, *Cerebello-pontile tumor diagnosed for six years as Tic Douloureux: the symptoms of irritation of the ninth and twelfth cranial nerves,* Journal of the American Medical Association **54**, 1600 (1910), publisher: American Medical Association.

[5] J. E. Davies, *Origins, acquisition and dissemination,* Antibiotic resistance: origins, evolution, selection and spread **207**, 15 (2008), publisher: John Wiley & Sons.

[6] W. H. Organization, *Global Action Plan on Antimicrobial resistance,* (2015).

[7] W. H. Organization, *Global Priority List of Antibiotic-Resistance Bacteria to Guide Research, Discovery, and Development of New Antibiotics,* (2017).

[8] S. B. Vakulenko and S. Mobashery, *Versatility of aminoglycosides and prospects for their future,* Clinical microbiology reviews **16**, 430 (2003), publisher: Am Soc Microbiol.

[9] K. M. Krause, A. W. Serio, T. R. Kane, and L. E. Connolly, *Aminoglycosides: an overview,* Cold Spring Harbor perspectives in medicine **6**, a027029 (2016), publisher: Cold Spring Harbor Laboratory Press.

[10] J. Xie, A. E. Talaska, and J. Schacht, *New developments in aminoglycoside therapy and ototoxicity,* Hearing research **281**, 28 (2011), publisher: Elsevier.

[11] L. Leibovici, L. Vidal, and M. Paul, *Aminoglycoside drugs in clinical practice: an evidence-based approach,* Journal of Antimicrobial Chemotherapy **63**, 246 (2009), publisher: Oxford University Press.

[12] D. Gilbert and J. Leggett, *Principles and practice of infectious disease* (Churchill Livingstone Philadelphia, 2000) publication Title: Aminoglycosides.

[13] S. Magnet and J. S. Blanchard, *Molecular insights into aminoglycoside action and resistance,* Chemical reviews **105**, 477 (2005), publisher: ACS Publications.

[14] E. C. Böttger and D. Crich, *Aminoglycosides: Time for the Resurrection of a Neglected Class of Antibacterials?* ACS Infectious Diseases **6**, 168 (2019), publisher: ACS Publications.

[15] H. W. Taber, J. P. Mueller, P. F. Miller, and A. Arrow, *Bacterial uptake of aminoglycoside antibiotics.* Microbiological reviews **51**, 439 (1987), publisher: American Society for Microbiology (ASM).

[16] R. E. Hancock, *Aminoglycoside uptake and mode of action—with special reference to streptomycin and gentamicin: II. Effects of aminoglycosides on cells,* Journal of Antimicrobial Chemotherapy **8**, 429 (1981), publisher: Oxford University Press.

[17] M. Chittapragada, S. Roberts, and Y. W. Ham, *Aminoglycosides: molecular insights on the recognition of RNA and aminoglycoside mimics,* Perspectives in medicinal chemistry **3**, PMC (2009).

[18] D. Fourmy, M. I. Recht, and J. D. Puglisi, *Binding of neomycin-class aminoglycoside antibiotics to the A-site of 16 S rRNA,* Journal of molecular biology **277**, 347 (1998).

[19] B. François, R. J. Russell, J. B. Murray, F. Aboul-ela, B. Masquida, Q. Vicens, and E. Westhof, *Crystal structures of complexes between aminoglycosides and decoding A site oligonucleotides: role of the number of rings and positive charges in the specific binding leading to miscoding,* Nucleic acids research **33**, 5677 (2005), publisher: Oxford University Press.

[20] S. Shandrick, Q. Zhao, Q. Han, B. K. Ayida, M. Takahashi, G. C. Winters, K. B. Simonsen, D. Vourloumis, and T. Hermann, *Monitoring molecular recognition of the ribosomal decoding site,* Angewandte Chemie International Edition **43**, 3177 (2004), publisher: Wiley Online Library.

[21] P. Veyssier and A. Bryskier, *Aminocyclitol aminoglycosides,* in *Antimicrobial Agents* (American Society of Microbiology, 2005) pp. 453–469.

[22] R. Hancock, *Intrinsic antibiotic resistance of Pseudomonas aeruginosa,* Journal of Antimicrobial Chemotherapy **18**, 653 (1986), publisher: Oxford University Press.

[23] A. H. Delcour, *Outer membrane permeability and antibiotic resistance,* Biochimica et Biophysica Acta (BBA)-Proteins and Proteomics **1794**, 808 (2009).

[24] R. A. Moore, D. DeShazer, S. Reckseidler, A. Weissman, and D. E. Woods, *Efflux-mediated aminoglycoside and macrolide resistance in Burkholderia pseudomallei,* Antimicrobial agents and chemotherapy **43**, 465 (1999), publisher: Am Soc Microbiol.

[25] S. N. Hobbie, P. Pfister, C. Bruell, P. Sander, B. François, E. Westhof, and E. C. Böttger, *Binding of neomycin-class aminoglycoside antibiotics to mutant ribosomes with alterations in the A site of 16S rRNA,* Antimicrobial agents and chemotherapy **50**, 1489 (2006).

[26] F. Yeganeh Sefidan, Y. Mohammadzadeh-Asl, and R. Ghotaslou, *High-level resistance to aminoglycosides due to 16S rRNA methylation in Enterobacteriaceae isolates,* Microbial Drug Resistance **25**, 1261 (2019).

[27] M. S. Ramirez and M. E. Tolmasky, *Aminoglycoside modifying enzymes,* Drug resistance updates **13**, 151 (2010).

[28] A. I. M. Salah Ud-Din, A. Tikhomirova, and A. Roujeinikova, *Structure and functional diversity of gcn5-related n-acetyltransferases (gnat),* International journal of molecular sciences **17**, 1018 (2016).

[29] E. Azucena and S. Mobashery, *Aminoglycoside-modifying enzymes: mechanisms of catalytic processes and inhibition,* Drug Resistance Updates **4**, 106 (2001), publisher: Elsevier.

[30] B. Becker and M. A. Cooper, *Aminoglycoside antibiotics in the 21st century,* ACS chemical biology **8**, 105 (2013), publisher: ACS Publications.

[31] S. Shakil, R. Khan, R. Zarrilli, and A. U. Khan, *Aminoglycosides versus bacteria–a description of the action, resistance mechanism, and nosocomial battleground,* Journal of biomedical science **15**, 5 (2008).

[32] M. Hainrichson, I. Nudelman, and T. Baasov, *Designer aminoglycosides: the race to develop improved antibiotics and compounds for the treatment of human genetic diseases,* Organic & biomolecular chemistry **6**, 227 (2008), publisher: Royal Society of Chemistry.

[33] J. E. Michiels, B. Van den Bergh, N. Verstraeten, M. Fauvart, and J. Michiels, *In vitro emergence of high persistence upon periodic aminoglycoside challenge in the ESKAPE pathogens,* Antimicrobial agents and chemotherapy **60**, 4630 (2016).

[34] S. Schwarz, *Mechanisms of antimicrobial resistance in Pasteurellaceae* (Caister Academic Press Norfolk, UK, 2008).

[35] B. Llano-Sotelo, E. F. Azucena Jr, L. P. Kotra, S. Mobashery, and C. S. Chow, *Aminoglycosides modified by resistance enzymes display diminished binding to the bacterial ribosomal aminoacyl-tRNA site,* Chemistry & biology **9**, 455 (2002).

[36] J. B. Aggen, E. S. Armstrong, A. A. Goldblum, P. Dozzo, M. S. Linsell, M. J. Gliedt, D. J. Hildebrandt, L. A. Feeney, A. Kubo, R. D. Matias, and others, *Synthesis and spectrum of the neoglycoside ACHN-490,* Antimicrobial agents and chemotherapy **54**, 4636 (2010).

[37] Y. Berkov-Zrihen, K. D. Green, K. J. Labby, M. Feldman, S. Garneau-Tsodikova, and M. Fridman, *Synthesis and evaluation of hetero-and homodimers of ribosome-targeting antibiotics: antimicrobial activity, in vitro inhibition of translation, and drug resistance,* Journal of medicinal chemistry **56**, 5613 (2013), publisher: ACS Publications.

[38] S. G. Zárate, M. L. De la Cruz Claure, R. Benito-Arenas, J. Revuelta, A. G. Santana, and A. Bastida, *Overcoming aminoglycoside enzymatic resistance: design of novel antibiotics and inhibitors,* Molecules **23**, 284 (2018).

[39] A. G. Santana, S. G. Zárate, J. L. Asensio, J. Revuelta, and A. Bastida, *Selective modification of the 3"-amino group of kanamycin prevents significant loss of activity in resistant bacterial strains,* Organic & biomolecular chemistry **14**, 516 (2016), publisher: Royal Society of Chemistry.

[40] A. A. Bastian, E. M. Warszawik, P. Panduru, C. Arenz, and A. Herrmann, *Regioselective Diazo-Transfer Reaction at the C3-Position of the 2-Desoxystreptamine Ring of Neamine Antibiotics,* Chemistry–A European Journal **19**, 9151 (2013), publisher: Wiley Online Library.

[41] E. Krissinel and K. Henrick, *Inference of macromolecular assemblies from crystalline state,* Journal of molecular biology **372**, 774 (2007).

[42] A. L. Norris and E. H. Serpersu, *Interactions of coenzyme A with the aminoglycoside acetyltransferase (3)-IIIb and thermodynamics of a ternary system,* Biochemistry **49**, 4036 (2010), publisher: ACS Publications.

[43] K. D. Green, W. Chen, J. L. Houghton, M. Fridman, and S. Garneau-Tsodikova, *Exploring the substrate promiscuity of drug-modifying enzymes for the chemoenzymatic generation of N-acylated aminoglycosides,* ChemBioChem **11**, 119 (2010), publisher: Wiley Online Library.

[44] A. L. Norris, C. özen, and E. H. Serpersu, *Thermodynamics and kinetics of association of antibiotics with the aminoglycoside acetyltransferase (3)-IIIb, a resistance-causing enzyme,* Biochemistry **49**, 4027 (2010), publisher: ACS Publications.

[45] P. J. Stogios, M. L. Kuhn, E. Evdokimova, M. Law, P. Courvalin, and A. Savchenko, *Structural and biochemical characterization of Acinetobacter spp. aminoglycoside acetyltransferases highlights functional and evolutionary variation among antibiotic resistance enzymes,* ACS infectious diseases **3**, 132 (2017), publisher: ACS Publications.

[46] J. Vliegenthart, P. Ketelaar-van Gaalen, and J. van de Klundert, *Nucleotide sequence of the aacC3 gene, a gentamicin resistance determinant encoding aminoglycoside-(3)-N-acetyltransferase III expressed in Pseudomonas aeruginosa but not in Escherichia coli.* Antimicrobial agents and chemotherapy **35**, 892 (1991), publisher: Am Soc Microbiol.

[47] T. Lebleu, X. Ma, J. Maddaluno, and J. Legros, *Selective monomethylation of primary amines with simple electrophiles,* Chemical Communications **50**, 1836 (2014).

[48] S. B. Vakulenko and S. Mobashery, *Versatility of aminoglycosides and prospects for their future,* Clinical microbiology reviews **16**, 430 (2003).

[49] I. Wohlgemuth, R. Garofalo, E. Samatova, A. N. Günenç, C. Lenz, H. Urlaub, and M. V. Rodnina, *Translation error clusters induced by aminoglycoside antibiotics,* Nature communications **12**, 1830 (2021).

[50] E. D. Goddard-Borger and R. V. Stick, *An efficient, inexpensive, and shelf-stable diazotransfer reagent: imidazole-1-sulfonyl azide hydrochloride,* Organic letters **9**, 3797 (2007), publisher: ACS Publications.

3

Harnessing Light to Control Antibiotic Activity: Photo-Switchable Aminoglycosides as a Strategy Against Resistance

Jingyi Huang, Nicola Pontillo, Avishek Paul, Lifei Zheng, Xintong Yang, Albert Guskov, Andreas Herrmann

"Why kill bacteria in the dark when you can do it in style?"

— A photopharmacology enthusiast

ABSTRACT

The repertoire of antimicrobial drugs is becoming increasingly ineffective due to bacterial resistance. To address this issue, imminent bacterial threat, we designed two types of photo-switchable dimeric paromomycin derivatives, which undergo isomerization upon exposure to light of specific wavelengths. These isomers exhibit distinct antimictibial activities, with up to 2-3 fold diffecence in activity against Escherichia coli strains carrying aminoglycoside-modifying enzyme resistance genes. The reversible activation and deactivation of these antibiotics minimize evolutionary pressure for resistance development. The compounds were thoroughly characterized using UV-vis spectroscopy, NMR, ITC measurements, and X-ray crystallography, providing insights into their mechanism of action.

3.1. INTRODUCTION

BACKGROUND ON ANTIBIOTIC RESISTANCE

The emergence of bacterial resistance to antibiotics is one of the most pressing challenges in modern medicine. The widespread use, misuse, and overprescription of antibiotics have accelerated the evolution of resistant bacterial strains, rendering many conventional treatments ineffective, and resulting in prolonged illnesses, increased mortality rates, and a growing economic burden on healthcare systems worldwide.[1, 2]

The World Health Organization (WHO) and the European Union (EU) have both highlighted the urgent need for novel antimicrobial strategies to combat this growing threat. [3, 4] Over the past decades, intensive research efforts have been dedicated to understanding the mechanisms of bacterial resistance and developing innovative solutions to counteract them. Despite these efforts, bacterial pathogens continue to evolve, necessitating alternative approaches beyond traditional antibiotic development. [5, 6]

One of the key challenges in antibiotic resistance is the ability of bacteria to rapidly adapt to selective pressures imposed by drug treatments. When antibiotics are introduced into an environment, susceptible bacteria are eliminated, leaving behind resistant strains that continue to proliferate. This selection process is exacerbated by the accumulation of active antibiotics in the environment, which provides additional opportunities for bacteria to develop resistance mechanisms. As a result, there is an urgent need for antimicrobial solutions that not only target resistant bacteria effectively but also minimize environmental impact and resistance development. [7]

TARGETING THE RIBOSOME: MECHANISM OF ACTION

Protein biosynthesis is a fundamental process in all living cells, and bacterial ribosomes are key targets for many clinically useful antibiotics (see Figure 3.1). Aminoglycosidess (AGs) exert their antibacterial effect by binding to the ribosome and interfering with protein translation. Specifically, they target the aminoacyl-tRNA binding site (A-site) or the peptidyltransferase domain (P-site) of the ribosome, preventing proper decoding and peptide bond formation. [8, 9]

The prolonged and inappropriate use of aminoglycosides has driven the emergence of resistance mechanisms, which can be categorized into four main types: (i) enzymatic modification of the antibiotic, reducing its efficacy; (ii) decreased intracellular concentration of the drug through efflux pumps; (iii) reduced membrane permeability, preventing antibiotic entry; and (iv) structural modifications in the ribosomal target, such as mutations in ribosomal RNA or protein components and rRNA methylation. These modifications can significantly hinder the binding of aminoglycosides to the ribosome, leading to reduced antibacterial activity. [10, 11]

NOVEL STRATEGIES TO OVERCOME RESISTANCE

The increasing prevalence of these resistance mechanisms has significantly reduced the efficacy of traditional aminoglycoside treatments, necessitating the development of alternative



Figure 3.1 | Antibiotic binding sites on the 30S ribosomal subunit. Overview of representative antibiotic binding pockets along the mRNA-binding channel of the *E. coli* 30S ribosomal subunit. Helix 44 is shown for reference. The positions of the antibiotics are indicated as sticks: tetracycline (Tet, green), kasugamycin (Ksg, purple), pactamycin (Pct, yellow), edeine (Ede, red), hygromycin B (HygB, gray), neomycin (Neo, light blue), streptomycin (Str, light yellow), and thermorubin (Thb, cyan). The visualization highlights the spatial distribution of drug-binding pockets across the decoding center of the 30S subunit.

therapeutic strategies. [11]
One approach to counteract resistance is combination therapy, where multiple antibiotics are administered together to enhance bacterial eradication. Cocktails can be synergistic, antagonistic, or additive, each with distinct mechanisms and outcomes (see Figure 3.2).

Synergistic combinations amplify the antibacterial effect by targeting complementary pathways, such as weakening the bacterial cell membrane while simultaneously inhibiting protein synthesis. This increased potency often allows for lower dosages, reducing toxicity and side effects. However, a major concern is that while synergy enhances bacterial killing, it may also accelerate the selection of resistant strains by making it more beneficial for bacteria to acquire resistance to one or both drugs. [12]

Antagonistic combinations involve drugs that partially counteract each other's effects, leading to a reduced overall antibacterial activity compared to their individual use. While this may seem counterintuitive, studies suggest that such combinations can delay the emergence of resistance. The rationale is that bacteria face a weaker selective pressure to develop resistance when the combined drugs are less effective together than separately. However, the drawback of this approach is the potential for reduced treatment efficacy, requiring prolonged exposure to antibiotics and increasing the risk of persistent infections. [13]

Finally, additive combinations do not significantly enhance or reduce each other's effects but still provide the benefit of targeting multiple bacterial pathways. While this strategy can contribute to prolonged antibiotic effectiveness, it does not offer the amplified potency of synergy or the resistance-dampening effect of antagonism. [14] The challenge remains that any form of combination therapy, while temporarily effective, cannot entirely prevent resistance evolution. As bacteria continue to adapt, multidrug-resistant strains capable of circumventing combination regimens may still emerge, highlighting the need for alternative strategies such as hybrid antibiotics. [15]
An alternative and emerging strategy is the development of hybrid antibiotics, where two pharmacophores (usually but not necessarily with distinct bacterial targets) are covalently linked into a single molecule. This design ensures more predictable drug distribution while overcoming resistance mechanisms by simultaneously attacking multiple cellular pathways. Unlike combination therapy, hybrid antibiotics offer a controlled and unified pharmacokinetic profile, reducing the risk of resistance development associated with separate drug administration. [14]
By integrating two active components into a single molecular entity, hybrid antibiotics ensure that both pharmacophores reach the bacterial target at the same concentration, avoiding the discrepancies in drug absorption, distribution, and metabolism that often occur with combination therapy. This synchronization reduces the likelihood of bacteria developing resistance to one component before encountering the second, a common issue in cocktails where one drug may be eliminated or degraded faster than the other. [16] Furthermore, hybrid antibiotics can enhance bacterial uptake by leveraging the transport properties of one moiety to facilitate the entry of the other, effectively bypassing permeability-related resistance mechanisms. [17]

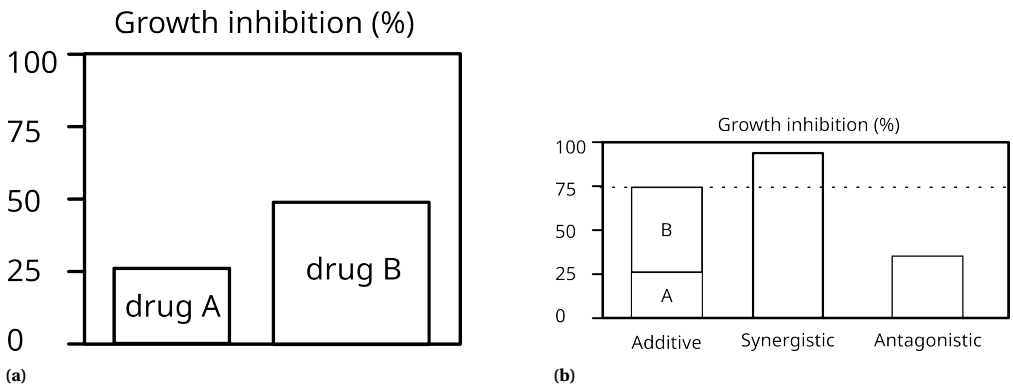


Figure 3.2 | (a) Growth inhibition effects of Drug A (25%) and Drug B (50%) when administered individually. (b) Three possible outcomes in combinatorial therapy: additive effect, where the combined inhibition equals the sum of individual effects (A + B = 75%); synergistic effect, where the combined inhibition is enhanced by the interaction between the drugs; and antagonistic effect, where the combined inhibition is lower than the sum of individual effects, potentially due to interference between the two drugs.

Another significant advantage of hybrid antibiotics is their ability to evade enzymatic degradation by resistance-conferring bacterial enzymes. In many cases, the structural modifications introduced by covalent linkage can prevent recognition by bacterial resistance enzymes, preserving the drug's activity. Additionally, rationally designed hybrids can exert dual or synergistic actions within bacterial cells, increasing efficacy while minimizing toxicity to host cells. [18]

Despite these advantages, challenges remain in designing hybrid antibiotics with optimal linkers that preserve the activity of both pharmacophores while ensuring metabolic stability and avoiding undesired interactions. Antibiotic dimerization may present challenges such as reduced cell permeability and unintended off-target effects.

Nonetheless, the potential of hybrid antibiotics to deliver enhanced efficacy while mitigating resistance development makes them a promising frontier in the fight against multidrug-resistant bacterial infections. [14, 19, 20]

Hybrid aminoglycoside molecules represent a promising avenue for antibiotic development, as they can exhibit enhanced binding to rRNA, improved resistance evasion, and greater bactericidal efficiency. Additionally, since most aminoglycosides have a single ribosomal binding site, homodimerization may improve their inhibitory effect by increasing local drug concentration and enhancing target affinity. [21, 22]

AMMINOGLYSIDE HYBRID ANTIBIOTICS

Over the past two decades, significant efforts have been made to develop aminoglycoside-containing hybrid antibiotics as a strategy to overcome bacterial resistance and reduce toxicity. Hybrid compounds have been designed by covalently linking aminoglycosides to various pharmacophores, including β-lactams, chloramphenicol, oxazolidinones, fluoroquinolones, and peptides. [22–24]

These structures aim to enhance bacterial targeting, improve drug uptake, and evade resistance mechanisms by simultaneously acting on multiple cellular pathways. Early work focused on β–lactam–aminoglycoside hybrids, leveraging the synergy between these two antibiotic classes, but challenges in synthesis and inconsistent antibacterial activity limited their development. [23, 25]
More recently, aminoglycoside-oxazolidinone and aminoglycoside-fluoroquinolone hybrids have been explored to broaden antibacterial spectra and improve ribosomal binding, showing enhanced affinities to bacterial RNA targets. Some of these hybrids have demonstrated promising effects in delaying the emergence of resistance, particularly antagonistic hybrids that balance activity across different bacterial targets. [26, 27]
Additionally, aminoglycoside–peptide hybrids have been developed to enhance membrane penetration and combat multidrug-resistant Gram-positive and Gram-negative pathogens. [28]
Multidrug-resistant (MDR) strains that have evolved resistance to multiple antibiotic families pose additional challenges, limiting the applicability of combination treatments. In contrast, hybrid antibiotics, where two pharmacophores with distinct bacterial targets are covalently linked, offer a more controlled and predictable pharmacokinetic profile. [14, 29]
This approach not only ensures simultaneous delivery of both active components but also allows one pharmacophore to enhance the penetration and activity of the other. Additionally, the rational design of hybrid antibiotics can overcome resistance mechanisms that affect individual drugs, reducing the likelihood of further resistance development. [30]
Despite these advances, many hybrid antibiotics face limitations, such as inconsistent antibacterial potency, cytotoxicity concerns, or pharmacokinetic challenges. To further expand the utility of aminoglycoside hybrids, we introduce a novel optically controlled hybrid antibiotic that incorporates light-responsive elements, allowing a more precise spatial and temporal activation to optimize therapeutic efficacy and pave the way to future developments in minimize resistance development.

OPTICAL CONTROL OF ANTIBIOTIC ACTIVITY

One of the primary challenges in antibiotic therapy is the lack of selectivity, which leads to uncontrolled drug activity in both time and space since. Conventional antibiotics remain active regardless of their location, resulting in off-target effects, toxicity, and the unintentional promotion of bacterial resistance. To address these issues, new molecular strategies are being explored to dynamically regulate antibiotic activity, allowing precise spatial and temoral control.
Light offers a precise and non-invasive means to regulate biological functions, making it a powerful tool for controlling antibiotic activity. [31]
Unlike chemical regulators, photons do not introduce contaminants into biological systems and exhibit minimal toxicity, making them ideal for bioorthogonal drug activation. By integrating photoactive compounds into antibiotics, light-triggered structural changes can be harnessed to modulate their function, an approach has already employed in enzyme activation, receptor modulation, and transport regulation. [31–33]
Optical control of antibiotics enables targeted activation at the site of infection, reducing

systemic exposure and preventing the accumulation of active drugs in the environment. Strategies include photodegradable antibiotics, such as light-inactivated β-lactams, and reversibly photoswitchable molecules that cycle between active and inactive states in response to light stimuli. [34, 35] Unlike traditional prodrugs, which undergo irreversible activation, photoswitchable antibiotics offer a reversible and tunable mechanism of control, allowing repeated activation and deactivation.

Recent advancements in photopharmacology have expanded this approach by developing molecular photoswitches responsive to visible and near-infrared light. [35] Photoswitches such as azobenzenes and diarylethenes undergo reversible structural changes upon light absorption, altering molecular properties like polarity, flexibility, and binding affinity (see Figure 3.3). This reversible transformation enhances pharmacokinetic control, enabling antibiotics to exhibit different properties at various stages of drug distribution. [36, 36]

The ability to precisely manipulate antibiotic activity with light presents a transformative strategy for antimicrobial therapy, improving treatment efficacy while minimizing resistance development and environmental contamination. [37] The following sections explore the synthesis, characterization, and biological evaluation of photo-switchable aminoglycoside dimers, with a focus on their potential to counteract bacterial resistance.

CHEMICAL MODIFICATIONS OF AZOBENZENES

To optimize the optical control of antibiotics, chemical modifications of azobenzenes are crucial in tuning their absorption properties and thermal stability.

The introduction of electron-withdrawing or electron-donating groups at strategic positions affects the UV-Vis absorption spectra, allowing red shifts that facilitate activation with longer wavelengths in the visible range. This shift is particularly beneficial for biological applications, as it enhances tissue penetration, reduces phototoxicity, and enables more precise antibiotic activation.

Additionally, these modifications influence the half-life of the Z-isomer, determining the duration of antibiotic activity before thermal relaxation occurs. [38]

Among various modifications, ortho-fluorination has emerged as one of the most effective strategies for optimizing azobenzene-based photoswitches. As shown in Figure 3.4, the incorporation of fluorine at the ortho positions significantly enhances the thermal stability of the Z-isomer, extending its half-life from minutes to several days or years, depending on the solvent. [39]

A summary of various azobenzene modifications, including their absorption properties, transition wavelengths, and half-lives, is provided in Table 3.1.

Ortho-fluorinated azobenzenes exhibit a maximum $n \rightarrow \pi^*$ band separation of approximately 50 nm, enabling selective $E \rightarrow Z$ and $Z \rightarrow E$ isomerization in the visible-light range without overlap between the two transitions.[40]

Moreover, ortho-fluorination significantly increases the thermal stability of the Z-isomer, with reported half-lives exceeding two years for certain derivatives.[39]

This remarkable stability is attributed to orbital stabilization effects, which raise the energy barrier for thermal relaxation. Compared to unmodified azobenzene, which thermally reverts to the trans state within hours to days, ortho-fluorinated derivatives provide long-term

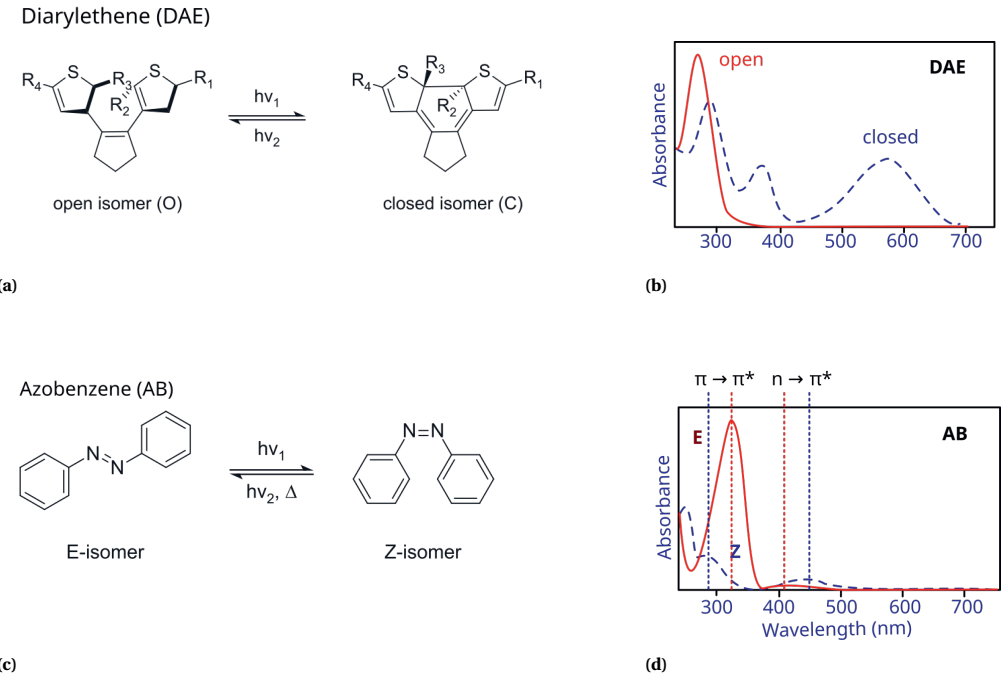


Figure 3.3 | (a) Structural representation of diarylethene (DAE) photochromic transition between open (O) and closed (C) forms; (b) UV–Vis absorption spectra of DAE in both states; (c) Azobenzene (AB) reversible E/Z (trans/cis) isomerization upon light irradiation; (d) UV–Vis absorption spectra of AB illustrating distinct profiles for trans and cis configurations.

stability, ensuring sustained antibacterial activity in the active state while preserving precise reversibility under light exposure.

The ability to selectively activate and deactivate photo-switchable hybrid antibiotics using visible light is critical for minimizing bacterial resistance development and reducing environmental drug accumulation. By leveraging these structural modifications, light-responsive aminoglycoside hybrids can be designed with enhanced efficacy, extended pharmacokinetic stability, and controlled antibiotic action, making them a powerful tool against multidrug-resistant bacterial infections.

3.2. RESULTS AND DISCUSSION

DESIGN AND DEVELOPMENT OF PHOTO-SWITCHABLE PAROMOMYCIN DIMERS

To explore the feasibility of photo-switchable hybrid antibiotics, paromomycin (PAR) was chosen as the parent drug due to its well-characterized structure and antibacterial activity. A key feature of PAR is the aminomethyl group at position 6”’, which offers a site for regiose-

Table 3.1 | Absorption properties, transition wavelengths, and half-lives of modified azobenzenes, highlighting the effects of different substitutions on photophysical behavior and stability. Half-life ($\tau_{1/2}$) refers to the thermal stability of the *Z* isomer.

Compound	$\lambda_{E\rightarrow Z}$ (nm)	$\lambda_{Z\rightarrow E}$ (nm)	$\lambda_{Z/E}$ (nm)	**Half-life** ($\tau_{1/2}$)	**Solvent**
Unmodified AB	320–360	~380–450	Overlapping	Hours–Days	Various
Ortho-Methoxy AB	~480–550	~450–530	Moderate shift	~5 h	Hexane, H_2O
Ortho-Fluorinated AB	400–500	450–550	50 nm separation	Up to 2 years	DMSO, $CHCl_3$
2,2'-Azonaphthalene	310–360	450	Overlap	Several hours	Various
Bis(Amido) Azobenzenes	400–410	~550	Separated bands	Minutes–Hours	CH_2Cl_2, H_2O
Disperse Red Derivatives	500–700	450–600	Red-shifted bands	Seconds–Minutes	THF, polymer matrices

lective modification due to its lower steric hindrance (see Figure 3.5 where the structure and ring nomenclature are detailed).

This site was particularly advantageous for introducing bulky substituents, as it is less critical for ribosomal binding and has a reduced impact on interactions with Aminoglycoside Modifying Enzymes (AMEs).

As part of this work, we solved the crystal structure of the APH(3')-Ia in a binary complex with PAR, confirming that position 6"' does not play a key role in the enzyme's active site interactions (see Figure 3.6). This structural insight, along with the previously known structure of AAC-IIIb bound to PAR (PDB code: 6MB7), further supports the non-essential role of this modification site in AME recognition.

This validation provided the rationale for modifying PAR at this site to introduce a photo-switchable moiety without significantly affecting its antibacterial function.

To introduce light-responsiveness into the molecule, two types of dimeric photo-switchable PAR derivatives were synthesized: H-dimer and F-dimer (Figure 3.7). These compounds incorporate either azobenzene or ortho-fluoroazobenzene as the photo-responsive linker. The ortho-fluorinated version (F-dimer) was designed to extend the absorption wavelength into the visible range and enhance the thermal stability of the Z-isomer, addressing key limitations of unmodified azobenzenes in biological applications.

We hypothesized that, despite the presence of azobenzene linkers, the dimeric PAR structures would maintain their antibacterial properties. Furthermore, we envisioned that the Z-isomer configuration would introduce steric hindrance at the enzymatic binding sites of AMEs, thereby reducing enzymatic modification and potentially overcoming AME-mediated bacterial resistance. This effect arises because, in the Z-isomer, the amino sugar rings are arranged in a more crowded spatial configuration, interfering with AME binding and enzymatic modification. By leveraging photo-switchable elements, these dimers offer a novel approach to spatial and temporal control over aminoglycoside activity, providing a promising strategy to combat bacterial resistance mechanisms while minimizing off-target effects and environmental antibiotic accumulation.

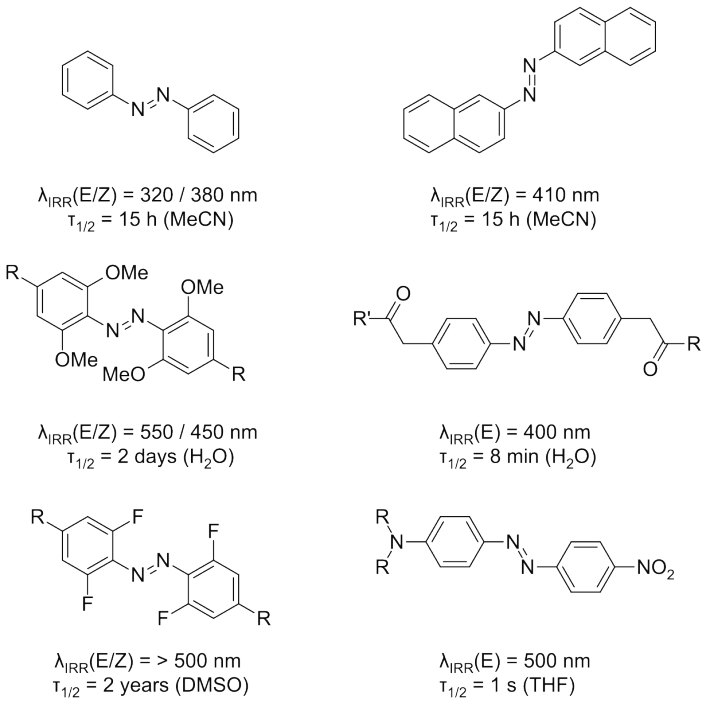


Figure 3.4 | Structural representation of azobenzene and ortho-substituted azobenzenes illustrating their photochemical properties. $\lambda_{E\rightarrow Z}$ and $\lambda_{Z\rightarrow E}$ indicate the wavelengths required for $E\rightarrow Z$ and $Z\rightarrow E$ isomerization, respectively. Additionally, the half-life of each Z isomer in various solvents is shown. The red shifts induced by different substituents highlight their influence on the absorption properties and thermal stability of the metastable Z state, which are key parameters in the design of photoresponsive antibiotics.

SYNTHESIS AND CHARACTERIZATION OF PHOTO-SWITCHABLE PAR DIMERS

The photo-switchable PAR dimers (H-dimer and F-dimer) were synthesized by coupling azobenzene-4,4'-dicarboxylic acid and fluoro-azobenzene-dicarboxylic acid with PAR through amide bond formation. The synthesis followed a well-established two-step process: first, the carboxylic acids were activated as N-hydroxysuccinimide (NHS) esters, and then these activated esters were reacted with the aminomethyl group at position 6"' of PAR (see Figure 3.7).

The regioselective modification at position 6"' was achieved due to the preferential reactivity of the aminomethyl group under mildly activated acylation conditions, ensuring minimal side reactions at other amine positions. The H-dimer (azobenzene-linked) and F-dimer (fluoro-azobenzene-linked) derivatives were obtained in moderate yields (20–35%), consistent with previous azobenzene-functionalization reports.

Following purification via High-Performance Liquid Chromatography (HPLC), both compounds were characterized using 1D-NMR spectroscopy and Heteronuclear Single Quantum

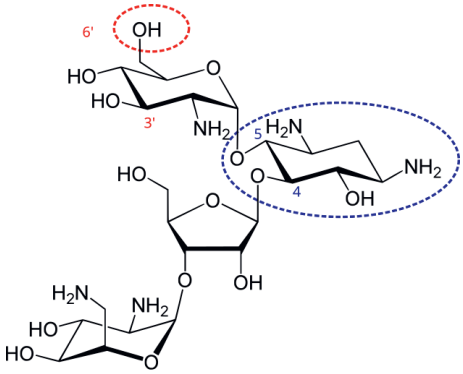
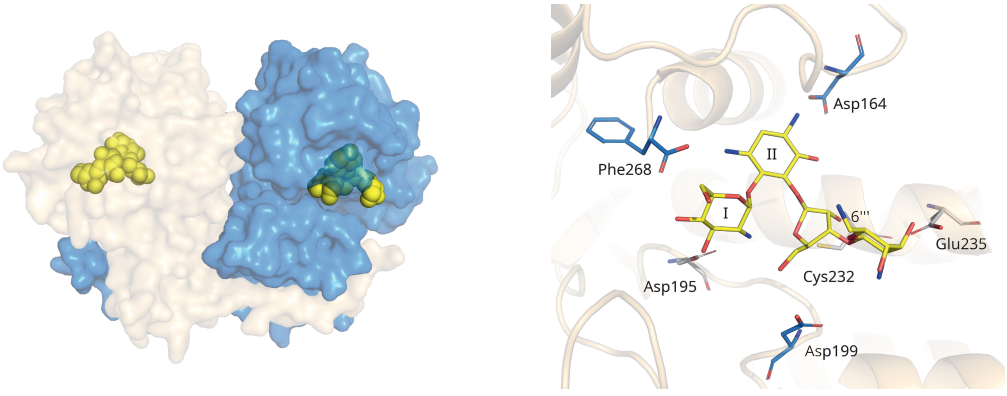


Figure 3.5 | Structural representation of PAR highlighting key functional elements: hydroxyl group in 6' position highlighted in red, the 2-deoxystreptamine (2-DOS) core is highlighted in blue, and labeled positions 3', 4, and 5 relevant for enzymatic modification and chemical diversification.



(a) **(b)**

Figure 3.6 | Crystal structure of APH(3')-Ia in complex with PAR. (a) Cartoon and surface representation of APH(3')-Ia with PAR bound (dark yellow), highlighting the quaternary structure of the enzyme-substrate complex. (b) Close-up view of the binding site, showing that the 6"' position of PAR is exposed to the solvent, confirming its minimal interaction with the enzyme's active site. This structural insight supports the feasibility of modifying this position without disrupting enzymatic recognition, forming the basis for the design of photo-switchable PAR derivatives.

Coherence (HSQC), confirming the successful conjugation of the photo-switchable moieties to PAR.
The structural integrity of the dimers was further validated by mass spectrometry and elemental analysis, ensuring that no unwanted modifications had occurred.

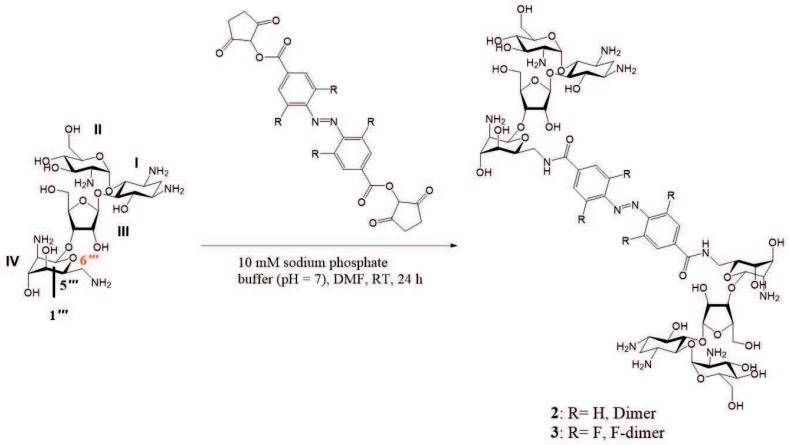
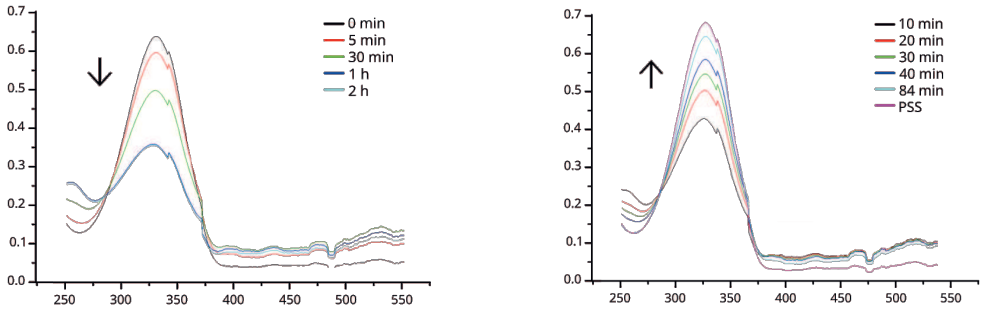


Figure 3.7 | Synthetic pathway for the preparation of H-dimer and F-dimer. The diagram illustrates the key functionalization step in the conjugation of PAR via azobenzene (H-dimer) or ortho-fluoroazobenzene (F-dimer) linkers.

3.3. PHOTOISOMERIZATION STUDIES

The photo-switching behavior of the H-dimer and F-dimer was assessed using UV–Vis spectroscopy and Ultra-Performance Liquid Chromatography (UPLC). The absorption spectra of the *E*-isomer of the H-dimer displayed a strong $\pi \rightarrow \pi^*$ transition band at 329 nm, characteristic of trans-azobenzene. Upon irradiation at 365 nm (UV light), a gradual $E \rightarrow Z$ isomerization was observed, resulting in a decrease of the 329 nm band and the formation of a photo-stationary state (PSS) containing approximately 30% of the *Z*-isomer (Figure 3.8).
Interestingly, the H-dimer spectrum exhibited two well-defined isosbestic points at 286 nm and 371 nm, indicating a clean and reversible isomerization process with no detectable side reactions. The conversion to the Z-isomer was achieved within 60 minutes, at which point the system reached equilibrium under continuous irradiation. The ability to reversibly photoswitch between E- and Z-isomers without degradation is a key feature of these compounds, making them suitable candidates for antibiotic activation control.
The F-dimer, in contrast, showed enhanced photo-stability and a red-shifted absorption profile, likely due to the electron-withdrawing effects of the fluorine substituents at the ortho-positions.
The introduction of fluorine atoms not only enabled activation in the visible range but also significantly prolonged the thermal stability of the Z-isomer, ensuring a longer residence time in the active conformation compared to the H-dimer. This finding aligns with previous



(a) (b)

Figure 3.8 | Photo-isomerization of H-dimer in MQ water monitored by UV-Vis spectroscopy. (a) Irradiation at 365 nm (UV light) induces hypochromism, leading to a decrease in absorbance as the E → Z isomerization progresses. (b) Exposure to 450 nm (blue light) triggers the Z → E isomerization, resulting in an increase in absorbance until the PSS is reached.

reports that ortho-fluorination increases the activation energy for thermal relaxation, thereby extending the half-life of the Z-state.

Further analysis using UPLC confirmed the stability of both dimers in aqueous solution, with minimal degradation observed under experimental conditions. The retention of structural integrity under prolonged irradiation supports their potential as light-activated antibiotics with controllable activity.

The reversible photoisomerization of the F-dimer was confirmed by ^{1}H Nuclear Magnetic Resonance (NMR) spectroscopy. Figure 3.10 shows the spectra of the F-dimer under different irradiation conditions and of the isolated E/Z isomers. Upon green-light irradiation ($> 500nm$), the system reached a PSS enriched in the E isomer, whereas blue-light exposure ($\tilde{4}50$ nm) generated the Z-enriched state.

HPLC purification allowed the isolation of the pure E and Z forms, confirming full spectral reversibility.

The UV-Vis absorption spectra of the F-dimer were recorded in water to assess its photo-isomerization behavior (Figure 3.9). The F-dimer exhibited a 42 nm separation between the n → π^* bands, a feature that contributes to its large switching factor. The Z-isomer spectrum displayed a strong $\pi \rightarrow \pi^*$ absorption band at 328 nm, along with a weaker n → π^* band centered at 418 nm. Spectral measurements revealed two isosbestic points at 275 nm and 390 nm.

During the $E \rightarrow Z$ transition, hypsochromic and bathochromic shifts were observed in the absorption spectra: the E-isomer peak at 328 nm decreased, accompanied by an increase in absorbance and a shift towards higher wavelengths relative to the 418 nm peak.

The ortho-fluorine substituents, acting as σ-electron withdrawing groups, lowered the n-orbital energy of the Z-isomer, leading to a separation of the $n \rightarrow \pi^*$ absorption bands between the E and Z states. This effect enabled selective excitation of the two isomers within the visible spectrum, facilitating precise photochemical control of isomerization.

The PSS composition was determined using UPLC analysis of the elution profile (Figure 3.11).

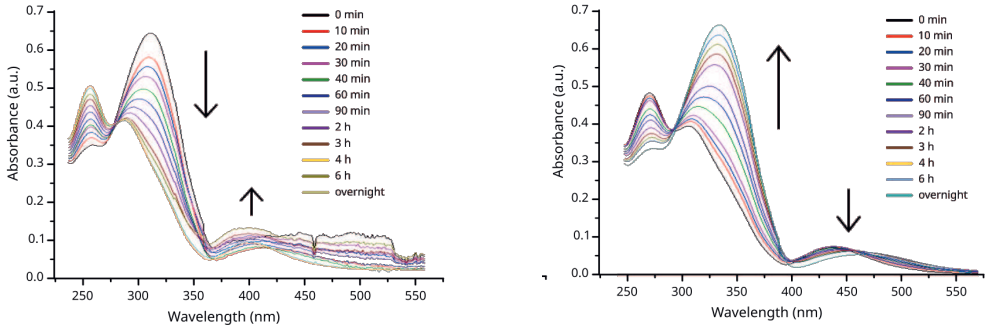


Figure 3.9 | Photo-isomerization of F-dimer in MQ water monitored by UV-Vis spectroscopy. (a) Irradiation at >500 nm (green light) induces $E \rightarrow Z$ isomerization, leading to a decrease in absorbance at the $\pi \rightarrow \pi^*$ transition and a concurrent increase at the n $\rightarrow \pi^*$ band. (b) Exposure to 450 nm (blue light) triggers $Z \rightarrow E$ isomerization, reversing the spectral changes. Arrows indicate the direction of absorbance changes over time during each transition.

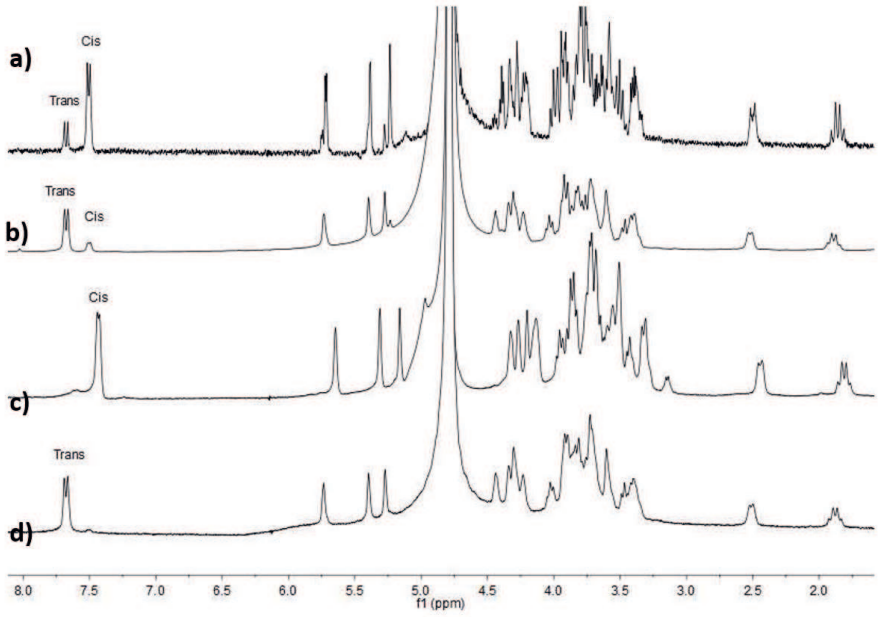
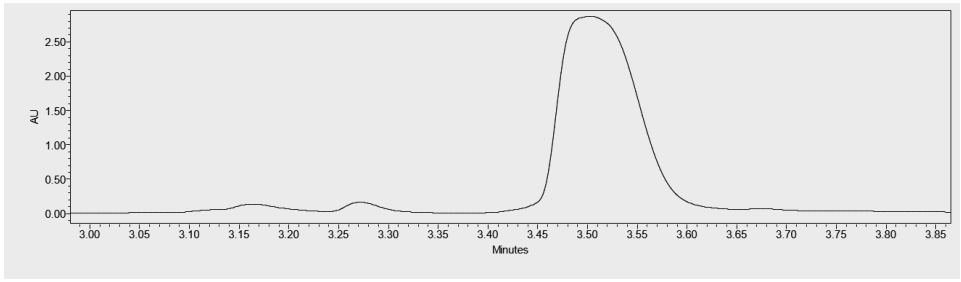


Figure 3.10 | ^{1}H NMR (500 MHz, D_2O) spectra of the F-dimer. (a) PSSobtained after irradiation with green light ($> 500nm$); (b) PSS after irradiation with blue light ($\bar{4}50$ nm); (c) pure Z-F-dimer isolated by HPLC; (d) pure E-F-dimer isolated by HPLC.

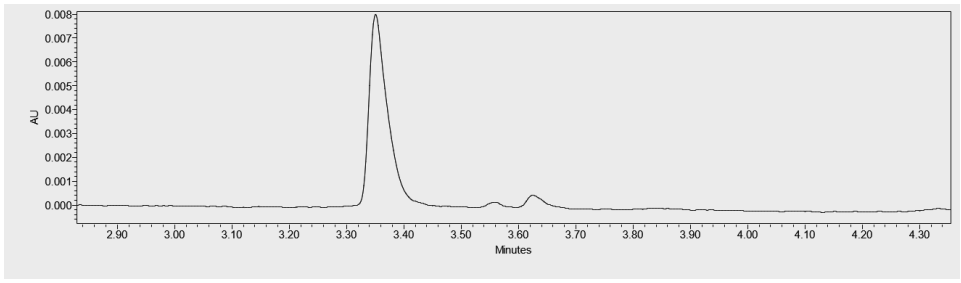
Irradiation with visible light successfully triggered E/Z isomerization in both directions, producing PSS compositions of 78% Z-1 under green light ($\lambda > 500$ nm) and 73% E-1 under blue light (450 nm). Multiple photo-switching cycles showed no noticeable degradation, indicating the high photochemical stability of the F-dimer scaffold (Figure 3.12).
In addition to photo-stability, the thermal relaxation properties of the F-dimer were examined to assess its stability in the absence of light activation (see Figure 3.13. The $Z \rightarrow E$ thermal isomerization was monitored in water at 37 °C in the dark, revealing a half-life of approximately 8 days, which is significantly longer than the H-dimer, which reverted within 1 hour under the same conditions.
The extended thermal stability of the F-dimer is attributed to the lowering of the n-orbital energy induced by ortho-fluoro substituents, which increases the activation energy required for isomerization, thereby slowing down the thermal reversion process.
This enhanced stability is a crucial factor in maintaining the Z-isomer population over extended periods, reducing the need for frequent light activation and making it a more practical candidate for potential biomedical applications.

ANTIBACTERIAL ACTIVITY OF PHOTO-SWITCHABLE PAROMOMYCIN DIMERS

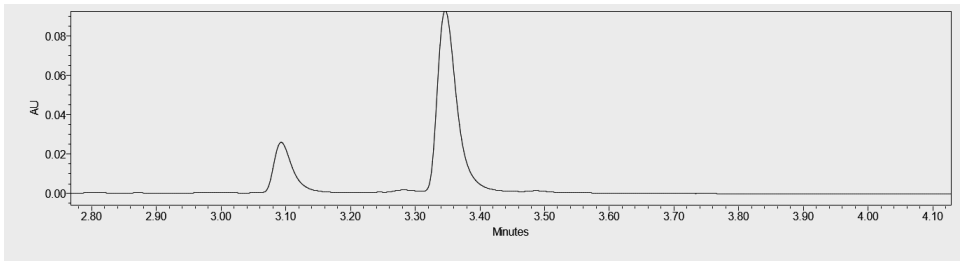
To further evaluate the impact of photoisomerization on antibiotic function, we analyzed the Minimal Inhibitory Concentration (MIC) of the H-dimer and F-dimer against *Escherichia coli* (ATCC 25922) and engineered strains expressing aminoglycoside-modifying enzymes (AMEs). MIC values were determined for both E- and Z-isomers. The MICs were measured against *E. coli* strains harboring pET9b(+) and pAT21-1, which encoded the APH(3')-Ia and APH(3')-IIIa, respectively. These enzymes transfer a phosphate group to the hydroxyl at position 3' of PAR, thereby reducing its ribosomal binding affinity. Additionally, a separate strain was engineered with pBluescript KS(+), encoding the *N*-acetyltransferase AAC(3)IV, which catalyzes acetylation of the amino group at position 3, similarly impairing antibiotic activity.
The growth inhibition assays (Figure 3.14) showed a marked difference in antibacterial activity between the E- and Z-isomers of the F-dimer (see Table 3.2. The E-isomer of the F-dimer at 256 μM strongly inhibited bacterial growth in *E. coli* expressing APH(3')IIIa, whereas the Z-isomer required a concentration of 1024 μM to achieve comparable inhibition. A similar trend was observed in *E. coli* carrying *O*-phosphotransferase (3') type Ia (APH(3')-Ia), where the E-isomer exhibited a MIC of 512 μM, while the Z-isomer required 1024 μM. In the strain expressing AAC(3)IV, the E-isomer maintained inhibitory activity at 512 μM, whereas bacterial growth persisted at 1024 μM in the presence of the Z-isomer.
When compared to pristine PAR, both H-dimer and F-dimer exhibited an approximately eightfold reduction in antibacterial efficacy against wild-type *E. coli*, resulting in a MIC of 32 μM. The Z-isomer of the H-dimer was not tested due to its limited thermal half-life, which restricted its stability under experimental conditions.
The reduced efficacy of the Z-isomer is likely attributable to increased steric hindrance, which interferes with AME recognition and modification while retaining antibiotic activity at the ribosomal binding site.
This hypothesis is further supported by crystallographic data from the APH(3')-Ia–PAR dimer



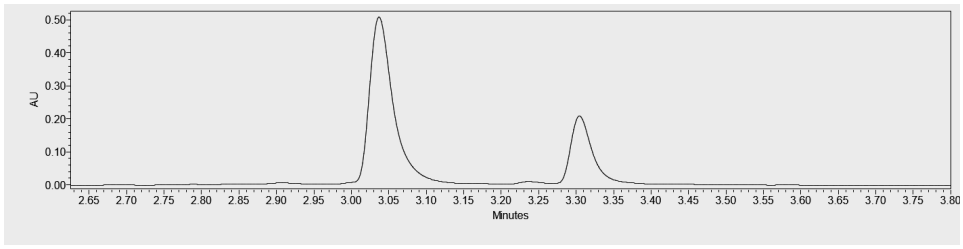
(a)



(b)

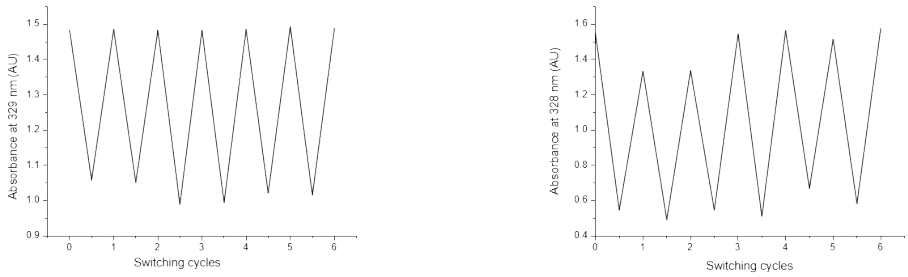


(c)



(d)

Figure 3.11 | UPLC traces of F-dimer recorded at the corresponding isosbestic points in water. (a) Pure Z-isomer after HPLC purification. (b) Pure E-isomer after HPLC purification. (c) PSS at >500 nm, showing a composition of 21.5% E and 78.5% Z. (d) PSS after exposure to 450 nm light, resulting in a mixture of 72.4% E and 27.6% Z.



(a) **(b)**

Figure 3.12 | Reversible photo-switching behavior of H-dimer and F-dimer in water at 25 °C. (A) Photochromic cycling of H-dimer (20 μM) upon alternating irradiation with UV light (λ = 365 nm) and visible light (λ = 450 nm). The absorbance was measured at 329 nm ($\pi \rightarrow \pi^*$ transition of the trans-isomer). Six consecutive E/Z cycles were performed without significant fatigue or reduction in absorbance. (B) Photochromic cycling of F-dimer (20 μM) using green light (λ > 500 nm) and blue light (λ = 450 nm). The absorbance was measured at 328 nm ($\pi \rightarrow \pi^*$ transition of the trans-isomer), demonstrating stable and reversible switching with no noticeable degradation over multiple cycles.

complex, which revealed key differences in the active-site pocket where one of the PAR moieties is bound to APH(3')-Ia.

Table 3.2 | MIC values (μg/mL) determined against *E. coli* ATCC 25922 wild type and strains expressing different AMEs. Due to its limited half-life, MIC for the *E*-isomer of H-dimer was evaluated only against wild-type *E. coli* for comparison with the F-dimer.

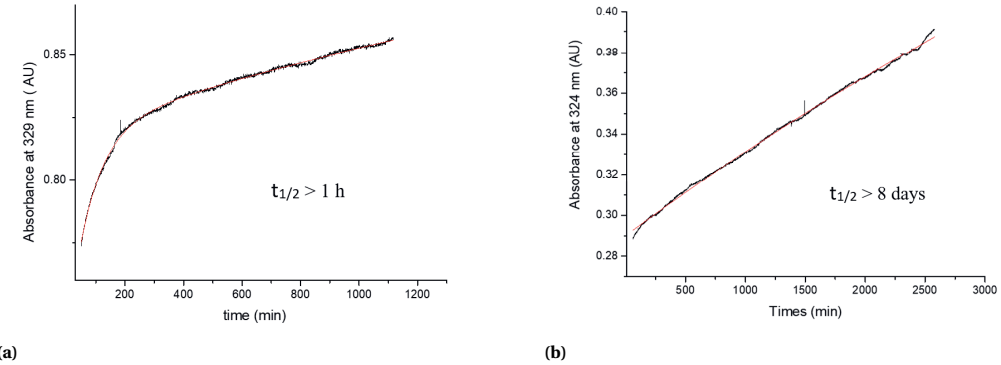
Compound	Wild Type	APH(3')-IIIa	APH(3')-IIIa	AAC(3)-IV
PAR	4	> 512	> 512	> 512
H-dimer (*E*)	32	–	–	–
F-dimer (*E*)	32	512	512	512
F-dimer (*Z*)	32	256	128	256

STRUCTURAL INSIGHTS INTO THE BINDING OF PHOTO-SWITCHABLE PAROMOMYCIN DIMERS TO APH(3')-IA

To better understand the effect of photo-switchable modification on antibiotic-enzyme interactions, we solved the crystal structure of APH(3')-Ia in complex with PAR H-dimer. The structural data revealed key differences in ligand binding when compared to pristine PAR (Figure 3.15).

While both ligands occupy the same active site, notable positional shifts, altered hydrogen bonding, and steric effects introduces by the H-dimer suggests a modified enzyme-ligand interaction that may contribute to reduced susceptibility to enzymatic modification.

The electron density maps displayed a well-defined region in the active site pocket, corresponding to one PAR unit of the H-dimer, indicating that the core aminoglycoside scaffold



(a) **(b)**

Figure 3.13 | Thermal half-life determination of H-dimer and F-dimer in aqueous solution. (a) Thermal relaxation of the photoisomerized H-dimer monitored at 37 °C in water under dark conditions. The PSS was first obtained upon 365 nm irradiation, and the subsequent decrease in absorption was followed at λ_{max} = 329 nm. (b) Thermal relaxation of the photoisomerized F-dimer under the same conditions. The PSS was reached upon > 500nm irradiation, and the decay was monitored at λ_{max} = 324 nm.

remains recognized by the enzyme. However, despite sufficient space for ligand accommodation, the azobenzene moiety and second PAR molecule could not be unambiguously resolved. This suggests that either multiple conformations of the dimer exist within the active site, or that the azobenzene linker introduces flexibility, preventing a stable single-state conformation.

When comparing this structure to the APH(3')-Ia–PAR complex, key deviations in ligand positioning and active site adaptation were observed. PAR binds deeply within the active site, with its 6"' amino group pointing towards Asp199, forming a stabilizing interaction. In contrast, in H-dimer, this group projects outward, likely due to the presence of the azobenzene linker, which, while unresolved in the electron density map, appears to interfere with deeper binding. This partial displacement suggests that H-dimer does not fit as tightly in the pocket as PAR, leading to a shift of its center of mass by approximately 1 Å and an overall RMSD of 0.53 Å between the two binding sites.

Despite these differences, the hydrogen bonding network remained largely conserved, with some local adjustments. In H-dimer, the O at 3"' interacts with Glu238, whereas in PAR, this position was solvent-exposed. Additionally, Asp162, and Phe268 exhibited slight shifts toward the exit of the binding pocket, suggesting structural accommodation for the modified ligand. One notable displacement was observed in the oxygen at the 3'-position, which in PAR is coordinated by Asp199, but in H-dimer, it shifts 2.4 Å away, bringing it closer to the backbone of Ser33 (2.7 Å), further supporting the idea of an altered ligand-enzyme interface.

These structural modifications align with the observed reduction in AME-mediated inactivation of the Z-isomer in MIC assays, where bacteria expressing APH(3')-Ia and APH(3')-IIIa exhibited higher tolerance to the E-isomer than the Z-isomer. The inability to model the full H-dimer within the active site further supports the hypothesis that steric interference from the azobenzene linker disrupts optimal ligand positioning, thereby reducing the efficiency of enzymatic modification.

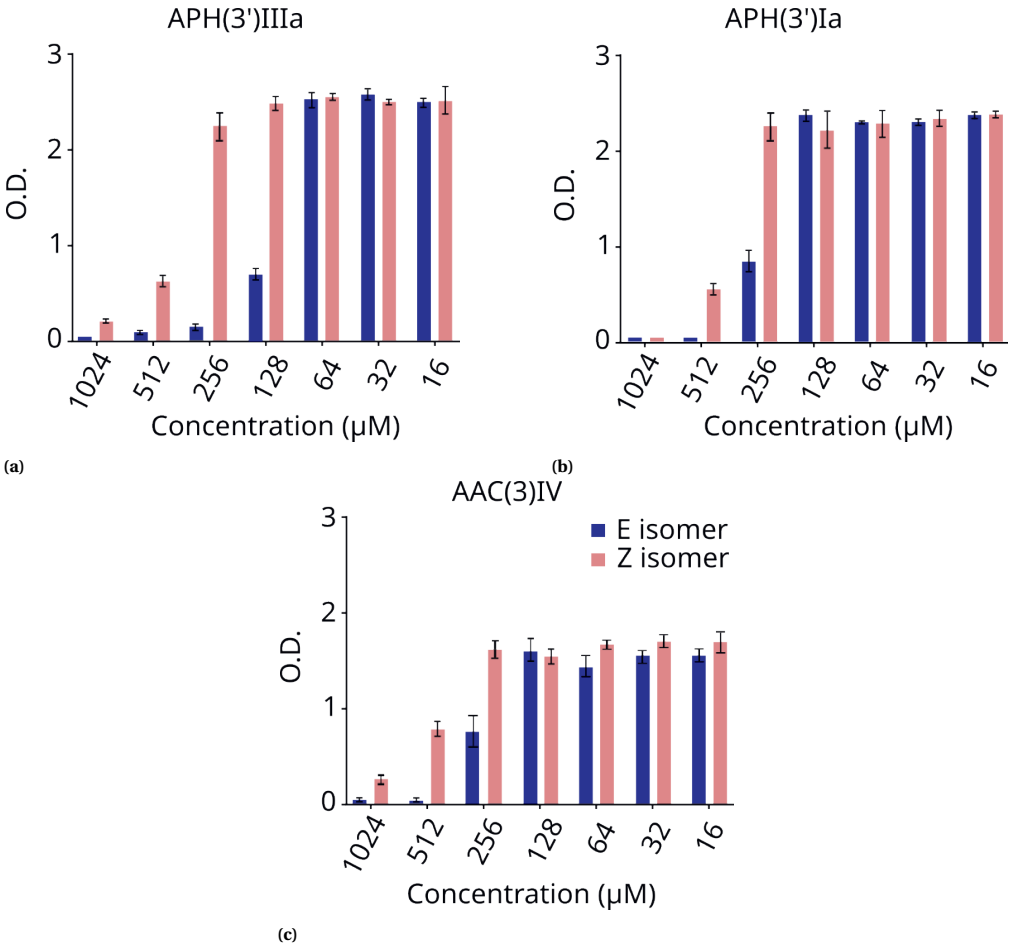
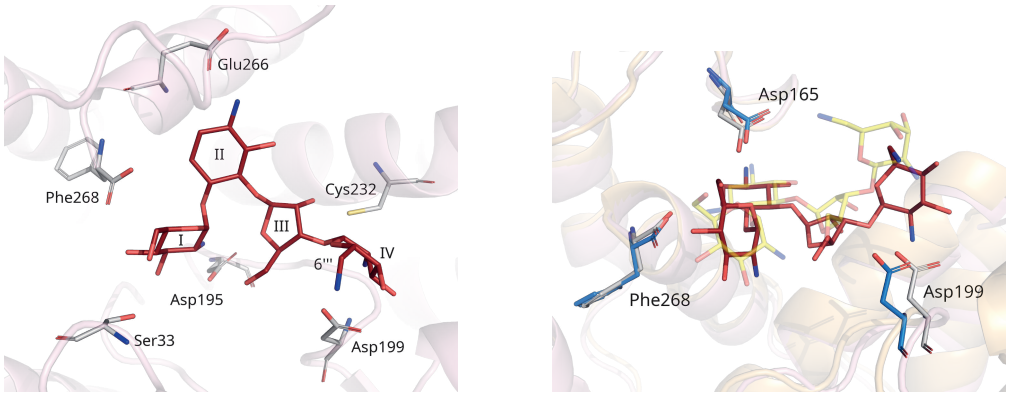


Figure 3.14 | Growth levels of *E. coli* expressing AMEs in the presence of F-dimer isomers. The growth of *E. coli* strains carrying APH(3')-IIIa, APH(3')-Ia, and AAC(3)-IV was measured after 16 hours of incubation with varying concentrations of E and Z isomers of the F-dimer, assessing the impact of photo-isomerization on antibiotic activity and resistance modulation.

The impact of photo-switching on ribosomal binding affinity remains an open question. Since the Z-isomer retains antibacterial activity, it suggests that steric hindrance affecting AME recognition does not significantly impair ribosomal interactions. Future studies will focus on resolving the ribosome-bound structure of the photo-switchable PAR dimers, aiming to fully elucidate how photo-switching influences antibiotic function and enzyme evasion mechanisms.



(a) **(b)**

Figure 3.15 | Structural comparison of APH(3')-Ia bound to PAR and H-dimer. (a) Structure of APH(3')-Ia bound to H-dimer (red), and main interactions within the binding site. (c) Superposition of the two complexes (PAR, yellow transparent; H-dimer, red). The figure highlights the difference in the positioning of ring IV whose centroids are displaced by approximately 3 Å. The azobenzene linker of H-dimer extends outward from the active site and is not resolved in the electron density. Residues involved in binding PAR are highlighted in blue.

3.4. CONCLUSIONS

In this study, we successfully synthesized and characterized H-dimer and F-dimer, two photo-switchable aminoglycoside dimers in which PAR molecules were covalently linked to an azobenzene or ortho-fluoroazobenzene moiety, respectively. These novel constructs represent the first example of conformationally restricted aminoglycosides that can be externally modulated using light, providing a unique tool for controlling antibiotic activity in a spatiotemporal manner.

A comprehensive structural and functional characterization was performed using NMR, UV–Vis spectroscopy, and ITC, alongside antimicrobial assays against *E. coli* strains expressing aminoglycoside-modifying enzymes (AMEs). Crystallographic analysis of the APH(3')-Ia–F-dimer complex provided molecular-level insights into the differential antibiotic activity of the *E*- and *Z*-isomers, revealing how photo-induced steric hindrance may interfere with AME recognition while preserving ribosomal binding. Structural analysis showed that H-dimer binds within the same active site as PAR but is partially displaced from the pocket, with key residues such as Asp162 and Phe268 shifting toward the exit of the binding pocket. These changes may contribute to reduced enzymatic phosphorylation efficiency, supporting the

observed higher MIC for the *Z*-isomer in bacterial growth assays.
Among the two dimers, the F-dimer demonstrated the most promising activity, with its *E*-isomer effectively overcoming AME-mediated resistance. The introduction of ortho-fluoro substituents not only enhanced the photophysical properties of the system—extending activation into the visible spectrum and stabilizing the *Z*-isomer—but also contributed to an improved antibiotic profile by restricting enzymatic inactivation.
Interestingly, the photo-switchable aminoglycoside dimers also exhibited antagonistic interactions in bacterial growth assays. While the *E*-isomer of F-dimer showed lower MIC values compared to its *Z* counterpart, indicating increased potency, this antagonistic effect presents both advantages and limitations. On the positive side, antagonistic behavior can reduce the selective pressure for resistance development, as bacteria are less likely to evolve resistance against weaker antibiotic combinations. However, a lower MIC does not necessarily translate to higher clinical efficacy, and in some cases, the reduced overall potency may limit the bactericidal effect. These findings suggest that while photo-switchable aminoglycosides offer a new level of control over antibiotic function, further optimization is required to balance antagonism and efficacy for clinical translation.
This work highlights the potential of photo-switchable antibiotics as a next-generation strategy to combat aminoglycoside resistance. By designing light-activated antibiotics that can be selectively switched between active and inactive states, it may be possible to minimize evolutionary pressure on bacterial populations, reducing the emergence of new resistant strains while preventing the uncontrolled accumulation of active antibiotics in the environment. The F-dimer synthesized in this study emerges as a particularly promising lead compound, demonstrating how photo-switchable modifications can be leveraged to evade enzymatic inactivation while maintaining antibiotic function. Further studies will focus on ribosome-bound structural characterization, pharmacokinetic optimization, and potential synergy with other antibiotic classes, paving the way for the development of clinically relevant light-controllable antibiotics.

FUTURE DEVELOPMENTS

Building on these findings, several key areas of future research could further advance the development of photo-switchable aminoglycoside antibiotics:

- **Optimization of the F-dimer for enhanced potency.** While the F-dimer has demonstrated promising activity, further structural modifications could improve its antibiotic potency and resistance evasion. Fine-tuning the fluorination pattern, linker rigidity, or molecular size may optimize its interaction with both bacterial ribosomes and AMEs, maximizing its therapeutic potential.

- **Ribosome-bound structural studies.** The current crystallographic data provide valuable insights into enzyme binding; however, the ribosomal interactions of the photo-switchable dimers remain unexplored. High-resolution cryo-EM or X-ray crystallography of ribosome–F-dimer complexes could reveal the precise conformational changes and their effects on translation inhibition.

- **Investigating pharmacokinetics and stability in biological systems.** Detailed pharmacokinetic studies are needed to evaluate the stability, bioavailability, and metabolic profile of these compounds in bacterial and mammalian systems. Understanding how the isomerization state affects drug distribution and clearance will be essential for future development.
- **Developing targeted light-delivery systems.** One limitation of photo-switchable antibiotics is the need for external light exposure to trigger isomerization. Strategies such as nanoparticle-based drug delivery, light-penetrating biomaterials, or upconversion nanoparticles (UCNPs) that convert near-infrared light to visible wavelengths could enable deep-tissue activation in clinical settings.
- **Expanding the photo-pharmacology approach to other antibiotic classes.** The successful application of photo-switching in aminoglycosides opens the door to extending this concept to other ribosome-targeting antibiotics, such as macrolides, tetracyclines, and oxazolidinones. The development of photo-switchable variants of these drugs could establish a broader framework for light-controlled antimicrobial therapy.

By pursuing these future directions, photo-switchable aminoglycoside antibiotics could evolve into clinically viable antimicrobial agents, providing a novel and sustainable strategy to combat aminoglycoside resistance in bacterial infections.

AUTHOR CONTRIBUTIONS

J.H., N.P., L.Z., A.G., and A.H. designed the research. J.H. and L.Z. contributed to the conceptualization of the study.

- J.H.: Conceptualization; initial study design.
- N.P.: Manuscript writing; assistance in study design; generation and interpretation of structural data.
- A.P.: Photochemical kinetics measurements and data analysis.
- L.Z.: Conceptualization; synthesis of photo-switchable dimers.
- X.Y.: Chemical synthesis and HPLC purification.
- A.G.: Supervision of structural biology; manuscript revision.
- A.H.: Project supervision; manuscript revision.

3.5. MATERIALS AND METHODS

GENERAL PROCEDURES

^{1}H-NMR and heteronuclear single-quantum correlation (HSQC) spectroscopy were performed on Varian Unity Inova (500 MHz for ^{1}H, ^{13}C, and HSQC) and Oxford AS400 (400 MHz for ^{1}H and 100.6 MHz for ^{13}C) spectrometers at 25 °C. High-resolution mass spectrometry (HRMS) was carried out using an LTQ ORBITRAP XL (Thermo Scientific) equipped with electron impact ionization in positive ion mode (EI^{+}).
Chromatographic separations were performed on a Shimadzu VP series HPLC modular system equipped with a DGU-14A3 vacuum degasser, two LC-20AT pumps, a SIL-20A autosampler, a CTP-20A column oven, an RID-10 refractive index detector, an FRC-10A fraction collector, and controlled via Shimadzu LCsolution software. HPLC purification was carried out on Waters Spherisorb ODS-2 C18 analytical (250 × 4.6 mm) and semi-preparative (250 × 10 mm) columns using isocratic elution at 20 °C.
pH adjustments of reaction buffers were performed using a Hanna Instruments pH 209 meter equipped with a glass combination electrode.

MATERIALS

All chemicals and reagents were obtained from commercial suppliers and used without further purification unless otherwise specified. PAR sulfate salt (98%) was purchased from Sigma-Aldrich and used as received. HPLC purification utilized heptafluorobutyric acid (HFBA, Fluka, *puriss. p.a.*, for ion chromatography) and acetone (Sigma-Aldrich, HPLC grade). Ultrapure water (specific resistance > 18.4 MΩ·cm) was obtained from a Milli-Q water purification system (Sartorius®).
Chromatographic separations were conducted using a Eurospher-100 C18 column (5 μm, 250 × 4 mm, 3 mL/min) with solvent A (H_2O, HPLC grade + 0.028% v/v trifluoroacetic acid, TFA) and solvent B (H_2O/MeCN, 2:1 + 0.028% v/v TFA). Detection was performed at 314 nm and 275 nm, unless otherwise stated.
All synthesized compounds, including intermediates, were stored at +5 °C unless specified otherwise. Reactions were monitored by thin-layer chromatography (TLC) on Merck silica gel 60 F_{254} plates. Column chromatography was carried out using Merck silica gel 60 (0.04–0.063 mm), with compressed air applied for MeCN/H_2O mixtures to overcome high column resistance.

PROTEIN PREPARATION

CLONING OF *aph(3')Ia*

The open reading frame (ORF) of the *aph(3')Ia* gene was codon-optimized for *E. coli* expression and synthesized by IDT Technologies (Belgium). To facilitate cloning, *NdeI* and *HindIII* restriction sites were introduced at the 5' and 3' ends, respectively. The synthesized gene was first blunt-end ligated into the pJET1.2/blunt vector (Thermo Fisher) and transformed into chemically competent *E. coli* DH5α cells for propagation.
The target gene was subsequently excised using *NdeI* and *HindIII* and subcloned into the pET28b(+) vector (Merck), yielding the construct pET28b(+)-*aph(3')Ia*, which encodes

APH(3')-Ia with an N-terminal His-tag and a thrombin-cleavable site. The final plasmid was transformed into *E. coli* BL21(DE3) (Merck) for protein overexpression.

OVEREXPRESSION AND PURIFICATION OF APH(3')-IA

The APH(3')-Ia protein was overexpressed in *E. coli* BL21(DE3)/pET28b(+)-*aph(3')Ia* following standard expression protocols. Briefly:

Expression induction Bacterial cultures were grown in LB medium supplemented with 50 μg/mL kanamycin A at 37 °C. Expression was induced at an optical density (OD_{600}) of approximately 0.6 by adding 1 mM IPTG, followed by incubation for 16 h at 16 °C. Cells were harvested by centrifugation (6000*g*, 10 min, 4 °C) and resuspended in lysis buffer (50 mM KPO_4, 500 mM NaCl, 10 mM imidazole, 1 mM PMSF, 1 μg/mL DNase, pH 7.5).

Cell lysis and soluble fraction isolation Cells were lysed using a Constant Cell Disruptor (Constant Systems Ltd.) at 25 kpsi. Insoluble material was removed by ultracentrifugation (267,000*g*, 80 min, 4 °C).

Affinity purification The cleared lysate was loaded onto a Ni-sepharose column (GE Healthcare) pre-equilibrated with Buffer A (50 mM KPO_4, 500 mM NaCl, 30 mM imidazole, 5 mM $MgCl_2$, pH 7.5). Bound protein was eluted with Buffer B (50 mM KPO_4, 500 mM NaCl, 300 mM imidazole, 5 mM $MgCl_2$, 10% glycerol, pH 7.5). Fractions containing purified protein were pooled and flash-frozen in liquid nitrogen.

Size exclusion chromatography (SEC) Further purification was achieved using a Superdex 200 10/300 GL gel filtration column (GE Healthcare) equilibrated with Buffer C (20 mM HEPES, 100 mM NaCl, 1 mM $MgCl_2$, pH 7.0). Peak fractions were concentrated to 20 mg/mL using a Vivaspin 10 kDa MWCO concentrator (GE Healthcare) and used immediately for crystallization experiments.

Protein Concentration Measurement The concentration of purified APH(3')-Ia was determined spectrophotometrically using a calculated molar extinction coefficient of 32,117$M^{-1}cm^{-1}$ (1.325 $g^{-1}Lcm^{-1}$).

CRYSTALLIZATION

APH(3')-Ia was crystallized using the hanging-drop vapor diffusion technique, following previously reported protocols [41].
The protein was crystallized at concentrations between 10 and 20 mg/mL, with 2 μL of protein solution mixed in a 1:1 ratio with crystallization solution containing 0.1 M calcium acetate and 7% PEG 3350. The drops were allowed to equilibrate against the reservoir at room temperature, leading to the formation of cubic crystals within 3 days, which ceased growing after one week.
Attempts to co-crystallize APH(3')-Ia with the H-dimer (E-isomer) were unsuccessful. Instead, ligand soaking was employed to obtain binary complex structures. Crystals of the apo enzyme

were soaked with either 3.33 mM PAR or 8 mM H-dimer, yielding well-diffracting crystals of the two binary complexes. Prior to data collection, crystals were cryoprotected using 33% glycerol and flash-frozen in liquid nitrogen.

DATA COLLECTION, PROCESSING, AND STRUCTURE DETERMINATION

X-ray diffraction data for APH(3')-Ia crystals soaked with PAR dimer were collected in-house using an ENRAF-Nonius CuKα rotating anode generator equipped with a MacScience DIP2030 image plate detector. Data for APH(3')-Ia co-crystallized with PAR (monomer) were collected at beamline P13 at the European Molecular Biology Laboratory (EMBL) outstation at Deutsches Elektronen-Synchrotron (DESY), Hamburg, Germany, using 0.99 Å wavelength radiation.

Diffraction data were processed using XDS, and phases were solved by Molecular Replacement (MR) using the program PHASER[42, 43] implemented in Phenix [44, 45], with chain A from the previously reported APH(3')-Ia structure (PDB code: 4EJ7) used as a search model. Space group determination using Pointless[46, 47] confirmed that all crystals belonged to $P3_121$ (space group 152), with two molecules in the asymmetric unit.

The electron density map was well-defined, allowing for unambiguous interpretation, with all residues from position 20 onward successfully modeled. The structure was built using Coot and refined with Phenix, applying non-crystallographic symmetry restraints during refinement. Final data collection and refinement statistics are provided in Table 3.3.

Table 3.3 | Data processing, refinement, and model statistics for the structures of APH(3')-Ia with different ligands. Statistics for the highest-resolution shell are shown in parentheses.

Parameter	**H-dimer (*E*)**	**PAR**
Wavelength (Å)	Cu Kα	1.000
Resolution range (Å)	14.42–2.046 (2.119–2.046)	46.83–1.74 (1.77–1.74)
Space group	$P3_12_1$	$P3_12_1$
Unit cell		
a, b, c (Å)	127.7, 127.7, 83.8	130.49, 130.49, 83.67
α, β, γ (°)	90.0, 90.0, 120.0	90.0, 90.0, 120.0
Total reflections	267,200 (19,548)	418,687 (22,540)
Unique reflections	49,611 (4,536)	83,671 (4,376)
Multiplicity	5.4 (4.2)	5.0 (5.2)
Completeness (%)	97.91 (82.59)	99.4 (99.9)
$\langle I \rangle / \sigma(I)$	15.76 (7.76)	13.5 (0.6)
Wilson B factor	14.22	36.42
$\mathbf{R_{merge}}$	0.1176 (0.8276)	0.053 (2.319)
$\mathbf{R_{meas}}$	0.1328 (1.003)	0.059 (2.587)
$\mathbf{R_{pim}}$	0.0598 (0.5507)	0.025 (1.128)
$\mathbf{CC_{1/2}}$	0.955 (0.603)	0.999 (0.294)
CC*	0.988 (0.868)	~1.0 (~0.87)
Reflections		

Table 3.3 (continued): Data processing, refinement, and model statistics for the structures of APH(3')-Ia with different ligands.

Parameter	H-dimer (*E*)	PAR
Total	48,961 (4,069)	78,634 (2,796)
R_{free} set	2,344 (208)	4,093 (148)
R_{work}	0.2133 (0.7035)	0.2167 (0.45)
R_{free}	0.2507 (0.7180)	0.2474 (0.44)
No. non-H atoms	4,894	4,937
Macromolecules	4,326	4,492
Ligands	161	183
Solvent	407	293
Protein residues	534	541
RMS(bonds) (Å)	0.008	0.0075
RMS(angles) (°)	0.94	1.674
Ramachandran		
Favored (%)	97.92	96.7
Allowed (%)	2.08	3.0
Outliers (%)	0.00	0.3
Rotamer outliers (%)	1.90	2.4
Clashscore	5.08	4.66
B-factors (Å^2)		
Average	42.27	48.54
Macromolecules	40.33	47.84
Ligands	74.74	59.62
Solvent	50.05	52.32
No. of TLS groups	9	0

AKNOWLEDGMENTS

The authors acknowledge DESY (Hamburg, Germany), a member of the Helmholtz Association HGF, for the provision to experimental facilities. Part of this research was carried out at PETRA III and we thank Dr. Panneerselvam Saravanan for the assistance in using photon beamline P13.

FUNDING

This project has received funding from the European Union's Horizon 2020 research and innovation program under the Marie Sklodowska Curie grant agreement No 713482, and the European Research Council Advanced Grant SUPRABIOTICS No. 694610.

3.6. SUPPORTING INFORMATION

SYNTHESIS OF AZOBENZENE-4,4'-DICARBOXYLIC ACID (5)

COMPOUND SYNTHESIS

Compound **5** was synthesized following the procedure described by Panthappally S. Zacharias.
4-Nitrobenzoic acid (**4**, 15.00 g, 89.8 mmol) was added to a solution of sodium hydroxide (50 g in 225 mL H_2O), and the mixture was heated until complete dissolution.
A hot aqueous glucose solution (100 g in 150 mL H_2O) was then added dropwise at 50 °C. During the addition, a yellow precipitate initially formed, which gradually turned into a brown solution as the reaction progressed.
The solution was stirred at room temperature overnight, resulting in a dark solution that, after standing for several hours, yielded a bright brown precipitate. The solid was filtered, dissolved in water, and acidified with 20 mL of acetic acid, upon which a light pink precipitate was obtained.
The product was filtered, washed thoroughly with water (300 mL), and dried to yield compound **5** (6.18 g, 22.9 mmol, 51%).

SPECTROSCOPIC DATA

^{1}H NMR (400 MHz, DMSO-d_6): δ 8.01–8.03 (d, 4H), 8.16–8.18 (d, 4H), 13.25 (brs, 1H).
^{13}C NMR 100 MHz, DMSO-d_6): δ 122.84, 130.70, 132.87, 154.18, 167.75.
HRMS (ESI$^-$): m/z = 269.2054 (calculated for [M – H]$^-$, 269.2440).

SYNTHESIS OF 4,4'-BIS(2,5-DIOXOPYRROLIDIN-1-YL ESTER) AZOBENZENE (6)

SYNTHESIS

Azobenzene-4,4'-dicarboxylic acid (**5**, 3.00 g, 11.1 mmol) was dissolved in dimethylformamide (DMF) and heated to 60 °C. To this solution, N-hydroxysuccinimide (NHS, 3.07 g, 26.7 mmol), EDC·HCl (5.12 g, 26.7 mmol), and a catalytic amount of DMAP were added sequentially.
The reaction mixture was stirred at room temperature for 12 h. Subsequently, pure water (200 mL) was added slowly until a red precipitate formed, which was then collected by filtration.
The solid was washed repeatedly with water (100 mL) and dried to yield compound **6** as a light red powder (4.85 g, 10.4 mmol, 94%).

SPECTROSCOPIC DATA

^{1}H NMR (400 MHz, DMSO-d_6): δ 2.93 (s, 8H), 8.17–8.19 (d, 4H), 8.35–8.37 (d, 4H).
^{13}C NMR (100 MHz, DMSO-d_6): δ 25.59, 124.57, 126.47, 129.23, 152.70, 161.23, 168.00.

SYNTHESIS OF PAROMOMYCIN–AZOBENZENE CONJUGATES

SYNTHESIS

All PAR–azobenzene conjugates were synthesized following the general strategy outlined in Figure 3.16. PAR sulfate salt was first converted to its free base form using ion-exchange resin

treatment.
To obtain the photoswitchable PAR derivatives, azobenzene units were introduced through their carboxylic acid functionality. The azobenzenes were dissolved in dry DMF and activated using NHS in the presence of N,N'-dicyclohexylcarbodiimide (DCC).
The activated azobenzene esters (1 equiv) were then reacted with an excess of PAR (10 equiv) in a water/DMF mixture. This reaction scheme is also suitable for parallel synthesis.
The transformation of PAR with azo–NHS yielded monoacetylated PAR derivatives, corresponding to the 6"'N-acetyl PAR–azobenzene conjugate in a 1:1 stoichiometry, as well as dimeric photoswitchable 6"'N-acetyl PAR species.
Final purification of the photoswitchable aminoglycosides was achieved by HPLC.

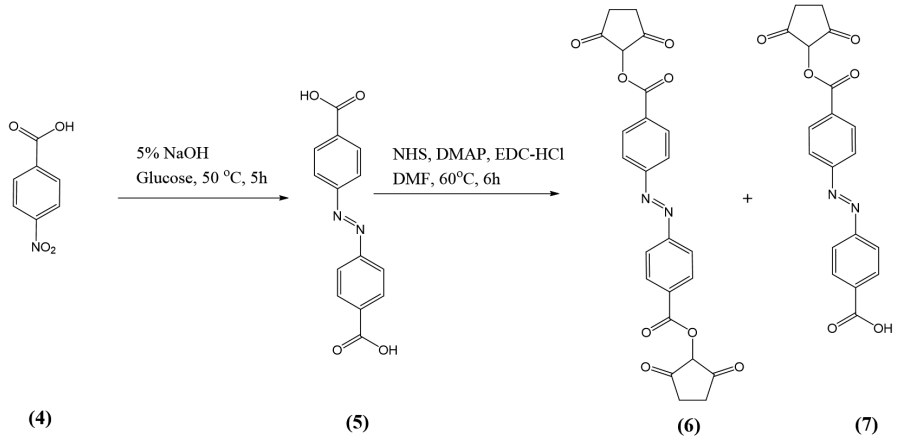


Figure 3.16 | Synthetic routes to compounds 5, 6 and 7.

SYNTHESIS OF H-DIMER (COMPOUND 2)

SYNTHESIS

In a 5 mL round-bottom flask, azobenzene-4,4′-dicarboxylic acid (16.2 mg, 0.060 mmol) and *N*-hydroxysuccinimide (13.8 mg, 0.120 mmol) were dissolved in dry DMF (20 mL). After the addition of *N,N*′-dicyclohexylcarbodiimide (24.8 mg, 0.120 mmol), the reaction mixture was stirred for 12 h under an inert atmosphere at room temperature. The precipitated dicyclohexylurea (DCU) was removed by filtration. The resulting 4,4′-bis(2,5-dioxopyrrolidin-1-yl)azobenzene was used for coupling without further purification.
PAR (0.30 mmol) was dissolved in 20 mM sodium phosphate buffer (20 mL, pH 7.0). A solution of 4,4′-bis(2,5-dioxopyrrolidin-1-yl)azobenzene in DMF (2.5 mL) was added dropwise over 3 h. The reaction was continued overnight under an inert atmosphere at room temperature. The solvent was evaporated, and the crude residue was purified by column chromatography using a homogeneous dichloromethane/methanol/aqueous 25% ammonia mixture (from 2:2:1 to 2:3:2 v/v/v). After evaporation of the solvents, the residue was redissolved in water (3 mL),

and traces of silica were removed by filtration through 0.45 μm syringe filters. Lyophilization afforded compound **2** as an orange solid (53.6 mg, 0.030 mmol, 61%).

SPECTROSCOPIC DATA

^{1}**H NMR** (500 MHz, D_2O, *E*-isomer): δ 8.09–8.07 (d, 4H, *azo*), 8.01–8.00 (d, 4H, *azo*), 5.71 (d, J = 3.5 Hz, 1H, 1-H′), 5.40 (d, J = 1.5 Hz, 1H, 1-H″), 5.27 (s, 1H, 1-H‴), 4.43 (t, J = 5.5 Hz, 1H, 3-H″), 4.33 (m, 1H, 2-H″), 4.32 (m, 1H, 3-H‴), 4.31 (t, J = 5.5 Hz, 1H, 5-H‴), 4.24 (m, 1H, 4-H″), 4.04 (t, J = 7.8 Hz, 1H, 4-H), 3.95–3.81 (m, 4H, 5a-H″, 6a-H′, 3-H′, 5-H), 3.83–3.71 (m, 4H, 5-H′, 5b-H″, 6b-H′, 4-H‴), 3.75 (t, J = 9.5 Hz, 1H, 6-H), 3.62 (t, J = 9.75 Hz, 1H, 3-H), 3.61 (m, 1H, 2-H‴), 3.46 (t, J = 7.75 Hz, 1H, 4-H′), 3.38 (dd, J = 11.0, 4.0 Hz, 1H, 2-H′), 3.41 (m, 1H, 1-H), 2.54 (dt, J = 13.0, 4.0 Hz, 1H, 2-He), 1.90 (dd, J = 12.0 Hz, 1H, 2-Ha).

^{13}**C NMR** (HSQC-assisted assignments, 500 MHz, D_2O): δ 127.48 (*azo*), 122.49 (*azo*), 109.67 (C-1″), 96.23 (C-1′), 93.25 (C-1‴), 84.19 (C-5), 82.05 (C-4″), 77.67 (C-4), 76.49 (C-3″), 73.98 (C-5′), 73.90 (C-2″), 72.56 (C-5‴), 72.30 (C-6), 69.43 (C-4′), 69.03 (C-3′), 67.74 (C-3‴), 66.46 (C-4‴), 60.50 (2C, C-5″, C-6′), 53.82 (C-2′), 51.17 (C-2‴), 49.78 (C-1), 49.02 (C-3), 40.35 (C-6‴), 28.15 (C-2).

HRMS (ESI): m/z = 1466.4542 (calculated for $[M + H]^+$, $C_{64}H_{88}N_{14}O_{22}$, 1466.4820).

SYNTHESIS OF 2,6-DIFLUORO-4-BROMOANILINE (COMPOUND 9)

SYNTHESIS

NBS (35.6 g, 200 mmol) was added to a solution of 2,6-difluoroaniline (**8**, 25.8 g, 200 mmol) in acetonitrile (300 mL) and the mixture was stirred overnight at room temperature. The reaction mixture was diluted with water and hexanes, the layers were separated, and the organic phase was dried over $MgSO_4$, filtered, and concentrated *in vacuo*. The residue was purified by column chromatography (DCM/hexanes 1:1) to give **9** as a purple solid (33.5 g, 80%).

SPECTROSCOPIC DATA

^{1}**H NMR** (300 MHz, $CDCl_3$): δ 7.00 (dd, J = 6.1, 1.3 Hz, 2H), 3.75 (br s, 2H).

^{13}**C NMR** (75 MHz, $CDCl_3$): δ 153.36, 150.12, 123.50, 114.72, 107.09.

SYNTHESIS OF 4-AMINO-3,5-DIFLUOROBENZONITRILE (10)

SYNTHESIS

Compound **9** (20 g, 96 mmol) and CuCN (25.6 g, 288 mmol) were dissolved in DMF (100 mL) and the mixture was refluxed overnight. After cooling, the mixture was poured into 12% aqueous NH_3 and extracted with EtOAc. The combined organic layers were dried over $MgSO_4$, filtered, and concentrated *in vacuo*. Purification by column chromatography (DCM/hexanes 2:1) afforded **10** as a white solid (9.2 g, 62%).

SPECTROSCOPIC DATA

^{1}**H NMR** (300 MHz, $CDCl_3$): δ 7.16 (dd, J = 6.1, 2.2 Hz, 2H), 4.29 (br s, 2H).

SYNTHESIS OF 4-AMINO-3,5-DIFLUOROBENZOIC ACID (11)

SYNTHESIS

Compound **10** (6.9 g, 45 mmol) was suspended in 1 M NaOH (150 mL) and refluxed overnight. After cooling, 1 M HCl was added until the hydrochloride salt of **11** precipitated. The precipitate was dissolved in EtOAc, dried over $MgSO_4$, filtered, and concentrated *in vacuo*. The product was obtained as a white solid and used without further purification.

SPECTROSCOPIC DATA

^{1}**H NMR** (300 MHz, DMSO-d_6): δ 7.40 (dd, J = 4.2, 1.4 Hz, 2H), 3.81 (br s, 2H).
^{13}**C NMR** (75 MHz, DMSO-d_6): δ 165.96, 150.65, 148.74, 130.65, 115.59, 112.22.
HRMS (ESI$^-$): m/z = 172.0278 (calculated for $[M-H]^-$, 172.0204).

SYNTHESIS OF ETHYL 4-AMINO-3,5-DIFLUOROBENZOATE (12)

SYNTHESIS

To a solution of acid **11** (5.92 g, 28 mmol) in EtOH (100 mL) was added H_2SO_4 (2 mL), and the mixture was refluxed for 5 h. Saturated $NaHCO_3$ was added to neutralize (pH 7). The mixture was extracted with DCM; the combined organic layers were dried over $MgSO_4$ and filtered. Concentration under reduced pressure gave **12** as a pale brown solid (4.2 g, 69% over two steps).

SPECTROSCOPIC DATA

^{1}**H NMR** (300 MHz, $CDCl_3$): δ 7.50 (dd, J = 7.2, 2.2 Hz, 2H), 4.30 (q, J = 7.1 Hz, 2H), 4.07 (br s, 2H), 1.34 (t, J = 7.1 Hz, 3H).
^{13}**C NMR** (75 MHz, $CDCl_3$): δ 165.19, 152.21, 149.03, 128.78, 118.38, 112.55, 61.04, 14.25.
HRMS (ESI$^+$): m/z = 202.0535 (calculated for $[M+H]^+$, 202.0680).

SYNTHESIS OF DIETHYL 4,4'-(2,2',6,6'-TETRAFLUORO)AZOBENZENE-4,4'-DICARBOXYLATE (13)

SYNTHESIS

Compound **12** (600 mg, 3.0 mmol) was dissolved in DCM (100 mL), and a freshly ground mixture of $KMnO_4$ (5.1 g) and $FeSO_4{\cdot}7H_2O$ (5.1 g) was suspended in this solution. The mixture was refluxed overnight, filtered through Celite, dried over $MgSO_4$, filtered, and concentrated *in vacuo*. Purification by column chromatography (DCM/hexanes 1:1) afforded **13** as an orange–red solid (136 mg, 23%).

SPECTROSCOPIC DATA
^{1}H NMR (300 MHz, $CDCl_3$, *E*-isomer): δ 7.76 (m, 4H), 4.45 (q, J = 7.0 Hz, 4H), 1.45 (t, J = 7.0 Hz, 6H).
^{13}C NMR (75 MHz, $CDCl_3$, *E*-isomer): δ 163.63, 156.75, 153.24, 133.80, 113.90, 62.18, 14.20.
HRMS (ESI$^+$): m/z = 399.0999 (calculated for $[M + H]^+$, 399.0968).

SYNTHESIS OF 4,4'-(2,2',6,6'-TETRAFLUORO)AZOBENZENE-4,4'-DICARBOXYLIC ACID (14, F_4-DIACID)

SYNTHESIS
Compound **13** (F_4-diester; 136 mg, 0.34 mmol) and KOH (67 mg, 1.19 mmol) were dissolved in H_2O/THF (2:1, 4 mL) and heated at 70 °C for 2 h. The mixture was diluted with water and EtOAc, the layers were separated, and the aqueous layer was washed twice with EtOAc. The aqueous layer was then acidified with 1 M HCl until an orange precipitate formed. Filtration afforded **14** as an orange solid (113 mg).
The reaction scheme from compound **8** to **14** is outlined in Figure 3.17

SPECTROSCOPIC DATA
HRMS (ESI$^-$): m/z = 342.0264 (calculated for $[M - H]^-$, 342.2056).

Conversion of PAR sulfate to the free base A solution of PAR sulfate (0.30 mmol) in H_2O/MeOH (1:1, 10 mL) was treated with ion-exchange resin and stirred for 2 h at room temperature. The resin was removed by filtration, the aqueous solution was concentrated under reduced pressure to remove MeOH, and the residue was lyophilized.

SYNTHESIS OF F-DIMER (COMPOUND 3)

SYNTHESIS
In a 5 mL round-bottom flask, F_4-diacid (**14**, 20.4 mg, 0.060 mmol) and *N*-hydroxysuccinimide (13.8 mg, 0.120 mmol) were dissolved in dry DMF (20 mL). After addition of *N,N'*-dicyclohexylcarbodiimide (24.8 mg, 0.120 mmol), the reaction mixture was stirred for 12 h under an inert atmosphere at room temperature. The precipitated dicyclohexylurea (DCU) was removed by filtration. The resulting F_4-diacid–NHS ester was used for coupling without further purification.
PAR (0.30 mmol) was dissolved in 20 mM sodium phosphate buffer (20 mL, pH 7.0). A solution of the F_4-diacid–NHS ester in DMF (2.5 mL) was added dropwise over 3 h. The reaction was stirred overnight under an inert atmosphere at room temperature. The solvent was evaporated, and the crude mixture was purified by column chromatography using a homogeneous DCM/MeOH/aq. 25% NH_3 gradient (from 2:2:1 to 2:3:2 v/v/v). After evaporation of solvents, the residue was redissolved in water (3 mL) and traces of silica were removed by filtration

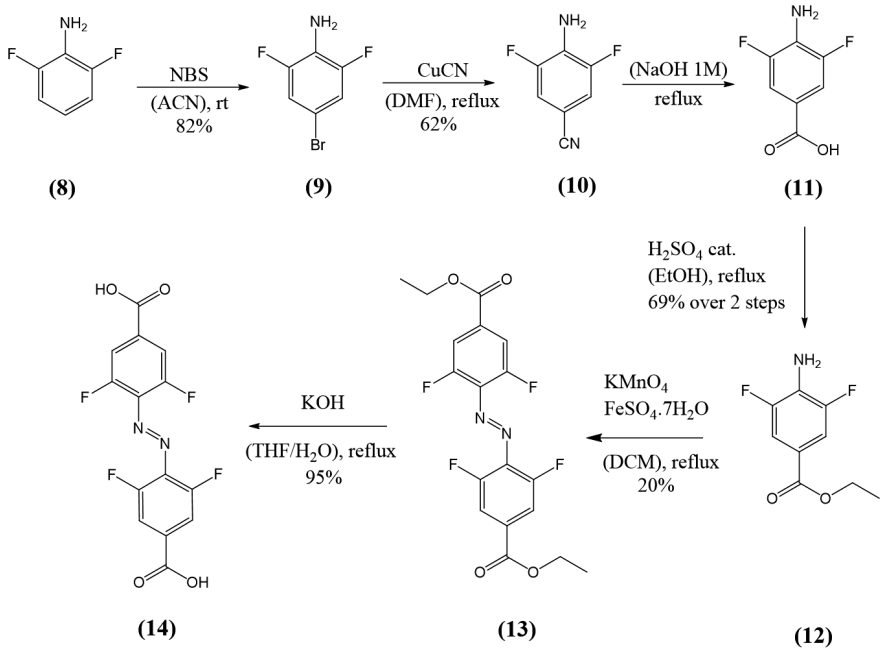


Figure 3.17 | Synthetic routes to F_4-diacid compound 14.

through 0.45 μm syringe filters. Lyophilization afforded the *F*-dimer **3** as an orange solid (51.2 mg, 0.030 mmol, 56%).

SPECTROSCOPIC DATA

^{1}H NMR (500 MHz, D_2O, *E*-isomer): δ 7.69 (m, 4H, *azo*), 5.73 (d, J = 3.5 Hz, 1H, 1-H′), 5.40 (d, J = 1.5 Hz, 1H, 1-H″), 5.27 (s, 1H, 1-H‴), 4.44 (t, J = 5.5 Hz, 1H, 3-H″), 4.34 (m, 1H, 2-H″), 4.31 (m, 1H, 3-H‴), 4.28 (t, J = 5.5 Hz, 1H, 5-H‴), 4.24 (m, 1H, 4-H″), 4.04 (t, J = 7.8 Hz, 1H, 4-H), 3.92–3.81 (m, 4H, 5a-H″, 6a-H′, 3-H′, 5-H), 3.84–3.71 (m, 4H, 5-H′, 5b-H″, 6b-H′, 4-H‴), 3.73 (t, J = 9.5 Hz, 1H, 6-H), 3.61 (m, 1H, 2-H‴), 3.57 (t, J = 9.75 Hz, 1H, 3-H), 3.47 (t, J = 7.75 Hz, 1H, 4-H′), 3.40 (dd, J = 11.0, 4.0 Hz, 1H, 2-H′), 3.85–3.72 (m, 3H, 6a-H‴, 6b-H‴), 3.38 (m, 1H, 1-H), 2.50 (dt, J = 13.0, 4.0 Hz, 1H, 2-He), 1.86 (dd, J = 12.0 Hz, 1H, 2-Ha).

^{13}C NMR (HSQC-assisted assignments, 500 MHz, D_2O): δ 111.76 (*azo*), 109.64 (C-1″), 96.02 (C-1‴), 92.12 (C-1′), 84.12 (C-5), 81.97 (C-4″), 77.59 (C-4), 76.31 (C-3″), 73.90 (C-5′), 73.87 (C-2″), 72.48 (C-5‴), 72.22 (C-6), 69.25 (C-4′), 68.82 (C-3′), 67.67 (C-3‴), 66.33 (C-4‴), 60.36 (2C, C-5″, C-6′), 53.75 (C-2′), 51.09 (C-2‴), 49.61 (C-1), 48.81 (C-3), 40.31 (C-6‴), 28.07 (C-2).

HRMS (ESI$^+$): m/z = 1539.242 (calculated for $[M + H]^+$, 1538.443).

SYNTHESIS OF P-(PHENYLAZO)BENZOIC ACID (16)

SYNTHESIS

A solution of nitrosobenzene (**15**, 2.00 g, 18.69 mmol) in glacial AcOH (20 mL) was added to a suspension of *p*-aminobenzoic acid (**4**, 3.07 g, 22.43 mmol) in glacial AcOH (15 mL). The mixture was stirred at room temperature for 24 h. The solvent was evaporated to dryness and the residue was suspended in water and lyophilized. Recrystallization from EtOAc afforded **16** as an orange solid (3.37 g, 14.91 mmol, 80%). M.p. 247 °C.

SPECTROSCOPIC DATA

IR (KBr) ν_{max} 3200–2300, 1678, 1429, 1289 cm^{-1}.

^{1}H NMR (400 MHz, DMSO-d_6): δ 7.56–7.65 (m, 3H), 7.88–7.99 (m, 4H), 8.10–8.17 (m, 2H), 13.13 (br s, 1H).

HRMS (ESI$^-$): m/z = 225.0661 (calculated for $[M - H]^-$, 225.0670).

SYNTHESIS OF P-(PHENYLAZO)BENZOIC ACID-PAR CONJUGATE (17)

SYNTHESIS

In a 5 mL round-bottom flask, *p*-(phenylazo)benzoic acid (**16**, 20.3 mg, 0.090 mmol) and *N*-hydroxysuccinimide (12.4 mg, 0.110 mmol) were dissolved in dry DMF (20 mL). After addition of *N,N′*-dicyclohexylcarbodiimide (24.8 mg, 0.120 mmol), the reaction mixture was stirred for 12 h under an inert atmosphere at room temperature. The precipitated dicyclohexylurea (DCU) was removed by filtration, and the resulting *p*-(phenylazo)benzoic acid–NHS ester was used for coupling without further purification.

PAR (1.00 mmol) was dissolved in 20 mM sodium phosphate buffer (20 mL, pH 7.0). A solution of the *p*-(phenylazo)benzoic acid–NHS ester in DMF (10 mL) was added dropwise over 3 h.

The reaction was stirred overnight under an inert atmosphere at room temperature. The solvent was evaporated, and the crude residue was purified by column chromatography using a DCM/MeOH/aq. 25% NH_3 gradient (from 5:3:1 to 2:2:1 v/v/v). After evaporation of solvents, the residue was redissolved in water (3 mL), and traces of silica were removed by filtration through 0.45 μm syringe filters. Lyophilization afforded **17** as an orange solid (49.3 mg, 0.060 mmol, 67%).

SPECTROSCOPIC DATA

^{1}**H NMR** (500 MHz, D_2O, *E*-isomer): δ 7.83–7.90 (m, 6H, *azo*), 7.62 (m, 3H, *azo*), 5.64 (d, J = 3.5 Hz, 1H, 1-H′), 5.40 (d, J = 1.5 Hz, 1H, 1-H″), 5.28 (s, 1H, 1-H‴), 4.41 (t, J = 5.5 Hz, 1H, 3-H″), 4.34 (m, 1H, 2-H″), 4.31 (m, 1H, 3-H‴), 4.30 (t, J = 5.5 Hz, 1H, 5-H‴), 4.23 (m, 1H, 4-H″), 3.93 (t, J = 7.8 Hz, 1H, 4-H), 3.92–3.80 (m, 4H, 5a-H″, 6a-H′, 3-H′, 5-H), 3.84–3.72 (m, 4H, 5-H′, 5b-H″, 6b-H′, 4-H‴, 6-H), 3.63 (m, 1H, 2-H‴), 3.90–3.60 (m, 3H, 6a-H‴, 6b-H‴), 3.58 (t, J = 9.75 Hz, 1H, 3-H), 3.42 (t, J = 7.75 Hz, 1H, 4-H′), 3.32 (dd, J = 11.0, 4.0 Hz, 1H, 2-H′), 3.39 (m, 1H, 1-H), 2.51 (dt, J = 13.0, 4.0 Hz, 1H, 2-He), 1.86 (dd, J = 12.0 Hz, 1H, 2-Ha).
^{13}**C NMR** (HSQC-assisted assignments, 500 MHz, D_2O): δ 132.36 (*azo*), 129.54 (*azo*), 128.36 (*azo*), 122.60 (*azo*), 109.66 (C-1″), 96.09 (C-1′), 95.97 (C-1‴), 84.08 (C-5), 81.83 (C-4″), 77.59 (C-4), 76.26 (C-3″), 73.84 (C-5′), 73.82 (C-2″), 72.75 (C-5‴), 72.23 (C-6), 69.27 (C-4′), 68.80 (C-3′), 67.70 (C-3‴), 66.48 (C-4‴), 60.34 (2C, C-5″, C-6′), 53.70 (C-2′), 51.07 (C-2‴), 49.58 (C-1), 48.74 (C-3), 40.28 (C-6‴), 28.05 (C-2).
HRMS (ESI$^+$): m/z = 824.8014 (calculated for $[M + H]^+$, 824.8540).

SYNTHESIS OF AZOBENZENE-4,4'-DICARBOXYLIC ACID-MONO-NHS-PAR CONJUGATE (18)

SYNTHESIS

In a 5 mL round-bottom flask, azobenzene-4,4′-dicarboxylic acid (26.9 *mg*, 0.10 mmol) and *N*-hydroxysuccinimide (13.8 mg, 0.120 mmol) were dissolved in dry DMF (20 mL). After addition of *N,N*′-dicyclohexylcarbodiimide (24.8 mg, 0.120 mmol), the reaction mixture was stirred for 12 h under an inert atmosphere at room temperature. The precipitated dicyclohexylurea (DCU) was removed by filtration, and the azobenzene-4,4′-dicarboxylic acid *mono*-NHS ester was used for coupling without further purification.
PAR (1.00 mmol) was dissolved in 20 mM sodium phosphate buffer (20 mL, pH 7.0), and a solution of the azobenzene-4,4′-dicarboxylic acid *mono*-NHS ester in DMF (10 mL) was added dropwise over 3 h. The reaction was stirred overnight under an inert atmosphere at room temperature. The solvent was evaporated, and the crude residue was purified by column chromatography using a DCM/MeOH/aq. 25% NH_3 gradient (from 5:3:1 to 2:2:1 v/v/v). After evaporation of solvents, the residue was redissolved in water (3 mL), and traces of silica were removed by filtration through 0.45 μm syringe filters. Lyophilization afforded **18** ("Azo-COOH–PAR") as an orange solid (63.7 mg, 0.070 mmol, 72%).

SPECTROSCOPIC DATA

^{1}**H NMR** (500 MHz, D_2O, *E*-isomer): δ 7.98–8.00 (d, 2H, *azo*), 7.78–7.84 (m, 6H, *azo*), 5.61 (d, J = 3.5 Hz, 1H, 1-H′), 5.37 (d, J = 1.5 Hz, 1H, 1-H″), 5.24 (s, 1H, 1-H‴), 4.39 (t, J = 5.5 Hz, 1H, 3-H″), 4.33 (m, 1H, 2-H″), 4.32 (m, 1H, 3-H‴), 4.24 (t, J = 5.5 Hz, 1H, 5-H‴), 4.19 (m, 1H, 4-H″), 3.88 (t, J = 7.8 Hz, 1H, 4-H), 3.88–3.81 (m, 4H, 5a-H″, 6a-H′, 3-H′, 5-H), 3.79–3.63 (m, 4H, 5-H′, 5b-H″, 6b-H′, 4-H‴), 3.65 (t, J = 9.5 Hz, 1H, 6-H), 3.60 (m, 1H, 2-H‴), 3.50 (t, J = 9.75 Hz, 1H, 3-H), 3.39 (t, J = 7.75 Hz, 1H, 4-H′), 3.29 (dd, J = 11.0, 4.0 Hz, 1H, 2-H′), 3.77–3.48 (m, 3H, 6a-H‴, 6b-H‴), 3.36 (m, 1H, 1-H), 2.45 (dt, J = 13.0, 4.0 Hz, 1H, 2-He), 1.84 (dd, J = 12.0 Hz, 1H, 2-Ha).

^{13}**C NMR** (HSQC-assisted assignments, 500 MHz, D_2O): δ 129.53 (*azo*), 127.90 (*azo*), 122.20 (*azo*), 109.33 (C-1″), 95.68 (C-1′), 95.40 (C-1‴), 83.72 (C-5), 81.35 (C-4″), 77.74 (C-4), 77.74 (C-3″), 73.28 (C-5′), 73.28 (C-2″), 72.18 (C-5‴), 71.90 (C-6), 68.83 (C-4′), 68.47 (C-3′), 67.31 (C-3‴), 65.95 (C-4‴), 59.92 (2C, C-5″, C-6′), 53.33 (C-2′), 50.64 (C-2‴), 49.34 (C-1), 48.43 (C-3), 39.70 (C-6‴), 28.11 (C-2).

HRMS (ESI$^+$): m/z = 868.8462 (calculated for $[M + H]^+$, 868.8637).

REFERENCES

[1] H. Brüssow, *The antibiotic resistance crisis and the development of new antibiotics,* Microbial Biotechnology **17**, e14510 (2024).

[2] M. Terreni, M. Taccani, and M. Pregnolato, *New antibiotics for multidrug-resistant bacterial strains: latest research developments and future perspectives,* Molecules **26**, 2671 (2021).

[3] A. Region, S.-E. A. Region, E. M. Region, and W. P. Region, *Global action plan on antimicrobial resistance,* (2015).

[4] W. H. Organization *et al.*, *Antimicrobial resistance surveillance in europe 2022–2020 data,* (2022).

[5] A. R. Coates, G. Halls, and Y. Hu, *Novel classes of antibiotics or more of the same?* British journal of pharmacology **163**, 184 (2011).

[6] S. Garneau-Tsodikova and K. J. Labby, *Mechanisms of resistance to aminoglycoside antibiotics: overview and perspectives,* Medchemcomm **7**, 11 (2016).

[7] L. P. Kotra, J. Haddad, and S. Mobashery, *Aminoglycosides: perspectives on mechanisms of action and resistance and strategies to counter resistance,* Antimicrobial agents and chemotherapy **44**, 3249 (2000).

[8] E. Azucena and S. Mobashery, *Aminoglycoside-modifying enzymes: mechanisms of catalytic processes and inhibition,* Drug resistance updates **4**, 106 (2001).

[9] M.-P. Mingeot-Leclercq, Y. Glupczynski, and P. M. Tulkens, *Aminoglycosides: activity and resistance,* Antimicrobial agents and chemotherapy **43**, 727 (1999).

[10] M. S. Ramirez and M. E. Tolmasky, *Aminoglycoside modifying enzymes,* Drug resistance updates **13**, 151 (2010).

[11] L. A. Richardson, *Understanding and overcoming antibiotic resistance,* PLoS biology **15**, e2003775 (2017).

[12] G. Cottarel and J. Wierzbowski, *Combination drugs, an emerging option for antibacterial therapy,* Trends in biotechnology **25**, 547 (2007).

[13] J. B. Bremner, J. I. Ambrus, and S. Samosorn, *Dual action-based approaches to antibacterial agents,* Current medicinal chemistry **14**, 1459 (2007).

[14] V. Pokrovskaya and T. Baasov, *Dual-acting hybrid antibiotics: a promising strategy to combat bacterial resistance,* Expert opinion on drug discovery **5**, 883 (2010).

[15] P. J. Yeh, M. J. Hegreness, A. P. Aiden, and R. Kishony, *Drug interactions and the evolution of antibiotic resistance,* Nature Reviews Microbiology **7**, 460 (2009).

[16] I. A. Bliziotis, G. Samonis, K. Z. Vardakas, S. Chrysanthopoulou, and M. E. Falagas, *Effect of aminoglycoside and β-lactam combination therapy versus β-lactam monotherapy on the emergence of antimicrobial resistance: a meta-analysis of randomized, controlled trials,* Clinical infectious diseases **41**, 149 (2005).

[17] H. Brötz-Oesterhelt and N. A. Brunner, *How many modes of action should an antibiotic have?* Current opinion in pharmacology **8**, 564 (2008).

[18] M. R. Barbachyn, *Recent advances in the discovery of hybrid antibacterial agents,* Annual reports in medicinal chemistry **43**, 281 (2008).

[19] Y. Berkov-Zrihen, K. D. Green, K. J. Labby, M. Feldman, S. Garneau-Tsodikova, and M. Fridman, *Synthesis and evaluation of hetero-and homodimers of ribosome-targeting antibiotics: antimicrobial activity, in vitro inhibition of translation, and drug resistance,* Journal of medicinal chemistry **56**, 5613 (2013).

[20] N. T. Chandrika and S. Garneau-Tsodikova, *Comprehensive review of chemical strategies for the preparation of new aminoglycosides and their biological activities,* Chemical Society Reviews **47**, 1189 (2018).

[21] C. Hubschwerlen, J.-L. Specklin, D. K. Baeschlin, Y. Borer, S. Haefeli, C. Sigwalt, S. Schroeder, and H. H. Locher, *Structure–activity relationship in the oxazolidinone–quinolone hybrid series: influence of the central spacer on the antibacterial activity and the mode of action,* Bioorganic & medicinal chemistry letters **13**, 4229 (2003).

[22] J. Lee, M. Kwon, K. H. Lee, S. Jeong, S. Hyun, K. J. Shin, and J. Yu, *An approach to enhance specificity against rna targets using heteroconjugates of aminoglycosides and chloramphenicol (or linezolid),* Journal of the American Chemical Society **126**, 1956 (2004).

[23] I. Grapsas, S. A. Lerner, and S. Mobashery, *Conjoint molecules of cephalosporins and aminoglycosides,* Archiv der Pharmazie: An International Journal Pharmaceutical and Medicinal Chemistry **334**, 295 (2001).

[24] J. Zhou, G. Wang, L.-H. Zhang, and X.-S. Ye, *Modifications of aminoglycoside antibiotics targeting rna,* Medicinal Research Reviews **27**, 279 (2007).

[25] H. Giamarellou, *Aminoglycosides plus beta-lactams against gram-negative organisms: Evaluation of in vitro synergy and chemical interactions,* The American journal of medicine **80**, 126 (1986).

[26] V. Pokrovskaya, V. Belakhov, M. Hainrichson, S. Yaron, and T. Baasov, *Design, synthesis, and evaluation of novel fluoroquinolone- aminoglycoside hybrid antibiotics,* Journal of medicinal chemistry **52**, 2243 (2009).

[27] J. Yu, J. Lee, M. Kwon, A. Pae, and H. Koh, *Heterodimeric conjugates of neomycin-oxazolidinone, their preparation and their use,* (2005), uS Patent App. 10/502,539.

[28] S. Bera, G. G. Zhanel, and F. Schweizer, *Evaluation of amphiphilic aminoglycoside–peptide triazole conjugates as antibacterial agents,* Bioorganic & medicinal chemistry letters **20**, 3031 (2010).

[29] A. H. Alkhzem, T. J. Woodman, and I. S. Blagbrough, *Design and synthesis of hybrid compounds as novel drugs and medicines,* RSC advances **12**, 19470 (2022).

[30] V. Gupta and P. Datta, *Next-generation strategy for treating drug resistant bacteria: Antibiotic hybrids,* Indian Journal of Medical Research **149**, 97 (2019).

[31] M. Baroncini, J. Groppi, S. Corra, S. Silvi, and A. Credi, *Light-responsive (supra) molecular architectures: Recent advances,* Advanced Optical Materials **7**, 1900392 (2019).

[32] M. Izquierdo-Serra, M. Gascón-Moya, J. J. Hirtz, S. Pittolo, K. E. Poskanzer, E. Ferrer, R. Alibès, F. Busquè, R. Yuste, J. Hernando, *et al.*, *Two-photon neuronal and astrocytic stimulation with azobenzene-based photoswitches,* Journal of the American Chemical Society **136**, 8693 (2014).

[33] A. A. Beharry and G. A. Woolley, *Azobenzene photoswitches for biomolecules,* Chemical Society Reviews **40**, 4422 (2011).

[34] J. Chang, Y. Chen, Z. Xu, Z. Wang, Q. Zeng, and H. Fan, *Switchable control of antibiotic activity: a shape-shifting "tail" strategy,* Bioconjugate Chemistry **29**, 74 (2018).

[35] W. A. Velema, J. P. Van Der Berg, M. J. Hansen, W. Szymanski, A. J. Driessen, and B. L. Feringa, *Optical control of antibacterial activity,* Nature chemistry **5**, 924 (2013).

[36] J. Zhu, T. Guo, Z. Wang, and Y. Zhao, *Triggered azobenzene-based prodrugs and drug delivery systems,* Journal of Controlled Release **345**, 475 (2022).

[37] W. A. Velema, W. Szymanski, and B. L. Feringa, *Photopharmacology: beyond proof of principle,* Journal of the American Chemical Society **136**, 2178 (2014).

[38] D. Bléger and S. Hecht, *Visible-light-activated molecular switches,* Angewandte Chemie International Edition **54**, 11338 (2015).

[39] C. Knie, M. Utecht, F. Zhao, H. Kulla, S. Kovalenko, A. M. Brouwer, P. Saalfrank, S. Hecht, and D. Bléger, *ortho-fluoroazobenzenes: visible light switches with very long-lived z isomers,* Chemistry–A European Journal **20**, 16492 (2014).

[40] D. Bléger, J. Schwarz, A. M. Brouwer, and S. Hecht, *o-fluoroazobenzenes as readily synthesized photoswitches offering nearly quantitative two-way isomerization with visible light,* Journal of the American Chemical Society **134**, 20597 (2012).

[41] P. J. Stogios, P. Spanogiannopoulos, E. Evdokimova, O. Egorova, T. Shakya, N. Todorovic, A. Capretta, G. D. Wright, and A. Savchenko, *Structure-guided optimization of protein kinase inhibitors reverses aminoglycoside antibiotic resistance,* Biochemical Journal **454**, 191 (2013).

[42] A. J. McCoy, R. W. Grosse-Kunstleve, P. D. Adams, M. D. Winn, L. C. Storoni, and R. J. Read, *Phaser crystallographic software,* Applied Crystallography **40**, 658 (2007).

[43] A. J. McCoy, *Solving structures of protein complexes by molecular replacement with phaser,* Biological Crystallography **63**, 32 (2007).

[44] P. D. Adams, P. V. Afonine, G. Bunkóczi, V. B. Chen, I. W. Davis, N. Echols, J. J. Headd, L.-W. Hung, G. J. Kapral, R. W. Grosse-Kunstleve, *et al.*, *Phenix: a comprehensive python-based system for macromolecular structure solution,* Biological crystallography **66**, 213 (2010).

[45] P. D. Adams, R. W. Grosse-Kunstleve, L.-W. Hung, T. R. Ioerger, A. J. McCoy, N. W. Moriarty, R. J. Read, J. C. Sacchettini, N. K. Sauter, and T. C. Terwilliger, *Phenix: building new software for automated crystallographic structure determination,* Biological crystallography **58**, 1948 (2002).

[46] M. D. Winn, C. C. Ballard, K. D. Cowtan, E. J. Dodson, P. Emsley, P. R. Evans, R. M. Keegan, E. B. Krissinel, A. G. Leslie, A. McCoy, *et al.*, *Overview of the ccp4 suite and current developments,* Biological crystallography **67**, 235 (2011).

[47] P. Evans, *Scaling and assessment of data quality,* Biological crystallography **62**, 72 (2006).

4

Site-Selective Modifications of Aminoglycosides: Overcoming Phosphorylation-Mediated Antibiotic Resistance

Nicola Pontillo, Simona Bianca, Michele Partipilo, Klara Haldimann, Marina Gysin, Ineke Land-Kuper, Katja Becker, Nabil Tahiri, Albert Guskov, Andreas Hermann, Dirk J. Slotboom, Sven Hobbie, Martin D. Witte, Adriaan J. Minnaard

"The details are not the details. They make the design."

— Charles Eames

ABSTRACT

Aminoglycosides are vital antibiotics, but their efficacy is compromised by phosphorylation via aminoglycoside O-phosphotransferases. This study explores 3'-OH modifications as a strategy to evade APH(3')-Ia-mediated resistance while retaining antibacterial activity. Synthetic modifications of kanamycin and paromomycin yielded novel derivatives (SBI209, SBI214, SBI233, SBI238, SBI236, and SBI237). MIC assays confirmed that SBI237 (3'-epi-PAR) and SBI209 (3'-propyl-KAN) remained effective against strains of E. coli expressing APH(3')-Ia, with SBI237 showing 16-fold improved activity over unmodified paromomycin. In vitro phosphorylation assays revealed that none of the modified aminoglycosides served as enzymatic substrates, while SBI214 and SBI237 acted as competitive inhibitors of APH(3')-Ia. X-ray crystallography of APH(3')-Ia in complex with SBI233 and SBI238 revealed steric hindrance at the ATP-binding site, impairing ATP hydrolysis and phosphorylation efficiency. These structural disruptions explain the reduced susceptibility of 3'-OH-modified aminoglycosides to enzymatic inactivation. These findings support 3'-OH modification as a viable strategy to overcome APH(3')-mediated resistance, while preserving ribosomal inhibition.

4.1. INTRODUCTION

AMINOGLYCOSIDES ANTIBIOTICS

Aminoglycosidess (AGs) are broad-spectrum bactericidal antibiotics that have played a critical role in treating bacterial infections since their discovery [1]. They were first identified as a natural product class of antibiotics in the 1940s, when Waksman, Schatz, and Bugie isolated streptomycin (STR) from *Streptomyces griseus* [2]. This breakthrough provided the first effective antibiotic treatment for tuberculosis (TB) [3]. Since then, AGs have been widely used to combat infections caused by Gram-positive and Gram-negative bacteria, particularly aerobic pathogens, either alone or in combination with other antibiotics [4, 5].

AGs are effective against a broad range of bacterial species, including Gram-positive bacteria such as *Staphylococcus aureus* and *Staphylococcus epidermidis*, as well as Gram-negative pathogens from the *Enterobacteriaceae* family, such as *Escherichia coli*, *Klebsiella* spp., *Salmonella* spp., *Shigella* spp., *Proteus* spp., *Serratia* spp., and *Enterobacter* spp. [6]. Additionally, AGs are active against non-*Enterobacteriaceae* Gram-negative species such as *Acinetobacter* spp., *Moraxella* spp., and *Pseudomonas* spp., as well as mycobacteria, making them an important option for Multi-Drug Resistant (MDR) TB treatment. However, they exhibit limited efficacy against *Streptococcus* and *Pneumococcus*, and anaerobic bacteria are inherently resistant due to their oxygen-dependent uptake mechanism [6, 7].

The first AGs were isolated from species belonging to the genera *Streptomyces* and *Micromonospora* [8]. Those derived from *Streptomyces* carry the suffix "-mycin", such as kanamycin (KAN), apramycin (APR), neomycin (NEO), and tobramycin (TOB) [9]. In contrast, AGs from *Micromonospora* carry the suffix "-micin", including gentamicin (GEN) and sisomycin (SIS)[10, 11]. Over time, semisynthetic derivatives were developed to improve pharmacokinetic properties and combat antimicrobial resistance [12]. These include amikacin (AMK), netilmicin (NET), isepamicin (ISE), arbekacin (ARB), etimicin (ETI), and plazomicin (PLA) [6].

The majority of AGs share key structural characteristics, notably the presence of an aminocyclitol core, which forms the backbone of their antimicrobial activity. The defining structural component of most AG antibiotics is 2-deoxystreptamine (2-DOS), a central aminocyclitol ring that determines the binding affinity and mechanism of action. AGs are broadly classified into two major subclasses based on the glycosylation position on the 2-DOS core: 4,6-disubstituted and 4,5-disubstituted.

The 4,6-disubstituted AGs, represented in Figure 4.1 by KAN, GEN, and AMK, exhibit broad-spectrum activity and potent bactericidal effects. Their structural features contribute to enhanced resistance against enzymatic modifications when compared to other AGs [13]. In contrast, the 4,5-disubstituted series, exemplified in Figure 4.2 by paromomycin (PAR) and NEO, share structural similarities but are generally more susceptible to Aminoglycoside Modifying Enzymes (AMEs), which can significantly reduce their antimicrobial efficacy.

STR belongs to a distinct class with a different core structure, lacking the 2-DOS scaffold and instead incorporating a streptidine moiety. AGs entered widespread clinical use due to their effectiveness against infections caused by *Enterobacterales*, including *Escherichia coli* and *Klebsiella pneumoniae* [12]. They have also demonstrated strong activity against non-

fermentative Gram-negative pathogens, including *Pseudomonas aeruginosa* and methicillin-resistant *Staphylococcus aureus* (MRSA) [14, 15].

MECHANISM OF ACTION AND BACTERICIDAL EFFECTS

AGs exert their bactericidal activity primarily through disruption of bacterial protein synthesis by targeting the 16S rRNA in the 30S ribosomal subunit. Several mechanisms contribute to their bactericidal effect. Binding of AGs to the ribosomal A-site induces a conformational change in the 16S rRNA, leading to erroneous decoding of mRNA and the synthesis of defective proteins. As misfolded proteins accumulate in the bacterial membrane, cell permeability increases, allowing more AGs to enter the cell, thereby amplifying their bactericidal effect.
AGs can also immobilize peptidyl-tRNA at the A-site, preventing normal ribosomal movement and effectively halting translation [16, 17]. Additionally, some AGs, including KAN, NEO B, and GEN, have been found to interact with an allosteric site on the 23S rRNA within the 50S ribosomal subunit, further impairing translation [18].
STR, which differs structurally from other AGs, binds near the ribosomal decoding center, inhibiting formation of the 70S initiation complex and interfering with protein synthesis termination [19]. Additionally, AGs have been shown to bind eukaryotic 80S ribosomes, altering ribosome intersubunit mobility and disturbing protein synthesis in mammalian cells, which may contribute to their toxicity profile [20, 21].

GRAM-NEGATIVE RESISTANCE AND THE NEED FOR NEW ANTIMICROBIAL STRATEGIES

Gram-negative bacteria have been classified as a *critical-priority group* due to their increasing resistance to third-generation cephalosporins and carbapenems [22]. Among the twelve most hazardous bacterial pathogens, nine are Gram-negative, emphasizing the urgency of developing novel antibiotics. One of the primary challenges in treating Gram-negative infections is their outer membrane, which acts as a permeability barrier limiting antibiotic penetration [6, 22].
AGs are often used in combination therapy with β-lactams or glycopeptides (such as vancomycin) to enhance their efficacy and broaden their antibacterial spectrum [23]. Their synergistic effect with β-lactams arises because cell wall disruption facilitates enhanced AG penetration into bacterial cells, leading to increased intracellular concentrations and more effective bacterial eradication [24].
Until recently, colistin was one of the few remaining last-line antibiotics for carbapenem-resistant *Enterobacterales* (CRE), including *Escherichia coli* and *Klebsiella pneumoniae* [25, 26]. However, colistin-resistant strains have now been identified in multiple regions, leading to infections for which no effective antibiotic treatments are available [27, 28]. The COVID-19 pandemic has further exacerbated the antimicrobial resistance (AMR) crisis, as increased antibiotic usage for preventing or treating bacterial co-infections has accelerated the emergence of resistance [29].
Given these challenges, AGs remain an essential class of antibiotics, particularly due to their broad-spectrum activity against Gram-positive and Gram-negative pathogens and their

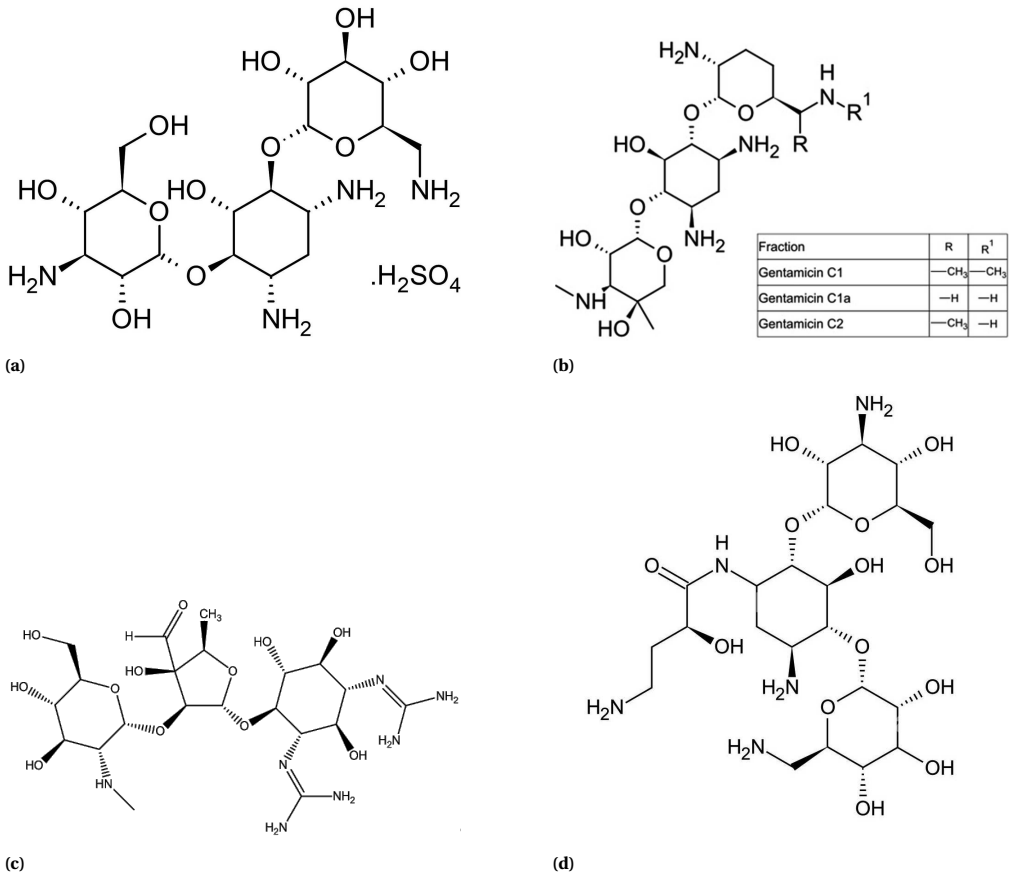


Figure 4.1 | Chemical structures of representative aminoglycosides. (a) Kanamycin A, (b) Gentamicin, (c) Streptomycin, and (d) Amikacin.

efficacy against mycobacteria. Despite their clinical importance, AGs are associated with notable toxicities, particularly nephrotoxicity (kidney damage) and ototoxicity (hearing loss), which limit their long-term use. However, advances in pharmacokinetics, dosing strategies, and structural modifications continue to improve their therapeutic profile [30].

4.2. THE GROWING CHALLENGE OF AMINOGLYCOSIDE RESISTANCE

The clinical efficacy of AGs is increasingly threatened by the emergence and global spread of resistance mechanisms that can significantly reduce or nullify their antibacterial activity. Resistance to AGs occurs through multiple pathways, including reduced antibiotic uptake,

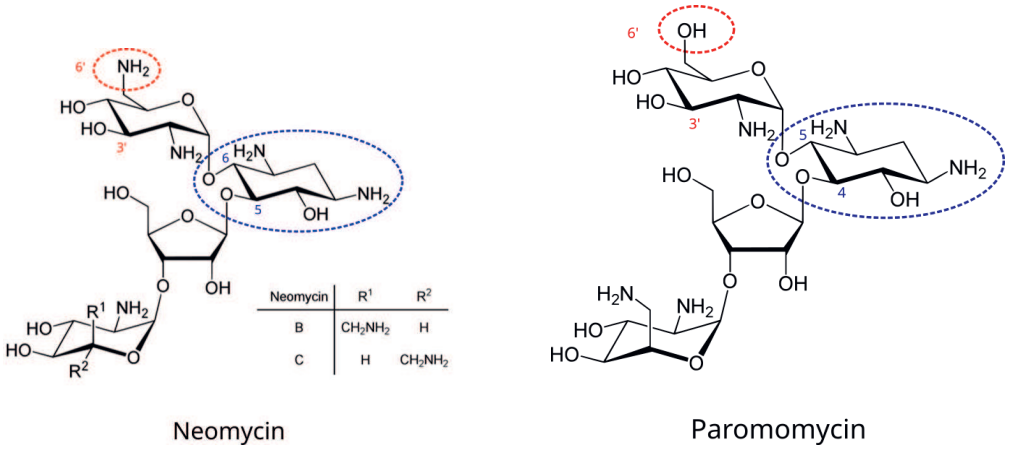


Figure 4.2 | Chemical structures of (a) NEO and (b) PAR. The red circle highlights position 6′, where NEO contains an –NH_2 group, while PAR carries an –OH group. The blue circle marks the aminocyclitol ring connecting two aminosugars at positions 4 and 5. Additionally, the 3′–OH group is labeled for reference.

active efflux, and alterations in porins in the outer bacterial membrane that decrease permeability. Some bacteria actively pump out AGs using efflux transporters, such as those found in *Pseudomonas aeruginosa* and *Acinetobacter baumannii*. Nevertheless, two mechanisms are primarily responsible for AG resistance: ribosomal target modification and enzymatic inactivation by AMEs.

Methylation of the ribosomal A-site by 16S rRNA methyltransferasess (RMTs) prevents AG binding, conferring high-level resistance to most AGs. This mechanism is particularly concerning, as RMT genes (*armA*, *rmtA–rmtH*, *npmA*) are frequently located on plasmids, facilitating horizontal gene transfer and rapid dissemination of resistance.

On the other hand, AMEs represent the most widespread and clinically relevant resistance mechanism and are classified into three main groups:

- O-phosphotransferasess (APHs), which catalyze hydroxyl phosphorylation;
- O-adenosyltransferases (ANTs), which mediate nucleotidylation reactions; and
- N-acetyltransferasess (AACs), which acetylate amine groups, reducing aminoglycoside affinity for the ribosome [8].

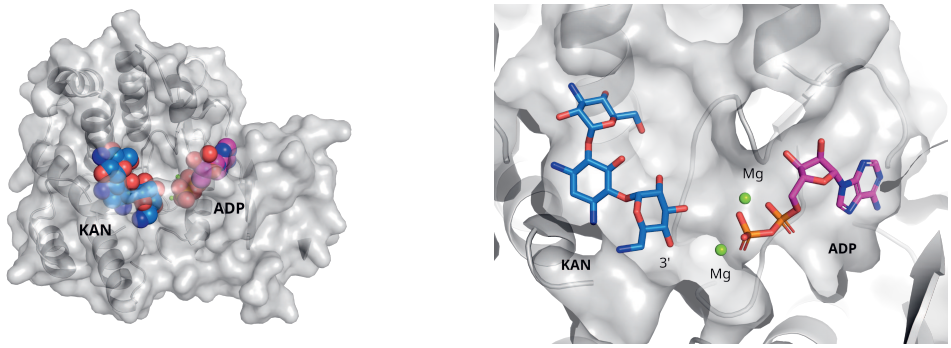
Among the various AMEs, APHs play a central role in clinical resistance. APHs are ATP-dependent enzymes that transfer the γ-phosphoryl group from ATP to specific hydroxyl positions on AGs, thereby preventing the antibiotics from binding effectively to their ribosomal target. As a result, bacteria expressing APHs exhibit high-level resistance to many first- and second-generation AGs [31].

APHs are named based on the site of phosphorylation, with genes encoding 3′-hydroxyl-modifying enzymes designated as APH(3′), where the regiospecificity of phosphorylation is

indicated in parentheses. A Roman numeral represents the phenotype, while letters differentiate distinct genes, as seen in APH(3′)-Ia and APH(3′)-IIIa [32].
Among the various APH subfamilies, APH(3′) enzymes are particularly ubiquitous and represent one of the most clinically significant AMEs. The APH(3′) family is found across both Gram-positive and Gram-negative pathogens, frequently carried on MDR plasmids, transposons, and integrons, facilitating their rapid dissemination among bacterial populations. The most extensively studied member of this family, APH(3′)-IIIa, exhibits both 3′- and 5″-regiospecific phosphoryl transfer capabilities, conferring resistance to a broad spectrum of AGs, including KAN, AMK, and NEO. However, it does not modify GEN or TOB, as these compounds lack the critical 3′-hydroxyl group required for phosphorylation [33, 34].
Structural studies have revealed that APH(3′) enzymes share a remarkable structural similarity with Ser, Thr, and Tyr protein kinases, despite lacking sequence homology, suggesting a convergent evolutionary relationship between AG kinases and eukaryotic phosphorylation enzymes. Like other kinases, APH(3′) enzymes require divalent metal cations (typically Mg^{2+}) as cofactors for ATP hydrolysis and catalysis [33, 34].
Given the prevalence and enzymatic efficiency of APH(3′), efforts to combat AG resistance have increasingly focused on structural modifications that prevent phosphorylation while preserving antibiotic function. In this study, we investigate the impact of site-selective modifications at the 3′-OH position, a critical site for APH(3′)-mediated phosphorylation, to develop AGs that can evade enzymatic inactivation while maintaining strong ribosomal binding and antibacterial activity.

4.3. CHEMICAL MODIFICATIONS TO OVERCOME AMINOGLYCOSIDE RESISTANCE

Building on previous advancements, our study focuses on resistance associated with APH(3′)-expressing bacterial strains and explores site-selective glycoside oxidation as a strategy to inhibit ATP hydrolysis and phosphorylation by APH(3′) enzymes. Given that hydroxyl groups in AGs are common targets of modification by APHs, ANTs, and AACs, late-stage selective modification of AGs has emerged as a promising approach to overcoming enzymatic inactivation [35].
To address this challenge, we employed a synthetic approach combining glycoside oxidation and structural modification to prevent enzymatic inactivation of KAN and PAR while preserving antibacterial potency and ribosomal binding. Using X-ray structures of APH(3′)-IIIa in complex with KAN, we identified that modifying the 3′-OH configuration could interfere with enzyme–substrate recognition (see Figure 4.3).
To achieve selective oxidation, we utilized the catalyst $[(\text{neocuproine})\text{Pd}(\text{OAc})]_2(\text{OTf})_2$, which has been demonstrated to facilitate highly regioselective oxidation of unprotected carbohydrate hydroxyl groups [36]. Similar methodologies have been applied successfully to monosaccharide oxidation, including selective C3′-hydroxyl oxidation of glucopyranosides, demonstrating the feasibility of such transformations even in complex molecular environments [37].
Our hypothesis is that 3′-OH inversion, in combination with alkyl chain modifications, will



(a) (b)

Figure 4.3 | (a) X-ray crystal structure of APH(3′)-IIIa in complex with KAN (blue) and ADP (magenta). (b) A zoomed-in view highlighting key interactions, where KAN is shown in cyan and ADP in magenta. The 3′-OH position of KAN is emphasized, illustrating its role in enzyme-substrate recognition and how modifications at this site could potentially interfere with enzymatic binding.

impede phosphorylation by APH(3′) while preserving ribosomal binding, thereby enhancing antibacterial effects against resistant strains. This approach is inspired by previous studies, such as the work of Mobashery et al., who introduced a self-regenerating AG derivative by incorporating a keto-group at the C3′-position, allowing for spontaneous nonenzymatic phosphate elimination and restoration of antibiotic activity. [38] While this strategy demonstrated improved activity against APH(3′)-expressing pathogens, its synthetic complexity (>10 synthetic steps) significantly limited its accessibility.

Other research efforts have explored alternative structural modifications at different hydroxyl positions to circumvent APH(3′)-mediated phosphorylation. *Baasov* and coworkers developed synthetic NEO B analogs in which the C5″-position was systematically modified with mono- and disaccharides, demonstrating altered substrate recognition by APH(3′)-III/ [39, 40] These findings reinforce the potential of targeted modifications at critical hydroxyl sites to disrupt enzyme interaction and restore antibacterial efficacy.

Despite the promising potential of late-stage AG modifications, accessibility remains a major challenge due to the structural complexity and reactivity of functional groups. Since 1990, PLA has been the only new semisynthetic AG to enter the market, underscoring the need for more efficient synthetic strategies to modify AGs while preserving their pharmacological activity. [41] Late-stage chemical modifications of unprotected or partially protected AGs are critical for streamlining drug development and accelerating the introduction of new antibacterial agents.

This study seeks to expand the applicability of site-selective oxidation strategies to AGs, demonstrating that selective oxidation at the C3′-position can be leveraged as a tool to evade APH(3′) phosphorylation. By introducing a keto handle amenable to further chemical diversification, we generate AG derivatives with improved resistance profiles and retained ribosomal binding capabilities. Through strategic chemical modifications, we provide a biochemical and structural framework for the development of next-generation AGs, offering

a rational approach to overcoming enzymatic resistance mechanisms while maintaining efficacy against MDR bacterial infections.

4.4. RESULTS AND DISCUSSION

SYNTHESIS AND CHEMICAL MODIFICATIONS OF AMINOGLYCOSIDES

To develop novel AG derivatives, we employed a site-selective oxidation strategy targeting the gluco-configured ring in KAN and PAR. The key transformation involved regioselective oxidation at the 3'-OH position, a site crucial for interactions with AMEs, particularly the APH(3') sub-family.

A major challenge in this oxidation reaction was the coordination of free amino groups in KAN and KAN to the catalyst [(neocuproine)Pd(OAc)]$_2$(OTf)$_2$, which could potentially inhibit the reaction. Moreover, the high polarity of unprotected AGs limited their solubility in organic solvents, necessitating selective protection strategies. The amino groups in PAR were successfully protected using Cbz-OSu under basic conditions, whereas KAN required Boc protection using (Boc)$_2$O and triethylamine in DMSO.

Following protection, oxidation was performed using [(neocuproine)Pd(OAc)]$_2$(OTf)$_2$ in the presence of benzoquinone (see Figure 4.4 for PAR, and Figure 4.5 for KAN). While oxidation of mono-glycosides proceeded rapidly, full conversion of protected *kan* and PAR remained incomplete (50–60% conversion), even with increased catalyst loadings or prolonged reaction times. The lower reactivity of these AGs compared to mono-glycosides may be attributed to steric hindrance or limited solubility.

Despite incomplete oxidation, we proceeded with functionalization of the keto- intermediates via indium-mediated allylation and propargylation. This strategy yielded single- and double-modified KAN and PAR derivatives, which were subsequently deprotected using trifluoroacetic acid in dichloromethane.

The resulting derivatives — SBI209, SBI214, SBI233, and SBI238 for KAN, and SBI236 and SBI237 for PAR — were purified and isolated in their respective trifluoroacetate or acetate forms (see Figure 4.6).

MICROBIOLOGICAL ACTIVITY AND MECHANISM OF ACTION

To evaluate whether modifications at the C3' position can overcome APH(3')-mediated resistance, we conducted Minimal Inhibitory Concentration (MIC) assays on a panel of AG derivatives.

The assays were performed using the *Escherichia coli* DH5α laboratory strain, genetically engineered to express specific APH(3') enzymes with varying promoter strengths, as outlined in Table 4.1.

This approach allowed us to assess both the direct impact of the modifications on antibacterial activity and whether transcriptional levels of *aph(3')* genes influenced the effectiveness of the modified AGs.

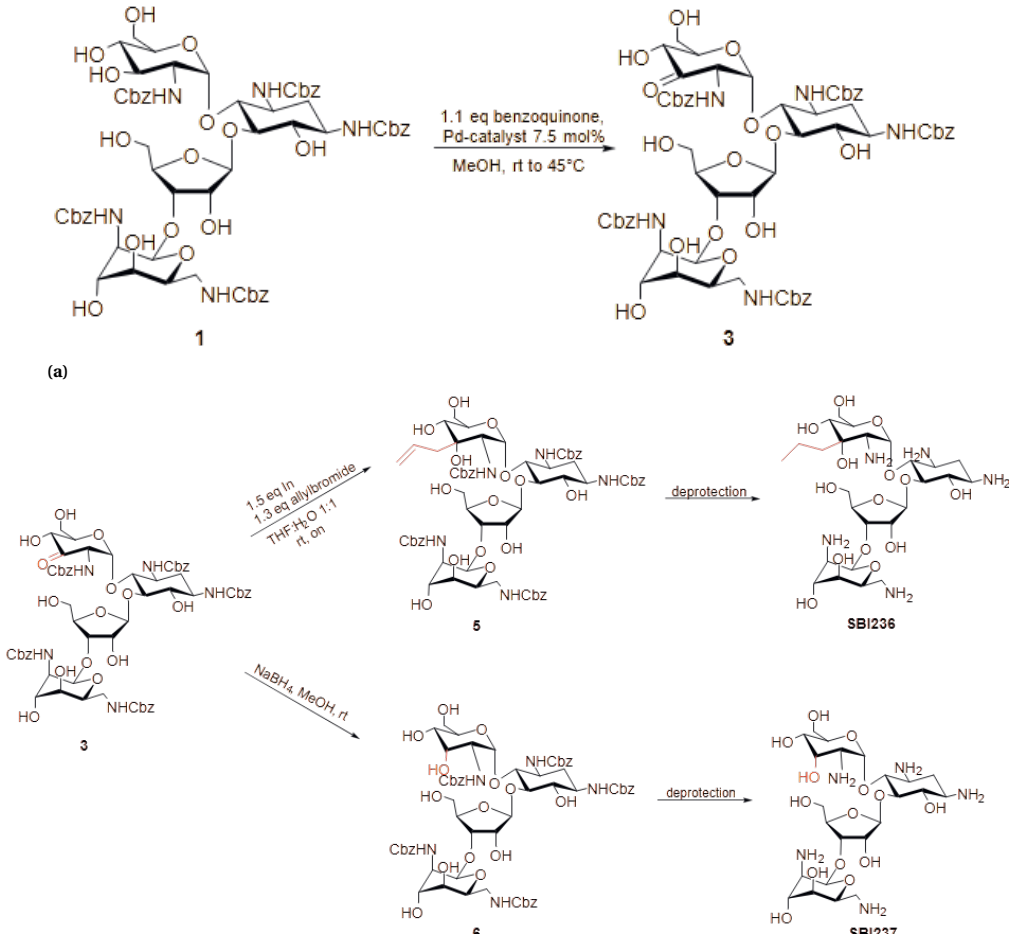


Figure 4.4 | (a) Selective Cbz protection of PAR (THF:water 1:2) followed by (b) oxidation using [(neocuproine)Pd $(OAc)]_2(OTf)_2$ and benzoquinone. The Cbz-protected PAR undergoes partial oxidation to yield the corresponding keto intermediate, which serves as a precursor for further functionalization.

EFFECT OF 3'-OH MODIFICATIONS ON AG ACTIVITY

The MIC assays revealed that only minor modifications at the 3'-position were tolerated without a significant loss of activity, while larger substitutions generally compromised antibacterial efficacy in both wild-type and engineered strains.

Among the synthesized compounds, SBI237 (3'-epi-PAR) and SBI209 (3'-propyl-KAN) exhibited the highest potency, retaining strong antibacterial activity against resistant strains expressing APH(3')-IIa and APH(3')-IIb.

SBI237 (3'-epi-PAR) maintained activity comparable to PAR against wild-type *E. coli*, but

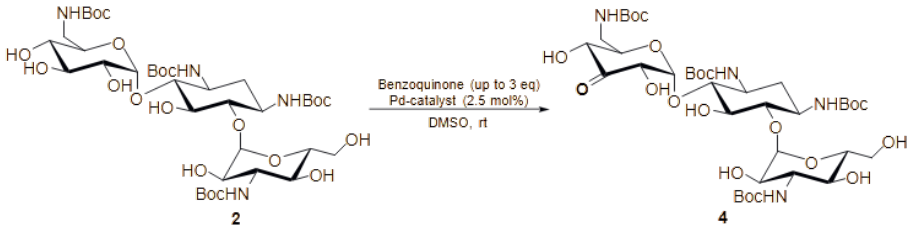


Figure 4.5 | Boc protection of KAN using Boc_2O and triethylamine in DMSO, followed by oxidation with [(neo cuproine)$Pd(OAc)]_2(OTf)_2$ and benzoquinone. Similar to PAR, the reaction yields a keto intermediate, albeit with incomplete conversion.

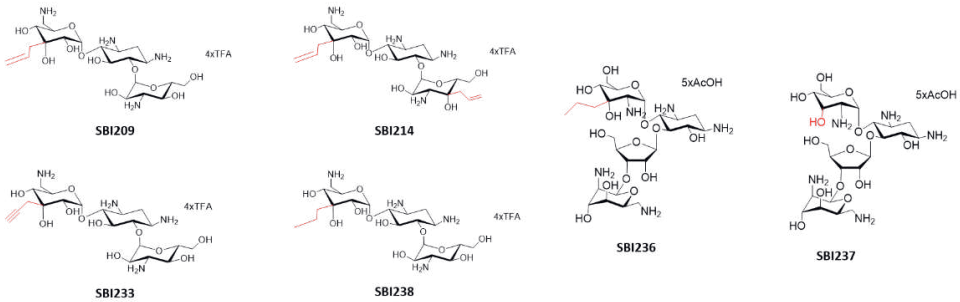


Figure 4.6 | Final modified derivatives of KAN and PAR. The structures of SBI209, SBI214, SBI233, and SBI238 (KAN derivatives) and SBI236 and SBI237 (PAR derivatives) are shown after indium-mediated allylation/propargylation and subsequent deprotection. These compounds were purified and isolated in their respective trifluoroacetate or acetate forms. Modifications at the 3'-position are highlighted in red.

showed a 16-fold improvement in potency against APH(3')-expressing strains EC125 and EC191.

This enhancement suggests that stereochemical inversion at the 3'-OH position disrupts recognition by APH(3'), reducing enzymatic inactivation while preserving ribosomal binding. SBI209 (3'-propyl-KAN) displayed enhanced MIC values against multiple resistant strains, reinforcing the hypothesis that steric hindrance at the 3'-OH site prevents phosphorylation by APH(3') enzymes.

LIMITATIONS OF 3'-OH MODIFICATION IN 4,5-DISUBSTITUTED AGS

While C3'-modifications were effective in certain cases, they were not universally protective across all APH(3') subtypes. The MIC data indicated that strains expressing APH(3')-Ia and APH(3')-IIIa remained highly resistant, likely due to their ability to modify additional hydroxyl sites beyond the 3'-OH. These findings suggest that structural diversification at the 3'-position must be complemented by further modifications targeting secondary phosphorylation sites to achieve broader protection against AME-mediated resistance.

In 4,5-disubstituted AGs such as PAR, APH(3')-Ia and APH(3')-IIIa can also phosphorylate the 5"-OH of the ribose ring, enabling these enzymes to bypass the protective effects of 3'-

Table 4.1 | MICs in mg/L of modified AGs and their parent compounds against *Escherichia coli* strains expressing different APH(3') isoenzymes.

Strain	Resistance	Promoter strength	KAN	SBI209	SBI214	SBI233	SBI238	PAR	SBI236	SBI237
DH5α	None	none	2	16	512	64	128	4	>512	8
EC122	APH(3')-Ia	++	>512	>512	256	128	>512	>512	>512	>512
EC189	APH(3')-Ia	+	256	>512	>512	128	>512	128	>512	256
EC191	APH(3')-IIa	+	256	>512	>512	256–512	>512	64	>512	4
EC125	APH(3')-IIb	++	256	>512	>512	256–512	>512	128–256	>512	8–16
EC126	APH(3')-IIIa	++	>512	>512	>512	512	>512	>512	>512	>512
EC193	APH(3')-VI	+	8	32	256–512	128–256	128–256	4	>512	4

modifications. Thus, while 3'-OH modifications enhance resistance against certain APH(3') subtypes, a dual-modification strategy targeting both the 3'- and 5"-OH groups may be necessary for broader resistance evasion.

These findings suggest that targeted 3'-OH modifications represent a promising strategy for overcoming AG resistance, particularly in 4,5-disubstituted AGs such as PAR. However, future studies should explore dual modifications to evaluate their potential in reducing susceptibility to phosphorylation and expanding the efficacy of aminoglycosides against resistant strains.

IMPACT OF 3'-OH MODIFICATIONS ON PROTEIN SYNTHESIS INHIBITION

To further investigate how 3'-OH modifications affect bacterial translation, we evaluated the ability of modified AGs to inhibit protein synthesis using a cell-free luciferase mRNA translation assay with *Escherichia coli* ATCC 25922 extracts. This assay provides direct insight into whether derivatization at the 3'-position alters the ability of AGs to interfere with ribosomal function.

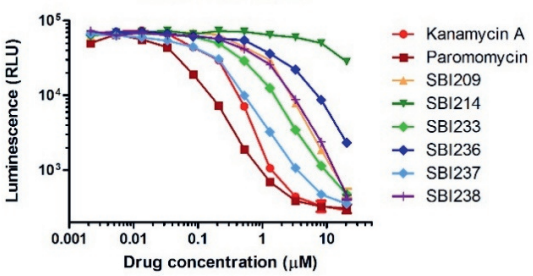
The luminescence readout revealed that most derivatives retained ribosomal inhibition, though generally with reduced efficiency compared with their parent compounds (Figure 4.7). Notably, SBI237 (3'-epi-PAR) exhibited potent inhibition of luciferase synthesis, closely resembling the activity of PAR, which aligns with its strong antibacterial effect observed in MIC assays. In contrast, SBI214 (3',4"-di-allyl-KAN) displayed weak inhibition, suggesting that the second allyl group disrupts ribosomal binding and reduces translation inhibition.

These findings reinforce the correlation between protein synthesis inhibition and antibacterial activity, particularly for SBI237, which remains effective against resistant *E. coli* strains expressing APH(3')-IIa and APH(3')-IIb.

EFFECT OF 3'-OH MODIFICATIONS ON PHOSPHORYLATION BY APH(3')

As a first step, we estimated the kinetic parameters (K_m and V_{max}) for the parent AG KAN and PAR (see Figure 4.8 and Table 4.2).

Both molecules exhibited weak substrate inhibition, consistent with previous reports on APHs and the general catalytic behavior of AMEs. Next, we evaluated whether the synthetic AG derivatives—SBI209, SBI214, SBI236, and SBI237—could serve as substrates for APH(3')-Ia,



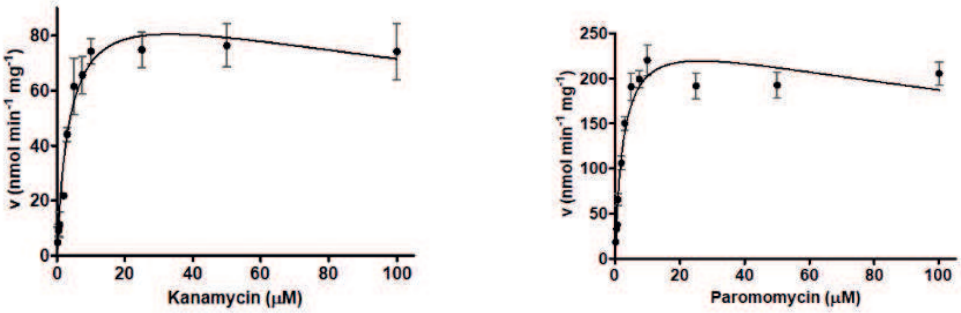
(a)

Compound	IC_{50} (average)
Kanamycin A	0.14 ± 0.00035
Paromomycin	0.056 ± 0.0076
SBI209	1.176 ± 0.041
SBI214	48.6 ± 13.98
SBI233	0.47 ± 0.012
SBI236	0.88 ± 0.099
SBI237	1.87 ± 0.59
SBI238	0.16 ± 0.042

(b)

Figure 4.7 | Effect of 3'-OH modifications on bacterial translation inhibition. (a) Luminescence-based cell-free luciferase mRNA translation assay using *E. coli* ATCC 25922 extracts. (b) Calculated IC_{50} values for the modified and parent aminoglycosides. SBI237 (3'-epi-PAR) retained strong inhibition, comparable to PAR, whereas SBI214 (3',4"-di-allyl-KAN) showed reduced activity, indicating impaired ribosomal binding.

replacing the natural antibiotics in the reaction. Increasing concentrations of each compound (ranging from 500 to 2000 μM, depending on solubility) were tested. However, no detectable ADP release was observed for any of the modified AGs, except for the basal ATPase activity. This background activity was comparable to that measured in control reactions with both binary (enzyme + ATP) and ternary (enzyme + ATP + AG) complexes, further supporting the notion that the synthetic AGs were not phosphorylated by APH(3')-Ia, consistent with previous studies on APH(3')-Ia [42].



(a) (b)

Figure 4.8 | Kinetic parameters of APH(3')-Ia for KAN and PAR. Enzyme kinetics reveal that both natural aminoglycosides exhibit substrate inhibition, with reaction rates decreasing at higher substrate concentrations. Data were fitted using a substrate inhibition model.

Table 4.2 | Kinetic parameters of APH(3')-Ia for PAR and KAN. The table reports the Michaelis constant (K_M), maximum reaction rate (V_{max}), turnover number (k_{cat}), and inhibition constant (K_i) obtained from enzyme kinetics experiments. Data were fitted using a substrate inhibition model, and values represent the mean ± standard deviation from at least two independent experiments.

Compound	K_M **(**μ**M)**	V_{max} **(**μ**mol·min^{-1}·mg^{-1})**	k_{cat} **(s^{-1})**	k_{cat}/K_M **(s^{-1}·M^{-1})**	K_i **(**μ**M)**
Kanamycin A	3.80 ± 1.21	0.10 ± 0.01	0.11 ± 0.01	2.89×10^4	289.2 ± 195.4
Paromomycin	2.65 ± 0.49	0.26 ± 0.02	0.31 ± 0.02	1.17×10^5	263.1 ± 104.7

BASAL ATPASE ACTIVITY OF APH(3')-IA: CASE STUDY WITH SBI214

APH(3')-Ia displayed basal ATPase activity both in the presence and absence of the natural AG KAN and the AG derivative SBI214. Under standard assay conditions, the absorbance at 340 nm continuously decreased even in the absence of KAN or when both KAN and SBI214 were absent (see Figure 4.9). Upon kanamycin addition, ADP formation was detected. However, incubation with high concentrations of SBI214 inhibited kanamycin phosphorylation but did not completely suppress basal ATP hydrolysis.

Given that the synthesized AGs were not phosphorylated, we next investigated whether they could instead inhibit APH(3')-Ia activity by competing with the native substrates, KAN and PAR. To assess inhibition, we fixed the natural AG concentration at 25 μM (~7–9 times the estimated K_m) and measured APH(3')-Ia activity in the presence of increasing concentrations of synthetic AGs.

Encouragingly, SBI209, SBI214, SBI236, and SBI237 effectively competed with their parent compounds in the APH(3')-Ia-mediated phosphorylation reaction, preventing modification in a dose-dependent manner. The IC_{50} values for each derivative are summarized in Table 4.3. The results indicated notable differences in inhibition efficiency between KAN and PAR derivatives. The PAR derivatives SBI236 and SBI237 exhibited comparable IC_{50} values (~80 μM), indicating that neither compound was phosphorylated by APH(3')-Ia. This suggests that modifications at the 3'-OH position effectively prevent enzymatic recognition without compromising their ability to interact with bacterial ribosomes.

In contrast, the KAN derivatives SBI209 and SBI214 displayed markedly different inhibition profiles. SBI214, which carries a 3',4"-di-allyl modification, showed the strongest inhibition, with an IC_{50} of 24.6 ± 15.9 μM, requiring approximately eight times the K_m of kanamycin (3.80 ± 1.21 μM) to halve the APH(3')-Ia activity. On the other hand, SBI209 (3'-propyl-KAN) was the least effective inhibitor, with an IC_{50} of 130 μM, and was the only derivative that failed to achieve complete inhibition of APH(3')-Ia. Even at a 2 mM concentration (500-fold excess over the K_m of KAN), SBI209 only reached 80% inhibition of ATPase activity, suggesting that the propyl modification at the 3'-OH position does not effectively block enzyme activity.

ASSAY VALIDATION AND POTENTIAL OVERESTIMATION OF IC_{50} VALUES

To verify the reliability of the IC_{50} values, we tested whether the synthetic AGs or potential impurities interfered with the PK–LDH spectrophotometric assay. Using high concentrations of SBI214 and SBI237, we compared PK–LDH-mediated NADH oxidation in the presence

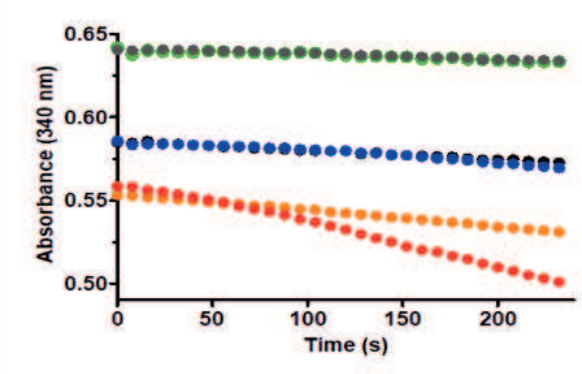


Figure 4.9 | Basal ATPase activity of APH(3')-Ia in the presence and absence of AGs, highlighting the effect of SBI214. APH(3')-Ia exhibited basal ATPase activity either in absence of KAN (orange line) or when both KAN and SBI214 were absent (100 μM SBI214, black line; 500 μM SBI214, dark green line). Addition of 25 μM KAN (red line) led to ADP formation. High concentrations of SBI214 (100 μM, blue line; 500 μM, light green line) inhibited KAN phosphorylation but did not suppress basal ATP hydrolysis.

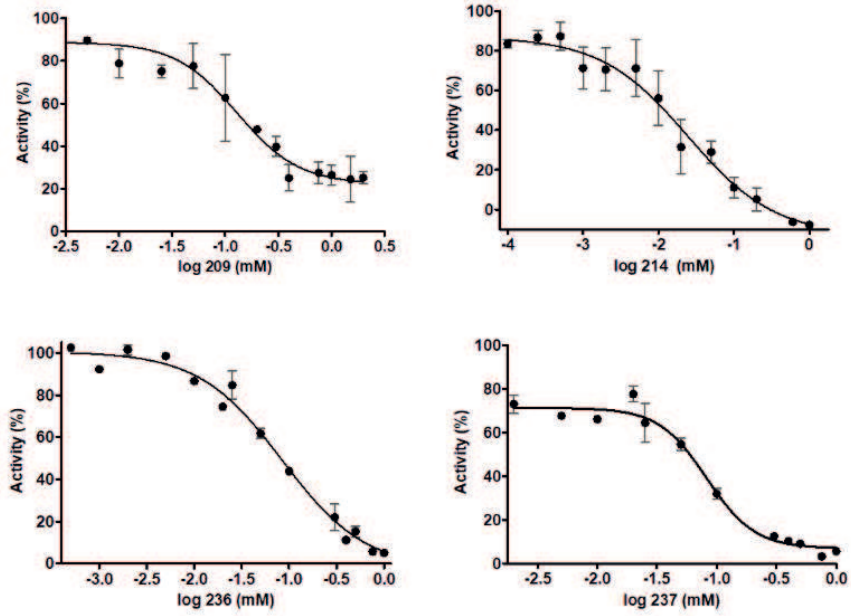


Figure 4.10 | IC_{50} values of AG derivatives for APH(3')-Ia inhibition. The inhibition of APH(3')-Ia was assessed at varying concentrations of synthesized AG derivatives. Enzymatic activity was plotted using a four-parameter logistic regression model to determine IC_{50} values.

Table 4.3 | Inhibition of APH(3')-Ia by modified AGs. IC_{50} values for synthetic aminoglycoside analogs (SBI209, SBI214, SBI236, and SBI237) are reported. Each derivative is compared to its parent compound and described by the specific substitution at the 3'-position. Data represent mean ± standard deviation from at least two independent experiments.

Compound	Parent compound	Substitution	IC_{50} (μM)
SBI209	KAN	3'-allyl	129.8 ± 43.9
SBI214	KAN	3',4"-di-allyl	24.6 ± 15.9
SBI236	PAR	3'-propyl	84.4 ± 14.1
SBI237	PAR	3'-epi	82.3 ± 5.9

and absence of the derivatives under conditions where APH(3')-Ia was absent, allowing us to isolate any unintended interactions with the detection system.

The results indicated that 200 μM SBI237 did not significantly alter NADH oxidation, confirming that its IC_{50} (~80 μM) was accurately determined. However, SBI214 at 100 μM caused a two-fold reduction in NAD^+ formation compared to control conditions, suggesting that the IC_{50} value for SBI214 might be overestimated due to assay interference. Since the APH(3')-Ia enzymatic assay involves gradual ADP formation, whereas the PK–LDH control experiment used an excess of 5.0 mM ADP, direct comparisons were challenging. The PAR derivatives did not show any signs of interference, supporting the reproducibility of their inhibition data.

To further assess the reliability of the coupled PK/LDH assay, we examined its response to ATP and ADP under standard conditions. The system provided a readout for ADP at 340 nm, tracking NADH oxidation over time. When tested in the absence of aminoglycosides, the reaction showed full NADH oxidation within one minute when 5.0 mM ADP was added (ochre triangles), whereas 5.0 mM ATP (orange triangles) did not trigger significant oxidation, confirming that ATP alone did not contribute to the spectrophotometric signal.

The assay was then performed in the presence of 100 μM SBI214 or 200 μM SBI237, along with their corresponding natural AG (25 μM KAN or PAR). As illustrated in Figure 4.11, conditions containing ATP alone did not lead to NAD^+ formation. In contrast, when SBI237 (black diamonds) was present, the initial reaction velocity slightly deviated from the ADP control but leveled off within the same time range. However, in the presence of SBI214 (black asterisks), the ATPase reaction required twice the time to fully oxidize NADH upon ADP injection, suggesting that SBI214 delayed the reaction's initial velocity. Despite this disturbance, complete NADH oxidation was achieved within two minutes.

These results demonstrate that structural modifications at the 3'-OH position not only protect AGs from enzymatic inactivation but also enable them to competitively inhibit APH(3')-Ia, potentially reducing resistance in bacterial strains expressing this enzyme. While SBI214 exhibited the strongest inhibition among KAN derivatives, its interaction with the detection assay suggests that further evaluation may be needed to confirm its precise inhibitory potency.

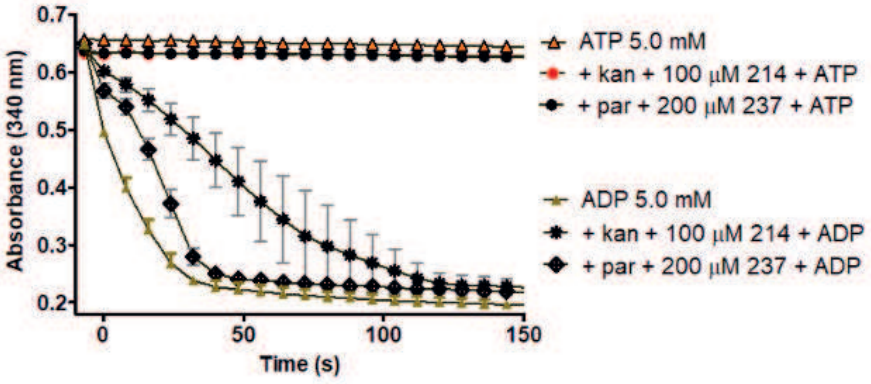


Figure 4.11 | Validation of the PK/LDH-coupled assay and SBI214's effect on ATPase activity. ADP triggered full NADH oxidation within one minute, while ATP had no effect. In the presence of SBI237, reaction velocity slightly deviated but stabilized. SBI214 delayed oxidation, doubling the reaction time, yet full NADH oxidation was achieved within two minutes.

STRUCTURAL INSIGHTS INTO APH(3')-IA RECOGNITION OF MODIFIED AMINOGLYCOSIDES

To further validate the findings from the MIC assays and APH(3')-Ia inhibition studies, we employed X-ray crystallography to characterize the binding interactions between the synthesized aminoglycoside derivatives and APH(3')-Ia. Recombinant apo-APH(3')-Ia was crystallized, and both co-crystallization and soaking experiments were attempted for all derivatives. Successful complex formation was achieved through soaking with SBI233 and SBI238 (5–9 mM). Crystallographic analysis revealed that all crystals belonged to the trigonal space group $P3_12_1$, with two molecules per Asymmetric Unit (AU). High-resolution diffraction data enabled an unambiguous interpretation of the electron density map (EDM), allowing complete modeling of all 271 residues in the enzyme. The dimeric state observed in the crystal structure was consistent with solution-state data, as supported by solvent-accessible surface area calculations (24,584 $Å^2$) and a buried surface area of 34.8%, confirming dimer formation through the Protein Interfaces, Surfaces, and Assemblies (PISA) analysis. [43]

Structurally, the APH(3')-Ia monomer consists of two distinct domains. Domain A (residues 34–104) contributes to structural stabilization through interactions with the flexible N-terminal tail (residues 1–33) from the second monomer, while Domain B (residues 105–271) contains the substrate-binding groove and the ATP-binding site located at the domain interface (Figure 4.12).

To investigate how 3'-OH modifications influence AG binding to APH(3')-Ia, we superimposed the structures of ATP-bound APH(3')-Ia (PDB: 4EJ7) with the newly solved APH(3')-Ia complexes containing SBI233 (3'-propargyl-KAN) and SBI238 (3'-propyl-KAN) (Figure 4.13). This comparative analysis revealed key structural adaptations explaining the reduced phos-

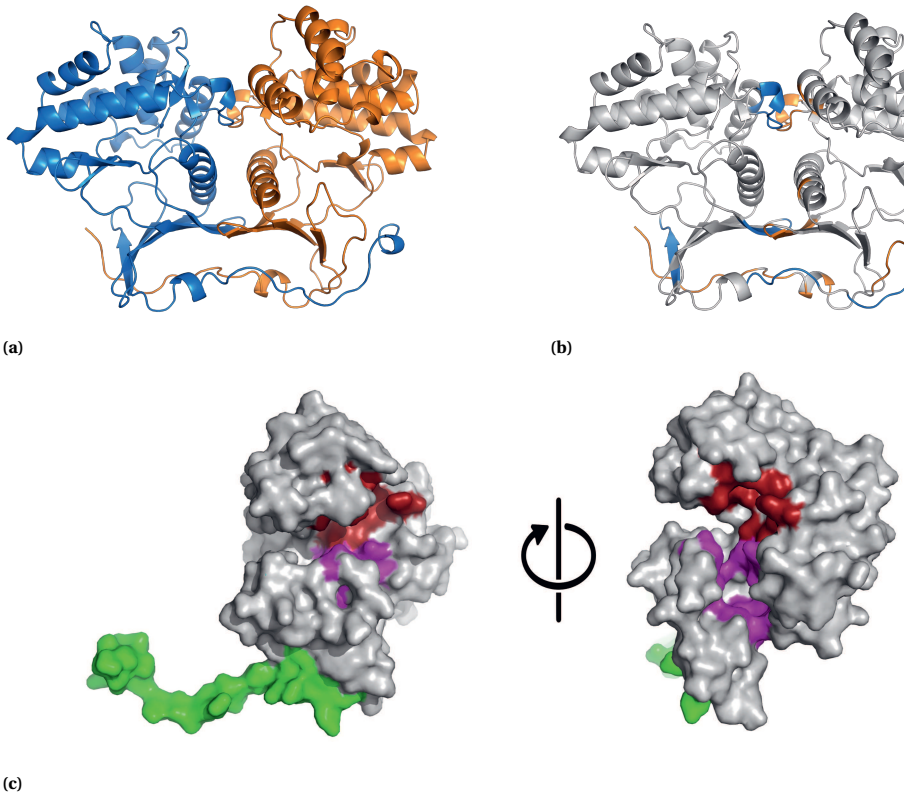


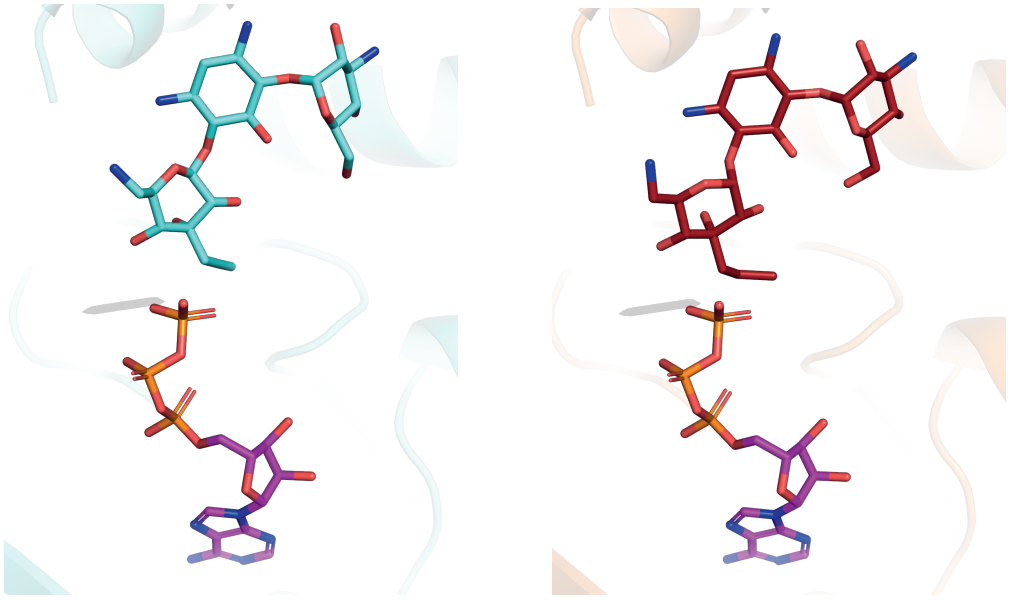
Figure 4.12 | (a) Dimeric interface of APH(3')-Ia. The crystal structure confirms the dimeric state, with monomer A shown in blue, monomer B in orange. In (b), the dimer interface is highlighted in yellow and light blue, to emphasize inter-monomer interactions. (c) Monomeric structure of APH(3')-Ia. The protein backbone is displayed in grey, with the substrate-binding groove highlighted in red, the ATP-binding site in magenta, and the N-terminal tail in green.

phorylation susceptibility of the modified compounds.

A notable hydrogen bond was observed between the epimerized 3'-OH group and the Oδ atom of Asp198 (Domain B), with distances ranging between 2.7 and 4.0 Å. This interaction deviates from the unmodified KAN structure, where the native equatorial 3'-OH group is positioned too far to form such a bond. The rearrangement suggests that 3'-OH modification facilitates additional stabilizing interactions within the enzyme active site, thereby altering AG recognition.

In addition to hydrogen bonding, structural analysis indicated that substituents introduced at the equatorial 3'-OH position are oriented toward the ATP-binding pocket, potentially creating steric clashes with ATP or key catalytic residues. This steric interference likely disrupts ATP hydrolysis, reducing enzymatic phosphorylation efficiency—consistent with the lack of ADP release observed in *in vitro* assays. SBI233 and SBI238, in particular, exhibit

clear disruptions within the ATP-binding region, aligning with their ability to function as APH(3')-Ia inhibitors rather than substrates.
Overall, the crystallographic data provide direct molecular evidence for how strategic 3'-OH modifications influence APH(3')-Ia recognition. These structural insights complement the biochemical assays, supporting the hypothesis that 3'-OH modifications alter substrate positioning to evade enzymatic phosphorylation while preserving ribosomal binding affinity. The results establish a framework for designing next-generation AGs able to overcome APH(3')-Ia-mediated inactivation.



(a) (b)

Figure 4.13 | Structural comparison of APH(3')-Ia in complex with SBI233 (A, cyan sticks) and SBI238 (B, red sticks), superimposed with the ATP-bound APH(3')-Ia structure (PDB: 4EJ7; ATP in magenta). In both cases, the third phosphate group of ATP points toward the aminoglycoside, but phosphorylation is hindered by chemical modifications at the 3' position. Steric clash is evident between the ligand substituent and the ATP γ-phosphate impeding proper ATP-substrate alignment.

4.5. CONCLUSIONS

This study demonstrates that structural modifications at the 3'-OH position of AGs can effectively reduce susceptibility to APH(3')-mediated phosphorylation while maintaining antibacterial activity. Through a combination of synthetic chemistry, microbiological assays, enzymatic inhibition studies, and X-ray crystallography, we have provided compelling evidence that specific modifications at the 3'-OH site disrupt enzyme recognition and phosphorylation without compromising ribosomal binding.

The MIC assays confirmed that 3'-modified aminoglycosides retain antibacterial potency against resistant *E. coli* strains, with SBI237 (3'-epi-PAR) and SBI209 (3'-propyl-KAN) showing particularly promising activity. Notably, SBI237 exhibited a 16-fold lower MIC against APH(3')-expressing strains compared to unmodified PAR, highlighting the potential of stereochemical inversion as a strategy to evade enzymatic inactivation.
In vitro phosphorylation assays using purified APH(3')-Ia further demonstrated that none of the modified AGs served as enzymatic substrates, effectively preventing phosphorylation. Additionally, several derivatives, particularly SBI214 (3',4"-di-allyl-KAN) and SBI237, exhibited strong competitive inhibition of APH(3')-Ia, suggesting that specific 3'-OH modifications not only block phosphorylation but actively inhibit enzyme function.
Structural insights from X-ray crystallography provided a molecular basis for these observations, revealing that epimerization and steric bulk at the 3'-OH position introduce steric hindrance at the ATP-binding site of APH(3')-Ia. This structural disruption likely contributes to reduced ATP hydrolysis efficiency and impaired phosphorylation, further explaining the resistance-evasive properties of the modified AGs.
Together, these findings support the viability of targeted aminoglycoside modifications as a strategy to combat enzymatic resistance mechanisms. The observed structure–activity relationships provide a foundation for future aminoglycoside design, suggesting that dual modifications at the 3'- and 5"-OH positions could further expand the spectrum of resistance evasion.
These results contribute to the broader field of antibiotic resistance mitigation, reinforcing the importance of structural optimization in the development of next-generation aminoglycosides. The insights gained from this study pave the way for further rational drug design efforts, with the goal of developing aminoglycosides that can effectively combat multidrug-resistant bacterial infections.

AUTHOR CONTRIBUTIONS

N.P., S.B., A.J.M., A.G., A.H., and D.J.S. designed the research. S.B. and N.P. contributed to the conceptualization of the study.

- N.P.: Cloning, protein expression and purification; protein crystallization and diffractino data collection, analysis, and structure determination; manuscript writing.
- S.B.: Chemical synthesis of aminoglycoside derivatives; contribution to study design and manuscript draft.
- M.P.: Enzymatic activity and kinetic assays.
- A.G., A.H., D.J.S., S.H., M.D.W., A.J.M.: Supervision, conceptual input, and manuscript revision.
- K.H., M.G., I.L.-K., K.B., N.T.: General contributions to experimental work, chemical synthesis, and supervision.

4.6. MATERIALS AND METHODS

SYNTHESIS OF MODIFIED AMINOGLYCOSIDES

Cbz Protection of Paromomycin (PAR). PAR (500 mg, 0.9 mmol) was dissolved in THF:water (1:2, 10 mL) and reacted with Cbz-OSu (1.1 equiv.) in the presence of $NaHCO_3$ (2 equiv.) at room temperature for 16 hours. The product was purified via flash column chromatography using a DCM:methanol gradient.

Boc Protection of Kanamycin (KAN). KAN (500 mg, 1.2 mmol) was dissolved in DMSO (10 mL) and reacted with Boc_2O (1.2 equiv.) in the presence of triethylamine (2 equiv.). After 12 hours, water (10 mL) was added to precipitate the product, which was collected via filtration and drying.

Oxidation and Functionalization. The protected AGs underwent oxidation using [(neocuproine)$Pd(OAc)]_2(OTf)_2$ (5 mol) and benzoquinone (3 equiv.). Subsequent indium-mediated allylation and propargylation were carried out in the presence of In(0), allyl bromide, or propargyl bromide in MeOH:water (1:1) for 12 h. Detailed synthetic protocols are provided in the Supporting Information in Section 4.7.

MICROBIOLOGY

GENERAL

Stock solutions of aminoglycoside derivatives were prepared in deionized water at 10 or 20 mM and stored at –20 ° C. The concentrations were corrected based on qNMR-determined purity. Antibacterial activity was assessed using disk diffusion and MIC assays on various *E. coli* strains (Table 4.1). The IC_{50} values for protein synthesis inhibition were determined using a cell-free translation assay with *E. coli* ATCC 25922.

MIC ASSAYS

MIC were determined using a 96-well microdilution method. Wells 2–12 were filled with 50 μ L of cation-adjusted Müller–Hinton broth (CAMHB). The working antibiotic solutions were prepared by diluting stock solutions (see Table 3) into CAMHB. Well 1 was filled with 100 μ L of the working antibiotic solution, followed by serial two-fold dilutions across wells 2–10.
The bacterial inoculum was prepared by resuspending 3–4 colonies from LB–ampicillin agar plates in NaCl solution, adjusting the turbidity to 0.5 McFarland standard, and diluting 1:100 in CAMHB. Fifty microliters of this bacterial suspension was added to each well. Growth control contained no antibiotic, while sterile control contained no bacteria.
Plates were sealed and incubated at 37 ° C for 18 h. MIC values were determined as the lowest antibiotic concentration that completely inhibited visible bacterial growth under a lamp. The protocol was adapted from literature sources. Each experiment was performed in duplicate, and MIC values were calculated as the average of $\log_2$-transformed results.

CELL-FREE TRANSLATION ASSAYS

Stock solutions (1 mM) for *in vitro* translation assays were prepared by diluting 10 or 20 mM antibiotic stock solutions in 0.3% v/v Tween-20. The solutions were vortexed, centrifuged, and dispensed onto 96-well plates using a Tecan D300e dispenser, yielding a final concentration range of 20.5 μM to 0.002 μM. The dispensed volume was normalized to 1.5 μL of 0.3% Tween-20 in H_2O.

The translation master mix was freshly prepared using 0.2 mM amino acid mix, 0.4 μg luciferase mRNA, 6 μg tRNA, protease inhibitor, RNase inhibitor, S30 premix, and *E. coli* ATCC 25922 S30 lysate in Milli-Q water. After vortexing, 13.5 μL of this mix was added per well, plates were sealed, centrifuged (600 rpm), and incubated at 37 °C for 1 h. Post-incubation, 75 μL of LAR (luciferase assay reagent) was added per well, and chemiluminescence was immediately measured using an FLx800 plate reader. Luciferase activity was measured based on chemiluminescence intensity, where higher luminescence indicates higher protein biosynthesis, and lower luminescence reflects stronger inhibition of translation. The IC_{50} values ($n = 2$) were calculated from dose–response curves.

BIOCHEMICAL ASSAYS

GENERAL

The following chemicals were obtained from Sigma–Aldrich (St. Louis, MO) and used for enzyme assays:

- Phospho(enol)pyruvic acid (PEP), cyclohexylammonium salt
- β-Nicotinamide adenine dinucleotide, reduced disodium salt hydrate (β-NADH)
- Adenosine 5'-triphosphate (ATP) disodium salt trihydrate
- Pyruvate kinase (PK) and lactate dehydrogenase (LDH) enzyme solution (rabbit muscle)

KINETIC ASSAYS

The activity and kinetic parameters of APH(3')-Ia were determined using a spectrophotometric assay adapted from Goldman & Northrop. The AG phosphorylation reaction was monitored at 340 nm by coupling ATP hydrolysis with PK/LDH-catalyzed reactions, which result in β-NADH oxidation. The absorbance change at 340 nm provided the kinetic readout, as NADH ($\varepsilon_{340} = 6.22\ mM^{-1}\ cm^{-1}$) was oxidized by LDH, facilitating the conversion of pyruvate to lactate.

Reactions were conducted in a 96-well flat-bottom transparent polystyrene plate, and absorbance was measured using a Spark 10M microplate reader (Tecan). Light-path correction to 1 cm was applied using the absorbance difference between 977 nm and 900 nm for 200 μL of Milli-Q water.

Standard assay conditions (200 μL reaction volume): 50 mM HEPES buffer (pH 7.0), 100 mM NaCl, 10 mM $MgCl_2$, 4.0 mM PEP, 6–10 units of PK, 5.0 mM ATP, 0.2 mM NADH, 9–14 units of LDH, 0.2 μM APH(3')-Ia, and 10 μL of 20× aminoglycoside stock at the desired concentration. Reactions were pre-incubated for 3 min at 30 ° C before antibiotic addition, maintaining a constant temperature throughout the assay.

The kinetic parameters for kanamycin A and paromomycin were determined by fitting the initial velocities to a substrate inhibition model, where:

$$v = \frac{V_{\max}[S]}{K_M + [S]\left(1 + \frac{[S]}{K_i}\right)} \tag{4.1}$$

Equation | 4.1 Where K_i is the inhibitory constant, v is the reaction rate, V_{max} is the maximum reaction rate, $[S]$ is the substrate concentration, and K_M is the Michaelis constant. The k_i parameter was interpolated from the corresponding V_{max} value, considering the enzyme concentration used in the assay.

APH(3')-IA INHIBITION ASSAYS

IC_{50} experiments for AG derivatives were performed similarly to the standard kinetic assays, with the addition of the tested compound at varying concentrations in the reaction mixture. The concentration range tested for each compound varied between 10^{-3} M and 10^{-7} M, while a fixed 25 μM concentration of the natural AG (7–8-fold excess of the K_M value) was used to trigger the enzymatic reaction.
Statistical analysis was performed using GraphPad Prism (GraphPad Software, Inc.), fitting the data corresponding to the initial velocities at each inhibitor concentration (log-transformed in mM) to a four-parameter logistic equation (Equation 4.2). The enzymatic activity was reported as a percentage:

$$\text{Activity (\%)} = \text{MIN} + \frac{(\text{MAX} - \text{MIN})}{1 + 10^{(\log \text{IC}_{50} - x)\cdot \text{Hill}}} \tag{4.2}$$

Equation | 4.2 Four-parameter logistic model used for IC_{50} determination of the AG derivatives where: MIN represents the basal hydrolase activity of APH(3')-Ia in the absence of any antibiotics; MAX corresponds to the enzymatic phosphorylation activity of the natural aminoglycoside without an inhibitor; IC_{50} is the inhibitor concentration required to reduce enzymatic activity by 50%; Hill is the Hill slope of the linear portion of the curve between the lower and upper activity extremes.

STRUCTURAL DETERMINATION OF APH(3')-IA

CLONING OF *aph(3')Ia*

The Open Reading Frame (ORF) of *aph(3')-Ia* was codon-optimized for *E. coli* and synthesized by IDT Technologies (Belgium) with *NdeI* and *HindIII* restriction sites at the 5' and 3' ends, respectively. The gene was first blunt-end ligated into the pJET1.2/blunt vector (Thermo Fisher) and transformed into chemically competent *E. coli* DH5α. It was then subcloned into pET28b(+) (Merck) using *NdeI* and *HindIII*, generating pET28b(+)-*aph(3')Ia*, which encodes APH(3')-Ia with an N-terminal thrombin-cleavable His-tag. The final plasmid was transformed into *E. coli* BL21(DE3) (Merck) for protein overexpression.

OVEREXPRESSION AND PURIFICATION PROTOCOL

APH(3')-Ia was overexpressed following standard protocols. LB medium containing 50 μg/mL kanamycin A was inoculated with an overnight culture of BL21(DE3)/pET28b(+)-*aph(3')Ia* (initial OD ~ 0.05) and grown at 37 °C until OD ~ 0.9, then induced with 0.4–0.6 mM IPTG.

After 16 h at 22 °C, cells were harvested by centrifugation (6000 *g*, 10 min) and resuspended in lysis buffer (50 mM K_3PO_4, 500 mM NaCl, 10 mM imidazole, 1 mM PMSF, 1 μg/mL pancreatic bovine DNase, pH 7.5).
All purification steps were carried out at 4 °C. Cells were disrupted using a Constant Systems Ltd. cell disruptor (~25 kpsi), and cell debris was removed by centrifugation at 267,000 *g* for 60 min. The lysate was loaded onto a Ni-Sepharose column equilibrated with washing buffer (50 mM KPO_4, 500 mM NaCl, 30 mM imidazole, 5 mM $MgCl_2$, pH 7.5) and eluted with elution buffer (50 mM KPO_4, 500 mM NaCl, 300 mM imidazole, 5 mM $MgCl_2$, 20% glycerol, pH 7.5). For crystallization, the protein was further purified via size-exclusion chromatography (SEC) on a Superdex 200 10/300 GL column (GE Healthcare) equilibrated with crystallization buffer (10 mM HEPES, 100 mM NaCl, pH 7.0). For enzymatic assays, the elution was carried out using activity buffer (50 mM HEPES, 100 mM NaCl, 10 mM $MgCl_2$, pH 7.0). Peak fractions were concentrated to 20 mg/mL using a Vivaspin 10 kDa MWCO concentrator (GE Healthcare) and used immediately for crystallization.
Protein concentration was determined spectrophotometrically using a molar extinction coefficient of 32,117 M^{-1} cm^{-1} (1.325 g^{-1} L cm^{-1}).

CRYSTALLIZATION, DIFFRACTION DATA COLLECTION, AND PROCESSING

Crystallization of APH(3')-Ia was performed by mixing equal volumes of protein solution (10–20 mg/mL) and reservoir solution (0.1 M $CaCl_2$, 7–14% PEG 3350). Crystals appeared overnight, reached full size within one week, and diffracted close to atomic resolution when harvested within 15 days. Protein–ligand complexes were obtained by soaking crystals in reservoir solution supplemented with 20% glycerol and 5–9 mM of each compound.
X-ray diffraction data for the APH(3')-Ia–paromomycin complex were collected at beamline X31 at the European Molecular Biology Laboratory (EMBL) outstation, Deutsches Elektronen-Synchrotron (DESY), Hamburg, Germany, using a 0.99 Å wavelength. Data for other structures were collected in-house on an ENRAF–Nonius CuKα rotating anode generator equipped with a MacScience DIP2030 image plate detector. All diffraction data were collected at 110 K.
Data were processed using `XDS` and reduced with `Aimless`. Phases were determined by molecular replacement (MR) using `PHASER`, with chain A from PDB entry 4EJ7 as the search model. `Pointless` confirmed that all crystals belonged to the $P3_12_1$ space group, with two molecules per asymmetric unit. The electron density map allowed for unambiguous interpretation, and residues from position 20 onward were fully modeled.
The structure was built using `Coot`, and refinement and validation were carried out with `Phenix`. Data collection and refinement statistics are summarized in Table 4.4.

Table 4.4 | Data processing, refinement, and model statistics for the structures of APH(3')Ia in complex with 3'-modified kanamycin derivatives. Statistics for the highest-resolution shell are shown in parentheses.

Parameter	**SBI233** (3'-Propargyl-KAN)	**SBI238** (3'-Propyl-KAN)
Wavelength (Å)	0.99	0.99
Resolution (Å)	2.22	2.19
Space group	$P3_12_1$	$P3_12_1$
Unit cell		
a, b, c (Å)	130.125, 130.125, 83.855	128.554, 128.554, 83.711
α, β, γ (°)	90.0, 90.0, 120.0	90.0, 90.0, 120.0
Total reflections	391,406 (34,914)	467,285 (45,271)
Unique reflections	40,680 (3,972)	41,320 (4,055)
Multiplicity	9.6 (8.8)	11.3 (11.2)
Completeness (%)	99.73 (98.17)	99.91 (99.95)
$\langle I \rangle / \sigma(I)$	29.69 (7.61)	10.50 (1.38)
Wilson B factor (Å^2)	29.89	34.37
$\mathbf{R_{merge}}$	0.0558 (0.2775)	0.2297 (1.87)
$\mathbf{R_{meas}}$	0.0589 (0.2944)	0.2407 (1.96)
$\mathbf{R_{pim}}$	0.0189 (0.0968)	0.0713 (0.5852)
$\mathbf{CC_{1/2}}$	0.999 (0.961)	0.996 (0.439)
CC*	1.000 (0.990)	0.999 (0.781)
Reflections		
Total	40,650 (3,972)	41,291 (4,053)
R_{free} set	1,994 (195)	2,095 (168)
$\mathbf{R_{work}}$	0.1753 (0.2428)	0.1998 (0.3007)
$\mathbf{R_{free}}$	0.2134 (0.3042)	0.2454 (0.3602)
CC(work)	0.958 (0.869)	0.960 (0.672)
CC(free)	0.941 (0.723)	0.941 (0.534)
No. non-H atoms	4,829	4,551
Macromolecules	4,368	4,263
Ligands	72	83
Solvent	319	205
Protein residues	537	529
RMS(bonds) (Å)	0.004	0.008
RMS(angles) (°)	0.65	0.98
Ramachandran		
Favored (%)	97.94	97.32
Allowed (%)	2.06	2.68
Outliers (%)	0.00	0.00
Rotamer outliers (%)	0.42	2.15
Clashscore	3.96	4.84
B-factors (Å^2)		

Table 4.4 (continued): Data processing, refinement, and model statistics.

Parameter	**SBI233**	**SBI238**
Average	38.16	41.21
Macromolecules	37.45	41.23
Ligands	48.83	41.48
Solvent	41.34	40.72

4.7. SUPPORTING INFORMATION

GENERAL METHODS

All solvents used for extraction, filtration, and chromatography were of commercial grade and used without further purification. [(neocuproine)Pd(OAc)]$_2$(OTf)$_2$ was prepared according to a literature procedure. Benzoquinone was purified by recrystallization from ethanol. Celite® 545 was purchased from Merck, and palladium on carbon (10% Pd/C, Type 487, dry) was obtained from Alfa Aesar. Other reagents were sourced from Sigma-Aldrich, TCI, Fluorochem, and Acros, and used as received.
Flash chromatography was performed manually using SiliaFlash P60 silica (230–400 mesh, Silicycle) or using an automated Reveleris flash chromatography system (Büchi). Thin-layer chromatography (TLC) was conducted on Merck silica gel 60 (0.25 mm plates) and visualized using either anisaldehyde stain (135 mL EtOH, 5 mL H_2SO_4, 1.5 mL AcOH, 3.7 mL *p*-anisaldehyde) or ninhydrin stain (1.5 g ninhydrin, 100 mL *n*-butanol, 3 mL AcOH).
NMR spectra (^{1}H, ^{13}C, APT, HSQC, TOCSY) were recorded on a Bruker Avance NEO 600 MHz spectrometer (^{1}H: 600 MHz, ^{13}C: 150.9 MHz) at 25 °C, using MeOD-d_4, DMSO-d_6, or D_2O as solvents. Chemical shifts (δ) are reported in ppm, using solvent resonances as internal standards (MeOD-d_4: δ 3.31 (^{1}H), δ 49.00 (^{13}C); DMSO-d_6: δ 2.50 (^{1}H), δ 39.52 (^{13}C); D_2O: δ 4.79 (^{1}H)). Data are reported as follows: chemical shifts (δ), multiplicity (s = singlet, d = doublet, dd = doublet of doublets, ddd = doublet of doublet of doublets, dddd = doublet of doublet of doublet of doublets, dt = doublet of triplets, ddt = doublet of doublet of triplets, dq = doublet of quartets, t = triplet, td = triplet of doublets, q = quartet, m = multiplet, bs = broad singlet), coupling constants J (Hz), and integration.
High-resolution mass spectrometry (HRMS) was performed on a Thermo Scientific LTQ Orbitrap XL. Residual palladium was removed using MP-TMT resin (Biotage).

UPLC-MS ANALYSIS AND QNMR-BASED PURITY DETERMINATION

UPLC-MS Analysis Graph 1 illustrates the UPLC solvent gradient and MS settings used for reaction monitoring. Solvent A consisted of water with 0.1% formic acid, while Solvent B was acetonitrile with 0.1% formic acid.

Quantitative NMR (qNMR) for Purity Determination The purity of the final compounds was determined by quantitative NMR (qNMR) using dimethyl sulfone (DMS) TraceCERT (Sigma) as the standard. qNMR experiments were performed using either internal or external calibration.
For internal calibration, an accurately weighed amount of the sample (3.00–5.00 mg) and DMS internal calibrant (IC) was dissolved in MeOD-d_4 or D_2O (0.6 mL). The experiment was recorded on a Bruker Avance NEO 600 MHz spectrometer at 25 °C, using a 90° pulse width, relaxation delay ($d1$) of 60 s, acquisition time (AQ) of 4 s, and 32 scans (nt). The purity (%) of the compound was calculated using:

$$P\ (\%) = \frac{n_{IC} \times \mathrm{Int}_t \times MW_t \times m_{IC}}{n_t \times \mathrm{Int}_{IC} \times MW_{IC} \times m_s} \times P_{IC} \tag{4.3}$$

Equation | 4.3 Where Int = integral; MW = molecular weight; m = mass; n = number of protons; P = purity (%); IC = internal calibrant; s = sample; t = target analyte/molecule.

For external calibration, qNMR purity was determined using a DMS dilution series. The most concentrated solution (0.128 mol/L) was prepared by dissolving 14.5 mg DMS in 1.2 mL DMSO-d_6 and subjected to serial two-fold dilutions to obtain eight concentration points down to 0.001 mol/L. ^{1}H NMR spectra were recorded at 25 °C on a Bruker Avance NEO 600 MHz spectrometer, using 16 scans, relaxation delay of 60 s, a 90° pulse, and an acquisition time of 4.99 s. Integrated resonance lines were fitted using linear regression (correlation coefficient = 0.999893). The purity (%) of unknown samples was calculated by dividing the qNMR-determined concentration by the concentration based on the weighed amount of analyte, multiplied by 100%.

qNMR was used to adjust compound concentrations for biological assays, accounting for NMR-silent impurities (salts) and water content. Due to the high hygroscopicity of aminoglycosides, paromomycin derivatives exhibited lower apparent purity due to high acetate salt and water content, which could not be fully removed despite multiple freeze-drying cycles. Therefore, qNMR-adjusted purity values were used for calculating final yields and compound concentrations in biological assays.

4.8. SYNTHESIS

SYNTHESIS OF N-(CBZ)$_5$-PAROMOMYCIN (1)

SYNTHESIS

To a solution of paromomycin sulfate (4.0 g, 5.6 mmol, 1 eq) in H_2O (29 mL), a solution of K_2CO_3 (2.7 g, 19.6 mmol, 3.5 eq) in H_2O (18 mL) was added. THF (30 mL) was then introduced, followed by the dropwise addition of *N*-(benzyloxycarbonyloxy)-succinimide (12.6 g, 50.4 mmol, 9 eq) in THF (62 mL) over 30 min at room temperature, forming a white suspension, which was stirred overnight at room temperature.

Upon complete conversion (monitored by TLC, DCM:MeOH 95:5, visualized with anisaldehyde stain), the reaction was quenched with glycine (3.8 g, 50.4 mmol, 9 eq) in a saturated $NaHCO_3$ solution (20 mL) and stirred for 1 h at room temperature. The solvent (THF) was removed *in vacuo*, and the mixture was basified to pH 9 using 1 M NaOH. The aqueous layer was extracted with EtOAc, and the combined organic layers were dried over $MgSO_4$, filtered, and concentrated under reduced pressure.

The crude white solid was purified by flash column chromatography (DCM:MeOH, 0–10% gradient), affording N-(Cbz)$_5$-Paromomycin as a white foam (4.1 g, 3.2 mmol, 86%). The yield was adjusted based on the qNMR-determined purity (64%) of the starting paromomycin sulfate.

SPECTROSCOPIC DATA

^{1}H NMR (400 MHz, MeOD-d_4) δ 7.45–7.22 (m, 25H), 5.28–4.94 (m, 12H), 4.82 (d, 1H), 3.98 (s, 1H), 3.91 (m, 3H), 3.81 (m, 3H), 3.78–3.69 (m, 3H), 3.69–3.54 (m, 5H), 3.49 (m, 3H), 3.42–3.33 (m, 4H), 1.98 (br d, J = 12.7 Hz, 1H), 1.40 (m, 1H).

^{13}C NMR (151 MHz, MeOD-d_4) δ 174.9, 174.5, 159.2, 159.1, 159.0, 158.8, 158.7, 138.3, 138.2, 138.1, 129.6, 129.5, 129.4, 129.3, 129.2, 129.1, 129.0, 128.9, 128.8, 128.6, 110.6, 100.5, 100.2, 100.1, 87.3, 83.7, 81.2, 79.0, 78.1, 75.8, 74.9, 74.5, 72.6, 71.6, 71.5, 70.3, 69.2, 67.9, 67.8, 67.7, 67.6, 67.4, 63.4, 63.1, 62.8, 57.8, 54.1, 52.3, 52.2, 49.9, 49.4, 49.3, 49.1, 49.0, 48.9, 48.7, 48.6, 43.5, 42.6, 35.4.

HRMS (ESI) m/z $[M+Na]^+$ calcd for $C_{63}H_{75}O_{24}N_5Na$: 1308.4694, found: 1308.4714.

SYNTHESIS OF N-(CBZ)$_5$-3'-KETO-PAROMOMYCIN (3)

SYNTHESIS

N-(Cbz)$_5$-Paromomycin (1.0 g, 0.7 mmol, 1 eq) was dissolved in MeOH (8 mL), followed by the addition of benzoquinone (92 mg, 0.9 mmol, 1.1 eq). Once dissolved, [(neocuproine)Pd(OAc)]$_2$(OTf)$_2$ (20.4 mg, 0.02 mmol, 2.5 mol) was added, resulting in a dark orange solution, which was stirred overnight at room temperature.

After 16 h, an additional 5 mol of catalyst was added (total: 61.1 mg, 0.06 mmol, 7.5 mol) and the mixture was heated to 45 °C. The reaction was continued for 5 days, after which it was stopped despite incomplete conversion (TLC, DCM:MeOH 9:1, stained with anisaldehyde). The reaction mixture was concentrated *in vacuo*, yielding an orange foam, which was purified via manual column chromatography (DCM:MeOH 0–10% gradient). The desired product was obtained as a light orange foam (871 mg, 0.68 mmol, 87%), though it contained traces of catalyst and benzoquinone.

To determine the real yield, the actual product mass was calculated using:

$$m_3 = \frac{m_{\text{tot}}}{\left(\frac{i_3}{N_3}\right)MW_3 + \left(\frac{i_{\text{BQ}}}{N_{\text{BQ}}}\right)MW_{\text{BQ}} + \left(\frac{i_{\text{catalyst}}}{N_{\text{catalyst}}}\right)MW_{\text{catalyst}}} \tag{4.4}$$

where m = mass; i = integral of the corresponding NMR peak; N = number of nuclei represented by the peak; MW = molecular weight; BQ = benzoquinone; catalyst = [(neocuproine)Pd(OAc)]$_2$(OTf)$_2$. The actual isolated product mass was 644.5 mg (0.5 mmol, 65%) after correcting for impurities.

Small-Scale Reaction (500 mg Scale)

- N-(Cbz)$_5$-Paromomycin (500 mg, 0.39 mmol, 1 eq)
- MeOH (3.9 mL)
- Benzoquinone (46.2 mg, 0.43 mmol, 1.1 eq)
- [(neocuproine)Pd(OAc)]$_2$(OTf)$_2$ (30.5 mg, 0.03 mmol, 7.5 mol)

Due to the smaller scale, purification led to a cleaner isolated product, with a final yield of 48% (240 mg, 0.19 mmol).

SPECTROSCOPIC DATA
^{1}H NMR (400 MHz, MeOD-d_4) δ 7.32 (m, 25H), 5.08 (m, 12H), 4.69 (d, J = 4.4 Hz, 1H), 4.33 (d, J = 9.8 Hz, 1H), 4.05–3.80 (m, 8H), 3.79–3.69 (m, 2H), 3.67–3.56 (m, 3H), 3.50 (bs, 3H), 3.44–3.34 (m, 4H), 2.03–1.91 (m, 1H), 1.50–1.35 (m, 1H).
^{13}C NMR (101 MHz, MeOD-d_4) δ 205.0, 159.0, 158.0, 151.0, 147.8, 138.3, 129.7, 129.5, 129.4, 129.2, 129.0, 128.9, 128.84, 128.81, 128.7, 116.8, 102.4, 96.4, 86.0, 73.5, 71.6, 69.2, 67.7, 67.6, 61.8, 54.0, 42.6, 26.3.
HRMS (ESI) m/z $[M+H]^+$ calcd for $C_{63}H_{74}O_{24}N_5$: 1284.4718, found: 1284.4755.

SYNTHESIS OF N-(BOC)$_4$-KANAMYCIN (2)

Kanamycin A sulfate (5.0 g, 8.6 mmol, 1 eq) was suspended in H_2O (20 mL). Triethylamine (4.8 mL, 34.3 mmol, 4 eq) was added, followed by a solution of di-*tert*-butyl dicarbonate (15.0 g, 68.7 mmol, 8 eq) in DMSO (60 mL). The reaction mixture was stirred overnight at room temperature, and progress was monitored by UPLC-MS.
Upon completion, the solid was filtered through a glass sintered funnel, washed with H_2O, and dried under vacuum, yielding the desired product as a white solid (7.0 g, 92%).

SPECTROSCOPIC DATA
^{1}H NMR (400 MHz, DMSO-d_6) δ 6.97–6.85 (m, 1H), 6.59 (d, J = 7.1 Hz, 1H), 6.51 (d, J = 9.1 Hz, 1H), 6.36 (t, J = 5.0 Hz, 1H), 5.44–5.35 (m, 1H), 5.26 (bs, 1H), 4.99–4.85 (m, 4H), 4.72 (d, J = 6.4 Hz, 1H), 4.24 (t, J = 5.5 Hz, 1H), 3.81 (dt, J = 10.3, 3.2 Hz, 1H), 3.57 (dd, J = 8.6, 5.1 Hz, 1H), 3.49 (t, J = 4.6 Hz, 3H), 3.36 (d, J = 10.3 Hz, 1H), 3.32–3.16 (m, 3H), 3.06 (dt, J = 12.5, 6.1 Hz, 1H), 1.85–1.75 (m, 1H), 1.44–1.32 (m, 37H).
^{13}C NMR (101 MHz, DMSO-d_6) δ 156.5, 156.3, 155.5, 155.1, 101.2, 97.9, 84.1, 80.3, 77.99, 77.94, 77.4, 75.1, 73.0, 72.8, 72.2, 70.4, 70.2, 67.4, 60.3, 56.0, 50.2, 49.1, 41.5, 40.4, 34.9, 28.5*, 28.3*, 28.2* (12 CH_3 in total).
HRMS (ESI) m/z $[M+H]^+$ calcd for $C_{38}H_{69}O_{19}N_4$: 885.4551, found: 885.4561.

SYNTHESIS OF N-(BOC)$_4$-3'-KETO-KANAMYCIN (4)

N-(Boc)$_4$-Kanamycin (1 eq) was dissolved in DMSO, followed by the addition of benzoquinone (3 eq). Upon dissolution, [(neocuproine)Pd(OAc)]$_2$(OTf)$_2$ (2.5 mol) was added, forming a dark brown solution, which was stirred at room temperature.
The reaction was monitored by UPLC-MS and quenched when at least 50% of the starting material was converted to the desired mono-oxidized product. To quench the reaction, five volumes of water (relative to the DMSO used) were added, causing precipitation. The solid was filtered using a sintered-glass funnel, washed with water, and dried under vacuum, yielding N-(Boc)$_4$-3'-Keto-Kanamycin.
Different batches of starting material required varying reaction times to reach the 50% conversion target. However, in some cases, over-oxidation resulted in the formation of an undesired di-oxidized product, as confirmed by UPLC-MS analysis. To prevent over-oxidation, the reaction was stopped before full conversion. The crude product was used without further purification.

The site of the second oxidation was confirmed via TOCSY-NMR, following indium-mediated allylation and subsequent separation of the mono- and di-allylated Boc-protected kanamycin derivatives. The material obtained from several oxidation attempts was used for indium-mediated alkylation, as described in the procedures for derivatives 7, 8, and 9.

SYNTHESIS OF N-(CBZ)$_5$-3'-ALLYL-PAROMOMYCIN (5)

A solution of N-(Cbz)$_5$-3'-Keto-Paromomycin (530 mg, 0.4 mmol, 1 eq) in THF:H_2O (14 mL, 1:1 v/v) was prepared. Indium powder (61.6 mg, 0.5 mmol, 1.3 eq) and allyl bromide (54 μL, 0.6 mmol, 1.5 eq) were added, and the reaction was stirred at room temperature.
The reaction progress was monitored by TLC (DCM:MeOH 5%) and visualized with *p*-anisaldehyde stain. After two days, full conversion to a more apolar product was observed. The mixture was filtered over filter paper to remove indium salts and concentrated *in vacuo*. Purification by flash column chromatography (DCM:MeOH, 2–15% gradient) afforded N-(Cbz)$_5$-3'-Allyl-Paromomycin as a dark orange amorphous solid (297 mg, 74%), calculated based on the actual amount of 3'-Keto-Paromomycin used (392 mg, 0.22 mmol).

SPECTROSCOPIC DATA

^{1}H NMR (600 MHz, MeOD-d_4) δ 7.42–7.20 (m, 25H), 5.91–5.74 (m, 1H), 5.30–4.91 (m, 15H), 4.09–3.77 (m, 8H), 3.77–3.51 (m, 7H), 3.52–3.43 (m, 3H), 3.43–3.33 (m, 3H), 2.44 (dd, J = 13.7, 8.4 Hz, 1H), 2.31–2.21 (m, 1H), 2.05–1.95 (m, 1H), 1.49–1.38 (m, 1H).
^{13}C NMR (151 MHz, MeOD-d_4) δ 164.3, 159.2, 159.0, 141.0, 138.3, 138.1, 134.2, 129.7, 129.6, 129.5, 129.4, 129.1, 129.0, 128.9, 128.8, 128.7, 127.7, 127.6, 119.9, 119.6, 101.2, 100.7, 100.5, 86.4, 83.6, 78.0, 76.0, 75.1, 74.4, 72.2, 71.5, 68.3, 67.8, 67.6, 67.5, 64.3, 63.2, 62.8, 54.1, 53.5, 42.6, 39.1, 30.7, 30.0, 29.5, 24.2.
HRMS (ESI) m/z $[M+Na]^+$ calcd for $C_{66}H_{79}O_{24}N_5Na$: 1348.5007, found: 1348.5022.

SYNTHESIS OF N-(CBZ)$_5$-3'-EPI-PAROMOMYCIN (6)

N-(Cbz)$_5$-3'-Keto-Paromomycin (295 mg, 0.2 mmol, 1 eq) was dissolved in MeOH (8.2 mL). Sodium borohydride (43.5 mg, 1.2 mmol, 5 eq) was added, and the reaction mixture was stirred overnight at room temperature.
Upon full conversion (confirmed by TLC, DCM:MeOH 9:1, anisaldehyde stain), the mixture was stirred for 1 h with Amberlite-IR120 resin (H^+ form, 50 mg) to quench excess reducing agent. The mixture was then filtered and concentrated *in vacuo*.
Purification by flash column chromatography (DCM:MeOH 0–10% gradient) yielded N-(Cbz)$_5$-3'-epi-Paromomycin as a light orange foam (103.5 mg, 47%), considering the actual amount of 3'-keto-paromomycin used (218.3 mg, 0.08 mmol).

SPECTROSCOPIC DATA

^{1}H NMR (600 MHz, MeOD-d_4) δ 7.59–7.07 (m, 25H), 5.28–4.94 (m, 13H), 4.78 (s, 1H), 3.98 (t, 1H), 3.93 (dt, J = 6.6, 3.2 Hz, 3H), 3.90–3.85 (m, 2H), 3.85–3.80 (m, 3H), 3.69–3.63 (m, 2H), 3.62–3.52 (m, 4H), 3.51–3.48 (m, 1H), 3.48–3.36 (m, 4H), 2.07–1.95 (m, 1H), 1.45 (s, 1H).
^{13}C NMR (151 MHz, MeOD-d_4) δ 159.2, 159.0, 158.6, 158.5, 138.3, 138.1, 137.8, 129.7, 129.65, 129.53, 129.52, 129.4, 129.1, 129.0, 128.97, 128.93, 128.9, 128.8, 128.7, 100.5, 99.96, 99.93, 86.2,

83.6, 78.2, 78.17, 75.8, 75.3, 74.5, 72.1, 72.0, 71.5, 69.5, 69.2, 68.2, 67.9, 67.6, 67.5, 62.6, 54.1, 53.4, 49.9, 48.6, 42.6, 30.7, 21.0.
HRMS (ESI) m/z $[M+Na]^+$ calcd for $C_{63}H_{75}O_{24}N_5Na$: 1308.4694, found: 1308.4710.

SYNTHESIS OF 3'-EPI-PAROMOMYCIN × 5 ACOH (SBI237)

SYNTHESIS

A three-neck flask was purged with three vacuum/nitrogen cycles before adding Pd/C (25 mg, 0.02 mmol, 0.3 eq) and $Pd(OH)_2$ (16.4 mg, 0.02 mmol, 0.3 eq) under an inert atmosphere. A small amount of ethyl acetate was added, followed by careful addition of methanol (1.2 mL) via syringe.
N-$(Cbz)_5$-3'-epi-Paromomycin (100 mg, 0.08 mmol, 1 eq) was dissolved in methanol (2 mL) and added to the reaction flask. Acetic acid (22 μL, 0.4 mmol, 5 eq) was introduced, and the mixture was degassed by evacuating the air until the solvent began to boil, then backfilled with nitrogen (repeated 3 times).
A balloon of hydrogen was attached, and the flask was degassed again by evacuation until the solvent boiled, then backfilled with hydrogen (3 cycles). The reaction mixture was stirred overnight at room temperature, and completion was confirmed by UPLC-MS.
Upon completion, the hydrogen balloon was closed and detached, and the flask was filled with nitrogen. The reaction mixture was filtered through a Whatman filter, and the filter was washed with water. The resulting aqueous solution was stirred with MP-TMT resin for 1 h, then filtered. The final solution was freeze-dried overnight, yielding 3'-epi-Paromomycin × 5 AcOH (SBI237) as a white fluffy powder (96 mg, 26%). The qNMR-determined purity was 20% (qNMR experiment with internal standard).

SPECTROSCOPIC DATA

^{1}H NMR (600 MHz, D_2O) δ 5.51 (d, J = 4.3 Hz, 1H), 5.37 (d, J = 2.6 Hz, 1H), 5.23 (d, J = 1.9 Hz, 1H), 4.51 (dd, J = 6.5, 4.9 Hz, 1H), 4.35 (dd, J = 5.0, 2.6 Hz, 1H), 4.28 (d, J = 5.4 Hz, 1H), 4.19 (m, 3H), 3.98 (ddd, J = 9.0, 6.0, 2.5 Hz, 1H), 3.93–3.90 (m, 1H), 3.89 (t, J = 2.2 Hz, 1H), 3.82–3.73 (m, 4H), 3.72–3.65 (m, 2H), 3.56 (dd, J = 10.4, 9.3 Hz, 1H), 3.52 (tdt, J = 13.5, 6.8, 3.9 Hz, 1H), 3.46 (s, 1H), 3.41 (dd, J = 13.6, 7.0 Hz, 1H), 3.35 (dd, J = 13.6, 3.9 Hz, 1H), 3.24–3.11 (m, 2H), 2.27 (dt, J = 12.7, 4.3 Hz, 1H), 1.58 (q, J = 12.6 Hz, 1H).
^{13}C NMR (151 MHz, D_2O) δ 106.1, 93.0, 92.6, 81.0, 78.0, 76.5, 72.1, 70.6, 70.0, 67.2, 65.7, 65.1, 64.4, 64.0, 62.5, 57.3, 57.1, 48.0, 47.2, 47.0, 46.0, 37.2, 27.7.
HRMS (ESI) m/z $[M+H]^+$ calcd for $C_{23}H_{46}O_{14}N_5$: 616.3041, found: 616.3035.

SYNTHESIS OF 3'-PROPYL-PAROMOMYCIN × 5 ACOH (SBI236)

A three-neck flask was purged with three vacuum/nitrogen cycles before adding Pd/C (48 mg, 0.05 mmol, 0.3 eq) and $Pd(OH)_2$ (31.8 mg, 0.05 mmol, 0.3 eq) under an inert atmosphere. A small amount of ethyl acetate was added, followed by the careful addition of methanol (2.2 mL) via syringe. N-$(Cbz)_5$-3'-Allyl-Paromomycin (200 mg, 0.2 mmol, 1 eq) was dissolved in methanol (3 mL) and added to the flask. Acetic acid (43 μL, 0.8 mmol, 5 eq) was then introduced. The reaction was degassed by evacuating the flask until the solvent started to

boil, then backfilling with nitrogen (repeated 3 times). A balloon of hydrogen was attached, and the flask was evacuated again and backfilled with hydrogen (3 cycles).
After 2 days, no conversion to the desired product was observed, and LC–MS indicated partial deprotection. The reaction was therefore filtered over Celite, and fresh Pd/C (48 mg, 0.05 mmol, 0.3 eq) and $Pd(OH)_2$ (31.8 mg, 0.05 mmol, 0.3 eq) were added. The reaction was placed under hydrogen again and stirred overnight at room temperature, leading to partial conversion.
Since partially protected paromomycin remained, an additional 0.2 eq of both Pd/C and $Pd(OH)_2$ was added as a slurry in ethyl acetate, along with an additional 5 eq of acetic acid. The reaction was stirred overnight, and this time, full conversion was observed via UPLC–MS. Upon completion, the hydrogen balloon was closed and detached, and the flask was backfilled with nitrogen. The reaction mixture was filtered through a Whatman filter, and the filter was washed with water. The resulting aqueous solution was stirred with MP–TMT resin for 1 hour, then filtered. The final solution was freeze-dried overnight, yielding 3'-Propyl-Paromomycin × 5 AcOH (SBI236) as a white powder (322 mg, 22%). qNMR-determined purity was 10% (qNMR experiment with internal standard).

SPECTROSCOPIC DATA
^{1}**H NMR** (600 MHz, D_2O) δ 5.59 (d, J = 4.5 Hz, 1H), 5.39 (d, J = 2.9 Hz, 1H), 5.29 (d, J = 1.8 Hz, 1H), 4.55–4.49 (dd, 1H), 4.36–4.29 (m, 2H), 4.24 (t, J = 3.1 Hz, 1H), 4.21–4.17 (m, 1H), 3.98–3.91 (m, 2H), 3.89 (d, J = 3.1 Hz, 1H), 3.88–3.83 (dd, J = 6.9, 2.8 Hz, 1H), 3.82 (dt, J = 3.0, 1.3 Hz, 1H), 3.80–3.73 (m, 2H), 3.72–3.61 (m, 2H), 3.60–3.53 (td, 2H), 3.43 (dd, J = 13.6, 6.8 Hz, 2H), 3.36 (dt, J = 13.5, 4.2 Hz, 1H), 3.30 (ddt, J = 13.8, 7.6, 3.7 Hz, 1H), 2.42 (dt, J = 12.7, 4.6 Hz, 1H), 1.79–1.74 (m, 1H), 1.61–1.49 (m, 2H), 1.34–1.21 (m, 2H), 0.93 (t, J = 7.1 Hz, 3H).
^{13}**C NMR** (151 MHz, D_2O) δ 100.0, 95.7, 95.6, 81.4, 73.3, 73.29, 73.1, 72.7, 70.3, 69.6, 67.7, 67.3, 60.9, 60.2, 59.8, 50.9, 50.0, 49.2, 47.0, 46.9, 41.7, 40.4, 23.2, 18.4, 16.8, 13.4.
HRMS (ESI) m/z $[M+H]^+$ calcd for $C_{26}H_{52}O_{14}N_5$: 658.3511, found: 658.3506.

SYNTHESIS OF N-(BOC)$_4$-3'-ALLYL-KANAMYCIN (7) AND N-(BOC)$_4$-3',4"-DIALLYL-KANAMYCIN (8)

First Batch – Indium-Mediated Allylation Leading to Compound 7 A crude reaction mixture (total 4 g starting material) was used for indium-mediated allylation to obtain N-(Boc)$_4$-3'-Allyl-Kanamycin (7). The estimated conversion of N-(Boc)$_4$-3'-Keto-Kanamycin (4) was ~50%, as determined by UPLC–MS analysis:

- Retention time = 16.07 min → corresponding to unreacted N-(Boc)$_4$-Kanamycin (2) (m/z = 782.51, loss of 1 Boc group).
- Retention time = 16.44 min → corresponding to N-(Boc)$_4$-3'-Keto-Kanamycin (4) (m/z = 780.52, loss of 1 Boc group).

Based on these observations, the indium-mediated allylation was conducted using an estimated 2 g of N-(Boc)$_4$-3'-Keto-Kanamycin (4).
A solution of N-(Boc)$_4$-3'-Keto-Kanamycin (2 g, 2.27 mmol, 1 eq) in THF:H_2O (60 mL, 1:1 v/v) was prepared. Indium powder (390 mg, 3.4 mmol, 1.5 eq) and allyl bromide (0.3 mL, 3.4 mmol,

1.5 eq) were added. The color changed from dark orange to dark green. The reaction mixture was stirred at room temperature and monitored by TLC (DCM:MeOH 5%, ninhydrin stain) and UPLC–MS.
After five days, a more apolar product was observed. The reaction was filtered through filter paper to remove indium salts and concentrated *in vacuo*, yielding a poorly soluble material. A small amount of unreacted starting material was observed.
Purification by silica gel column chromatography (DCM:MeOH 2–15% gradient) afforded:

- N-$(Boc)_4$-3'-Allyl-Kanamycin (7) as an orange solid (210 mg, 0.23 mmol, 10%) (5% yield over two steps).

The low recovery was attributed to mixed fractions and poor solubility of the kanamycin derivative.

Second Batch – Indium-Mediated Allylation Leading to Compounds 7 and 8 A crude reaction mixture (total 1.9 g starting material) was subjected to another indium-mediated allylation. The estimated conversion of N-$(Boc)_4$-3'-Keto-Kanamycin (4) was difficult to determine due to poor retention time resolution.
The reaction was set up assuming the entire 1.9 g was keto-derivative (4). Excess reagents were used, but no side reactions were expected. UPLC–MS analysis showed:

- Almost full conversion to the desired keto-derivative (m/z = 780.70, loss of 1 Boc group).
- Formation of a minor by-product (N-$(Boc)_4$-3',4"-Diketo-Kanamycin) (m/z = 778.75, loss of 1 Boc group).

To a solution of N-$(Boc)_4$-3'-Keto-Kanamycin (containing some diketo by-product) (1.9 g, 2.2 mmol, 1 eq) in THF:H_2O (60 mL, 1:1 v/v), the following reagents were added:

- Indium powder (329 mg, 2.9 mmol, 1.3 eq)
- Allyl bromide (0.3 mL, 3.3 mmol, 1.5 eq)

The suspension changed color from dark orange to dark green. The reaction mixture was stirred at room temperature and monitored by TLC (DCM:MeOH 5%, ninhydrin stain) and UPLC–MS.
After three days, full conversion to a more apolar product was observed. The reaction was filtered through filter paper, and the filtrate was concentrated *in vacuo*.
Purification by silica gel column chromatography (DCM:MeOH 2–15% gradient) yielded:

- N-$(Boc)_4$-3'-Allyl-Kanamycin (7) as a grey solid (290 mg, 0.31 mmol, 28%).
- N-$(Boc)_4$-3',4"-Diallyl-Kanamycin (8) as a brown solid (112 mg, 0.12 mmol, 10%).

Structural Characterization. In the TOCSY–NMR spectrum of the diallylated product (8), a spin system correlation was observed between C5" and C6" protons, but not C4" protons, strongly suggesting the presence of the second allyl substituent at C4". The low recovery was attributed to mixed fractions and poor solubility of the kanamycin derivatives.

SPECTROSCOPIC DATA N-(BOC)$_4$-3'-ALLYL-KANAMYCIN (7)
^{1}H NMR (600 MHz, MeOD-d_4) δ 5.80 (ddt, J = 17.6, 10.0, 7.7 Hz, 1H), 5.20–5.05 (m, 4H), 4.02 (m, 1H), 3.90 (d, J = 10.1 Hz, 1H), 3.80 (dd, J = 11.7, 2.4 Hz, 1H), 3.72–3.63 (m, 3H), 3.56–3.47 (m, 5H), 3.43–3.37 (m, 3H), 3.34 (s, 1H), 3.26 (d, J = 10.1 Hz, 1H), 2.48 (d, J = 7.7 Hz, 2H), 2.10 (m, 1H), 1.45 (m, 37H).
^{13}C NMR (151 MHz, MeOD-d_4) δ 159.5, 158.0, 157.7, 134.7, 119.5, 103.2, 99.9, 85.6, 80.6, 80.4, 80.1, 76.8, 76.7, 74.5, 72.2, 69.9, 69.2, 69.0, 67.8, 62.4, 54.5, 50.8, 42.0, 40.4, 38.3, 28.9–28.8 (9 CH_3).
HRMS (ESI) m/z $[M+Na]^+$ calcd for $C_{41}H_{72}O_{19}N_4Na$: 947.4683, found: 947.4694.

SPECTROSCOPIC DATA N-(BOC)$_4$-3',4"-DIALLYL-KANAMYCIN (8)
^{1}H NMR (600 MHz, MeOD-d_4) δ 5.92–5.74 (m, 2H), 5.13 (m, 6H), 4.21 (dd, J = 7.0, 2.6 Hz, 1H), 3.90–3.84 (m, 2H), 3.83–3.74 (m, 2H), 3.74–3.62 (m, 3H), 3.60–3.46 (m, 5H), 3.38 (m, 1H), 3.27 (d, J = 10.1 Hz, 1H), 2.57–2.42 (m, 3H), 2.23–2.13 (m, 2H), 2.10–2.04 (m, 1H), 1.51–1.39 (m, 37H).
^{13}C NMR (151 MHz, MeOD-d_4) δ 159.4, 158.6, 157.9, 157.7, 134.5, 133.6, 119.6, 119.1, 102.9, 99.9, 85.3, 82.6, 76.7, 76.6, 76.4, 73.4, 73.3, 70.1, 68.9, 67.6, 62.2, 61.7, 55.9, 54.7, 50.7, 41.9, 40.8, 38.3, 29.5–28.7 (12 CH_3).
HRMS (ESI) m/z $[M+Na]^+$ calcd for $C_{44}H_{76}O_{19}N_4Na$: 987.4996, found: 987.5007.

SYNTHESIS OF N-(BOC)$_4$-3'-PROPARGYL-KANAMYCIN (9)

A crude reaction mixture (total weight 147 mg) was subjected to indium-mediated propargylation to obtain N-(Boc)$_4$-3'-Propargyl-Kanamycin (9). The conversion to N-(Boc)$_4$-3'-Keto-Kanamycin (4) was difficult to determine due to poor retention time resolution and improper peak separation in UPLC–MS analysis:

- Retention time = 0.98 min → corresponding to N-(Boc)$_4$-Kanamycin (2) and N-(Boc)$_4$-3'-Keto-Kanamycin (4).
- Retention time = 1.93 min → corresponding to N-(Boc)$_4$-3'-Keto-Kanamycin (4) and its double-oxidized by-product.

Given the complexity of determining the exact ratio, the indium-mediated propargylation was conducted assuming all 147 mg was N-(Boc)$_4$-3'-Keto-Kanamycin (4). Since no reaction with other functional groups was expected, an excess of reagents was safely used. Therefore, the final yield may be higher than reported, as it was calculated based on an overestimated amount of starting material.

Procedure A solution of N-(Boc)$_4$-3'-Keto-Kanamycin (147 mg, 0.2 mmol, 1 eq) in THF:H_2O (4 mL, 1:1 v/v) was prepared. Indium powder (28.7 mg, 0.3 mmol, 1.5 eq) and propargyl bromide (24 μL, 0.3 mmol, 1.5 eq) were added. The reaction mixture was stirred at room temperature and monitored by TLC (DCM:MeOH 5%, ninhydrin stain) and UPLC–MS.
After two days, full conversion to a more apolar product was observed. The reaction was filtered through filter paper to remove indium salts and concentrated *in vacuo*. Purification by

flash column chromatography (DCM:MeOH, 0–10% gradient) yielded N-$(Boc)_4$-3'-Propargyl-Kanamycin (9) as a light grey solid (16 mg, 0.017 mmol, 10%).

SPECTROSCOPIC DATA

^{1}**H NMR** (600 MHz, MeOD-d_4) δ 5.20–5.03 (m, 2H), 4.01 (ddd, J = 9.7, 5.1, 2.3 Hz, 1H), 3.92–3.88 (m, 1H), 3.88–3.75 (m, 2H), 3.73–3.63 (m, 4H), 3.58–3.46 (m, 5H), 3.46–3.32 (m, 4H), 2.61 (t, J = 3.1 Hz, 1H), 2.37–2.30 (m, 1H), 2.10 (s, 1H), 1.48–1.42 (m, 37H).
^{13}**C NMR** (151 MHz, MeOD-d_4) δ 144.4, 137.7, 127.5, 124.5, 122.6, 97.1, 89.5, 80.5, 76.7, 75.4, 72.1, 65.7, 62.4, 59.8, 58.3, 55.6, 42.8, 33.4, 30.8, 29.0, 28.9, 28.8, 24.2, 20.9, 18.8, 18.4, 15.0, 14.5.

SYNTHESIS OF N-$(BOC)_4$-3'-PROPYL-KANAMYCIN (10)

A three-neck flask was purged with three vacuum/nitrogen cycles before adding Pd/C (130 mg, 0.1 mmol, 0.3 eq) and $Pd(OH)_2$ (86 mg, 0.1 mmol, 0.3 eq) under an inert atmosphere. A small amount of ethyl acetate was added, followed by the careful addition of methanol (2 mL) via syringe.
N-$(Boc)_4$-3'-Propyl-Kanamycin (377 mg, 0.4 mmol, 1 eq) was dissolved in methanol (4 mL) and added to the reaction flask. The mixture was stirred and degassed by evacuation until the solvent started to boil, then backfilled with nitrogen (3 cycles).
A balloon of hydrogen was attached, and the flask was evacuated and backfilled with hydrogen (3 cycles). After overnight stirring, no conversion was observed. The reaction mixture was filtered over Celite, and the reaction was restarted and left to stir overnight.
Upon completion (confirmed by UPLC–MS), the hydrogen balloon was closed and detached, and the flask was backfilled with nitrogen. The reaction mixture was filtered through Celite and washed with water. The water layer was freeze-dried overnight, and column chromatography (DCM:MeOH, 0–11% gradient) yielded N-$(Boc)_4$-3'-Propyl-Kanamycin (10) as a dark orange solid film (22 mg, 0.024 mmol, 6%).

SPECTROSCOPIC DATA

^{1}**H NMR** (600 MHz, MeOD-d_4) δ 5.14 (s, 1H), 5.06 (d, J = 3.7 Hz, 1H), 4.55 (s, 1H), 4.02 (ddd, J = 10.0, 5.0, 2.5 Hz, 1H), 3.93–3.86 (m, 1H), 3.80 (dd, J = 11.7, 2.5 Hz, 1H), 3.72–3.63 (m, 3H), 3.58–3.46 (m, 5H), 3.45–3.33 (m, 4H), 2.14–2.07 (m, 1H), 1.45 (m, 37H), 1.29 (d, J = 4.2 Hz, 2H), 0.94 (t, 3H), 0.92–0.84 (m, 2H).
^{13}**C NMR** (151 MHz, MeOD-d_4) δ 157.7 (4 C), 126.2 (4 C), 105.7, 101.6, 101.4, 86.4, 80.6, 80.4, 76.8, 76.7, 74.5, 72.2, 69.5, 69.0, 62.4, 48.6, 42.2, 36.5, 28.9–28.8 (12 CH_3), 18.4, 15.0, 13.3.
HRMS (ESI) m/z $[M+Na]^+$ calcd for $C_{41}H_{74}O_{19}N_4Na$: 949.48395, found: 949.48394.

4.9. DEPROTECTION TO GIVE SBI209, SBI214, SBI233, SBI238

SYNTHESIS OF 3'-ALLYL-KANAMYCIN × 4 TFA (SBI209)

A suspension of N-$(Boc)_4$-3'-Allyl-Kanamycin (100.2 mg, 0.1 mmol, 1 eq) in DCM (1.3 mL) was prepared. Triisopropylsilane (89 μL, 0.4 mmol, 4 eq) and trifluoroacetic acid (0.7 mL,

8.7 mmol, 80.7 eq) were added via syringe. The reaction mixture turned clear and was stirred at room temperature for 1 hour. Upon completion (confirmed by UPLC–MS), toluene (2 mL) was added, and the mixture was concentrated *in vacuo*, yielding 3'-Allyl-Kanamycin × 4 TFA (SBI209) as a grey solid (100 mg, 66%). qNMR-determined purity was 66% (qNMR experiment with internal standard).

SPECTROSCOPIC DATA

^{1}H NMR (600 MHz, D_2O) δ 5.82 (ddt, J = 17.5, 10.2, 7.6 Hz, 1H), 5.45 (d, J = 4.4 Hz, 1H), 5.27–5.19 (m, 2H), 5.11 (d, J = 3.6 Hz, 1H), 4.11 (ddd, J = 10.7, 8.0, 3.2 Hz, 1H), 3.97–3.92 (m, 2H), 3.88–3.82 (m, 2H), 3.79 (d, J = 4.9 Hz, 3H), 3.60 (dt, J = 9.9, 2.6 Hz, 1H), 2.59–2.46 (m, 2H), 1.91 (q, J = 12.5 Hz, 1H).

SYNTHESIS OF 3',4"-DIALLYL-KANAMYCIN × 4 TFA (SBI214)

A suspension of 3',4"-Diallyl-$(Boc)_4$-Kanamycin (112.5 mg, 0.1 mmol, 1 eq) in DCM (1.4 mL) was prepared. Triisopropylsilane (96 μL, 0.5 mmol, 4 eq) and trifluoroacetic acid (0.7 mL, 9.4 mmol, 80.7 eq) were added via syringe. The reaction mixture turned clear and was stirred at room temperature for 1 hour. Upon completion (confirmed by UPLC–MS), toluene (2 mL) was added, and the mixture was concentrated *in vacuo*, yielding 3',4"-Diallyl-Kanamycin × 4 TFA (SBI214) as a white solid (70 mg, 30%). qNMR-determined purity was 48% (qNMR experiment with internal standard).

SPECTROSCOPIC DATA

^{1}H NMR (600 MHz, MeOD-d_4) δ 5.85 (ddt, J = 17.7, 10.2, 7.5 Hz, 2H), 5.53 (d, J = 4.3 Hz, 1H), 5.34–5.11 (m, 4H), 4.13–4.04 (m, 2H), 3.99–3.86 (m, 3H), 3.73 (ddd, J = 10.2, 8.3, 4.2 Hz, 1H), 3.65–3.51 (m, 4H), 3.39 (dd, J = 13.0, 2.9 Hz, 1H), 3.00 (dd, J = 13.1, 9.2 Hz, 1H), 2.50 (m, 4H), 2.06 (q, J = 12.4 Hz, 1H).
^{13}C NMR (151 MHz, MeOD-d_4) δ 134.1, 132.2, 121.0, 120.0, 101.4, 96.4, 86.0, 77.8, 76.9, 76.6, 74.1, 73.2, 69.4, 68.6, 68.2, 67.2, 60.7, 54.7, 51.0, 49.8, 42.5, 39.6, 38.9, 28.7.
HRMS (ESI) m/z $[M+H]^+$ calcd for $C_{24}H_{45}O_{11}N_4$: 565.3085, found: 565.3079.

SYNTHESIS OF 3'-PROPARGYL-KANAMYCIN × 4 TFA (SBI233)

A suspension of 3'-Propargyl-$(Boc)_4$-Kanamycin (15 mg, 0.02 mmol, 1 eq) in DCM (0.2 mL) was prepared. Triisopropylsilane (13 μL, 0.07 mmol, 4 eq) and trifluoroacetic acid (0.1 mL, 1.3 mmol, 0.7 eq) were added via syringe. The reaction mixture turned clear and was stirred at room temperature for 1 hour. Upon completion (confirmed by UPLC–MS), toluene (0.5 mL) was added, and the mixture was concentrated *in vacuo*, yielding 3'-Propargyl-Kanamycin × 4 TFA (SBI233) as a light orange solid (9 mg, 37%). qNMR-determined purity was 63% (qNMR experiment with external standard calibration).

SPECTROSCOPIC DATA

^{1}H NMR (600 MHz, MeOD-d_4) δ 5.54 (d, J = 4.4 Hz, 1H), 5.10 (d, J = 3.7 Hz, 1H), 4.15 (td, J = 9.7, 2.8 Hz, 1H), 3.98 (d, J = 4.4 Hz, 1H), 3.90 (m, 5H), 3.81 (dd, J = 10.7, 3.7 Hz, 1H), 3.74 (dd, J = 10.4, 8.2 Hz, 1H), 3.68–3.63 (m, 2H), 3.57–3.53 (m, 2H), 3.49 (t, J = 9.8 Hz, 1H), 3.44–3.35

(m, 3H), 3.04–2.98 (m, 1H), 2.66 (d, J = 2.7 Hz, 1H), 2.50 (dt, J = 12.2, 4.2 Hz, 1H), 2.44 (t, J = 2.6 Hz, 1H), 2.04 (q, J = 12.5 Hz, 1H).
^{13}**C NMR** (151 MHz, MeOD-d_4) δ 101.8, 96.1, 85.9, 80.7, 78.8, 76.3, 75.3, 73.9, 72.5, 70.1, 69.2, 68.3, 67.7, 67.2, 62.1, 56.8, 51.3, 49.6, 42.5, 28.7, 24.6.

SYNTHESIS OF 3'-PROPYL-KANAMYCIN × 4 TFA (SBI238)

A suspension of (Boc)$_4$-3'-Propyl-Kanamycin (22 mg, 0.02 mmol, 1 eq) in DCM (0.3 mL) was prepared. Triisopropylsilane (19 μL, 0.1 mmol, 4 eq) and trifluoroacetic acid (0.2 mL, 1.9 mmol, 80.7 eq) were added via syringe. The reaction mixture turned clear and was stirred at room temperature for 1 hour. Upon completion (confirmed by UPLC–MS), toluene (1 mL) was added, and the mixture was concentrated *in vacuo*, yielding 3'-Propyl-Kanamycin × 4 TFA (SBI238) as a yellow solid (17 mg, 36%). qNMR-determined purity was 47% (qNMR experiment with external standard calibration).

SPECTROSCOPIC DATA

^{1}**H NMR** (600 MHz, MeOD-d_4) δ 5.51 (d, J = 4.3 Hz, 1H), 5.08 (d, J = 3.7 Hz, 1H), 4.09 (td, J = 9.5, 2.9 Hz, 1H), 3.90 (d, J = 2.3 Hz, 1H), 3.89–3.87 (m, 1H), 3.85 (dd, J = 7.8, 4.7 Hz, 2H), 3.80 (dd, J = 10.7, 3.6 Hz, 1H), 3.71 (t, J = 9.4 Hz, 1H), 3.67–3.63 (m, 2H), 3.50 (t, J = 9.8 Hz, 3H), 2.48 (dt, J = 12.3, 4.2 Hz, 1H), 1.80–1.66 (m, 5H). free

REFERENCES

[1] B. Becker and M. A. Cooper, *Aminoglycoside antibiotics in the 21st century,* ACS chemical biology **8**, 105 (2013).

[2] A. Schatz, E. Bugle, and S. A. Waksman, *Streptomycin, a substance exhibiting antibiotic activity against gram-positive and gram-negative bacteria.* Proceedings of the Society for Experimental Biology and Medicine **55**, 66 (1944).

[3] A. T. Pezzella, *History of pulmonary tuberculosis,* Thoracic surgery clinics **29**, 1 (2019).

[4] M. Avent, B. Rogers, A. Cheng, and D. Paterson, *Current use of aminoglycosides: indications, pharmacokinetics and monitoring for toxicity,* Internal medicine journal **41**, 441 (2011).

[5] J. Jackson, C. Chen, and K. Buising, *Aminoglycosides: how should we use them in the 21st century?* Current opinion in infectious diseases **26**, 516 (2013).

[6] A. Tevyashova and K. Shapovalova, *Potential for the development of a new generation of aminoglycoside antibiotics,* Pharmaceutical Chemistry Journal **55**, 860 (2021).

[7] C. M. Webster and M. Shepherd, *A mini-review: environmental and metabolic factors affecting aminoglycoside efficacy,* World Journal of Microbiology and Biotechnology **39**, 7 (2023).

[8] S. Jana and J. Deb, *Molecular understanding of aminoglycoside action and resistance,* Applied microbiology and biotechnology **70**, 140 (2006).

[9] R. S. EDSON and C. L. TERRELL, *The aminoglycosides: streptomycin, kanamycin, gentamicin, tobramycin, amikacin, netilmicin, and sisomicin,* in *Mayo Clinic Proceedings*, Vol. 62 (Elsevier, 1987) pp. 916–920.

[10] M. J. Weinstein, G. M. Luedemann, E. M. Oden, G. H. Wagman, J. P. Rosselet, J. A. Marquez, C. T. Coniglio, W. Charney, H. L. Herzog, and J. Black, *Gentamicin, 1 a new antibiotic complex from micromonospora,* Journal of medicinal chemistry **6**, 463 (1963).

[11] G. H. Miller, G. Arcieri, M. J. Weinstein, and J. A. Waitz, *Biological activity of netilmicin, a broad-spectrum semisynthetic aminoglycoside antibiotic,* Antimicrobial Agents and Chemotherapy **10**, 827 (1976).

[12] K. M. Krause, A. W. Serio, T. R. Kane, and L. E. Connolly, *Aminoglycosides: an overview,* Cold Spring Harbor perspectives in medicine **6**, a027029 (2016).

[13] Y. Zhang, N. Zhang, M. Wang, M. Luo, Y. Peng, Z. Li, J. Xu, M. Ou, B. Kan, X. Li, *et al.*, *The prevalence and distribution of aminoglycoside resistance genes,* Biosafety and Health **5**, 14 (2023).

[14] J. A. Karlowsky, D. C. Draghi, M. E. Jones, C. Thornsberry, I. R. Friedland, and D. F. Sahm, *Surveillance for antimicrobial susceptibility among clinical isolates of pseudomonas aeruginosa and acinetobacter baumannii from hospitalized patients in the united states, 1998 to 2001,* Antimicrobial agents and chemotherapy **47**, 1681 (2003).

[15] C.-J. Yao, Y.-L. Li, M.-J. Pu, L.-H. Luo, Q. Xiong, F.-J. Xie, T.-L. Li, and P.-M. Feng, *Aminoglycosides with anti-mrsa activity: a concise review,* Current Topics in Medicinal Chemistry **21**, 2483 (2021).

[16] M. E. O'Sullivan, F. Poitevin, R. G. Sierra, C. Gati, E. H. Dao, Y. Rao, F. Aksit, H. Ciftci, N. Corsepius, R. Greenhouse, *et al.*, *Aminoglycoside ribosome interactions reveal novel conformational states at ambient temperature,* Nucleic acids research **46**, 9793 (2018).

[17] B. D. Davis, *Mechanism of bactericidal action of aminoglycosides,* Microbiological reviews **51**, 341 (1987).

[18] M. A. Borovinskaya, R. D. Pai, W. Zhang, B. S. Schuwirth, J. M. Holton, G. Hirokawa, H. Kaji, A. Kaji, and J. H. D. Cate, *Structural basis for aminoglycoside inhibition of bacterial ribosome recycling,* Nature structural & molecular biology **14**, 727 (2007).

[19] L. Zhang, J. He, L. Bai, S. Ruan, T. Yang, and Y. Luo, *Ribosome-targeting antibacterial agents: Advances, challenges, and opportunities,* Medicinal Research Reviews **41**, 1855 (2021).

[20] I. Prokhorova, R. B. Altman, M. Djumagulov, J. P. Shrestha, A. Urzhumtsev, A. Ferguson, C.-W. T. Chang, M. Yusupov, S. C. Blanchard, and G. Yusupova, *Aminoglycoside interactions and impacts on the eukaryotic ribosome,* Proceedings of the National Academy of Sciences **114**, E10899 (2017).

[21] D. C. Eustice and J. M. Wilhelm, *Mechanisms of action of aminoglycoside antibiotics in eucaryotic protein synthesis,* Antimicrobial agents and chemotherapy **26**, 53 (1984).

[22] B. A. Pontefract, H. T. Ho, A. Crain, M. K. Kharel, and S. E. Nybo, *Drugs for gram-negative bugs from 2010–2019: a decade in review,* in *Open forum infectious diseases*, Vol. 7 (Oxford University Press US, 2020) p. ofaa276.

[23] N. Wang, J. Luo, F. Deng, Y. Huang, and H. Zhou, *Antibiotic combination therapy: A strategy to overcome bacterial resistance to aminoglycoside antibiotics,* Frontiers in Pharmacology **13**, 839808 (2022).

[24] Y. Hu, A. Liu, J. Vaudrey, B. Vaiciunaite, C. Moigboi, S. M. McTavish, A. Kearns, and A. Coates, *Combinations of β-lactam or aminoglycoside antibiotics with plectasin are synergistic against methicillin-sensitive and methicillin-resistant staphylococcus aureus,* PLoS One **10**, e0117664 (2015).

[25] K. S. Kaye, D. Marchaim, V. Thamlikitkul, Y. Carmeli, C.-H. Chiu, G. Daikos, S. Dhar, E. Durante-Mangoni, A. Gikas, A. Kotanidou, *et al.*, *Colistin monotherapy versus combination therapy for carbapenem-resistant organisms,* NEJM evidence **2**, EVIDoa2200131 (2022).

[26] P. I. Rafailidis and M. E. Falagas, *Options for treating carbapenem-resistant enterobacteriaceae,* Current opinion in infectious diseases **27**, 479 (2014).

[27] M. Hamel, J.-M. Rolain, and S. A. Baron, *The history of colistin resistance mechanisms in bacteria: progress and challenges,* Microorganisms **9**, 442 (2021).

[28] N. H. Hussein, I. M. Al-Kadmy, B. M. Taha, and J. D. Hussein, *Mobilized colistin resistance (mcr) genes from 1 to 10: a comprehensive review,* Molecular biology reports **48**, 2897 (2021).

[29] S. Ghosh, C. Bornman, and M. M. Zafer, *Antimicrobial resistance threats in the emerging covid-19 pandemic: Where do we stand?* Journal of infection and public health **14**, 555 (2021).

[30] T. A. Le, T. Hiba, D. Chaudhari, A. N. Preston, Z. R. Palowsky, S. Ahmadzadeh, S. Shekoohi, E. M. Cornett, and A. D. Kaye, *Aminoglycoside-related nephrotoxicity and ototoxicity in clinical practice: a review of pathophysiological mechanism and treatment options,* Advances in therapy **40**, 1357 (2023).

[31] G. D. Wright, *Aminoglycoside-modifying enzymes,* Current opinion in microbiology **2**, 499 (1999).

[32] M. S. Ramirez and M. E. Tolmasky, *Aminoglycoside modifying enzymes,* Drug resistance updates **13**, 151 (2010).

[33] D. M. Daigle, G. A. McKay, P. R. Thompson, and G. D. Wright, *Aminoglycoside antibiotic phosphotransferases are also serine protein kinases,* Chemistry & biology **6**, 11 (1999).

[34] D. Nurizzo, S. C. Shewry, M. H. Perlin, S. A. Brown, J. N. Dholakia, R. L. Fuchs, T. Deva, E. N. Baker, and C. A. Smith, *The crystal structure of aminoglycoside-3'-phosphotransferase-iia, an enzyme responsible for antibiotic resistance,* Journal of molecular biology **327**, 491 (2003).

[35] A. A. Bastian, M. Bastian, M. Jäger, M. Loznik, E. M. Warszawik, X. Yang, N. Tahiri, P. Fodran, M. D. Witte, A. Thoma, *et al.*, *Late-stage modification of aminoglycoside antibiotics overcomes bacterial resistance mediated by aph (3') kinases,* Chemistry–A European Journal **28**, e202200883 (2022).

[36] M. Jäger and A. J. Minnaard, *Regioselective modification of unprotected glycosides,* Chemical Communications **52**, 656 (2016).

[37] N. N. Eisink, J. Lohse, M. D. Witte, and A. J. Minnaard, *Regioselective oxidation of unprotected 1, 4 linked glucans,* Organic & Biomolecular Chemistry **14**, 4859 (2016).

[38] J. Haddad, S. Vakulenko, and S. Mobashery, *An antibiotic cloaked by its own resistance enzyme,* Journal of the American Chemical Society **121**, 11922 (1999).

[39] V. Pokrovskaya, V. Belakhov, M. Hainrichson, S. Yaron, and T. Baasov, *Design, synthesis, and evaluation of novel fluoroquinolone- aminoglycoside hybrid antibiotics,* Journal of medicinal chemistry **52**, 2243 (2009).

[40] K.-S. Fung, A. A. Joseph, A. Khononov, T. Pieńko, V. Belakhov, and T. Baasov, *Towards catalytic aminoglycoside: Probing the modification of kanamycin b at the 3'-and 4'-positions,* Tetrahedron **136**, 133342 (2023).

[41] L. D. Saravolatz and G. E. Stein, *Plazomicin: a new aminoglycoside,* Clinical Infectious Diseases **70**, 704 (2020).

[42] C. Kim, J. Y. Cha, H. Yan, S. B. Vakulenko, and S. Mobashery, *Hydrolysis of atp by aminoglycoside 3'-phosphotransferases: an unexpected cost to bacteria for harboring an antibiotic resistance enzyme,* Journal of Biological Chemistry **281**, 6964 (2006).

[43] E. Krissinel and K. Henrick, *Protein interfaces, surfaces and assemblies service PISA at European Bioinformatics Institute,* J Mol Biol **372**, 774 (2007).

5

IN-SILICO FRAGMENT-BASED APPROACHES TO IDENTIFY POTENTIAL METHYLTRANSFERASE INHIBITORS

Nicola PONTILLO, Albert GUSKOV, Andreas HERRMANN

"The greatest challenge to any thinker is stating the problem in a way that allows a solution."

— Bertrand Russell

ABSTRACT

The widespread distribution of 16S rRNA methyltransferase genes contributes to the escalating global crisis of antimicrobial resistance. It hampers the efficacy of antibiotic therapies, limits treatment options, and poses a significant threat to public health. Efforts to combat antimicrobial resistance must consider the complex interplay between these resistance determinants and devise new strategies to address their dissemination. There is a growing consensus among the scientific community to explore novel strategies and targets to overcome resistance mechanisms that hinder the effectiveness of many aminoglycoside antibiotics. In this study, we explore an in-silico approach to generate and identify potential inhibitors of ArmA, a 16S methyltransferase enzyme responsible for pan-aminoglycoside resistance. To accomplish this, we designed a library of fragments derived from natural products with substructures represented in marketed drugs. We performed in-silico docking screening and fragment evolution against ArmA, and generated two chemotypes with predicted inhibitory effect on ArmA. Notably, these compounds can be synthesized using an affordable 2-step process. Experimental evaluation of our compounds to test their potential to inhibit ArmA was not possible due to unforeseen delays in the research project, and remains on our to-do list. However, by exploring this approach, we aim to contribute to the development of effective strategies to combat antimicrobial resistance and safeguard the efficacy of aminoglycoside antibiotics in clinical practice.

5.1. INTRODUCTION

rRNA METHYL-TRANSFERASES

Post-transcriptional methylation of the ribosome has emerged as a novel mechanism of resistance to aminoglycosides (AG) antibiotics, posing challenges to the surveillance of antibiotic resistance and the study of the related resistance mechanisms in pathogenic bacteria [1].
Recent trends, particularly in the context of the COVID-19 pandemic, have shown an increasing incidence of AG-resistant bacteria causing nosocomial infections [2, 3]. Co-infections caused by *Staphylococcus* spp., *Escherichia coli*, *Acinetobacter* spp., *Pseudomonas* spp., and *Klebsiella pneumoniae*, often carrying virulence plasmids with resistant determinants, can contribute to high mortality rates even when broad-spectrum antibiotics like AGs are administered [4, 5].
AGs, often used in combination with β-lactams, have been crucial in the treatment of various serious infections in humans and animals [6, 7]. Their antimicrobial activity stems from binding to the conserved A site of the 16S rRNA within prokaryotic 30S ribosomal subunits, thereby disrupting protein translation [8]. However, with the use of AGs we have witnessed the emergence of multiple resistance mechanisms, which ensure bacterial survival by drug deactivation, reduction of intracellular drug concentration, or target modification.
Enzymatic modification through drug deactivation is the most prevalent mechanism observed in clinical isolates. Three classes of enzymes catalyze *N*-acetylation, *O*-nucleotidylation, and *O*-phosphorylation of AGs, thereby reducing their affinity for the ribosome [9, 10].
Reduction of intracellular concentration involves nonspecific or species-specific mechanisms such as changes in membrane permeability, decreased inner membrane transport, active efflux, or drug trapping [11–13].
Target mutation, particularly observed in actinomycetes intrinsically resistant to AGs, involves methylation of the 30S ribosomal subunit as a self-protective measure. Plasmid-mediated methylases targeting the 16S rRNA have emerged as a new mechanism of resistance in clinically relevant pathogens, primarily in *Enterobacteriaceae* and non-fermentative Gram-negative bacilli [14, 15]. The main methyltransferase genes, their target residues, and associated resistance profiles are summarized in Table 5.1.
ArmA, the first of this enzyme class, was originally identified in France and quickly spread across different geographical areas including Europe, the USA, Mexico, and several Asian countries. Subsequent reports revealed additional transferase genes, mostly responsible for nosocomial infections [16, 17]. The geographical distribution of pathogenic isolates carrying these genes is shown in Table 5.2.
The origin of these genes remains a topic of debate. The methylase enzyme ArmA naturally occurs in AG producers that have developed high-level self-resistance through methylation of the AG binding site. Its biochemical characteristics suggest it belongs to the Agr family of methyltransferases, which includes the m7G-methyltransferases, anti-suicide genes from actinomycete species [16, 18]. However, known actinomycete methylase genes exhibit low sequence identity (37–40%) compared to ArmA, which, combined with the low (<30%) GC content between these genes, suggests either non-recent transfer events or an unknown microbial origin [17].

ArmA catalyzes the covalent addition of a methyl group from *S*-adenosyl-*L*-methionine (AdoMet or SAM) to G1405 of the bacterial A-site. It confers high-level resistance to clinically important AGs used in systemic therapy, with the exception of streptomycin (STR) [19–22]. The *armA* gene is frequently found within multi-resistance loci that are commonly linked to extended-spectrum β-lactamasess (ESBLs). As with other methylases, the gene is typically located on transferable plasmids and transposons, facilitating the spread of genetic elements associated with multidrug resistance. The transferability of plasmids and transposons carrying *armA* across different bacterial strains, species, and even ecological niches significantly contributes to the widespread dissemination of antimicrobial resistance [19, 23].
Moreover, the coexistence of ArmA with other resistance determinants, particularly ESBLs, enhances the overall resistance profile of pathogens. As a result, the effectiveness of antibiotic treatments becomes increasingly compromised, potentially limiting therapeutic options [24]. Inhibiting the activity of ArmA methylase could restore the efficacy of many commercially available AG antibiotics and revive this class of drugs heavily impacted by antimicrobial resistance.
To this end, the structural characterization of ArmA, RmtB, and NpmA methylases has provided a foundation for the development of potential resistance inhibitors [25, 26].
In this study, we describe the design of a library of compounds tailored for *in-silico* fragment-based drug design (FBDD) with the explicit aim of targeting ArmA and identifying potential inhibitors of its activity. Our approach involves leveraging docking, neural network scoring functions, and open-source fragment-evolution software to craft potential inhibitors. The most promising lead compounds are accessible through a two-step synthesis using commercially available building blocks and will be synthesized and tested for their inhibitory power in the near future. We believe they can serve as valuable templates deserving experimental validation in further studies.

Table 5.1 | Methylation sites targeted by 16S rRNA methyltransferases and associated resistance profiles.

Genotype	Residue modified	Known subtypes	Resistance profile
armA	N7 of G1405	—	Amk, Apr, Gen, Tob, Kan, Sis
rmtA		—	Abk, Amk, Gen, Tob, Kan
rmtB		B1, B2, B4	Amk, Gen, Tob, Kan
rmtC		—	Abk, Amk, Gen, Tob
rmtD		D1, D2, D3	Abk, Amk, Gen, Tob, Kan
rmtE		E1, E2, E3	Amk, Gen, Tob, Kan
rmtF		F1, F2	Amk, Gen, Tob
rmtG		—	Amk, Abk, Gen, Tob
rmtH		—	Amk, Abk, Gen, Tob
npmA	N1 of A1408	A1, A2	Apr, Neo, Tob, Kan
npmB		B1, B2	Amk, Apr, Gen, Neo, Tob

Abbreviations: Abk, Arbekacin; Amk, Amikacin; Apr, Apramycin; Gen, Gentamicin; Kan, Kanamycin; Neo, Neomycin; Tob, Tobramycin; Sis, Sisomycin.

Table 5.2 | Geographical distribution of pathogenic isolates with confirmed 16S rRNA methyltransferase genes.

Resistance gene	Organisms	Geographical distribution	Source
ArmA	*A. baumannii, E. coli, E. cloacae, E. aerogenes, E. xiangfangensis, C. amalonaticus, C. freundii, S. enterica, K. pneumoniae, S. marcescens, K. oxytoca*	PL, US, FR, BE, IT, IR, JP, BR, IN, GR, IN, CN, UK, MM, TR	[15, 27–30]
RmtA	*P. aeruginosa, K. pneumoniae, E. coli, E. cloacae*	IR, JP, KR, CN, CH, IN	[19, 31]
RmtB	*E. cloacae, K. pneumoniae, E. coli, P. mirabilis, S. marcescens, S. enterica, K. terrigena, K. aerogenes, A. baumannii, K. variicola, P. rettgeri, P. aeruginosa*	MX, US, BR, BE, JP, CH, KR, IN, FR, UK, GR, CN, IR, US, MM, EG	[31]
RmtC	*P. mirabilis, K. pneumoniae, E. coli*	JP, AT, SA, UK, CH, UK, CN, ZA, IN, UA, BR, MM	[31]
RmtD	*C. freundii, K. pneumoniae, E. cloacae, E. aerogenes, P. aeruginosa*	CL, MX, AR, BR, US, TR, IN, AR, MM, PO, UK	[31]
RmtE	*E. coli, A. baumannii, P. aeruginosa, E. xiangfangensis*	US, CN, IN, MM, UK	[31]
RmtF	*K. pneumoniae, E. coli, P. aeruginosa, C. freundii, E. cloacae, C. koseri, P. mirabilis*	FR, IN, NP, UK, US, EG, CH, IE, ZA, MM	[31]
RmtG	*K. pneumoniae, P. aeruginosa, E. coli, K. aerogenes, E. hormaechei*	BR, US, CL, IN, CH	[31]
RmtH	*K. pneumoniae, E. coli*	IQ, IN, LB	[31]
NpmA	*E. coli, P. aeruginosa, E. coli, C. difficile*	JP, CN, US	[31]
NpmB	*E. coli*	UK	[32]

5.2. COMPUTER-BASED METHODS IN DRUG DISCOVERY

The last decades have seen an increasingly important contribution from computer-based *in-silico* design techniques [33], and they have been intensely employed in the discovery of therapeutic compounds such as anti-Human Immunodeficiency Virus (HIV) compounds and influenza A neuraminidase inhibitors, among others [34–38].

Typically, *in-silico* approaches are divided into two categories: structure-based and ligand-based design [39]. The structure-based approach aims to identify and optimize potential ligands for a known 3D structure of a drug target. The classical approach involves virtual screening (VS), such as docking of a library of compounds, estimating the target–ligand

interactions, and evaluating the structural requirements to optimize binding [40, 41].
To keep pace with increasingly large libraries of compounds, docking has been adapted to include machine-learning (ML) emulation of docking scores, which proved successful in ultra-large screenings [42], yielding novel ligands targeting relevant proteins such as Keap1, SARS-CoV-2 M_{pro} and Nsp3 Mac1, CB1/CB2, and PKA [43–48].
The combined strengths of docking and ML significantly reduced the computational demands of large screening by introducing fragment-based representations of docking libraries or by using ML approaches to emulate docking scores (see Figure 5.1).
Conversely, ligand-based approaches try to estimate the structure-activity relationship (SAR) in the absence of structural data. Ligands known to bind the target are analyzed to understand the structural and physico-chemical properties that correlate with a desired pharmacological activity. Although ligand-based drug design has proven to be an effective method, its main limiting factors are that the selection of the pharmacophoric features is often user-dependent, and that extensive molecular dynamics (MD) simulations are required to sample the conformational space of the chemical groups that might impact the biological activity [49–51].

FRAGMENT-BASED DRUG DESIGN

FBDD aims at identifying potential fragments that bind the target site and feeds this information into the design of novel inhibitors. FBDD represents a change in the paradigm of drug discovery and has proven to be a more successful approach to identify lead-like and drug-like compounds compared to virtual screening of high molecular weight compounds [52, 53]. The evolution of a fragment into a higher molecular weight compound is a more attractive and efficient approach than pruning a high molecular weight compound, which is typically the outcome of conventional high-throughput screening (HTS) of drug-like compound libraries. The higher efficiency of FBDD is achievable due to the greater chemical diversity explored by this approach compared to HTS [54]. Moreover, the dynamic nature of the ligand-receptor interactions favors binding events involving compounds with lower complexity, where there is less chance of steric hindrance [55, 56].
The FBDD technique relies on three main strategies (see Figure 5.2):

Fragment linking This technique aims to covalently join two fragments that bind to adjacent regions of the target site to yield a single, more potent compound. However, it is generally considered the least successful strategy due to the significant influence of the linker's nature on the binding process. In cases where this strategy has been consistently effective, researchers typically begin with a fragment whose binding has been validated through orthogonal methods. This initial fragment serves as a specific "warhead" targeting the desired site. Subsequently, a screening process is initiated to identify a second fragment that binds in proximity to the first one [57].

Fragment merging or cross-over Fragments which share the same substructure and/or binding space are found to bind to the same region and are joined or merged into a bigger fragment to improve the interactions with the required target [58].

Fragment growing A central fragment is increased in size to enhance the binding affinity

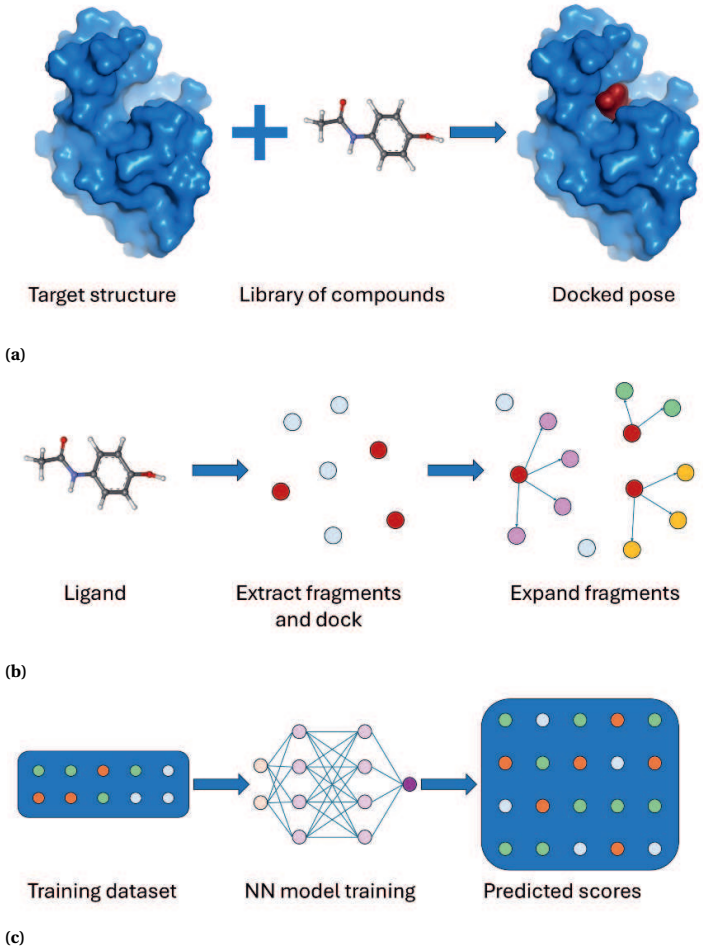


Figure 5.1 | Structure-based methods used in virtual screening. (a) brute force: all molecules of a library are subjected to docking. (b) fragment-based: a library I s decomposed into synthons or building blocks (fragments) and docked onto a target. The top scoring compounds are then used to expand the library or merged into bigger compounds. (c) In machine learning, neural networks (NNs) are trained on a subset of docked compounds and used as a model to predict docking scores of the remainder of the library. In this study, we did not train neural networks; we used existing platforms with pre-trained models.

and specificity to the target. By growing the central fragment and strategically introducing new functional groups, the binding affinity and specificity to the target can be optimized.

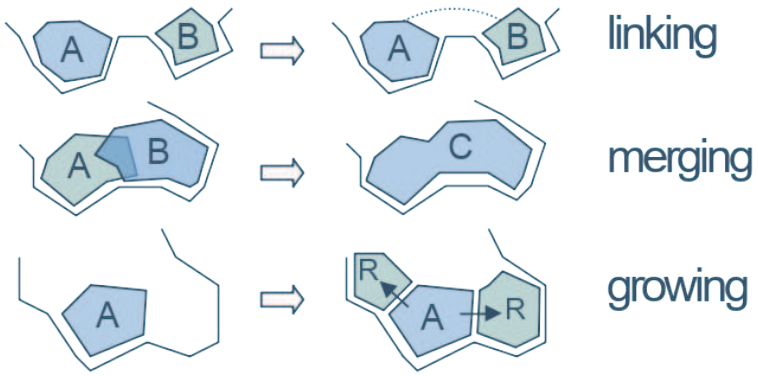


Figure 5.2 | The three primary strategies to drive the evolution of a small fragment are: linking, merging, and growing. In fragment linking, fragments that bind to adjacent regions of the target site are connected through a linker to create a more potent compound. Fragment merging or cross-over involves the fusion of fragments that bind to overlapping spaces within the target site. In fragment growing, a rational design approach is employed to expand a core fragment and incorporate additional groups that interact with adjacent regions of the binding site.

5

FRAGMENT PROFILING

Due to the absence of a standardized fragment definition, a wide array of approaches is typically employed in constructing fragment libraries. Different chemoinformatic criteria can be utilized to define such libraries, tailoring them to achieve optimal fragment property profiles aligned with the specific target or screening technique, be it Nuclear Magnetic Resonance (NMR) or X-ray crystallography [59]. For instance, in the context of high-throughput crystallography, fragment selection often adheres to the "rule-of-3," analogous to Lipinski's rule-of-5).

However, the assembly of a fragment library presents several challenges: it must possess ample diversity for comprehensive chemical space exploration, compounds should be closely related to facilitate sSAR analysis, the library's size must be manageable for *in-vitro* screening and validation, and it should allow for subsequent medicinal chemistry elaboration.

Throughout the drug development continuum, in-silico computational methodologies play a crucial role and encompass an array of tools and approaches. These computational efforts have proven valuable across various stages of FBDD, including target identification and validation, library design, as well as identification, evaluation, and evolution of (putative) fragment binding.

Chemical suppliers generally provide an extensive array of compounds suitable for constructing a fragment library. However, there is a clear advantage in augmenting this library with substructures from biologically active molecules, or recurring privileged motifs found in established drugs. To achieve this, the initial step in library construction often involves the creation of a compound database. This database encompasses various constituents, such as known active compounds, commercially available compounds with drug- and lead-like characteristics, as well as structures of marketed drugs. The formulation of an initial

dataset of fragments can be accomplished by dissecting these compounds into meaningful building blocks. To facilitate this, different methodologies are available to ensure that the resultant fragments serve as effective starting points for synthesis and are amenable to further development using conventional synthetic chemistry techniques (see Table 5.3).
After establishing the initial collection of fragment candidates, a diversity algorithm can be employed to cluster molecules and create subsets to ensure appropriate dissimilarity. Tools such as similog keys, descriptors based on pharmacophores, and fingerprint-based similarity are instrumental in this stage [51, 60, 61]. To refine the selection, a series of meticulous steps are taken to ensure the viability of the fragments for biochemical and/or biophysical screening. These entail defining and refining fragment molecules based on specific physical properties (known or calculated) including parameters such as molecular weight (MW), water/octanol partition coefficient, solubility, heavy-atom count, number of hydrogen-bond donors and acceptors, and number of rotatable bonds.
Special consideration must be given to the chemical functional groups present in the building blocks. Compounds that are excessively reactive are unsuitable for fragment screening, and even functional groups with lower reactivity may pose issues if they are capable of forming strong hydrogen bonds or ionic interactions with the target, thereby directly influencing the interaction between the fragment and the protein [62].

Table 5.3 | Representative fragment-generation methodologies used in FBDD. These computational tools are used for fragmentation of molecules into meaningful building blocks.

Method	Description	Reference
RECAP	Fragmentation of complex compounds into fragments based on chemical knowledge	[63]
FLUX	Pseudo-retrosynthesis	[64, 65]
SHAPES	Shape descriptors to classify compounds	[66]
DAIM	Decomposition and identification of molecules into fragment libraries suitable for docking and database analysis	[67]

5.3. RESULTS AND DISCUSSION

ARMA POCKET ANALYSIS

The crystal structure of ArmA (PDB: 3FZG) was assessed using the DogSiteScorer server to investigate the presence and druggability of surface pockets [68]. This analysis unveiled two prominent surface pockets, as illustrated in Figure 5.3. Notably, the largest pocket, designated as P1, exhibited the highest drug score at 89%. P1 encompasses the SAM binding site and extends on both sides of this binding site, resulting in a total volume of 658 $Å^3$. Within the P1 pocket, two sub-pockets, P1a and P1b, were identified, with volumes and drug scores of 610 $Å^3$ (48%) and 48 $Å^3$ (29%), respectively.

Table 5.4 | Comparison of different criteria for profiling compounds based on their chemoinformatic properties.

Property	RO3	RO5	lead-like	Reduced complexity	Ghose	Egan	GSK (Verber)	Muegge
MW	≤300	≤500	≤460	≤350	160–480			200–600
LogP (w/o)	≤3	≤5	-4 to 4.2	≤2.2		≤5.88		-2 to +5
LogS (w)			-5 to 1					
Rotatable bonds	≤3[1]		≤10	≤6			≤10	≤15
Molar refractivity					20–70			
Rings			≤4					≤7
H-bond acceptors (HBA)	≤3	≤10[2]	≤9	≤8				≤10
H-bond donors (HBD)	≤3	≤5[3]	≤5	≤3				≤5
Heavy-atom count (HAC)				≤22	20–70			C≤4, Het.≤1
TPSA (Å^2)	≤60*					131.6	140	150

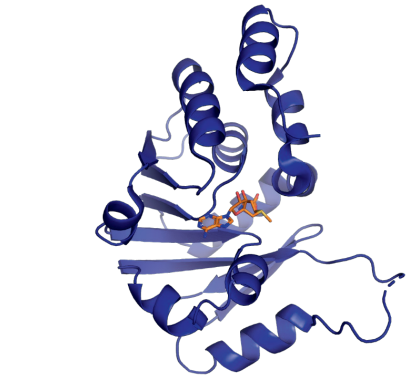
Notes: 1 facultative; 2 defines as number of O and N; 3 defines as number of NH and OH.
Abbreviations: RO3 = Rule-of-3; RO5 = Lipinski's rule-of-5; MW = molecular weight; w = water; o = octanol; TPSA = Topological Polar Surface Area; Het. = heteroatom number.

5

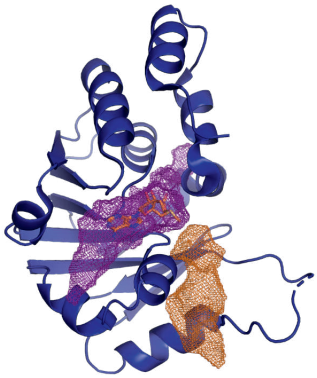
A second significant pocket, referred to as P2, was identified during the analysis, with a volume of 368 Å^3 and a drug score of 57%. This pocket can be further divided into two sub-pockets, P2a and P2b, with volumes and drug scores of 282 Å^3 (33%) and 86 Å^3 (27%), respectively.
Of particular interest is the sub-pocket P1b. The structural alignment of ArmA with the homologous protein NpmA (PDB: 4OX9) bound to the 30S ribosomal subunit suggests that the sub-pocket P1b is in close proximity to the binding site of A1408, which serves as the methyl-acceptor on the 30S ribosomal subunit, as depicted in Figure 5.4.
We hypothesized that by conducting an in-silico screening and evolution of compounds in the fragment space, we could develop candidate molecules that mimic the intermediate state of the methylation reaction and target additional interactions with residues lining the extensive pocket, potentially enhancing specificity towards ArmA.

BUILDING OF THE FRAGMENT LIBRARY

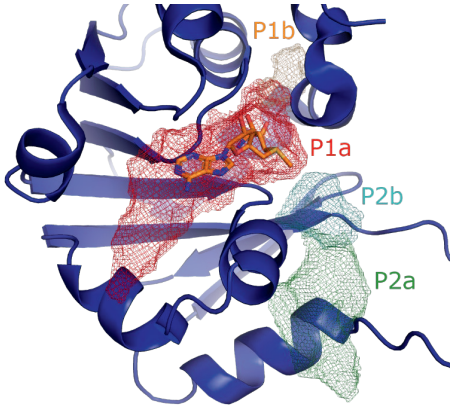
Natural compounds exert significant influence within the domain of chemical space, and their chemical moieties are present in over one third of marketed drugs. Therefore, we selected the ZINC natural products library as the foundational element of our initial database. The library comprises 134,060 unique compounds validated for their ability to interact with no fewer than two distinct proteins [69].
The ZINC library was subjected to a fragmentation process to identify their chemical moieties within the fragment space. The procedure was performed in adherence to the RECAP rules, visually represented in Figure 5.5 [63]. Subsequently, compounds were filtered to identify and remove any substructure that might match Pan Assay Interference Compounds (PAINS). This step resulted in a subset of 27,659 fragments, which were used as search queries for the identification of commercially available compounds with a Tanimoto coefficient of 0.8 or higher.
The retrieved compounds were filtered to ensure the absence of PAINS substructures, unde-



(a)



(b)



(c)

Pocket	Volume (Å^3)	Area (Å^2)	Score
P1	658	843	0.89
P1a	610	719	0.48
P1b	48	134	0.29
P2	368	706	0.57
P2a	282	565	0.33
P2b	86	180	0.27

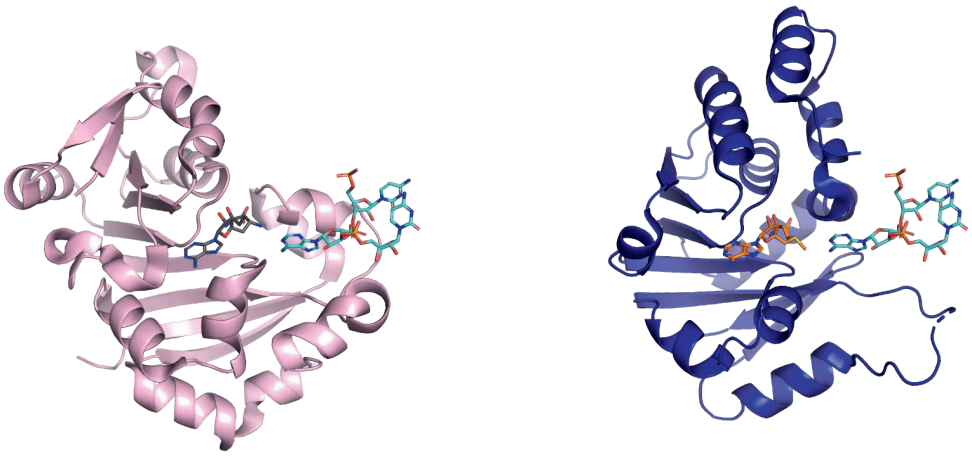
(d)

Figure 5.3 | (a) Cartoon representation of the crystal structure of the 16S rRNA methylase ArmA (blue, PDB code: 3FZG) in complex with SAM (orange). (b) The two main pockets, P1 and P2 are represented as mesh in purple and yellow, respectively. (c) The sub-pockets P1a (red), P1b (yellow), P2a (green), and P2b (cyan). (d) Properties and druggability of the pockets.

sirable reactive groups, and cheminformatic properties within the fragment space.

DOCKING RESULTS AND GROWING STRATEGY

Using the AutoGrow program, docking was effectively paired with fragment evolution to generate and optimize potential ligands by optimizing the ligand-receptor interactions. Each initial core fragment was processed by the algorithm, evolved into a series of larger fragments, and docked using QuickVina. The docking results were used to weight the results and influence the next iteration.



(a) (b)

Figure 5.4 | (a) Cartoon representation of NpmA (pink, PDB code: 4OX9) in complex with a SAM analog (SFG, gray) and the 30S ribosomal subunit (cyan). Only residues 1407-1409 of the 30S ribosomal subunit are shown for clarity. The binding interaction displaces the A1408, which is in the ideal position to act as the methyl acceptor in the catalysis. (c) Assuming that the ArmA (blue) binds the 30S ribosomal subunit (cyan) in a similar manner compared to NpmA, strongly suggests that pocket P2b might serve as the binding site for the methyl acceptor G1405.

Each docking and growing iteration generated up to 100,000 compounds, of which the top 500 were re-scored by averaging the Vina score with the neural-network-based NNScore function. Compounds amenable to further growing entered the next iteration. Ten successive iterations produced an extensive pool of approximately 5 million drug-like compounds obeying the relaxed Lipinski's rule-of-five.

LEAD SELECTION AND LINKER-ANGLE HYPOTHESIS

Among the highest-scoring candidates, we prioritized two chemotypes, **1** and **2** (Figure 5.6a,b), which exhibited comparable docking scores (Vina: −8.7 and −8.4 kcal/mol, respectively). Despite their similar cores, visual inspection of the docking poses revealed distinct orientations of the distal phenyl ring (Figure 5.6c,d). We attribute this divergence primarily to differences in linker geometry: the aryl–O–aryl ether in **1** (typical bond angle ~ 120°) versus the aryl–S–aryl thioether in **2** (~ 100°). This angular variation alters the exit vector and repositions the phenyl group toward a hydrophobic subpocket lined by Ile138, Leu185, and Met181.

Although heterocycle identity (tetrazole in **1** versus triazole in **2**) may influence hydrogen bonding and π-stacking, geometry appears to be the dominant factor driving pose differences (Figure 5.6e). To improve synthetic tractability while preserving the binding hypothesis, we replaced the thioether sulfur with a methylene linker (S→C), yielding analog-friendly scaffolds **3** and **4**, which can be synthesized in two steps from readily available building blocks.

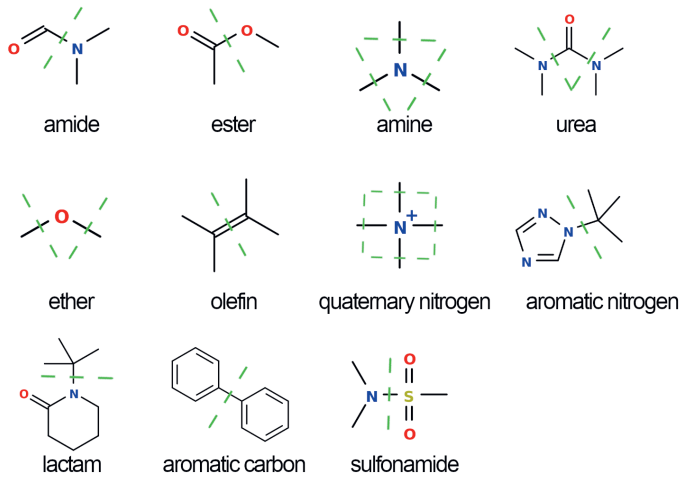


Figure 5.5 | The 11 RECAP rules originally defined by Lewell which specify the cleavage of a complex molecule into smaller fragments. The green dotted line represents the bond cleavage.

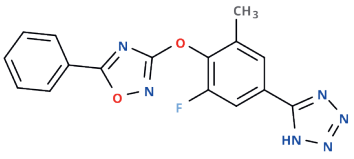
Moreover, to assess whether this substitution adversely affected binding, we redocked compounds **3** and **4**. Encouragingly, compounds **3** and **4** exhibited docking poses and scores similar to their parent compounds.

SYNTHETIC FEASIBILITY AND ACADEMIC ACCESSIBILITY

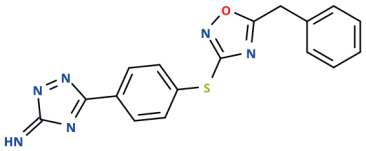
The two-step route outlined in Figure 5.7 demonstrates that the redesigned scaffolds (**3** and **4**) can be assembled from commercially available building blocks, significantly reducing synthetic complexity compared to the original ether/thioether cores.
This streamlined approach is particularly advantageous in academic settings, where resources for multi-step synthesis are limited. By leveraging simple transformations and widely accessible reagents, the proposed route ensures that initial candidates can be prepared rapidly, enabling early-stage biological evaluation without prohibitive cost or time investment.

COMMERCIAL BUILDING BLOCKS AND IN-SILICO COMBINATORIAL EXPANSION

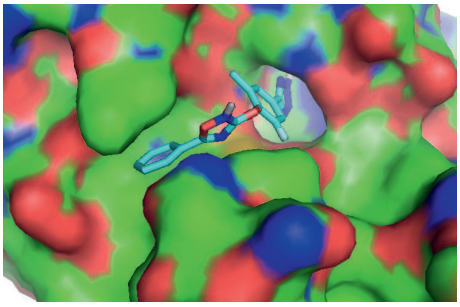
To enable rapid *in-silico* analog generation, we leveraged commercially available building blocks from the eMolecules database. The synthetic route (Figure 5.7) begins with building block **B1**, which is converted to intermediate **B2** via hydroxylamine treatment. From this intermediate, analog families are constructed by combining **B3** and **B4**, each offering diverse R-group substitutions.
The accessible chemical space is substantial: approximately 16,000 possible variants for the **B1**-derived chemotype (about 9,000 after applying a LogP ≤ 3 filter), 35,000 for **B3** (around 24,000 after filtering), and 9,500 for **B4** (approximately 7,800 after filtering).
The combinatorial reaction was performed *in silico* using AutoClickChem and RDKit, and all



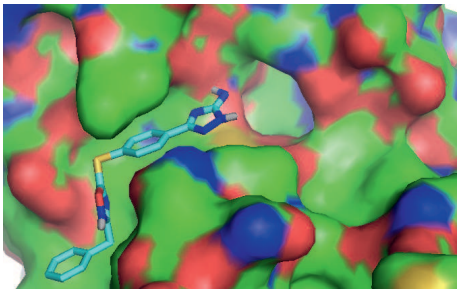
(a) Compound **1**



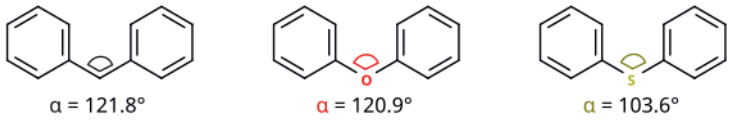
(b) Compound **2**



(c) Docking pose compound **1**



(d) Docking pose compound **2**

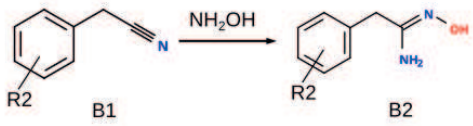


(e)

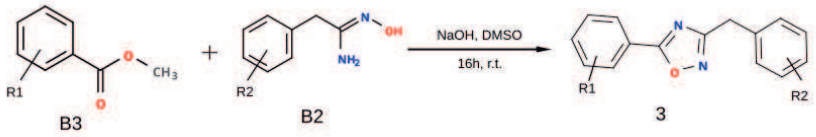
Figure 5.6 | Lead candidates and structural considerations. (**a**) Compound **1** featuring a tetrazole core and an aryl ether linker. (**b**) Compound **2** featuring a triazole core and an aryl thioether linker. (**c**) Docking pose of compound **1** within the ArmA pocket, partially overlapping the binding site of SAM and the methyl-acceptor residue A1408. (**d**) Docking pose of compound **2**, predicted to occupy the groove typically used by SAM. (**e**) Comparison of characteristic bond angles for ether ($\alpha \approx 120°$), thioether ($\alpha \approx 100°$), and benzylic linkers, illustrating the geometric basis for pose divergence and the rationale behind scaffold redesign.

compounds containing undesirable functional groups were removed during post-processing. This resulted in two curated libraries: **6,178,720** analogs for scaffold **3** and **1,872,660** analogs for scaffold **4**.

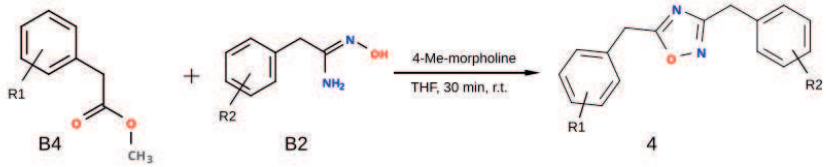
Accelerating ultra-large screening with AI TThe final pool of possible compounds contained 6,178,720 analogs for scaffold **3** and 1,872,660 analogs for scaffold **4**. Exhaustive docking was impractical; therefore, we employed the Deep Docking platform as provided, which uses its own pre-trained neural network to predict docking scores. Approximately 5% of each pool was randomly sampled and docked using QuickVina and GNINA on the Peregrine HPC cluster. These results were incorporated into the standard D2 workflow for fine-tuning the top layer of the included AI model. No custom AI model development or training was performed from scratch; all machine learning components were part of the existing software.



(a) Step 1: Synthetic route to building block



(b) Step 2: Synthetic route to compound **3**



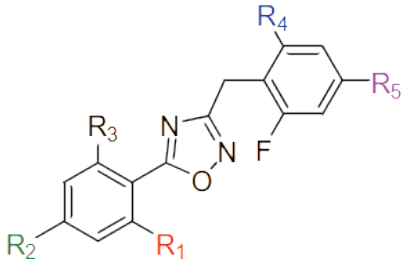
(c) Step 2: Synthetic route to compound **4**

Figure 5.7 | Two-step synthetic route to redesigned scaffolds **3** and **4** from commercially available building blocks. (a) Step 1: formation of the key intermediate B2 from precursor B1 via hydroxylamine addition. (b) Step 2: assembly of scaffold **3** through condensation of intermediate B2 with acyl component B3 under basic conditions. (c) Step 2: analogous coupling of B2 with B4 yielding scaffold **4**. Together, these concise routes demonstrate that the redesigned cores can be generated using simple, and resource-accessible transformations.

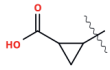
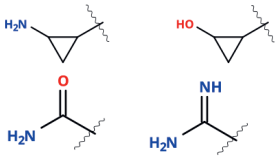
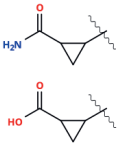
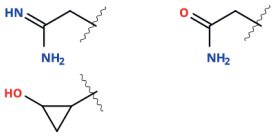
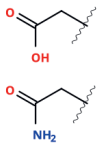
Docking outcomes for expanded libraries The combinatorial enumeration and docking campaign yielded several analogs with improved predicted affinity compared to the parent scaffolds. The best-performing derivatives achieved Vina scores in the range of −9.3 to −9.1 kcal/mol, surpassing the original leads (**1** and **2**). These improvements were primarily associated with substitutions that enhanced hydrophobic interactions within the P1 pocket and introduced favorable electrostatic contacts near residues Glu165 and Asp137.
After combinatorial enumeration and docking, analogs with similar predicted affinities were clustered to identify interchangeable substituent sets. Figure 5.8 shows representative groups for positions R_1–R_5. These clusters reveal that multiple chemical motifs can achieve comparable binding scores, suggesting flexibility in scaffold decoration and providing synthetic alternatives without compromising predicted activity.

5.4. CONCLUSIONS

Considerable progress has been made in computer assisted drug-design (CADD) where computational approaches are employed to accelerate the development of novel inhibitors,



(a) Scaffold with variable positions

Affinity	R1	R2	R3	R4	R5
−9.3	OH		F/H	OH	
−9.2	H/OH		F/H	H/OH	
−9.1	H/OH/NH_2		F/H	H/OH	

(b) Top-ranked analogs and substituent patterns

Figure 5.8 | Representative high-affinity analogs from the combinatorial library. (**a**) Core scaffold highlighting five substitution positions (R_1–R_5). (**b**) Table summarizing top-ranked analogs with predicted docking affinities and common substituent motifs.

mine chemical databases, and explore the relevant chemical space to generate structure-activity relationship (SAR) hypotheses and guide the design of focused libraries of compounds. In this study, we aimed to develop a library of fragments that can potentially produce drug-like candidates by leveraging *in-silico* methodologies, by specifically focusing on docking and the evolution of fragments. Our approach diverged from traditional fragment-based drug discovery, which typically on screening library of compounds using biophysical methods to identify promising hits. Instead, we sought to explore and validate a different strategy for obtaining initial hits and candidates, particularly within academic settings where access to extensive compound libraries and costly screening facilities may be limited.

SUMMARY OF FINDINGS

We began by constructing a comprehensive library of compounds, drawing from natural compound databases and FDA-approved drugs available through the *ZINC 15* repository. The initial step involved fragmenting these compounds. This fragmentation process allowed us to focus on chemical moieties frequently found in known drugs, enhancing the likelihood of identifying viable drug-like candidates.
Following fragmentation, we retrieved commercially available building blocks with high similarity to the selected fragments and applied a series of filters to select compounds that exhibit favorable chemical properties while allowing for structural diversity within the library. Subsequently, we utilized docking simulations and *in-silico* evolution techniques to generate lead candidates. Through docking, we assessed the binding affinities of the fragments to the target protein, identifying those with high binding potential. In-silico evolution allowed us to iteratively optimize these fragments, evolving them into more potent candidates by exploring chemical modifications that enhance interactions with target sites.

IMPLICATIONS FOR ACADEMIC RESEARCH

The approach we employed offers a practical alternative for academic researchers who face challenges associated with traditional fragment screening methods. In academia, accessing extensive libraries and conducting high-throughput screenings can be logistically challenging and financially prohibitive. By focusing on computational methods, we demonstrated that it is possible to generate viable drug-like candidates without the immediate need for physical screening.
Our work underscores the potential of *in-silico* methodologies to complement and, in some cases, substitute traditional fragment screening approaches. The ability to conduct initial screenings computationally allows researchers to identify and prioritize compounds that merit further investigation through experimental methods. This can streamline the drug discovery process, making it more accessible to academic institutions with limited resources.

ADDENDUM AND FUTURE DIRECTIONS

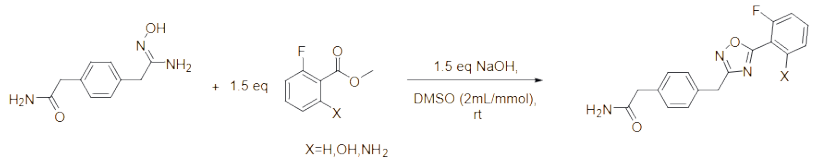
As the culmination of this Ph.D. thesis draws near, this addendum serves to provide an updated overview of the current status of our work and to acknowledge the challenges and limitations encountered.
Three analogs of compound 3 were successfully synthesized following the proposed two-step route. Figure 5.9 shows the synthetic scheme and representative characterization data for one analog. The ^1H NMR spectrum confirms the expected aromatic and linker protons, while ESI-MS analysis shows the molecular ion at m/z 312.4 $[M+H]^+$ and the dimer peak at m/z 623.2 $[2M+H]^+$, consistent with the calculated molecular formula ($C_{17}H_{15}FN_3O_2$).
However, we observed that the resulting compounds exhibit very poor solubility, which limits their immediate applicability in biological assays. This finding underscores the need to design new analogs with improved physicochemical properties to facilitate further testing.
In parallel, we successfully expressed and purified the ArmA protein. We were even able to

obtain crystals suitable for X-ray crystallography. Unfortunately, the crystals diffracted poorly, with resolution worse than 3 Å. Such diffraction quality is insufficient for detailed structural analysis and confirmation of compound binding. These results have prompted a new round of construct design aimed at improving crystal packing and enhancing diffraction quality for future experiments.

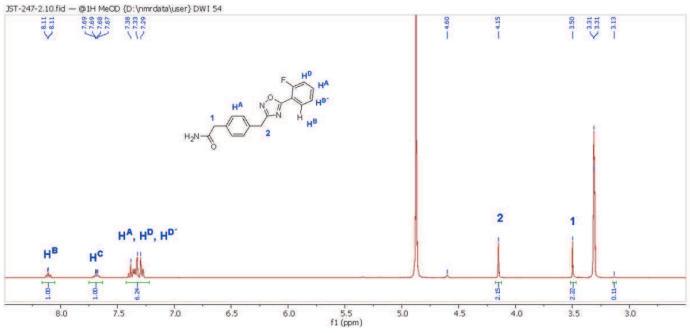
While these developments present technical challenges, they provide valuable insights that will guide the next steps in our project. Overcoming these obstacles is an integral part of the drug discovery process and will inform the design of novel inhibitors targeting aminoglycoside resistance.

While our study highlights the benefits of *in-silico* screening, it is essential to recognize the need for further validation of the identified candidates through experimental methods. Future research should focus on experimentally testing the *in-silico*-derived candidates to confirm their biological activity and drug-like properties. Additionally, exploring the integration of machine learning algorithms with *in-silico* screening processes may further enhance the accuracy and efficiency of candidate identification.

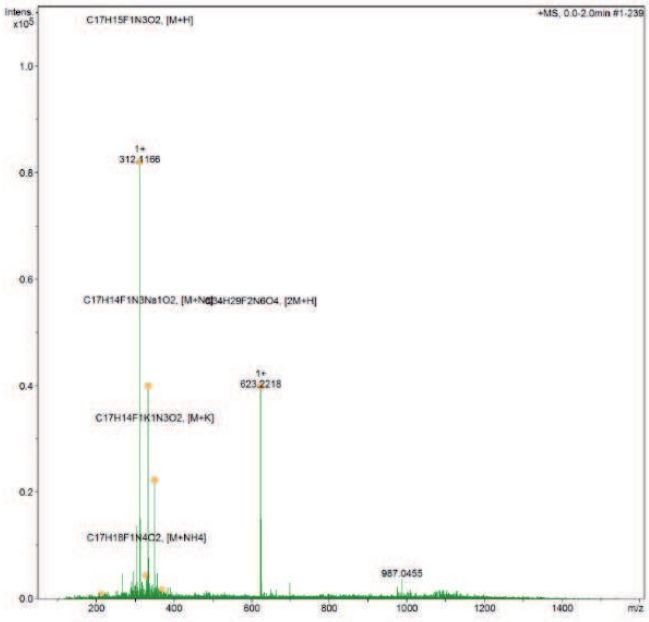
In conclusion, the library of compounds we developed and the computational approach we utilized provide a viable pathway for drug discovery in settings where traditional screening methods are not feasible. This study contributes to the growing body of evidence supporting the role of *in-silico* methods in drug development and encourages continued exploration of alternative strategies that can overcome the limitations faced by academia in this field.



(a)



(b)



(c)

Figure 5.9 | Characterization of synthesized analog of compound 3. (a) Two-step synthetic route using commercially available building blocks. (b) ^1H NMR spectrum recorded in MeOD, showing characteristic aromatic and aliphatic proton signals. (c) Mass spectrum confirming molecular ion at m/z 312.4 $[M+H]^+$ and dimer peak at m/z 623.2 $[2M+H]^+$.

AUTHOR CONTRIBUTIONS

N.P., A.G., and A.H. designed the research and carried out the computational work, data analysis, and manuscript writing.

- N.P.: Conceptualization; fragment library design; docking and fragment-evolution workflows; data analysis; manuscript writing.
- A.G.: Structural biology supervision; conceptual input; manuscript revision.
- A.H.: Project supervision; conceptual guidance; manuscript revision.

Acknowledgements: We thank Andreas Bastian and Jacob Whittaker for their efforts in extending the project through synthetic attempts, crystallization trials, and preliminary data collection.

5.5. METHODS

FORMULATION OF THE INITIAL COMPOUND LIBRARY

Several steps were taken to formulate the library of compounds used in this study (Table5.5). The process included sourcing natural compound libraries, fragmenting them to obtain chemical moieties, and then applying filters to select the most promising candidates. The steps are outlined below:

Formulation of the initial compound library Natural product fragments and FDA-approved drugs were sourced from the ZINC15 repository [69]. Fragmentation was performed using RECAP rules via FragIt, and fragments were filtered according to a relaxed Rule-of-3 (MW 140–350, ClogP –1 to 3, HBA/HBD ≤ 3, rotatable bonds ≤ 3). Commercially available analogs were retrieved from the eMolecules database and clustered to ensure diversity (see Table 5.5).

FRAGMENT EVOLUTION AND DOCKING

AutoGrow was used to evolve fragments into larger compounds through iterative growing and docking with AutoDock Vina. Each iteration generated up to 100,000 compounds, rescored using NNScore. Ten iterations produced 5 million compounds. Top-scoring candidates were visually inspected, leading to selection of Compounds **1** and **2**.

In-silico SYNTHESIS OF ANALOGS OF COMPOUNDS 3 AND 4

Combinatorial expansion was carried out *in silico* using AutoClickChem [70] and RDkit [71]. Building block family **B1** was converted to intermediate **B2** (hydroxylamine addition), then combined with families **B3** and **B4** to generate analogs for scaffolds **3** and **4**. All compounds containing undesirable reactive groups or PAINS motifs were removed. After filtering, the final libraries comprised:

Table 5.5 | Stepwise construction of the fragment library from ZINC natural compounds, showing the number of compounds at each stage of filtering and processing.

Steps	Nr. of compounds
ZINC natural compounds	134,060
Unique fragments (after fragmentation)	82,090
After filters	54,431
Selected fragments (after clustering)	27,659
Building blocks*	529,387
After reduced complexity filter	159,394

* Commercially available blocks with a Tanimoto coefficient of ≥ 0.8 to the selected fragments after clustering.

- **6,178,720** analogs for scaffold **3**
- **1,872,660** analogs for scaffold **4**

DEEP DOCKING WORKFLOW

To efficiently screen ultra-large libraries, we employed the Deep Docking (D2) platform [72], which uses deep learning to augment structure-based drug discovery. The workflow begins by randomly sampling a fraction of molecules (5% per batch) from the enumerated library. These molecules are docked using QuickVina and rescored with GNINA to generate initial training, validation, and test sets for the model. In iteration 1, the sampled set is split into three subsets for model initialization. From iteration 2 onward, additional randomly sampled molecules are docked and incorporated into the training set to refine predictions. This iterative approach enables accurate docking score prediction for the remaining compounds, dramatically reducing computational cost while maintaining ranking fidelity. Implementation followed the guidelines provided in the official D2 repository. Implementation followed the guidelines provided in the official D2 repository. We did not train any custom neural networks; the iterative refinement is part of the standard Deep Docking protocol.
Docking simulations were performed using AutoDock Vina and QuickVina for initial screening, followed by rescoring with GNINA (version 1). The docking grid was centered on the ArmA SAM-binding site (sub-pocket $P_{0,0}$) and extended to include the adjacent G1405-binding region (sub-pocket $P_{1,1}$). A cubic grid box of 16 Å per side was used to encompass both subpockets. Exhaustiveness was set to 16 for Vina and QuickVina runs, while GNINA employed its default convolutional neural network scoring function for pose rescoring. For each ligand, the top-ranked pose was retained for further analysis.

SYNTHETIC FEASIBILITY ANALYSIS

Synthetic routes for top-ranked scaffolds were designed to minimize complexity, using commercially available building blocks and two-step coupling strategies (Figure 5.7). Enumeration of substituent combinations was guided by synthetic accessibility and physicochemical filters (LogP ≤ 3, MW ≤ 500).
Analog enumeration was carried out in silico using RDKit. Reaction SMARTS templates were applied to combine building blocks B1, B3, and B4 with intermediate B2, generating initial libraries for scaffolds **3** and **4**. To ensure chemical tractability, compounds containing undesirable functionalities were removed. Examples of excluded motifs include multiple ester groups, acid halides, reactive aldehydes, long aliphatic chains, nitroso groups, peroxides, and heavy-metal-containing fragments. After filtering, the final libraries comprised 6,178,720 analogs for scaffold **3** and 1,872,660 analogs for scaffold **4**.

HIGH-PERFORMANCE COMPUTING ENVIRONMENT

Docking and neural network training were executed on the Peregrine HPC cluster at the University of Groningen. Jobs were distributed using SLURM arrays across CPU nodes for QuickVina and GPU nodes for GNINA rescoring. Each docking batch consisted of 10,000 ligands per job, with an average runtime of 2 hours per batch for QuickVina and 30 minutes for GNINA rescoring.

EXPERIMENTAL CHARACTERIZATION

Three analogs of compound **3** were synthesized following a two-step route. ^{1}H NMR spectra were recorded in MeOD, and ESI-MS confirmed the molecular weight and purity of the products. However, poor solubility was observed, which negatively impacted crystallization experiments. This outcome highlights the need for analog redesign to improve physicochemical properties.

ACKNOWLEDGMENTS

The author gratefully acknowledges Dr. Jens Köhler for his valuable contribution to the synthesis of the compounds used in this study.

REFERENCES

[1] T. R. Fritsche, M. Castanheira, G. H. Miller, R. N. Jones, and E. S. Armstrong, *Detection of methyltransferases conferring high-level resistance to aminoglycosides in enterobacteriaceae from europe, north america, and latin america,* Antimicrobial agents and chemotherapy **52**, 1843 (2008).

[2] O. B. Ahmed, A. H. Asghar, and F. S. Bahwerth, *Increasing frequency of aminoglycoside-resistant klebsiella pneumoniae during the era of pandemic covid-19,* Materials Today. Proceedings (2021).

[3] G. G. Gaspar, G. Tamasco, N. Abichabki, A. F. T. Scaranello, M. Auxiliadora-Martins, R. Pocente, L. N. Andrade, M.-E. Guazzaroni, R. Silva-Rocha, and V. R. Bollela, *Nosocomial outbreak of extensively drug-resistant (polymyxin b and carbapenem) klebsiella pneumoniae in a collapsed university hospital due to covid-19 pandemic,* Antibiotics **11**, 814 (2022).

[4] A. M. Marua, N. D. Shethwala, P. Bhatt, and S. Amar, *Evaluation of bacterial co-infections and antibiotic resistance in positive covid-19 patients,* Maedica **17**, 350 (2022).

[5] G. L. Dandagi, *Nosocomial pneumonia in critically ill patients,* Lung India: Official Organ of Indian Chest Society **27**, 149 (2010).

[6] E. Van Duijkeren, C. Schwarz, D. Bouchard, B. Catry, C. Pomba, K. E. Baptiste, M. A. Moreno, M. Rantala, M. Ružauskas, P. Sanders, *et al.*, *The use of aminoglycosides in animals within the eu: development of resistance in animals and possible impact on human and animal health: a review,* Journal of Antimicrobial Chemotherapy **74**, 2480 (2019).

[7] M. Block and D. L. Blanchard, *Aminoglycosides,* (2019).

[8] A. W. Serio, T. Keepers, L. Andrews, and K. M. Krause, *Aminoglycoside revival: review of a historically important class of antimicrobials undergoing rejuvenation,* EcoSal Plus **8**, 10 (2018).

[9] G. Miller, F. Sabatelli, R. Hare, Y. Glupczynski, P. Mackey, D. Shlaes, K. Shimizu, K. Shaw, and A. R. S. Groups, *The most frequent aminoglycoside resistance mechanisms—changes with time and geographic area: a reflection of aminoglycoside usage patterns?* Clinical infectious diseases **24**, S46 (1997).

[10] L. P. Kotra, J. Haddad, and S. Mobashery, *Aminoglycosides: perspectives on mechanisms of action and resistance and strategies to counter resistance,* Antimicrobial agents and chemotherapy **44**, 3249 (2000).

[11] S. Jana and J. Deb, *Molecular understanding of aminoglycoside action and resistance,* Applied microbiology and biotechnology **70**, 140 (2006).

[12] M.-P. Mingeot-Leclercq, Y. Glupczynski, and P. M. Tulkens, *Aminoglycosides: activity and resistance,* Antimicrobial agents and chemotherapy **43**, 727 (1999).

[13] S. Magnet, T.-A. Smith, R. Zheng, P. Nordmann, and J. S. Blanchard, *Aminoglycoside resistance resulting from tight drug binding to an altered aminoglycoside acetyltransferase,* Antimicrobial agents and chemotherapy **47**, 1577 (2003).

[14] K. Yamane, J.-i. Wachino, Y. Doi, H. Kurokawa, and Y. Arakawa, *Global spread of multiple aminoglycoside resistance genes,* Emerging infectious diseases **11**, 951 (2005).

[15] P. Bogaerts, M. Galimand, C. Bauraing, A. Deplano, R. Vanhoof, R. De Mendonca, H. Rodriguez-Villalobos, M. Struelens, and Y. Glupczynski, *Emergence of arma and*

rmtb aminoglycoside resistance 16s rrna methylases in belgium, Journal of antimicrobial chemotherapy **59**, 459 (2007).

[16] M. Galimand, P. Courvalin, and T. Lambert, *Plasmid-mediated high-level resistance to aminoglycosides in enterobacteriaceae due to 16s rrna methylation,* Antimicrobial agents and chemotherapy **47**, 2565 (2003).

[17] G. F. Liou, S. Yoshizawa, P. Courvalin, and M. Galimand, *Aminoglycoside resistance by arma-mediated ribosomal 16 s methylation in human bacterial pathogens,* Journal of molecular biology **359**, 358 (2006).

[18] T. Zarubica, M. R. Baker, H. T. Wright, and J. P. Rife, *The aminoglycoside resistance methyltransferases from the arma/rmt family operate late in the 30s ribosomal biogenesis pathway,* Rna **17**, 346 (2011).

[19] F. Yeganeh Sefidan, Y. Mohammadzadeh-Asl, and R. Ghotaslou, *High-level resistance to aminoglycosides due to 16s rrna methylation in enterobacteriaceae isolates,* Microbial Drug Resistance **25**, 1261 (2019).

[20] P. A. Skeggs, J. Thompson, and E. Cundliffe, *Methylation of 16s ribosomal rna and resistance to aminoglycoside antibiotics in clones of streptomyces lividans carrying dna from streptomyces tenjimariensis,* Molecular and General Genetics MGG **200**, 415 (1985).

[21] J. Thompson, P. A. Skeggs, and E. Cundliffe, *Methylation of 16s ribosomal rna and resistance to the aminoglycoside antibiotics gentamicin and kanamycin determined by dna from the gentamicin-producer, micromonospora purpurea,* Molecular and General Genetics MGG **201**, 168 (1985).

[22] J.-i. Wachino, K. Yamane, K. Shibayama, H. Kurokawa, N. Shibata, S. Suzuki, Y. Doi, K. Kimura, Y. Ike, and Y. Arakawa, *Novel plasmid-mediated 16s rrna methylase, rmtc, found in a proteus mirabilis isolate demonstrating extraordinary high-level resistance against various aminoglycosides,* Antimicrobial agents and chemotherapy **50**, 178 (2006).

[23] B. Gonzalez-Zorn, A. Catalan, J. A. Escudero, L. Domínguez, T. Teshager, C. Porrero, and M. A. Moreno, *Genetic basis for dissemination of arma,* Journal of Antimicrobial Chemotherapy **56**, 583 (2005).

[24] M. Roch, R. Sierra, K. Sands, W. M. Martins, J. Schrenzel, T. R. Walsh, A. C. Gales, and D. O. Andrey, *Vertical and horizontal dissemination of an incc plasmid harbouring rmtb 16s rrna methylase gene, conferring resistance to plazomicin, among invasive st258 and st16 kpc-producing klebsiella pneumoniae,* Journal of Global Antimicrobial Resistance **24**, 183 (2021).

[25] E. Schmitt, M. Galimand, M. Panvert, P. Courvalin, and Y. Mechulam, *Structural bases for 16 s rrna methylation catalyzed by arma and rmtb methyltransferases,* Journal of molecular biology **388**, 570 (2009).

[26] J. A. Dunkle, K. Vinal, P. M. Desai, N. Zelinskaya, M. Savic, D. M. West, G. L. Conn, and C. M. Dunham, *Molecular recognition and modification of the 30s ribosome by the aminoglycoside-resistance methyltransferase npma,* Proceedings of the National Academy of Sciences **111**, 6275 (2014).

[27] B. González-Zorn, T. Teshager, M. Casas, M. C. Porrero, M. A. Moreno, P. Courvalin, and L. Domínguez, *arma and aminoglycoside resistance in escherichia coli,* Emerging infectious diseases **11**, 954 (2005).

[28] J. P. Folster, R. Rickert, E. J. Barzilay, and J. M. Whichard, *Identification of the aminoglycoside resistance determinants arma and rmtc among non-typhi salmonella isolates from humans in the united states,* Antimicrobial agents and chemotherapy **53**, 4563 (2009).

[29] K. Piekarska, K. Zacharczuk, T. Wołkowicz, M. Rzeczkowska, E. Bareja, M. Olak, and R. Gierczyński, *Distribution of 16s rrna methylases among different species of aminoglycoside-resistant enterobacteriaceae in a tertiary care hospital in poland,* Advances in Clinical and Experimental Medicine **25**, 539 (2016).

[30] K. Zacharczuk, K. Piekarska, J. Szych, M. Jagielski, L. Hidalgo, A. San Millan, B. Gutierrez, W. Rastawicki, B. Gonzalez-Zorn, and R. Gierczyński, *Plasmid-borne 16s rrna methylase arma in aminoglycoside-resistant klebsiella pneumoniae in poland,* Journal of medical microbiology **60**, 1306 (2011).

[31] W. Yang and F. Hu, *Research updates of plasmid-mediated aminoglycoside resistance 16s rrna methyltransferase,* Antibiotics **11**, 906 (2022).

[32] A. Kawai, M. Suzuki, K. Tsukamoto, Y. Minato, and Y. Doi, *Functional and structural characterization of acquired 16s rrna methyltransferase npmb1 conferring pan-aminoglycoside resistance,* Antimicrobial agents and chemotherapy **65**, 10 (2021).

[33] J. Kirchmair, S. Distinto, D. Schuster, G. Spitzer, T. Langer, and G. Wolber, *Enhancing drug discovery through in silico screening: strategies to increase true positives retrieval rates,* Current medicinal chemistry **15**, 2040 (2008).

[34] P. Aparoy, K. Kumar Reddy, and P. Reddanna, *Structure and ligand based drug design strategies in the development of novel 5-lox inhibitors,* Current medicinal chemistry **19**, 3763 (2012).

[35] L. Krishnan, X. Li, H. L. Naraharisetty, S. Hare, P. Cherepanov, and A. Engelman, *Structure-based modeling of the functional hiv-1 intasome and its inhibition,* Proceedings of the National Academy of Sciences **107**, 15910 (2010).

[36] A. Speck-Planche, V. V. Kleandrova, F. Luan, and M. N. D. Cordeiro, *A ligand-based approach for the in silico discovery of multi-target inhibitors for proteins associated with hiv infection,* Molecular BioSystems **8**, 2188 (2012).

[37] V. Stoll, K. D. Stewart, C. J. Maring, S. Muchmore, V. Giranda, Y.-g. Y. Gu, G. Wang, Y. Chen, M. Sun, C. Zhao, *et al., Influenza neuraminidase inhibitors: structure-based design of a novel inhibitor series,* Biochemistry **42**, 718 (2003).

[38] N. P. Reddy, T. C. Reddy, P. Aparoy, C. Achari, P. R. Sridhar, and P. Reddanna, *Structure based drug design, synthesis and evaluation of 4-(benzyloxy)-1-phenylbut-2-yn-1-ol derivatives as 5-lipoxygenase inhibitors,* European journal of medicinal chemistry **47**, 351 (2012).

[39] K. M. Merz Jr, D. Ringe, and C. H. Reynolds, *Drug design: structure-and ligand-based approaches* (Cambridge University Press, 2010).

[40] M. H. Norman, L. Liu, M. Lee, N. Xi, I. Fellows, N. D. D'Angelo, C. Dominguez, K. Rex, S. F. Bellon, T.-S. Kim, *et al.*, *Structure-based design of novel class ii c-met inhibitors: 1. identification of pyrazolone-based derivatives,* Journal of Medicinal Chemistry **55**, 1858 (2012).

[41] E. Gregori-Puigjané and J. Mestres, *A ligand-based approach to mining the chemogenomic space of drugs,* Combinatorial chemistry & high throughput screening **11**, 669 (2008).

[42] J. Kuan, M. Radaeva, A. Avenido, A. Cherkasov, and F. Gentile, *Keeping pace with the explosive growth of chemical libraries with structure-based virtual screening,* Wiley Interdisciplinary Reviews: Computational Molecular Science **13**, e1678 (2023).

[43] J. Müeller, R. Klein, O. Tarkhanova, A. Gryniukova, P. Borysko, S. Merkl, M. Ruf, A. Neumann, M. Gastreich, Y. S. Moroz, *et al.*, *Magnet for the needle in haystack:"crystal structure first" fragment hits unlock active chemical matter using targeted exploration of vast chemical spaces,* Journal of Medicinal Chemistry **65**, 15663 (2022).

[44] S. Gahbauer, G. J. Correy, M. Schuller, M. P. Ferla, Y. U. Doruk, M. Rachman, T. Wu, M. Diolaiti, S. Wang, R. J. Neitz, *et al.*, *Iterative computational design and crystallographic screening identifies potent inhibitors targeting the nsp3 macrodomain of sars-cov-2,* Proceedings of the National Academy of Sciences **120**, e2212931120 (2023).

[45] A. A. Sadybekov, A. V. Sadybekov, Y. Liu, C. Iliopoulos-Tsoutsouvas, X.-P. Huang, J. Pickett, B. Houser, N. Patel, N. K. Tran, F. Tong, *et al.*, *Synthon-based ligand discovery in virtual libraries of over 11 billion compounds,* Nature **601**, 452 (2022).

[46] F. Gentile, M. Fernandez, F. Ban, A.-T. Ton, H. Mslati, C. F. Perez, E. Leblanc, J. C. Yaacoub, J. Gleave, A. Stern, *et al.*, *Automated discovery of noncovalent inhibitors of sars-cov-2 main protease by consensus deep docking of 40 billion small molecules,* Chemical science **12**, 15960 (2021).

[47] G. G. Rossetti, M. A. Ossorio, S. Rempel, A. Kratzel, V. S. Dionellis, S. Barriot, L. Tropia, C. Gorgulla, H. Arthanari, V. Thiel, *et al.*, *Non-covalent sars-cov-2 mpro inhibitors developed from in silico screen hits,* Scientific reports **12**, 2505 (2022).

[48] C. Gorgulla, A. Boeszoermenyi, Z.-F. Wang, P. D. Fischer, P. W. Coote, K. M. Padmanabha Das, Y. S. Malets, D. S. Radchenko, Y. S. Moroz, D. A. Scott, *et al.*, *An open-source drug discovery platform enables ultra-large virtual screens,* Nature **580**, 663 (2020).

[49] G. L. Wilson and M. A. Lill, *Integrating structure-based and ligand-based approaches for computational drug design,* Future medicinal chemistry **3**, 735 (2011).

[50] C. Chang, S. Ekins, P. Bahadduri, and P. W. Swaan, *Pharmacophore-based discovery of ligands for drug transporters,* Advanced drug delivery reviews **58**, 1431 (2006).

[51] C. Acharya, A. Coop, J. E Polli, and A. D MacKerell, *Recent advances in ligand-based drug design: relevance and utility of the conformationally sampled pharmacophore approach,* Current computer-aided drug design **7**, 10 (2011).

[52] T. J. Marrone, J. M. Briggs, and, and J. A. McCammon, *Structure-based drug design: computational advances,* Annual review of pharmacology and toxicology **37**, 71 (1997).

[53] P. J. Gane and P. M. Dean, *Recent advances in structure-based rational drug design,* Current opinion in structural biology **10**, 401 (2000).

[54] A.-D. Gorse, *Diversity in medicinal chemistry space,* Current topics in medicinal chemistry **6**, 3 (2006).

[55] M. N. Schulz and R. E. Hubbard, *Recent progress in fragment-based lead discovery,* Current opinion in pharmacology **9**, 615 (2009).

[56] D. C. Rees, M. Congreve, C. W. Murray, and R. Carr, *Fragment-based lead discovery,* Nature Reviews Drug Discovery **3**, 660 (2004).

[57] C. H. Röhrig, C. Loch, J.-Y. Guan, G. Siegal, and M. Overhand, *Fragment-based synthesis and sar of modified fkbp ligands: Influence of different linking on binding affinity,* ChemMedChem: Chemistry Enabling Drug Discovery **2**, 1054 (2007).

[58] M. A. El Hassab, T. M. Ibrahim, S. T. Al-Rashood, A. Alharbi, R. O. Eskandrani, and W. M. Eldehna, *In silico identification of novel sars-cov-2 2'-o-methyltransferase (nsp16) inhibitors: structure-based virtual screening, molecular dynamics simulation and mm-pbsa approaches,* Journal of enzyme inhibition and medicinal chemistry **36**, 727 (2021).

[59] B. A. Tounge and M. H. Parker, *Designing a diverse high-quality library for crystallography-based fbdd screening,* Methods in enzymology **493**, 3 (2011).

[60] M. J. McGregor and S. M. Muskal, *Pharmacophore fingerprinting. 1. application to qsar and focused library design,* Journal of chemical information and computer sciences **39**, 569 (1999).

[61] A. Schuffenhauer, P. Floersheim, P. Acklin, and E. Jacoby, *Similarity metrics for ligands reflecting the similarity of the target proteins,* Journal of chemical information and computer sciences **43**, 391 (2003).

[62] A. Schuffenhauer, S. Ruedisser, A. Marzinzik, W. Jahnke, P. Selzer, and E. Jacoby, *Library design for fragment based screening,* Current topics in medicinal chemistry **5**, 751 (2005).

[63] X. Q. Lewell, D. B. Judd, S. P. Watson, and M. M. Hann, *Recap retrosynthetic combinatorial analysis procedure: a powerful new technique for identifying privileged molecular fragments with useful applications in combinatorial chemistry,* Journal of chemical information and computer sciences **38**, 511 (1998).

[64] U. Fechner and G. Schneider, *Flux (1): a virtual synthesis scheme for fragment-based de novo design,* Journal of chemical information and modeling **46**, 699 (2006).

[65] U. Fechner and G. Schneider, *Flux (2): comparison of molecular mutation and crossover operators for ligand-based de novo design,* Journal of chemical information and modeling **47**, 656 (2007).

[66] J. Fejzo, C. A. Lepre, J. W. Peng, G. W. Bemis, M. A. Murcko, J. M. Moore, *et al.*, *The shapes strategy: an nmr-based approach for lead generation in drug discovery,* Chemistry & biology **6**, 755 (1999).

[67] P. Kolb and A. Caflisch, *Automatic and efficient decomposition of two-dimensional structures of small molecules for fragment-based high-throughput docking,* Journal of medicinal chemistry **49**, 7384 (2006).

[68] A. Volkamer, D. Kuhn, F. Rippmann, and M. Rarey, *Dogsitescorer: a web server for automatic binding site prediction, analysis and druggability assessment,* Bioinformatics **28**, 2074 (2012).

[69] T. Sterling and J. J. Irwin, *Zinc 15–ligand discovery for everyone,* Journal of chemical information and modeling **55**, 2324 (2015).

[70] J. D. Durrant and J. A. McCammon, *Autoclickchem: click chemistry in silico,* PLoS computational biology **8**, e1002397 (2012).

[71] G. Landrum *et al.*, *Rdkit: A software suite for cheminformatics, computational chemistry, and predictive modeling,* Greg Landrum **8**, 5281 (2013).

[72] F. Gentile, V. Agrawal, M. Hsing, A.-T. Ton, F. Ban, U. Norinder, M. E. Gleave, and A. Cherkasov, *Deep docking: a deep learning platform for augmentation of structure based drug discovery,* ACS central science **6**, 939 (2020).

6

General Discussion and Conclusions

Nicola Pontillo and Albert Guskov

"Prediction is very difficult, especially if it's about the future."

— Niels Bohr

6.1. OVERVIEW

Antimicrobial resistance (AMR) remains one of the most pressing challenges in global health, threatening the efficacy of antibiotics that have been cornerstones of modern medicine for decades. Among these, aminoglycosidess (AGs) occupy a unique position due to their broad-spectrum bactericidal activity and well-characterized mechanism of action. However, their clinical utility has been compromised by toxicity concerns and the rapid emergence of resistance mechanisms. This thesis addresses these challenges by exploring innovative strategies to revive AGs through chemical modification, structural biology, and novel concepts such as photopharmacology.

CHAPTER 1: FOUNDATIONS OF AMINOGLYCOSIDE RESEARCH

The first chapter provides an overview of AG antibiotics, detailing their historical significance, structural diversity, and mechanism of action. It emphasizes the unique bactericidal nature of AGs compared to other protein synthesis inhibitors and explains how their interaction with the ribosomal A-site underpins their therapeutic effect. Furthermore, Chapter 1 outlines the major resistance mechanisms—particularly Aminoglycoside Modifying Enzymes (AMEs) and 16S rRNA methyltransferasess (RMTs) that have eroded the clinical effectiveness of AGs. It motivated strategies that either re-design the drug to bypass enzymes or target the enzymes themselves, and anticipated the value of dynamic control (light) to modulate activity and selection pressure.[1, 2]

This foundational knowledge establishes the rationale for subsequent chapters, highlighting the urgent need for strategies that circumvent these resistance pathways while preserving ribosomal binding.

CHAPTER 2: OVERCOMING AAC(3)IIIA-MEDIATED RESISTANCE

Building on this foundation, Chapter 2 introduces a rational design approach to counteract AME-mediated resistance. The study focuses on the N-acetyltransferases (3) type IIIa (AAC(3)-IIIa), an enzyme notorious for its broad substrate promiscuity. Through structural and kinetic characterization, the chapter elucidates the enzyme's catalytic mechanism and binding interactions. The synthesis of 3-N-alkylated derivatives of neomycin B demonstrates that minimal chemical modifications—such as the addition of a single methyl group—can dramatically reduce enzymatic acetylation while maintaining ribosomal binding affinity. Cryo-EM analysis confirms that these derivatives preserve their interaction with the A-site, validating the strategy as a viable route to restore AG activity against resistant strains. This work underscores the potential of targeted chemical modifications to overcome resistance without compromising antibacterial potency.

CHAPTER 3: INTRODUCING PHOTO-SWITCHABLE AMINOGLYCOSIDES

While Chapter 2 addresses resistance through structural modification, Chapter 3 explores an entirely new paradigm: the spatial and temporal control of antibiotic activity using light.

The design of photo-switchable paromomycin dimers, incorporating azobenzene and ortho-fluoroazobenzene linkers, enables reversible isomerization between active and less active states upon irradiation with specific wavelengths. This approach offers two major advantages: (i) the ability to modulate antibiotic activity in situ, reducing off-target effects and environmental accumulation; and (ii) the potential to minimize evolutionary pressure for resistance development by activating the drug only when needed. Structural and photophysical characterization, combined with antimicrobial assays, demonstrate that photo-switching can influence enzymatic recognition and antibacterial efficacy. Although still at a conceptual stage, this strategy represents a significant step toward dynamic antibiotic therapies that integrate principles of photopharmacology with traditional antimicrobial design. Acess to spatiotemporal control will allow local activation (e.g., topical, or device-assisted) while minimizing systemic exposure, ecological dissemination, and continuous selection pressure.

CHAPTER 4: SITE-SELECTIVE MODIFICATIONS TO OVERCOME APH-MEDIATED RESISTANCE

Chapter 4 addresses one of the most pervasive aminoglycoside resistance mechanisms: enzymatic phosphorylation by aminoglycoside O-phosphotransferasess (APHs). These enzymes, particularly APH(3')-Ia and APH(3')-IIIa, catalyze ATP-dependent phosphorylation of hydroxyl groups on aminoglycosides, rendering them inactive. The study demonstrates that strategic chemical modifications at the 3'-OH position of kanamycin and paromomycin can effectively prevent phosphorylation while preserving ribosomal binding and antibacterial activity.

Through a combination of site-selective oxidation, indium-mediated allylation and propargylation, and stereochemical inversion, several derivatives were synthesized and evaluated. Among these, SBI237 (3'-epi-paromomycin) and SBI209 (3'-propyl-kanamycin) exhibited remarkable potency against APH-expressing strains, with SBI237 showing a 16-fold improvement in Minimal Inhibitory Concentration (MIC) compared to unmodified paromomycin. Enzymatic assays confirmed that none of the modified aminoglycosides served as substrates for APH(3')-Ia, and some derivatives acted as competitive inhibitors, further reducing enzymatic activity.

Structural insights from X-ray crystallography revealed that modifications at the 3'-OH position introduce steric hindrance within the ATP-binding site of APH(3')-Ia, disrupting catalytic alignment and preventing phosphorylation. These findings establish a rational framework for designing aminoglycosides that evade enzymatic inactivation. However, the study also highlights limitations: APH enzymes targeting multiple hydroxyl sites (e.g., 5"-OH) can bypass single-point modifications, suggesting that dual-site modification strategies may be necessary for broader resistance coverage.

CHAPTER 5: IN-SILICO DESIGN OF ARMA METHYLTRANSFERASE INHIBITORS

While Chapter 4 focuses on chemical modifications to protect aminoglycosides from enzymatic phosphorylation, Chapter 5 explores a complementary strategy: targeting resistance enzymes directly. The plasmid-mediated methyltransferase ArmA confers pan-aminoglycoside

resistance by methylating G1405 in the ribosomal A-site, preventing drug binding. Inhibiting ArmA could restore the efficacy of multiple aminoglycosides simultaneously. This chapter introduces an *in-silico* fragment-based drug design (FBDD) approach to identify potential ArmA inhibitors. Starting from natural product fragments and FDA-approved drug substructures, a library was constructed and iteratively evolved using docking and fragment-growing algorithms. Two lead chemotypes emerged, both predicted to occupy the SAM-binding pocket and interfere with methylation catalysis. Synthetic feasibility was prioritized, resulting in scaffolds amenable to two-step synthesis from commercially available building blocks, making them accessible for academic laboratories.
Combinatorial expansion and AI-assisted deep docking generated millions of analogs, with top candidates achieving predicted affinities surpassing initial leads. Although experimental validation was delayed, preliminary synthesis of three analogs confirmed synthetic tractability, albeit with solubility challenges. These results underscore the potential of computational approaches to accelerate early-stage drug discovery, particularly in resource-limited settings.

BROADER CONTEXT

This work illustrates a progressive trajectory from understanding AG biology and resistance mechanisms to implementing innovative solutions. The integration of structural biology, synthetic chemistry, computational design, and photopharmacology exemplifies a multidisciplinary approach to antibiotic development. These efforts align with global initiatives to combat AMR by expanding the chemical space of existing antibiotics and introducing novel control mechanisms that reduce selective pressure on bacterial populations.
In this thesis, three main strategies have been explored:

Chemical modification of aminoglycosides to evade enzymatic inactivation (e.g., acetylation and phosphorylation) while preserving ribosomal binding and antibacterial activity.

Design of inhibitors targeting resistance enzymes , such as ArmA methyltransferase, using fragment-based and AI-assisted *in-silico* approaches.

Modulation of antibiotic activity through photochemistry , introducing photo-switchable aminoglycoside derivatives for spatiotemporal control of antibacterial action.

These strategies exemplify the multidimensional approach required to combat AMR. Chemical modification offers immediate solutions for specific resistance phenotypes, while enzyme inhibition provides a broader, mechanism-based intervention. Together with the concepts introduced in Chapters 2 and 3 (structural optimization and photopharmacology) this thesis demonstrates that reviving aminoglycosides is feasible through integrated chemical, structural, and computational innovation.

MECHANISTIC LEVERAGE OVER AME SPECIFICITY

The work presented in this thesis shows that AME-driven resistance can be systematically weakened by precise stereochemical and substituent control at AG hydroxyl/amine posi-

tions. The resulting structure-activity relationship (SAR) suggests design rules: (i) maintain A-site contact geometry; (ii) introduce steric or electrostatic features that destabilize the enzyme–drug transition state; and (iii) exploit conformational biases (e.g., epimerization at 3'-OH) that redirect hydrogen-bond networks. This helps generalize beyond the single enzymes subject of thsi work, to other AMEs where catalytic pockets share kinase-like architecture.[1] One possible step to follow would be to combine 3'-OH inversion/bulky substituents with 5"-site protection to broaden APH evasion; evaluate effects of AGs derivatives on ribosomal fidelity and decoding accuracy.

ACTIVITY MODULATION AND EVOLUTIONARY DYNAMICS

Photopharmacology reframes antibiotic exposure as a controllable variable rather than a systemic constant. Intermittent or localized activation could reduce continuous selection pressure, slow resistance emergence, and minimize collateral damage to commensal microbiota. The broader implication is synergy with antimicrobial stewardship: dose only when and where needed, guided by rapid diagnostics and paired with light-delivery devices.
Potential applications extend beyond topical infections. The concept parallels localized cancer treatments, such as brachytherapy, where radioactive needles are inserted into solid tumors to deliver targeted radiation. In infectious disease, a safer and more versatile alternative would be to exploit existing clinical infrastructure, like endoscopic probes, fiber-optic catheters, and surgical light guides, to irradiate biofilms or deep-seated infection clusters. After systemic administration of an inactive, photo-switchable antibiotic, activation could occur exclusively at the infected site, reducing systemic toxicity and ecological impact. This approach could transform management of device-associated infections, chronic wounds, and localized abscesses, where conventional systemic therapy often fails due to poor penetration or biofilm resilience.
Future developments may include integration with minimally invasive imaging systems (e.g., fluorescence-guided surgery) to ensure precise targeting, and coupling with photonic technologies already approved for other indications. Compared to systemic escalation strategies, localized photopharmacology offers a paradigm shift: precision activation, reduced resistance pressure, and compatibility with existing hospital workflows.

TARGETING RMTS AS CLASS-WIDE LEVERAGE

ArmA inhibition promises class-wide restoration because G1405 methylation ablates binding of most 2-deoxystreptamine (2-DOS) AGs. The fragment/AI workflow demonstrates that academic laboratories can navigate ultra-large chemical spaces efficiently, enriching hit quality before costly wet screening. This approach reduces dependency on high-throughput infrastructure and democratizes early-stage antibiotic discovery.
The scientific implication is a scalable paradigm for resistance enzyme targeting across "One Health" contexts (human, animal, environmental microbiomes). From a strategic perspective, this also highlights a gap in industrial engagement: the antibiotic pipeline remains underfunded compared to oncology or chronic disease areas, largely due to lower profit margins

[1] Cf. structural homology with eukaryotic kinases [3, 4].

and stewardship-driven restrictions on usage. Consequently, academic and public-sector innovation is not merely complementary but essential to sustain progress in AMR mitigation. By leveraging open-source computational tools and affordable synthetic routes, universities can compete in niches where industry investment is minimal, accelerating the development of resistance breakers that may otherwise remain unexplored.

6.2. LIMITATIONS

Despite the promising outcomes, this work faces several limitations that must be acknowledged:

- **Partial coverage**: Single-site AG modifications cannot guarantee protection against all AMEs subtypes or secondary modification sites. AMEs are highly promiscuous and can adapt to structural changes in AGs unless a substantial chemotype shift is introduced. This raises the question of whether future research should move beyond incremental modifications toward designing entirely new antibiotic classes that mimic AG pharmacodynamics without sharing the canonical 2-DOS scaffold.

- ***In-silico* gaps**: Docking scores remain proxies for binding affinity and do not capture dynamic aspects of catalysis or solvation. Biochemical validation of ArmA inhibitors is pending, and solubility liabilities are significant. Furthermore, toxicity risks cannot be ignored—especially for inhibitors that partially overlap with SAM-binding sites or interact with conserved cofactor-binding motifs, which may lead to off-target effects in human methyltransferases.

- **Phototherapy constraints**: Light penetration limits systemic applications, confining photopharmacology primarily to topical or surgically accessible sites. Device logistics (such as fiber-optic delivery, wavelength calibration, and integration with clinical workflows) pose additional challenges for widespread adoption.

- **Evolutionary inevitability**: Resistance is an evolutionary certainty. Even with novel chemotypes and enzyme inhibitors, bacteria can adapt through compensatory mutations or horizontal gene transfer. These strategies can only delay resistance emergence, not eliminate it.

- **Non-standardized literature and methodological heterogeneity**: The aminoglycoside field suffers from a lack of standardized protocols for determining key parameters such as K_d, IC_{50}, and MIC values. These metrics have been reported using a wide range of techniques like solution-phase assays, isolated enzyme kinetics, cell extracts, without a unified reference scale and/or methodology. As a result, cross-study comparisons often assume equivalence where none exists, complicating meta-analyses and rational design. This fragmentation, combined with unwritten expectations in publications, may inadvertently hamper progress by discouraging systematic benchmarking and reproducibility. A comprehensive effort to normalize these measurements across platforms would significantly accelerate translational research.

PRECLINICAL PRIORITIES

This work is not conclusive and requires substantial follow-up to address the above limitations. Key priorities include:

- **Medicinal chemistry**: Improve solubility, permeability, and metabolic stability of ArmA inhibitors; explore dual-modification campaigns for AGs (e.g., simultaneous protection of 3'- and 5"-OH positions for APH-binding AGs) to broaden resistance evasion.
- **Mechanistic assays**: Conduct enzyme kinetics across diverse AME and RMT panels; validate ribosome binding using biophysical methods (SPR, ITC); obtain high-resolution structures of enzyme–ligand complexes to guide rational optimization.
- **Microbiology**: It would be good to compare MIC assays across clinical isolates with genotyped resistance determinants; evaluate time–kill curves, post-antibiotic effects, and resistance evolution under serial passage experiments.
- **Toxicology**: Assess ototoxicity and nephrotoxicity in relevant models; establish safety margins relative to parent AGs; investigate phototoxicity and tissue compatibility for light-activated agents.

6.3. CONCLUDING REMARKS

This thesis demonstrates that aminoglycosides, often considered legacy antibiotics, can be rationally revived through precise molecular editing, targeted enzyme inhibition, and dynamic activity control. The scientific payoff is a clearer map of enzyme recognition, ribosome-binding resilience, and resistance pressure management. The technical payoff is a set of accessible chemistries and computational workflows suited to academic and public-sector translation. The societal payoff is a pathway to equitable, stewardship-aligned, and environmentally sensitive antibiotic use.

Final perspective. Resistance is an evolutionary certainty; our task is to *buy time* responsibly. By integrating chemical, structural, computational, diagnostic, and device innovations, we can extend the useful lifespan of aminoglycosides and, crucially, learn a template for revitalizing other antibiotic classes under the AMR shadow.
A final observation concerns the structural incentives that shape research trajectories. Contemporary publishing culture often prioritizes novelty and complexity over incremental or confirmatory work. Methods perceived as "old" are frequently dismissed, even when simple, rigorous experiments could yield transformative insights. This bias discourages systematic benchmarking and reproducibility, fostering a cycle where promising avenues are abandoned prematurely in favor of fashionable paradigms. The aminoglycoside field exemplifies this: decades of fragmented data on K_d, IC_{50}, and MIC values, measured under incompatible conditions, remain largely unharmonized, and possibly slowing down the task of rational design of novel antimicrobial, despite the abundance of information.
On this line, I found praticulatly *enlightening* this observation from G. B. Barham in the context of technological innovation:

> "A point which is here worthy of notice, and which, curiously enough, has not received that attention from the student, or indeed from the inventor which it merits, is that there is a strong tendency on the part of human brain to think in grooves. In some way or another a discovery is made and an invention by means of which some pressing need of mankind can be filled is devised...
>
> At once the whole army of what may be termed improvers abandon their previous studies and rush... to the new line of investigation. The methods they have been following are abandoned and eventually forgotten and a new groove is laid down ...
>
> Possibly some student, years afterwards, turns back to the point where the previous rut came to a dead end, gives his attention to the old and abandoned experiments, sees that some good may result from carrying them further, and meets with some degree of success."
>
> — G. B. Barham, *Development of the Incandescent Electric Lamp [5]*

This reflection resonates deeply with the present work. Reviving aminoglycosides and integrating computational tools is, in essence, a return to an "abandoned groove", a deliberate act of rediscovery. Progress against antimicrobial resistance will depend not only on technological innovation but also on cultural shifts that value rigor, reproducibility, and the courage to revisit what was left behind.

REFERENCES

[1] A. W. Serio, T. Keepers, L. Andrews, and K. M. Krause, *Aminoglycoside revival: review of a historically important class of antimicrobials undergoing rejuvenation,* EcoSal Plus **8**, 10 (2018).

[2] K. M. Krause, A. W. Serio, T. R. Kane, and L. E. Connolly, *Aminoglycosides: an overview,* Cold Spring Harbor perspectives in medicine **6**, a027029 (2016).

[3] D. M. Daigle, G. A. McKay, P. R. Thompson, and G. D. Wright, *Aminoglycoside antibiotic phosphotransferases are also serine protein kinases,* Chemistry & biology **6**, 11 (1999).

[4] D. Nurizzo, S. C. Shewry, M. H. Perlin, S. A. Brown, J. N. Dholakia, R. L. Fuchs, T. Deva, E. N. Baker, and C. A. Smith, *The crystal structure of aminoglycoside-3'-phosphotransferase-iia, an enzyme responsible for antibiotic resistance,* Journal of molecular biology **327**, 491 (2003).

[5] G. Barham, *The Development of the Incandescent Electric Lamp* (Scott, Greenwood & Son, 1912).

ACKNOWLEDGEMENTS

Writing acknowledgments is supposed to be simple: make a neat list of names and thank everyone for the important things I am absolutely certain they did, even if, at this exact moment, I cannot for the life of me recall the details.
I've seen acknowledgments of every species: the professional ones that read like HR-approved press releases, the poetic ones that sound like the author wrote them barefoot in a forest, the nerdy ones full of inside jokes who managed to connect pipettes to the Lord of the Ring, and even the bold few who simply wrote nothing at all. And then there are the vengeance acknowledgments, the scorched-earth genre, which proves a well-known or at least widely suspected fact that a PhD tends to turn good guys into villains like Dr. Frankenstein, Dr. Octopus, or Dr. Evil, while heroes prudently stop at a Master's degree such as Master Yoda, Master Splinter, or Master Miyagi.
So, since I've already done enough "professional tone" to last me a lifetime, I'm not a poet (I checked), and my inner supervillain is currently off-duty, I've chosen a different approach.
Share some stories, events, out of context, memories of the people I have met, first impressions, funny facts, and hopefully I will recall enough of the best moments that everyone recognizes themselves just enough to feel acknowledged, and not quite enough to seriously consider withholding a signature.

My PhD began with my first conversation with **Andreas**, whose confidence in me preceded any evidence I was aware of. After that first meeting he put me forward for the ALERT interviews, having identified my main strength as atomic force microscopy. This was news to me. At the time, my hands-on experience with AFM could best be described as "theoretical optimism," raising the possibility that either I had gravely misunderstood my own strengths in crystallography, or that some talents reveal themselves only when written down by others. His trust opened the door to everything that followed. Those early months were full of enthusiasm and optimism as I tried to build a crystallography project inside a polymer-chemistry universe, and throughout it all he shaped the direction of my work with his characteristic mix of scientific insight and political fluency. Even when he relocated the group to Germany and my trajectory shifted, his influence remained the backbone of the project. I may not miss the meeting requests to be held from trains with the serene assumption that I could simply hop off somewhere between countries, but I am genuinely grateful for the opportunity he gave me and the path it set in motion.
In his group I learned a great deal about DNA construct design, protein expression, purification, and the broader world of molecular biology, which until then had existed for me mostly as diagrams. I owe this witchcraft knowledge to **Mark**, then a research assistant and the structural spine of the team, a man with patience, generosity, and an excellent sense of humor. I knew we were going to get along when he announced that my *crocodile* buffer had

arrived and, upon discovering it was arsenic-based, asked how large the cockroaches were that I was attempting to crystallize.
Then there was **Eliza**, whose energy and enthusiasm carried the project forward during that phase. Unfortunately, she was informed a little late that my task would be to crystallize her molecules in complex with our target, information that might have tempered the enthusiasm with which the work-in-progress was shared at several conferences. Nevertheless, we did good science together. The resulting work remains, appropriately, in a quantum state of being both publishable and unpublished, a situation we have both learned to accept with equanimity and a clear focus on the finish line.
Xintong and **Miancheng** introduced me to the practical art of not trusting my own assumptions both in science and when jumping on snacks. They once brought almond cookies, and in a moment of heroic confidence I gulped down what turned out to be a durian cookie. I did not learn the Chinese characters for "durian" which would've saved me repeating that mistake at least two more times. So for your own sake, please stay away from any box that says 榴莲饼 .
I would also like to thank all the other members of this group: **Ming**, **Shuaidong**, **Anne**, **Deniz**, **Hongyan**, **Jilin**, **Jing**, **Kai**, and **Moritz**. **Qing** and **Jan-Willem**, who, despite our short interaction and their persistent efforts, still did not manage to make me like Eminem's music. I clearly remember the atmosphere, the conversations, and the sense of learning through proximity, the kind of learning that happens not because someone is officially teaching you, but somehow absorbing knowledge through osmosis.

As I mingled with several other groups, **Bert**'s, **Cristina**'s, and **Dirk**'s, I collected more experiences that shaped the path of this PhD. **Dirk**, in particular, once gave me a mild heart attack and a few sleepless nights by suggesting that I restart my PhD in his group. It took us both a moment to realize that I was no longer exactly a fresh PhD chick, but had already been molten and recast a few times, making the plan somewhat impractical. Still, it remains one of my favorite "suggestions," and proof that his trust in me has always been slightly dangerous.
Eventually, I landed with **Albert**, the true shepherd of my wandering PhD soul, who became my main supervisor and helped me weave together all the loose ends I had accumulated along the way. Without his patience and his ability to turn chaos into direction, I could never have reached my goal today.
In this croockpot of collaborations, many deserve a place under the spotlight. **Jacopo**, a delight to have around, both as a friend and as a colleague. He brought color, intelligence, and a generous dose of left-wing commentary (everyone needs a nemesis), along with many other qualities that made the lab feel brighter. He has been a source of inspiration, scientifically, yes, but also in life, and for that I am deeply grateful.
Stephan who gifted me a diagram that I still rely on to this day, a single elegant overview capturing the logic of protein expression and purification. I continue to use it whenever troubleshooting threatens to turn philosophical. He once suspected me of removing an untouchable SEC column, a suspicion that was probably correct, since at the time I had no idea which instrument he meant. This left the matter pleasantly ambiguous and taught me the valuable lesson of labeling things more clearly.
Emanuela and **Masha**, we complained, we talked, we played, we ate, we confided in each

other. We waited together for the ultracentrifuge to stabilize… and then waited again for it to stop so we could enjoy the strangely soothing melody it made. We shared a hairdryer for our pants, which is the kind of detail that really cements a friendship. Some people bond over wine; we bonded over wet lab disasters.
Gianluca, we met at the university, we studied together, abbiamo sparlato dei sensi di colpa e dei tradimenti professionali su un mazzo di carte che non hanno predetto il futuro, ma di certo ci hanno azzeccato sul tema da discutere. Then we worked together again at ZoBio, until life sent us in different directions once more. I hope our paths cross again; statistically, we're due.
Michele, *che cazzo fai in Danimarca? È una vita che non ci sentiamo, ma hai comunque un posto fisso tra le mie memorie.* Thank you for loving everything I hated in the lab; we were, improbably, a very good team.
So many other people I've met along the way: **Eleonora**, **Lucas**, **Natalia** (is your cat still a devil?), **Alex**, **Aliza** and **Vakil**, for whom I had the honor of "re-performing their wedding" for a PhD video, during which I could not, for the life of me, get the words right. **Chancie**, **Aike**, **Jose**, **Fotini**, **Evi**, **Vanessa**. **Gea** (grumpy Gea, but she was right, and would have made PhD-student stew any time, hence everyone treaded lightly), **Valentina**, and **Hendrik**, a love story we all followed and learned from. I also learned to use always a full name and do not abbreviate unless explicitly permitted.

And then there is one more group of people, transcendent, heroic, slightly unhinged: the ALERT group. A desperate attempt to save the world whose password was commitment and teamwork. We didn't quite save the world, but we didn't fail either. We hovered in that noble middle ground where progress happens: not dramatic enough for a movie, but definitely good enough for a thesis.
YanYan, **Xintong**, **Patricia**, **Spyros**, **Roberto**, **Laszlo**, **Piermichele**, **Abigail**, **Simona**, **Miancheng**, each of you added something to the strange, wonderful ecosystem that was my PhD. Whether it was a conversation, a laugh, a shared complaint, or simply existing in the same chaotic orbit, I'm grateful.
But the honor goes to **Francis**, also my paranymph. It all started with a smirk, that silent, unmistakable form of communication that only noi terroni can pull off, some IKEA furniture, where you introduced me to your mother in a parallel universe scenario that should have been a recipe for disaster but instead blossomed into a friendship worthy of its own thesis. *Un mese di transizione italiano-dialetto per perdere dignità in una serata*, the bottles of wine at four in the morning after a litania of *me n'aggia ì*. Our *piccolo mondo* made of nonsense, confessions, and survival instincts. I cherish every single moment we shared. *Siamo stati polli insieme, non potevamo che diventare amici.*
Damla and **Elisa**, oh, the time we spent together at your place: movies, knitting, gossiping, and the kind of conversations that only happen when you're too comfortable to pretend otherwise. I wish you both all the best; you're firmly lodged in my heart.

The list of people who influenced this work, and its kinetics, goes far beyond academia. At some point I must stop writing, but how could I not thank the rotating cast of bold specialists across two hospitals, whose shared medical philosophy seemed to be "act first, verify later,"

while reserving the longest waiting lists for the one condition that was actually present and widely acknowledged. They unquestionably merit their own subsection here. It is not every day one encounters clinicians capable of diagnosing, with flawless confidence, two mutually exclusive endocrine conditions in the same patient, one requiring ovaries, the other requiring to have misplaced them with remarkable dedication.
My thanks also go to the people at **ZoBio**, who supported me through the final stretch of this thesis. **Rob** trusted me, pushed me, and gave me the space I needed to write; **Jan**, who once asked my opinion about a beer he never actually opened; **Marta**, whose patience and flexibility kept me afloat; **Pim**, with whom I shared scrolls of mutual suffering; **Marc**, for his endless rewervoir of little funny stories; **Ronald** and **Jeremy**, for the endless reservoir of stories I could tell thanks to you; and **Kasia**, who adopted me as a brother and still failed to convince me that there is only one God. I cannot list everyone, but each of you contributed to this work in ways that mattered.

To my dad, who kept asking, insistently, relentlessly, and to my mother, who gave me a very clear sense of time by telling me on a video call exactly how much I needed anti-aging cream 50+. It provided the sense of urgency I didn't know I needed.

To **Erwin**, there are things in this world that cannot be planned, earned, or reasoned into existence, and what we have is one of them. You brought a steadiness and a kindness into my days that still catches me by surprise, not because it is rare in you, but because it is rare in general. With you, everything has felt both simpler and richer, as if the ordinary had quietly expanded into something far more precious. You pushed me when I needed it, held space when I didn't know I needed it, and somehow made the whole journey feel lighter without ever diminishing its weight. I am profoundly grateful for what we have built together, something few people are lucky enough to find, and I look forward to the marriage that will carry it forward.

Dennis, life has a way of placing the right people in front of us long before we understand why, and you were one of those rare encounters that quietly rearrange everything. What began with a simple coffee opened a space I didn't know I had been missing: a space where curiosity, warmth, and a kind of effortless understanding could exist without explanation. You brought ideas into my days without even realizing it, small sparks that found their way into this thesis and into many other corners of my world. You reminded me of possibility, of imagination, of the kind of creativity that comes from being seen rather than instructed. There was a longing in me you recognized before I dared to name it, and the way you responded is something I will carry with me for life. To **Saskia**, whose openness and kindness made it possible for me to feel welcome from the very beginning; your presence turned something delicate into something safe.

Eduard. How the hell did we even meet? I mean, I know how and when, and yet… how? Some people arrive quietly and then somehow become the axis around which whole years turn, and you were exactly that. Over all this time, our friendship fed on unspoken words, moka machines, liqueur recipes, and distillation trials. You were the one who showed up

without being asked, who called whenever a single word would have made a difference, who took care of me in ways I didn't even know how to ask for. We joked, we worked, and you managed to make even the most ordinary moments feel like they carried an extra layer. Your presence, your help, your steadiness shaped more of me, and more of this thesis than you probably realize. Everything we built, from the smallest joke to the biggest project, was better because you were part of it. Thank you, for being here, for being my friend, and for being my paranymph.

En aan **Jeannette** en **Arend**: dank jullie wel voor het gevoel van familie dat ik meer miste dan ik ooit hardop heb toegegeven. Jullie warmte, openheid en de manier waarop jullie mij hebben verwelkomd, lieten iets in mij tot rust komen, alsof een deur waar ik al jaren op klopte eindelijk openging.

Scientia sine patientia nihil est.

"Don't start a PhD," they told me.
"Don't start a PhD?" I repeated.
And now it is my turn to tell you:
Don't start a PhD.

But of course… do.

In the end, every thesis is a regeneration scene: the lab coat smokes, the centrifuge hums like a dying TARDIS, the last paragraph refuses to align, and yet, somehow, you step out renewed, confused, and slightly singed, ready for whatever absurdity comes next.

Francis, ricordate sempre: **mettete paura d' 'e ll'uommene segnate d' o' Pateterno**.

Acta est fabula.

